Cenozoic Records of Seawater Chemistry: Chemical Proxies as Indicators of Past Climate.

Elaine M. Mawbey

Thesis submitted for the degree of Doctor of Philosophy.

March 2012

Declaration

This work has not previously been accepted in substance for any degree and is not concurrently submitted in candidature for any degree.

Signed …….… (candidate)

Date ……..

STATEMENT 1

This thesis is being submitted in partial fulfilment of the requirements for the degree of PhD.

Signed …….… (candidate)

Date ……..

STATEMENT 2

This thesis is the result of my own independent work/investigation, except where otherwise stated. Other sources are acknowledged by explicit references.

Signed …….… (candidate)

Date ……..

STATEMENT 3

I hereby give consent for my thesis, if accepted, to be available for photocopying and for inter-library loan, and for the title and summary to be made available to outside organisations.

Signed …….… (candidate)

Date ……..

STATEMENT 4

I hereby give consent for my thesis, if accepted, to be available for photocopying and for inter-library loans **after expiry of a bar on access previously approved by the Graduate Development Committee**.

Signed …….… (candidate)

Date …….

Abstract

The ratios of trace metals to calcium in the calcium carbonate tests of benthic foraminifera have been used as palaeoceanographic proxies for several decades and are now routinely used to reconstruct past climate change on a variety of Cenozoic timescales. Recent research, however, reveals gaps in our understanding of the effects of oceanic variables such as temperature and carbonate saturation state on these trace metal ratios, which limits their application as proxies. Additional uncertainties arise because of physiological effects ("vital effects") and microhabitat of the living foraminifera. Moreover, much of what is known about trace metal uptake into benthic foraminiferal calcite is derived from modern core-top calibrations and laboratory experiments and it is unknown as to what extent our understanding from these models can be applied to the early and mid Cenozoic.

This thesis attempts to address some of these questions using a novel depth transect approach and presenting benthic foraminiferal trace metal records across three major Cenozoic climate change events from Ocean Drilling Program (ODP) deep sea core material. The events are: (i) The Eocene-Oligocene transition (EOT), (ii) The Oligocene-Miocene boundary event (Mi-1) and (iii) The Middle Miocene Climatic Transition (MMCT). These records have allowed examination of the validity of the application of current knowledge of benthic foraminiferal trace metal proxies to Cenozoic records, and also the comparison of the records of two different benthic foraminiferal species, which has shed new light on the importance of foraminiferal habitat in the interpretation of the proxy data.

The identification of a dissolution effect operating on benthic foraminiferal Mg/Ca in undersaturated waters has allowed a reasonable estimate of cooling (~2-3˚C) to be obtained from deep-sea records across the Eocene-Oligocene Transition. The transient glaciation at the Oligocene-Miocene boundary is estimated to comprise of a deep-sea cooling of ~2°C and a sea level decrease of ~80 metres based on *Oridorsalis umbonatus* Mg/Ca. Comparison of new Middle Miocene trace metal records across a water depth transect has shed light on the relative interplay of temperature and saturation state on published Mg/Ca records, enabling more accurate estimates of temperature and ice volume change. The new interpretations suggest that deep sea temperatures cooled by ~4.5°C, and sea level fell by 70-100 metres between 16.2 and 11.6 Ma.

The recently developed paired Mg/Ca-Li/Ca approach to calculating simultaneous variations in bottom water temperature and saturation state has been used to assess inter-basinal differences in water mass composition for the first time. Down-core benthic foraminiferal Li/Ca records from Ceara Rise Sites do not behave as expected, indicating that there may be times when this proxy is affected by an additional environmental parameter. This is tentatively suggested to be a growth-rate related oxygenation signal. U/Ca in benthic foraminifera does not appear to work as a saturation state proxy in these records, again indicating either different behaviour to the observed modern behaviour, or additional factors absent from the modern calibration, such as bottom water oxygenation. Benthic foraminiferal Sr/Ca follows the linear negative water-depth relationship of Lear et al., (2003) suggesting a pressure-related effect.

This study demonstrates that benthic foraminiferal trace metal chemistry can be used to provide information about climate events in the Cenozoic, however additional empirical work is required to fully understand the systematics of trace metal incorporation into benthic foraminiferal tests.

Acknowledgements

Firstly would like to thank my supervisors Carrie Lear and Helen Coxall for their direction and encouragement throughout this project. Their incredible depth of knowledge and patience has improved my understanding of my work infinitely and has been inspirational.

Secondly I would like to thank all the office mates I have been lucky enough to have throughout this project. They have all been amazing and have challenged me to improve myself every day. I have really enjoyed our scientific (and non scientific) discussions throughout the last couple of years and look forward to many more in the future.

Thank you to all the technical staff at Cardiff University who have provided me with training and support, in particular Anabel Morte Rodenas, Huw Boulton, Julia Becker and Jenny Ricker.

Thank you to NERC for providing funding for this project (studentship NE/F016603/1).

Finally thank you to David Wallace for his endless support in life.

List of Contents

1 Introduction

Due to the absence of long term instrumental records (the longest instrumental temperature record being the Central England Temperature record starting from 1659 (Manley 1974)) geochemical analyses of various components of ocean sediments are key in the reconstruction of past climate change. These analyses can provide insights into not only temperature changes but also changes in ocean salinity, global ice volume, circulation patterns, palaeoproductivity and chemistry. The reconstruction of past climate is essential for the testing of global climate models to be used for the prediction of future climate change. This thesis applies a range of geochemical palaeoceanographic proxies to three different climatic events of the early Cenozoic; (i) The Eocene-Oligocene transition (EOT), (ii) The Oligocene-Miocene boundary event (Mi-1) and (iii) The Middle Miocene Climatic Transition (MMCT). The aim of this study is twofold; firstly to investigate the usefulness of benthic foraminiferal trace metal proxies in differing physical and geochemical environments (this is achieved through analysis of multiple sites) and secondly to gather information on the climatic events themselves. Section 1 of this introductory chapter provides background information into the proxies used in this research.

1.1 Stable Isotopes

1.1.1 Oxygen

One of the best established geochemical proxy for quantifying climate change throughout the Cenozoic is the ratio of oxygen isotopes ($\delta^{18}O$) in biogenic calcite. $\delta^{18}O$ is defined as the ratio of the two most abundant stable oxygen isotopes, O^{18} and O^{16} relative to a standard (Equation 1). Standards used in different laboratories are calibrated to international reference standards; initially these were the Pee Dee Belemnite (PDB) for carbonate and/or Standard Mean Ocean Water (SMOW) for water however as the original standards were exhausted isotopic compositions are now reported against standards of the International Atomic Energy of Vienna (VPDB and VSMOW).

$$\delta^{18}\mathrm{O\ sample}\ (‰) = 1000 \times \frac{\left[\left(\frac{^{18}\mathrm{O}}{^{16}\mathrm{O}}\right)\mathrm{sample} - \left(\frac{^{18}\mathrm{O}}{^{16}\mathrm{O}}\right)\mathrm{standard}\right]}{\left(\frac{^{18}\mathrm{O}}{^{16}\mathrm{O}}\right)\mathrm{standard}}$$

Equation 1

$\delta^{18}O$ values in biogenic calcite are dependent upon the $\delta^{18}O$ of the seawater from which they precipitate ($\delta^{18}O_{sw}$), and temperature. A change in $\delta^{18}O_{sw}$ will cause an equal change in the $\delta^{18}O$ of the measured calcite. Temperature and $\delta^{18}O$ have an inverse relationship where a change in temperature of 1ºC will give a ~0.23‰ change in the $\delta^{18}O$ of the biogenic calcite (Bemis et al., 1988). It has also been demonstrated that alkalinity may have a minor effect on isotope values (Spero et al., 1997). “Vital effects” (effects related to biological processes) can cause foraminifera, the proxy signals carriers, to calcify out of

equilibrium with seawater (e.g. Katz et al., 2003) so it is ideal to use the same species having a consistent biology and ecology, throughout a record.

It was first suggested by Urey (1947) that oxygen isotopes in biogenic calcite could be applied to determine marine temperatures. The first palaeotemperature equation was produced by Epstein et al., (1951) using the biogenic calcite of molluscs grown at different temperatures. The oxygen isotope record has played a vital role in palaeoceanography since the isotope record of planktonic foraminifera from a deep-sea core was first interpreted as a series of climate/temperature cycles (Emiliani, 1955) using the Epstein et al., equation. However at the time Emiliani did not realise that the $\delta^{18}O_{sw}$ is affected by ice volume and thus interpreted the signal as large temperature changes. Despite this he was the first to provide geochemical evidence for the Milankovich theory (the theory of how changes in the Earth's orbit affects climate). This work was followed by that of Shackleton (1987) who analysed benthic foraminifera in addition to planktonic foraminifera. From this work it was surmised that the primary control on the Pleistocene $\delta^{18}O$ records was ice volume changes affecting $\delta^{18}O_{sw}$ and temperature was secondary. Global ice volume affects $\delta^{18}O_{sw}$ because the $\delta^{18}O$ of water locked in ice sheets is isotopically much lighter (-35 to -40 ‰) than that of seawater (~0 ‰). This is caused by isotopically heavier water precipitating preferentially at lower latitudes due to Rayleigh fractionation and so isotopically lighter precipitation occurs at the poles where it is then stored in ice sheets.

The palaeotemperature equation of Epstein et al., (1951) has been refined by multiple workers. During times of supposedly ice free intervals such as the early Eocene climatic optimum, palaeotemperature equations can be used to determine temperature changes without correction for ice volume. However during times of changing ice volume $\delta^{18}O_{sw}$ cannot be easily estimated. Therefore an independent proxy is required for either temperature or ice volume in order to deconvolve the $\delta^{18}O$ signal. One such approach is to use Mg/Ca palaeothermometry (e.g. Lear et al., 2000). This proxy along with other trace metal proxies in benthic foraminifera is the main focus of this research.

1.1.2 Carbon

Stable carbon isotopes, as with oxygen isotopes have been used in palaeoceanography since Emiliani (1955) interpreted deep-sea core isotope records in terms of climate. Carbon isotopic records from carbonates are of interest in palaeoclimatology because they help understand how the carbon cycle functions. Shackleton (1987b) showed that carbon isotopes could be used in studying water mass movement and palaeoproductivity and proposed a connection between changes in the terrestrial biosphere with observed carbonate dissolution cycles and the flux of dissolved CO_2 into the oceans.

The $\delta^{13}C$ value of carbonates (the ratio of the two most abundant stable carbon isotopes, ^{12}C and ^{13}C relative to a standard, Equation 2) reflects the $\delta^{13}C$ of the dissolved inorganic carbon species in the ocean (DIC) at time of formation (Keith and Webber, 1964).

$$\delta^{13}\mathrm{C\ sample\ (‰)} = 1000\ \mathrm{x}\frac{\left[\left(\frac{^{13}\mathrm{C}}{^{12}\mathrm{C}}\right)\mathrm{sample} - \left(\frac{^{13}\mathrm{C}}{^{12}\mathrm{C}}\right)\mathrm{standard}\right]}{\left(\frac{^{13}\mathrm{C}}{^{12}\mathrm{C}}\right)\mathrm{standard}}$$

Equation 2

Shifts in seawater δ^{13}C are caused by movement of carbon between carbon reservoirs, including DIC organic matter and sedimentary carbonates. Different reservoirs have different δ^{13}C values; for example organic rich reservoirs have isotopically lighter δ^{13}C values due to fractionation during photosynthesis (O' Leary, 1988). The δ^{13}C of carbonates can therefore be dependent upon organic carbon burial rates relative to carbonate burial rates. An example of this being the Miocene Monterey Excursion during which positive carbon isotope excursions are associated with increased burial of organic matter which may have impacted global climate through the carbon cycle (e.g. Flower and Kennett, 1993).

1.2 Trace Metal/Calcium ratio proxies in benthic foraminifera

The research into trace metal chemistry in biogenic calcite has a long history. The first instance of the recognition that temperature could affect the quantity of trace metals in biogenic carbonate was in 1917 (Wigglesworth-Clarke and Wheeler, 1917). However, with mass spectrometry still in its infancy it was impossible to analyse single species as large amounts of material were needed for analysis. More recently, following advances in instrumentation, numerous studies have been carried out to investigate trace metal composition of biogenic calcite in relation to palaeoceanographic studies. Mg/Ca values in planktonic foraminifera initially were the focus of many studies (e.g. Savin and Douglas, 1973., Bender et al., 1975; Graham et al., 1982; Delaney et al., 1985). The first foray into benthic foraminifera as a bottom water temperature proxy was when Izuka (1988) proposed that temperature was the primary control on Mg content in the benthic foraminifera *Cassidulina*. Since then several benthic foraminifera Mg/Ca calibrations have been proposed (see details below), revealing Mg/Ca to be a powerful tool for reconstructing past ocean temperatures. Moreover, a number of other trace metals, including Sr, Ti, U and B have been investigated as palaeoceanographic proxies in foraminifera. Like all proxies, research has also revealed complications with the foraminifera trace metal proxies, and it is becoming clear that there are secondary effects other than water temperature that affect the concentrations of metals in the calcite crystal lattice. There are, therefore, still many unanswered questions regarding the reliability of trace metal proxies to palaeoceanographic questions, some of which this thesis attempts to address.

1.2.1 Mg/Ca

Temperature control on the ratio of magnesium to calcium in calcite.

Inorganic calcite

The partition coefficient of magnesium between inorganic calcite and a solution is strongly dependent on temperature. This can be explained thermodynamically as any reaction for which there is an enthalpy change will be dependent on temperature which can be defined by the van't Hoff equation. (Equation 3) (Garrels and Christ, 1965). The substitution of Mg into calcite is endothermic and thus higher temperatures lead to greater inclusion of magnesium. A ∆H estimate (Koziol and Newton, 1995) suggests that the Mg/Ca content of calcite will increase exponentially by about 3% per degree between 0° and 30°C.

$$\frac{dlnK}{d1/\mathrm{T}} = \frac{\Delta \mathrm{H}}{\mathrm{R}}$$

T = temperature in Kelvin, R = gas constant, and K = equilibrium constant

Equation 3

This has been supported by laboratory experiments during which calcite crystals were grown by the recrystallisation of aragonite at various temperatures (Chilingar, 1962; Katz, 1973; Burton and Walter, 1987; Mucci, 1987; Oomori et al., 1987). The Oomori data set fits well with the theoretical predictions.

Biogenic calcite

Experimental work has shown that as with inorganic calcite there is also a positive relationship between Mg/Ca and temperature in the formation of biogenic calcite. This work includes culture experiments investigating the growth of the planktonic species *Globigerinoides sacculifer* at varying temperatures and salinity (Nurnberg et al., 1996). This work provides evidence that in addition to temperature there are also biological controls on the uptake of magnesium into calcite as the change in the Mg/Ca partition coefficient with temperature is not the same as in inorganic carbonate. More recent work using core-top studies of planktonic foraminifera (Ferguson et al*.,* 2008, Kısakürek et al., 2008) indicates that salinity may be significant to Mg/Ca ratios and should be included in calibrations. The effects of salinity on Mg/Ca ratios of benthic foraminiferal are currently unknown; however the deep ocean location of the cores in this research project should reduce the likelihood of large scale salinity fluctuations.

Empirical core-top calibrations using benthic foraminifera also demonstrate the positive Mg/Ca temperature relationship (e.g., Rosenthal et al., 1997). In this study samples were obtained from box cores from Little Bahama Bank. These covered a temperature range of 4.5 – 18^{o}C. Eleven foraminifera species (ten calcitic, and one aragonitic) were analysed for their Mg/Ca composition by flame atomic absorption spectrometry. Mg/Ca was shown to have a strong correlation with water temperature. Again the temperature sensitivity was

higher than that in inorganic calcite, suggesting that “vital effects” were at work. Vital effects are signals imposed by biological activity and the living environment. In general, foraminifera, both planktonic and benthic, contain about an order of magnitude less Mg than inorganically precipitated calcite, and the response of Mg/Ca to temperature is larger. Calcification studies indicate that it is likely that foraminifera calcify from seawater that is encapsulated within an internal calcification pool, the composition of which may be altered by removal of magnesium through cellular pumps and channels (Erez 2003, Bentov and Erez, 2006).

From the samples collected in the Little Bahama Bank it was realised that the Mg/Ca content of benthic foraminifera could provide a new independent temperature proxy for studying palaeoceanography. Since then several different benthic foraminiferal Mg/Ca calibrations have been proposed in the literature.

The development of calibrations for benthic foraminifera

As this thesis focuses on benthic foraminiferal trace metal proxies rather than planktonic foraminifera the development of planktonic foraminiferal trace metal calibrations will not be discussed here. For a review of planktonic foraminiferal calibration development Rosenthal (2007) is recommended.

In order to use the Mg/Ca values of foraminifera for palaeothermometry calibrations are required. This may be expressed in the form of a general equation, (Equation 4) as most (but not all) calibrations are given an exponential fit.

$$Mg/Ca = B \exp(A \times Temperature)$$

Equation 4

An equation for determining seawater temperature from Mg/Ca was developed by Rosenthal et al., (1997) from data from Little Bahama Bank. (Equation 5)

$$T = 22.7 \exp(Mg/Ca) - 3.05$$

Equation 5

This equation is a single species calibration using data from the calcitic foraminifera *C.floridanus* (pachyderma). A single species calibration was produced due to large inter-specific differences although this limited its use. The exponential rather than linear fit for the data implies the sensitivity of foraminiferal Mg to temperature increases with temperature. Therefore at lower temperatures the method is less sensitive. The calibration doesn’t contain data for temperatures below 4°C and as most bottom water temperatures (BWT) are below this the calibration may not provide an accurate value for these. The calibration is only from one location and also the foraminifera were not prepared using the rigorous cleaning techniques as described in Boyle and Keigwin (1985/1986). Also

subsequent analyses of core top benthic foraminiferal Mg/Ca are not in agreement with the original calibration (Martin et al., 2002). Due to these factors a revised core top calibration was produced (Lear et al*.,* 2002).

The revised core top calibration (Lear et al., 2002) improved this initial calibration for several reasons. Core top samples from different ocean basins were used which prevents any bias from the use of just one location. These locations covered a temperature range of 0.8 to 18^{o}C thus improving the accuracy of the calibration with respect to lower temperatures. The foraminiferal tests were prepared using the rigorous techniques of Boyle and Keigwin (1985). The resulting calibration (equation 4) describes the relationship of three common species of *Cibicidoides (C.wuellerstorfi, C.pachyderma* and *C.compressus*).

$$Mg/Ca = 0.0867 \pm 0.049 \exp (0.109 \pm 0.007 \times BWT)$$

Equation 6

Other species in this study were also analysed and the values for A and B (Equation 4) produced. The benthic foraminifera included *P.ariminensis, Planulina* spp*., Uvigerina* spp*, M.barleeanum* and *M.pompilioides* and *O*. *umbonatu*s. Published benthic foraminifera calibrations are collated in Appendix 8.1.1.

More recently additional Mg/Ca calibrations for various species have been produced using core top samples (Elderfield et al*.,* 2006). This widens the potential use of Mg/Ca as a palaeothermometer.

In all calibrations discussed previously exponential fits are used to describe the Mg/Ca-temperature relationship. The exponent provides a means of describing the “sensitivity” of a foraminifera species to temperature so the higher the exponent the greater the absolute change in Mg/Ca per degree change in temperature. However one recent core top calibration dataset for the species *C.pachyderma* (Marchitto et al., 2007) indicates that a linear fit may be more suitable for this species data-set (Equation 7). Therefore care should be taken in deciding which fit is applicable to the calibration in question.

$$Mg/Ca = 0.116 \pm 0.014T + 1.2 \pm 0.18$$

Equation 7

If this calibration is applied to other down-core Mg/Ca records however it produces unrealistic temperature changes (e.g. Lear et al., 2008). Further calibration studies are required to resolve the issues described above and reduce uncertainty caused by inter-specific differences. This is especially the case for some of the earlier calibrations as the early *Cibicidoides* calibrations used a data set from the Little Bahama Bank (LBB) (Rosenthal et al., 1997) which is now thought to contain samples contaminated by inorganic precipitation of high Mg calcite (Lear et al., 2002, Marchitto et al., 2007).

Method limitations

Mg/Ca seawater through time

The rate at which Mg substitutes for Ca in calcite has been shown to be temperature dependent. However it is also dependent upon the concentration of Mg relative to Ca in the seawater at the time. This can be accounted for by including it within the calibration (Equation 8, Lear 2007).

$$Mg/Ca_{FORAM} = \frac{Mg/Ca_{sw\text{-}T}}{Mg/Ca_{sw\text{-}0}} \times B \exp(A \times T)$$

Where sw-0 is modern Mg/Ca in seawater and sw-T is estimated Mg/Ca in seawater for sample age.

Equation 8

As there are no direct records of ancient seawater Mg/Ca ratios indirect evidence has to be used to constrain variation through time. There are four lines of evidence available;

1. Fluid inclusions in evaporite minerals (Lowenstein et al., 1997),
2. Biogenic carbonate Mg/Ca ratios in greenhouse world of early Cenozoic (as there was very little or no continental ice volume during the early Cenozoic benthic foraminiferal oxygen isotopes can be used to calculate BWT. This can then be put into Equation 8 to determine seawater Mg/Ca (Lear et al*.,* 2002).
3. Modelling of processes which change concentrations of Mg^{2+} and Ca^{2+} in the oceans (e.g. Demicco et al*.,* 2005).
4. Calcium carbonate veins (Coggan, 2010).

The values from these different methods have quite a range (1.6 to 5 at 50 Ma, e.g. Lear, 2007) but provide some constraint. If these constraints were not available the long residence times of Mg^{2+} (1My) and Ca^{2+} (10My) in seawater (Broecker and Peng, 1982) means changes in seawater Mg/Ca must have occurred quite slowly. Therefore when looking at snapshots of time through the Cenozoic or comparing different localities of the same time period the calculated temperatures changes can still be deemed accurate as the Mg/Ca changes are very small. This thesis focuses on three discrete climate events and so constant seawater Mg/Ca has been assumed to calculate relative temperature variations.

Diagenetic effects

Post-mortem diagenetic processes such as neomorphism/cementation and/or dissolution of the foraminiferal test calcite may alter the trace metal signals found in down-core records. Impurities such as trace metals in the crystal lattice affect the solubility of calcite, with the more impure calcite dissolving preferentially (e.g. Brown and Elderfield, 1996). Therefore dissolution of the calcite would lead to lower Mg/Ca ratios. However, neomorphism, the replacement of a particular mineral such as biogenic calcite by the

same mineral but with different crystal form (for example inorganic calcite) and cementation during which inorganic calcite overgrowths and infilling of chambers may occur, may lead to an increase in Mg/Ca values. This is because the partition coefficient of the magnesium ion into inorganic is higher than biogenic calcite as shown by laboratory experiments (Katz, 1973).

It is observed however that deeply buried carbonate sediments do not trend towards the high values predicted by these experiments (Baker et al., 1982). A more recent study comparing the Mg/Ca values of two contrasting states of preservation; “glassy” (no alteration) vs. “frosty” (alteration) shows a much smaller increase in Mg/Ca in the “frosty” samples than would be expected from the data derived from inorganic experiments (Sexton et al., 2006).

Although these effects have been shown to be relatively small, methods have been proposed to correct for these processes. For example, in Pleistocene cores it has been shown that the extent of dissolution and therefore Mg/Ca depletion can be estimated using test weights (Rosenthal and Lohmann, 2002). There are problems with this however as the average test weight will probably have changed through time. Another way of avoiding the dissolution issue in planktonic foraminifera is to use samples from relatively shallow water depths well above the lysocline (e.g. Lear et al., 2008) although this is not always possible. Foraminifera preserved in clay rich sediments have been shown to retain their original microstructure and geochemistry (Wilson and Opdyke, 1996).

Secondary effects

Carbonate saturation state effect at low levels of saturation

The uptake of a number of trace metals into foraminiferal calcite has been shown to be affected by carbonate ion concentration (e.g. boron (Yu and Elderfield, 2007), lithium (Lear and Rosenthal, 2006) and zinc (Marchitto et al., 2000)). Subsequently a hypothesis has emerged and is now well established that there is a carbonate ion effect on the partition of magnesium into benthic foraminiferal calcite (e.g. Martin et al., 2002, Lear et al., 2004, Elderfield et al., 2006) affecting Mg/Ca temperature estimates. This was initially based on the observation of Martin et al. (2002) that core-top data for *Cibicidoides* spp. below 3ºC fall on steeper gradient than established temperature calibrations (Figure 1-1).

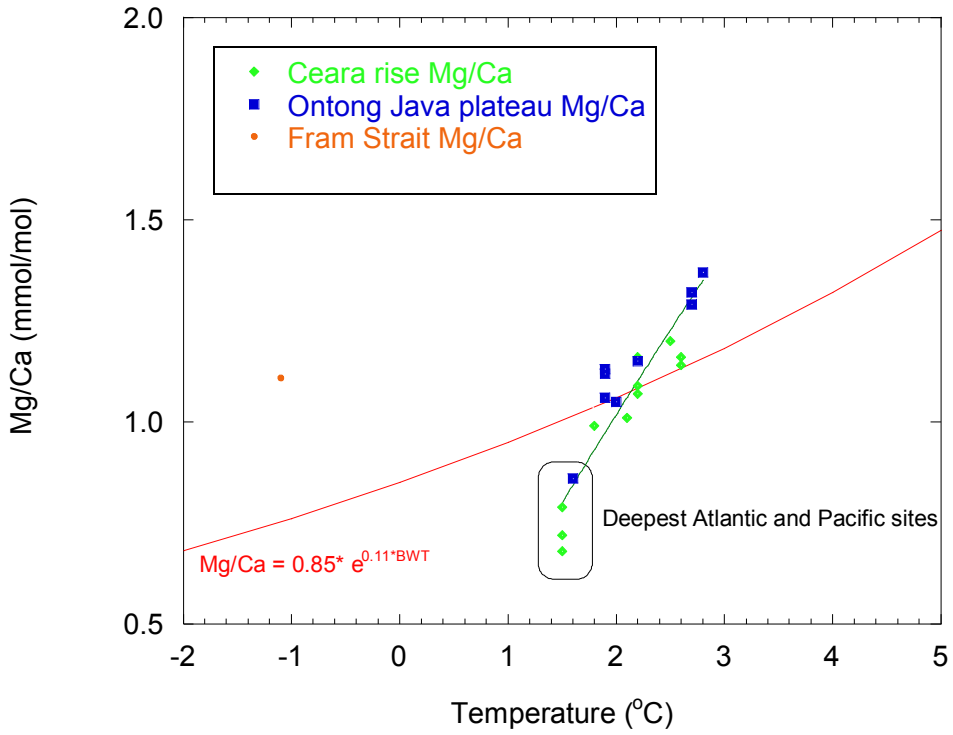

Figure 1-1 Core-top *Cibicidoides wuellerstorfi* Mg/Ca data from different ocean basins (Martin et al., 2002). Red line indicates the core-top calibration of Lear et al. (2002) for *Cibicidoides* spp. Green line indicates line of best fit through Ceara Rise and Ontong Java Plateau data.

An example of this effect in the paleoceanographic record is that during the establishment of the Antarctic ice sheet across the Eocene-Oligocene transition (EOT) where most deep sea benthic Mg/Ca records do not show any decrease in Mg/Ca values despite a predicted >2 °C deep ocean cooling (Lear et al., 2000, 2004; Billups and Scragg 2003; Peck et al., 2011; Pusz et al., 2011). At one site the Mg/Ca signal actually increases indicating warming. This is not a realistic temperature profile across a glaciation event and the oxygen isotope $\delta^{18}O$ increase across the Eocene-Oligocene transition is too great to be attributed solely to ice growth on Antarctica (Coxall et al., 2005). Bipolar glaciation is not compatible with current computer model simulations of the event (Deconto et al., 2008).

Concomitant with the EOT glaciation is a dramatic 1.2 km deepening of the CCD (Coxall et al., 2005). Therefore it is suspected that these Mg/Ca records also reflect this change in seawater chemistry (Lear et al., 2004). The sites which do not display an overall increase in Mg/Ca across the EOT are shallower suggesting that benthic foraminiferal Mg/Ca is less sensitive to changes in saturation state in more saturated waters (Lear et al., 2008). This is supported by two shallow water (shelf/slope) studies across the EOT where the Mg/Ca benthic foraminiferal temperature profile provides evidence for a cooling across the interval (Lear et al., 2008, Katz et al., 2008).

Further evidence for a carbonate ion effect on benthic foraminifera Mg/Ca is provided in a study using modern temperatures and Last Glacial Maximum (LGM) temperatures derived from pore water modelling (Elderfield et al., 2006). These were compared with Mg/Ca values and $\delta^{18}O$ values for the modern and LGM sediments and it was found that carbonate ion variations do affect Mg/Ca values. Elderfield et al., (2006) empirically quantified the carbonate ion effect in *C.wuellerstorfi* species as being 0.0086 mmol/mol/µmol/kg. The carbonate ion sensitivity for *C.mundulus* has also been quantified by Raitzsch et al. (2008) as 0.017 mmol/mol/µmol/kg. However, other species may have a different sensitivity due to vital effects, a possibility that is explored further in this study. Core-top data show that there might also be a saturation state threshold for Mg/Ca (Yu and Elderfield, 2008). When saturation state is less than 25 µmol/kg, *C. wuellerstorfi* Mg/Ca is thought to be more sensitive to saturation state changes (Yu and Elderfield, 2008). However this threshold has been proposed from a consideration of core-top samples and may in part reflect the relative influences of temperature and ΔCO_3^{2-} across different water depths in the modern ocean, as below 3°C in the ocean ΔCO_3^{2-} changes more rapidly than temperature (see Elderfield et al., 2006 for a detailed discussion). Therefore this notion of a saturation state threshold at 25 µmol/kg may not be applicable for time periods where ocean hydrography was significantly different from today. A threshold of saturation state at 25 µmol/kg was documented for the partition coefficient of Zn into *C. wuellerstorfi* (Marchitto et al., 2000). This threshold may be related to physiological processes related to calcification and a further research needs to be undertaken to constrain this threshold in Mg/Ca and potentially other trace metal proxies.

Micro-habitat

The saturation state effect may also be dependent upon the microhabitat of the benthic foraminifera, with species that are thought to be infaunal, such as *Oridorsalis umbonatus* and *Uvigerina* spp., potentially being subjected to less of a bottom water saturation state effect due to living in buffered pore waters (e.g. Elderfield et al., 2010) in which ΔCO_3^{2-} tends to be zero (Martin and Sayles, 1996). Species of *Cibicidoides*, in contrast are believed to be more typically epifaunal, i.e. living at or just above the seafloor/water interface and experiencing unbuffered deep ocean chemistry (McCorkle et al., 1990). *Oridorsalis umbonatus* is a common and cosmopolitan species that is being increasingly used in Cenozoic palaeoceanographic studies, including this one. Having been observed in modern box cores living in the uppermost layers (1-4 cm) of seafloor sediments (Rathburn and Corliss, 1994) this species is regarded as having a 'shallow infaunal' habitat. The variability in depth range observed, however, together with observations of large ranges in abundance and test size (Coxall, personal. communication, 2012), suggests that in reality it may be quite opportunistic in its nature, possibly tracking food supply (Coxall and Wilson, 2011), and/or having the ability to bloom during times of elevated surface ocean productivity. The long stratigraphic range of *Oridorsalis umbonatus*

(Late Cretaceous to present) is further testament to its adaptable nature. This possible ecological flexibility is considered in this thesis when interpreting trace metal records of *Oridorsalis umbonatus* and other species.

Salinity

It has been found that in regions of high salinity (e.g. Greater and Little Bahama Bank, Eastern Mediterranean Sea, and Red Sea) the Mg/Ca of planktonic foraminifera is higher than in regions of lower salinity (Rosenthal et al., 2000, Lear et al., 2002, Reuning et al., 2005, Fergusen et al., 2008). It has been suggested (Fergusen et al., 2008) that salinity influences the Mg/Ca of planktonic foraminifera which would have significant implications for the interpretations of down-core records. However more recent work by Hoogakker et al., 2009 determined these high Mg/Ca values to be related to secondary inorganic calcite coatings. This effect has not been studied in benthic foraminifera, however it may be a potential problem if the benthic foraminifera were inhabiting high salinity areas. As the sediments used in this study are deep sea sediments they are unlikely to have undergone large scale salinity fluctuations and would not have had high salinities across the intervals studied.

Summary

This section highlights the fact that there are still many unanswered questions related to the application of Mg/Ca in benthic foraminifera as a palaeothermometer. This thesis attempts to address some of these questions using a novel multi-proxy water depth transect approach in an attempt to quantify the relative effects of the differing environmental conditions described above, in particular the extent and magnitude of the carbonate saturation state effect on Mg/Ca.

1.2.2 Li/Ca

Controls on Li/Ca in foraminiferal calcite

Li/Ca measured in biogenic and inorganic calcite precipitated at various temperatures indicates that Li/Ca increases as temperature decreases (e.g. Hall and Chan, 2004; Hall et al., 2005; Marriott et al., 2004a; Marriott et al., 2004b) However, this temperature effect is small and down-core measurements of planktonic and benthic foraminifera show a systematic variation with $\delta^{18}O$ that is too large to be caused by the effect of temperature change alone (Hall et al., 2004). Instead, it is has been suggested that much of the variability in Li/Ca of these records is linked to changes in seawater carbonate ion concentration as this would affect calcification rate and thus the take up of lithium into the calcitic tests. This hypothesis is supported by data collected from a Norwegian holothermal depth transect (Lear and Rosenthal, 2006). Core top data collected for the species *Oridorsalis umbonatus* establishes the relationship between Li/Ca and $\Delta[CO_3]^{2-}$ (Figure 1-2; Lear and Rosenthal, 2006).

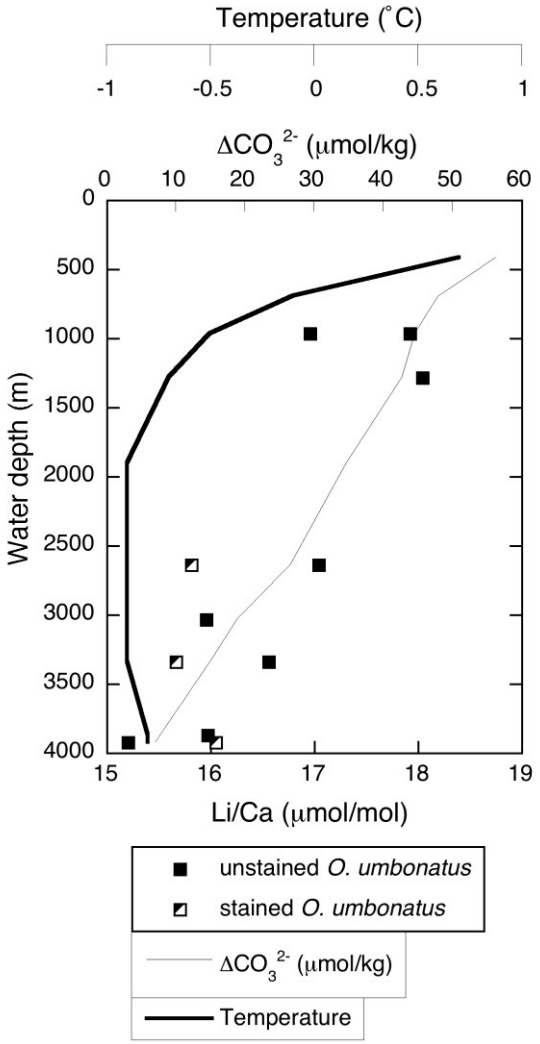

Figure 1-2 Benthic foraminiferal Li/Ca from a Norwegian Sea depth transect demonstrating the relationship between Li/Ca and Δ[CO_3^{2-}], from Lear and Rosenthal (2006).

Down-core records were then created covering the time intervals 0-12 Ma and 19-35 Ma and compared with CCD records (from Van Andel, 1975). The overall form of the data is similar in appearance to the CCD record again suggesting that Li/Ca may be largely dependent on Δ[CO_3^{2-}] (Lear and Rosenthal, 2006).

Limitations

The work described above indicates that Li/Ca ratios of foraminiferal calcite are dependent on both temperature and seawater carbonate saturation state. In order to determine Δ[CO_3^{2-}] variations the temperature aspect of the Li/Ca record must be resolved. This may be achieved through comparison of benthic foraminifera Li/Ca values in down-core deep sea records with better defined proxies for temperature and Δ[CO_3^{2-}], such as Mg/Ca and B/Ca respectively. This has already been attempted by Lear et al., (2010), who used

paired Mg/Ca and Li/Ca records to determine $\Delta[CO_3^{2-}]$ and temperature changes across the EOT and the MMCT. Using combined $\Delta[CO_3^{2-}]$ and temperature calibrations for both metals the authors successfully deconvolved temperature signals at some sites but not others, hinting towards secondary effects and calibration thresholds influencing the benthic Li/Ca concentrations. The exploration of these questions is a primary aim of this study. As with Mg/Ca the extent of the saturation state effect may be related to microhabitat.

Calibrations

It has been shown in studies of other proxies that there can be large inter-specific differences in the take up of trace metal ions into foraminiferal calcite. Therefore calibrations for individual species need to be acquired. An added difficulty is that the multi component (temperature and $\Delta[CO_3^{2-}]$) aspect to this proxy requires that one of the components be kept the same so while the effect of the other component can be measured. One way of doing this is to explore trace metal, including Li/Ca variability in a holothermal (i.e. constant water temperature) depth transect. Using this approach, Lear and Rosenthal (2006) determined the $\Delta[CO_3^{2-}]$ effect on *Oridorsalis umbonatus* Li/Ca without the complication of temperature. More core top and culture experiments need to be carried out to reduce the uncertainty envelope with respect to this proxy.

Changes in Li/Ca seawater composition

The residence time of lithium in seawater is greater than 1my (Huh et al., 1998). Therefore, when looking at more recent records, or looking at changes over a short time interval, changes in the Li/Ca seawater composition do not need to be taken into account. In order to compare intervals on a larger timeframe or obtain absolute values of seawater temperature/carbonate saturation state then Li/Ca seawater concentration changes need to be considered. As with other trace metals there are no direct records of seawater Li/Ca and at the time of writing no indirect records, so currently corrections for seawater Li/Ca cannot be made.

1.2.3 B/Ca

Controls on the ratio of B/Ca in benthic foraminifera

The B/Ca of benthic foraminiferal calcite has been shown empirically to be strongly dependent upon the carbonate saturation state ($\Delta[CO_3^{2-}]$) of the seawater from which they form (Yu and Elderfield, 2007). This is expected as boron is incorporated into foraminiferal calcite as the charged $B(OH)^{4-}$ ion and the amount of boron present as the borate ion is dependent upon pH. The relationship between B/Ca and $\Delta[CO_3^{2-}]$ has been shown to be a simple linear one as described by a generic equation (Equation 9).

$$B/Ca = A \times \Delta[CO_3^{2-}] + B$$

Equation 9

$\Delta[CO_3^{2-}]$ can be related to $[CO_3^{2-}]$ by the following equation (Broecker and Peng 1982).

$\Delta[CO_3^{2-}] = [CO_3^{2-}]_{INSITU} - [CO_3^{2-}]_{SAT}$

Equation 10

Four species of benthic foraminifera were investigated by Yu and Elderfield (2007) three calcitic (C*ibicidoides wuellerstorfi*, C*ibicidoides mundulus* and *Uvigerina* spp.) and one aragonitic (*Hoeglundina elegans*). The core-top data indicates there are large inter-species differences (Table 1-1) suggesting strong vital effects as with Mg/Ca in benthic foraminiferal calcite. More recent core-top calibrations have been carried out for the benthic foraminifera *Nuttallides umbonifera* and *Oridorsalis umbonatus* (Brown et al., 2011). It was found that *N. umbonifera* has a sensitivity to $\Delta[CO_3^{2-}]$ similar to that of *Cibicidoides wuellerstorfi* (Yu and Elderfield, 2007). The absolute B/Ca values and sensitivity to $\Delta[CO_3^{2-}]$ of the species *Oridorsalis umbonatus* were found to be much lower, which was interpreted as the result of pore water buffering of the species in an infaunal habitat. As with Mg/Ca and Li/Ca, therefore, the extent of the saturation state effect in benthic B/Ca may be related to microhabitat, which may vary depending on environmental conditions.

Species	A	B
C.wuellerstorfi	1.14 ± 0.048	177.1 ± 1.41
C. mundulus	0.69 ± 0.072	119.1 ± 2.62
H.elegans	0.27 ± 0.179	19.4 ± 2.99
Uvigerina spp.	0.51 ± 0.179	42.4 ± 3.12

Table 1-1 Empirical B/Ca sensitivities to saturation state of various benthic foraminiferal species from Yu and Elderfield (2007).

Limitations of the method

Changes in B/Ca of seawater

The B/Ca of benthic foraminiferal calcite is dependent on $\Delta[CO_3^{2-}]$ but it is also dependent on seawater B/Ca concentrations. Boron has a long seawater residence time although this is not well constrained (varying estimates between 10 my. (Simon et al., 2006) and 20 My

(Spivack et al., 1987). There are no direct records of Cenozoic seawater B/Ca, yet models indicate minimal change in the seawater [B] over the Cenozoic (~10%; (e.g. Lemarchand et al., 2000) whilst seawater [Ca] is thought to have declined (e.g. Horita et al., 2002). However, as discussed previously calcium has a relatively long residence time and so B/Ca changes over short time slices should reflect saturation state changes rather than seawater B/Ca changes.

Vital effects

Interspecific vital effects in geochemical proxies are corrected for using species-specific calibrations. Recent work, however, indicates that for B/Ca there may also be detectable differences in B/Ca between morphotypes of a single species, as shown in studies on morphotypes of *Cibicidoides mundulus* and *Cibicidoides wuellerstorfi* (Rae et al., 2011). This may be an issue if the morphotypes are not readily identifiable from or when there are insufficient numbers of a single morphotype for analysis. Currently only one morphotype of *Oridorsalis umbonatus*, which is the species upon which much of this study is based, is recognized.

Lack of calibrations for different species

The only current published B/Ca core top calibrations for benthic foraminifera are those described in Yu and Elderfield (2007) (Table 1-1) and Brown et al., (2011). More calibration data from different species are required because the calibrations produced so far show a large range in both absolute B/Ca values and $\Delta[CO_3^{2-}]$ sensitivities. The modern species with the lowest B/Ca is *Oridorsalis umbonatus* (~30µmol/mol) (Brown et al., 2011) and the species with the maximum B/Ca is *Cibicidoides wuellerstorfi* (~250 µmol/mol) (Yu and Elderfield, 2007). The species with lower absolute B/Ca seem to also have lower sensitivity to carbonate saturation state.

Application of B/Ca in benthic foraminifera

B/Ca in benthic foraminifera as a proxy for seawater saturation state is a relatively new proxy and there are various uncertainties in its use. However, the method has been validated through several applications to down-core records from the Holocene and LGM (Yu and Elderfield, 2007) and a study of sediments from the last 800 kyr (Rickaby et al., 2010). The method has also been applied to Pleistocene sediments (Raitzsch et al., 2011).The results were consistent with other proxies for saturation state changes which supports the further development and application of benthic foraminifera B/Ca to questions concerning past changes in deep ocean chemistry.

1.2.4 Sr/Ca

Controls on the ratio of Sr/Ca in Benthic Foraminifera

Core-top calcite benthic foraminiferal Sr/Ca has been shown to decrease linearly with increasing water depth (Elderfield et al., 1996, McCorkle et al., 1995, Rosenthal et al., 1997, Lear et al., 2003). The lack of correlation with temperature indicated by these studies suggests that Sr/Ca in benthic foraminifera is correlated to pressure or carbonate saturation state. The aragonitic foraminifera *H.elegans* however was found to have a positive correlation with both temperature and carbonate saturation state (Rosenthal et al., 2006). The effect is limited to aragonite saturation levels below 15 µmol/kg. Above this threshold temperature exerts the dominant control on Sr/Ca. Aragonitic benthic foraminiferal Sr/Ca was used to estimate a ~2.5°C cooling in shelf-slope waters across the EOT (Lear et al., 2008).

Limitations

The aragonite Sr/Ca temperature proxy cannot be used to for the determination of deep water temperatures that lay below the aragonite compensation depth (ACD). Furthermore below ~15 µmol/mol aragonite saturation there is a carbonate ion affect in addition to a temperature effect (Rosenthal et al., 2006).

The controls on calcitic benthic foraminifera Sr/Ca are still poorly understood and thus its use as a proxy is limited.

1.2.5 U/Ca

Use of U/Ca in biogenic calcite

Initially it was thought that U/Ca was dependent only upon seawater uranium content although decreases in U/Ca across the lysocline were observed this was attributed to dissolution rather than an affect of carbonate saturation state (Russell et al., 1994). Uranium availability for uptake by benthic foraminifera is dependent upon seawater redox conditions (Raitzsch et al., 2011) but in the majority of modern oceans the bottom water and the top centimetre of sediment in oxic and thus does not affect U/Ca availability.

Down-core U/Ca data generated prior to the culture studies showed that the U/Ca ratio of glacial planktonic foraminifera was approximately 25% lower than Holocene values (Russell et al., 1996). Because this change was too large to be explained in terms of changes in the uranium concentration of seawater, Russell et al. (1996) hypothesized that the U/Ca ratio of planktonic foraminifera is also controlled by changes in $\Delta[CO_3^{2-}]$ or temperature.

Later culture studies of planktonic foraminifera indicated that *O.universa* and *G.bulloides* U/Ca is inversely proportional to carbonate ion concentration (Figure 1-3; Russell et al., 2004). This is explained by the fact that the abundance of UO_2CO_3 and $UO_2(CO_3)_2^{2-}$

decrease with increasing carbonate concentration, and these are the two uranium bearing species that preferentially are incorporated into calcite.

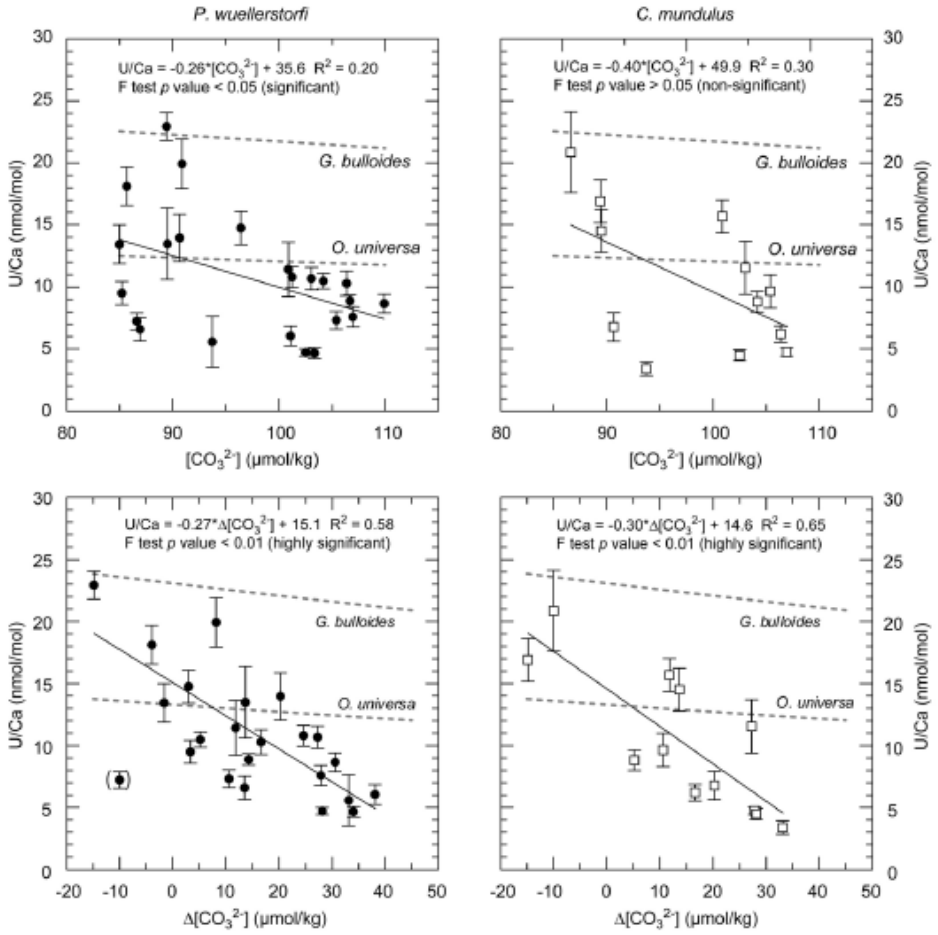

1-3 Benthic foraminiferal U/Ca vs. bottom water [CO_3^{2-}] and Δ[CO_3^{2-}] (Raitzsch et al., 2011). The solid lines are linear fits through the data, the dashed lines are the exponential regressions for planktonic foraminifera from Russell et al. (2004).

U/Ca in planktonic foraminifera is also negatively correlated with temperature. (Yu et al., 2008).

U/Ca changes in benthic foraminiferal species *Planulina wuellerstorfi* and *Cibicidoides mundulus* have recently been assessed using core top samples from the South Atlantic, (Raitzsch et al., 2011). As with the planktonic species the benthic foraminiferal U/Ca is significantly negatively correlated to carbonate saturation state with the sensitivity being an order of magnitude higher than with planktonic foraminifera.

Limitations

Currently only two benthic foraminiferal species (*Planulina wuellerstorfi* and *Cibicidoides mundulus*) and two planktonic species (*O.universa* and *G.bulloides*) have been assessed.

All the species have different vital effects however they all display an inverse relationship to saturation state which presumably applies to all species. Benthic foraminiferal U/Ca could therefore play a key part in deconvolving temperature and saturation state changes from other records. To date there are no published benthic foraminiferal U/Ca records.

Uranium is conservative in seawater and has a residence time of 300-600 kyr (Ku, 1977). It is removed from seawater into sediments overlain by anoxic bottom waters or into continental margin sediments bathed by low oxygen waters. Therefore if in the past there was a higher area of these sediments then the oceanic uranium inventory could have been more variable. However, it is currently not known whether down-core benthic foraminiferal U/Ca records will reflect more regional environmental parameters or more global changes in the seawater uranium inventory.

1.3 Climatic events

The transition of the Earth's climate from the warm ice-free world of the early Cenozoic to today's colder glaciated state has been punctuated by climatic events, both transitional and transient. This is easily observed through analysis of $\delta^{18}O$ records which display a 4 ‰ overall increase across the past 50 my (Zachos et al., 2001), which reflects both the transition to the present glacial state and a global temperature cooling. The climatic events that are studied in this thesis are outlined below.

1.3.1 Eocene-Oligocene Transition and Eocene Oligocene Glacial Maximum

The Eocene-Oligocene transition is recognised as a period of global climate change lasting around 500 kyr (from ~34.1 to ~33.6 Ma) that marks a major step towards the development of the glacial climate of the present. The event has been subject to several decades of research and consequently some ambiguity in the terminology has resulted. The terminology as described in Coxall and Pearson (2007) is used below.

The "Eocene-Oligocene Transition" (EOT) refers to the period of climatic and biotic change that began before and ended after the E-O boundary. The E-O boundary is formally defined as corresponding to the extinction of the planktonic foraminiferal family Hankeninidae (Coccioni et al., 1988). The "Early Oligocene Glacial Maximum" (EOGM), also known as Oi-1, refers to the period where $\delta^{18}O$ values are at a maximum after the transition and has a duration of ~ 400kyr.

High resolution records of the EOT show the increase in oxygen isotope values as a two step event (Coxall et al., 2011, Coxall et al., 2005 (Figure 1-5)). These are referred to as "Step 1" and "Step 2" throughout this study.

The Fossil Record

The fossil record during the E-O transition and subsequent glacial maximum has recently been reviewed by Coxall and Pearson (2007). The EOT was a time of extinction and ecological reorganisation in many groups with the radiation of cold adapted forms. It is

probable that the extinctions are related to the climatic changes across the E-O boundary but there could be several immediate causes including sea-level fall, temperature change, and ocean chemistry.

$\delta^{18}O$ records

The positive shift marking the EOT and the EOGM is clearly seem in a multi-site compilation of benthic foraminiferal $\delta^{18}O$ records (Zachos et al., 2008) (Figure 1-4).

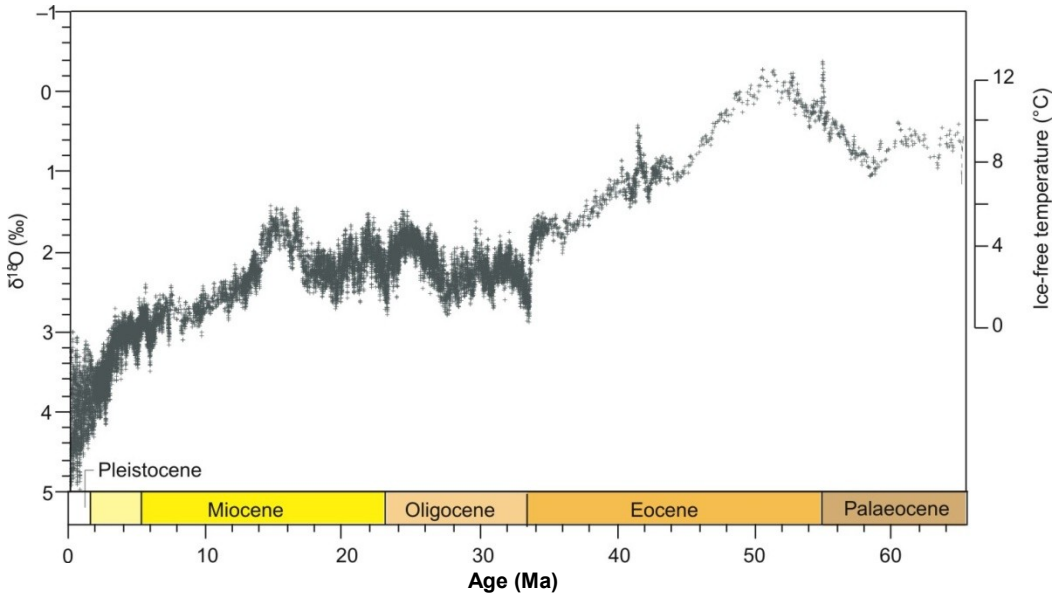

Figure 1-4 Multi-site compilation of benthic foraminiferal $\delta^{18}O$ (Zachos et al., 2008).

High resolution $\delta^{18}O$ and $\delta^{13}C$ records from ODP Leg 199 Site 1218 show a ~1.5 ‰ increase with most of the transition from a relatively deglaciated climate to one with well developed ice sheets taking place over 2 ~40kyr intervals (Coxall et al., 2005; Figure 1-5).

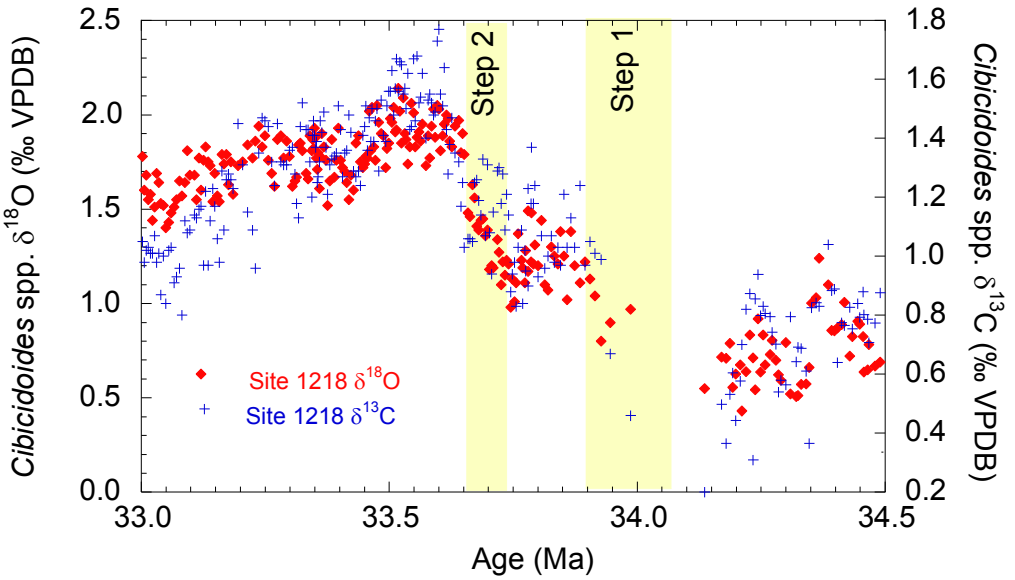

Figure 1-5 High resolution benthic foraminiferal $\delta^{18}O$ and $\delta^{13}C$ records from ODP Leg 199 Site 1218 (Coxall et al., 2005).

Calcite compensation depth (CCD)

A low resolution CCD record showed an increase in the CCD at the EOT (van Andel, 1975). High resolution $CaCO_3$ records from ODP Site 1218 allowed detailed comparison to the $\delta^{18}O$ record (Coxall et al., 2005). The record shows a very rapid increase in $CaCO_3$ content/MAR close to the E-O boundary. The $CaCO_3$ record is synchronous with the $\delta^{18}O$ and $\delta^{13}C$ records showing the same stepwise structure. This CCD was unlikely to be a driving mechanism for the Antarctic glaciation as it would have caused a relatively minor CO_2 drawdown of less than 25 µatm (Sigman and Boyle, 2000). It is thought instead that the CCD increase is a response to glaciation, as the sea level fall reduced the availability of continental shelf for neritic carbonates to form, shifting global $CaCO_3$ deposition from the shelf to the deep ocean basins (Berger and Winterer, 1974; Coxall et al., 2005; Merico et al., 2008).

Trace metal records

The EOT $\delta^{18}O$ shift is too large to reflect Antarctic ice accumulation alone, therefore it must either include a temperature component, or substantial ice sheet accumulation in the Northern hemisphere must have occurred (Coxall et al., 2005). Although there may have been small isolated glaciers on Greenland (Eldrett et al., 2007) significant Northern hemisphere glaciation at the time is not supported by climate modelling (Deconto et al., 2008) which suggests bipolar glaciation was initiated at much lower pCO_2 (~280 ppmV) levels than those estimated for the EOT. Therefore it seems most likely that there was a cooling aspect to the event. Despite this several studies using benthic foraminiferal Mg/Ca

palaeothermometry could not provide evidence for ocean cooling during the EOT (e.g. Lear et al., 2000; 2004; Billups and Schrag 2003), and one record actually indicates a slight warming (Lear et al., 2004). However as discussed in section 3.3.1 it is likely that these records were affected by the concomitant deepening of the CCD which may have exerted a saturation state effect on the benthic foraminiferal Mg/Ca records. Mg/Ca and Sr/Ca records from Tanzanian sediments well above the CCD indicate ~2.5^{o}C cooling associated with ice growth (Lear et al., 2008). This is also the case for records from the shallower site at St Stephens Quarry (Katz et al., 2008), thus supporting the idea that the deep sea Mg/Ca records include a saturation state component.

Proposed causes of the EOT

The cause of the EOT is not fully understood. There are two main mechanisms proposed; the tectonic opening of ocean gateways causing changes in oceanic and atmospheric heat transport (e.g. Toggweiler and Bjornsson, 2000) or declining atmospheric CO_2 coupled with a favourable orbital configuration for ice growth (e.g., Kennett and Shackleton, 1976; DeConto and Pollard, 2003; Zachos and Kump, 2005; Coxall et al., 2005; and Pearson et al., 2009). These contrasting mechanisms have different implications for a global temperature signal.

1.3.2 The Oligocene-Miocene Boundary.

The Oligocene-Miocene Boundary (OMB) was first defined in terms of the fossil record in order to separate observed distinctions in fossil molluscan faunas (Lyell, 1830). Oxygen isotope records spanning this period indicate that the turnover was accompanied by a global climatic event following a period of moderate warmth (Zachos et al., 2001).

Isotope evidence

Designation of Mi-1

The major glacial event (Figure 1-4) associated with the OMB was first defined from $\delta^{18}O$ records from six different Atlantic sites and designated “Mi-1” (Miller et al., 1991). The glacial event and post glacial recovery span from ~23.25 to 23.02 Ma.

High resolution stable isotopes from ODP Leg 154 show that the major glaciation at the OMB was favoured by a specific orbital configuration involving low amplitude variance in obliquity coupled with a minimum in eccentricity (Paul et al., 2000; Zachos et al., 2001b; Pälike et al., 2006).

Trace metal records

There are currently three published benthic foraminiferal Mg/Ca records across Mi-1: low resolution records of Billups and Schrag (2003) from ODP Sites 747 and 689 and a higher resolution record from ODP Site 1218 (Lear et al., 2004). The palaeowater depth of ODP

Site 1218 was ~4km at the OMB as so this record may potentially be affected by changes in bottom water saturation state.

Proposed causes of Mi-1

As with the EOT the proposed causal mechanisms of Mi-1 are tectonic opening of an ocean gateway (the Drake Passage) (Pfuhl and McCave, 2005), orbital configuration as Mi-1 coincides with a low amplitude variance in eccentricity and a minimum in obliquity (Zachos et al., 2001) and pCO_2 decline (Deconto and Pollard, 2003). These contrasting mechanisms have different implications for a global temperature signal.

1.3.3 Middle Miocene Climate Transition (MMCT)

The Middle Miocene Climate Transition (~13.8-14.2 Ma) is a major step in the evolution of Cenozoic climate towards a cooler more glaciated state. It is marked by a ~1‰ positive shift in $\delta^{18}O$ values (Miller et al., 1987). The fossil record, ice rafted debris and eustatic sea level changes across the interval indicate that it was a combination of temperature change and ice volume that caused the positive $\delta^{18}O$ excursion (Woodruff and Savin 1989; Haq et al., 1987). There is also a planktonic Mg/Ca record from the Southern Ocean which indicates sea surface cooling (Shevenell et al., 2008). However, to determine the absolute temperature and ice volume change a proxy independent of $\delta^{18}O$ is needed. Trace metal records have been produced at ODP Site 761 and suggest a bottom water 2°C cooling across the climate transition (Lear et al., 2010). However further records are needed to assess the global extent of this cooling and to reduce the uncertainty of the ODP Site 761 temperature records which depend on whether the site was above or below the Mg/Ca-$\Delta[CO_3^{2-}]$ threshold across the MMCT.

Possible causes of the MMCT

It has been hypothesised that increased burial rates of organic carbon led to atmospheric CO_2 drawdown and global cooling in the middle Miocene (Vincent and Berger, 1985; Flower and Kennett, 1993). While an alkenone based CO_2 record displays little variation through this interval (Pagani et al., 2009), boron isotope ratios and a leaf stomatal record do point to a decrease in pCO_2 at the MMCT (Pearson and Palmer, 2000; Kürschner et al., 2009). Recently published trace metal records from ODP Site 761 (Wombat Plateau) combined the Li/Ca and Mg/Ca from the benthic foraminifera *Oridorsalis umbonatus* to determine relative changes in saturation state and temperature through the MMCT. These indicate that the $\delta^{18}O$ excursion contains both an ice volume (sea level change ~60 m) and temperature decrease (~2°C). It also indicates a saturation state increase in the bottom waters which if other parameters remained equal could indicate a decrease in atmospheric CO_2. Deep ocean circulation changes may have played a major role in the evolution of the glacial climate across the MMCT. Reduction of warm, saline deep water flow to the Southern Ocean at ~14.8 Ma is thought to have decreased meridional heat transport to

the Antarctic, cooling the region and leading to increased production of Southern Component Water (Flower et al., 2003). A further mechanism to explain the MMCT is a favourable orbital configuration. The orbital configuration across the MMCT produced relatively constant, low summer insolation over Antarctica (Holbourn et al., 2005).

1.4 Aims of this study

The primary aims of this thesis are to determine the extent to which our current understanding of the controls on the trace metal composition of modern benthic foraminifera can be applied to Cenozoic records whilst furthering knowledge about key climatic events. In achieving these aims the key objectives were to;

1) Develop the analytical method on a recently installed inductively coupled plasma mass spectrometer (ICP-MS).
2) Construct a suite of trace metal records across the EOT from a water depth transect in the Pacific.
3) Compare EOT records with others sites on the same age model.
4) Construct a suite of trace metal records across the Mi-1 event from two sites with different water depths in the equatorial Atlantic.
5) Construct a suite of trace metal records across the MMCT event from two sites with different water depths in the equatorial Pacific.

1.5 Thesis layout

The developmental aspect of the research is described in chapter 2, while the principal scientific findings are set out in chapters 3-5. The thesis is outlined below;

Chapter 1: Sets out the current understanding of both the proxies and the climatic events that are the focus of this study.

Chapter 2: Sets out the methodology used to construct the records and steps taken during this study to develop these methods.

Chapter 3: Describes and discusses the scientific findings from the new EOT records produced in this study and compares these new results to previously published records.

Chapter 4: Describes and discusses the scientific findings from the new Mi-1 records produced in this study and compares these new results to previously published records.

Chapter 5: Describes and discusses the scientific findings from the new MMCT records produced in this study and compares these new results to previously published records.

Chapter 6: Integrates the main findings from the new records produced from the various sites during this study. Their significance within the context of paleoclimate research is discussed. Potential further work, resulting from the conclusions of this thesis are also discussed.

References and Appendices can be found at the back of the thesis.

2 Methods

The aim of this chapter is to provide background information on the sites, samples and analytical techniques used. The methods of analysis are described here with some method development experiments, the aims of which were to assess and improve the precision and accuracy of the trace metal analysis of foraminiferal calcite by ICP-MS.

2.1 Site Selection

In selecting material for this study the following criteria were considered;

(i) Geographical location, with a view to reducing regional influences such as terrestrial input, upwelling and water mass effects in order to try gain a global palaeoceanographic signal.

(ii) Sedimentation rate/ microfossil preservation state with the goal of obtaining high quality calcitic material for geochemical analysis.

(iii) A requirement for multiple sites in one region forming a paleodepth transect for exploring possible depth related effects such as carbonate saturation state. This section justifies the use of the sites in this study on the basis of the criteria outlined above and describes the sampling strategy.

Figure 2-1 Global map indicating site positions used in this study.

ODP Leg	Site	Sediment Depth (mbsf)		Latitude	Longitude	Modern water depth (m)
		top	bottom			
199	1218	204.1	224.6	8°53.378'N,	135°21.999'W	4826
199	1219	172.9	173.4	7°48.010'N	142° 0.939'W	5063
199	1220	76.3	76.9	10°10.600'N	142°45.503'W	5218
130	803	103.9	262.3	2°25.98'N	160°32.46'E	3412
130	806	409.5	595.8	0°l9.11 'N	159°21.69'E	2520
154	926	461.5	479.6	3°43.148'N	42°54.504'W	3598
154	929	315.2	331.0	5°58.573'N	43°44.394'W	4361

Table 2-1 Burial depths, locations and current water depths of studied sites.

Each depth transect was used to study a particular climate interval, ODP Leg 199 samples span the Eocene/Oligocene transition, ODP Leg 154 samples span the Oligocene-

Miocene boundary glacial event and the ODP Leg 130 samples span the Middle Miocene Climate Transition.

2.1.1 Eocene/Oligocene Transition sites

The material for the Eocene-Oligocene study is derived from three sites recovered from ODP Leg 199, which drilled Palaeogene sediments in the Equatorial Pacific (ODP Leg 199, Shipboard Scientific Party, 2002). The sites (ODP Sites 1218, 1219 and 1220) are presently located north of the equator in the eastern Equatorial Pacific Ocean (Figure 2-2). ODP Sites 1219 and 1220 are situated on crust ~56 million years in age whereas ODP Site 1218 is situated on younger crust ~42 million years in age which is why it has a shallower palaeowater depth. This crust was situated on or near the equator from the middle Eocene through Oligocene (based upon a fixed hotspot model (Engebretson et al., 1985)) and, thus, was under the high productivity equatorial zone during this interval, resulting in high sedimentation rates. As the Pacific plate drifted north over time the sites moved out of the high productivity zone causing the Paleogene carbonate sediments to be overlain by a relatively thin Neogene siliceous red clay sequence, a condition that favours enhanced foraminiferal preservation by reducing the infiltration of corrosive waters into the underlying sediments. This thin Neogene cover also resulted in relatively shallow burial depths for Eocene and Oligocene carbonate sediments (Table 2-1). The sites are likely to reflect a global deep water signal due to their palaeowater depths (Site 1218, 3700 m, Site 1219, 4200 m and Site 1220 4300 m) and central oceanic location (being distal from continental land masses reducing terrestrial influences).

Two standard coring systems were used during Leg 199: the advanced piston corer (APC) was used for ODP Site 1219 and ODP Site 1220 for the interval of interest, and the extended core barrel (XCB) for Site 1218 for the interval of interest. This led to a good recovery (on average between 80-100%) with minimal coring disturbance. This means it was possible to correlate physical property records between sites and thus generate a well defined stratigraphy that could be correlated between sites (Pälike et al., 2005; Pälike et al., 2006). This has allowed the age model to be well constrained for all three sites.

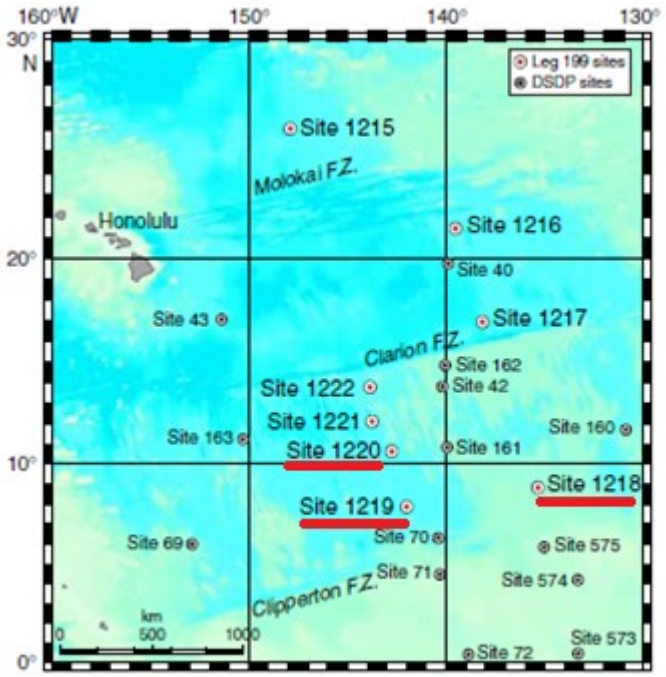

Figure 2-2 Site map of the Equatorial Pacific region including ODP Leg 199 Sites used in this study (underlined) (Shipboard Scientific Party 2002).

Across the Eocene-Oligocene boundary there is a rapid, 1.2 km deepening of the calcite compensation depth (CCD) (van Andel 1975). This is reflected in Site 1218 % carbonate records which increase from ~3% to ~90% across the EOT. Site 1218 was approximately at the same depth as the CCD prior to the EOT, and Site 1219 and Site 1220 were below the CCD prior to the deepening and then above the CCD after (Figure 2-3). These sites therefore provide an opportunity to study a significant change in saturation state due to CCD deepening across a palaeodepth transect.

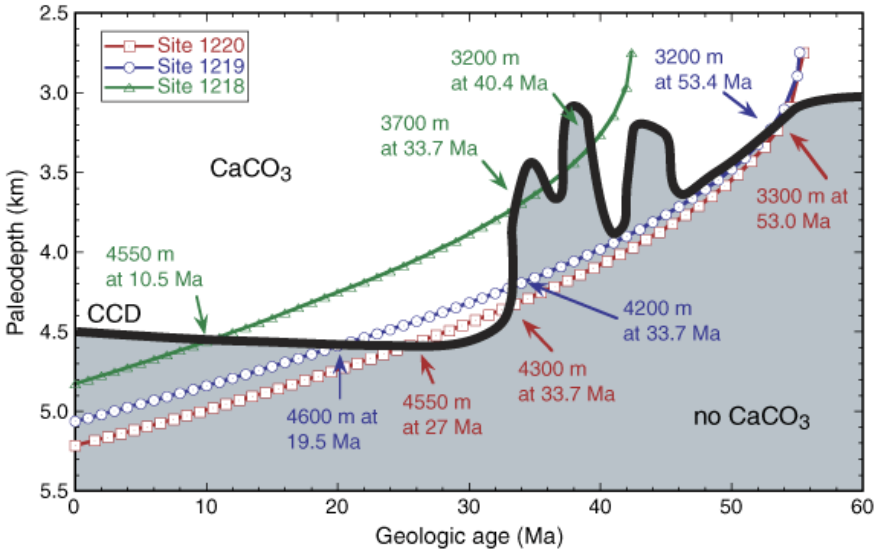

Figure 2-3 Subsidence histories for sites used in this study (green, blue and red lines) and estimated CCD depth (solid black line) (Leg 199 Shipboard Scientific Party, 2002).

ODP Holes 1218A/B (8°53.378'N, 135°21.999'W)

The lithology of ODP Site 1218 over the interval studied evolved from radiolarite ooze prior to the Eocene/Oligocene transition (EOT) to nannofossil ooze with decreasing diatom content (Shipboard Scientific Party, 2002). This abrupt change in lithology is coincident with “Step 1” of the transition, and reflects the deepening of the CCD (Shipboard Scientific Party, 2002). The EOT interval contains well-preserved benthic foraminifers but planktonic foraminifera are scarce and those preserved show the effects of dissolution.

As a detailed Mg/Ca and Li/Ca record has previously been generated for this site (Lear et al., 2004 and Lear and Rosenthal, 2006), samples from this site were taken at a lower resolution (every 50cm) than ODP Site 1219 and Site ODP 1220. Samples run from core 23 section 6 to core 24 section 7 for Hole 1218A and from core 23 section 1 to core 23 section 7 for Hole 1218B spanning an age range of 32.7Ma to 35.3 Ma. 36 samples were analysed.

ODP Hole 1219A (7°48.010'N, 142° 0.939'W)

As with Site 1218 the lithology of ODP Site 1219 evolved from radiolarite ooze prior to the EOT to nannofossil ooze with decreasing diatom content. However at ODP Site 1219 this change is coincident with “Step 2” of the transition indicating that the site remained below the CCD until this time. Therefore, geochemical proxy records in benthic foraminifera across the first step of the EOT cannot be generated for ODP Site 1219 as there are none in the sediment to analyse.

The sampling resolution for this site was every 2cm. The samples run from Hole 1219A core 17, section 2, interval 40-42cm (33.6 Ma) to core 17, section 2, interval 88-90cm (33.7 Ma). The total number of samples analysed was 25.

ODP Hole 1220B (10°10.600'N, 142°45.503'W)

The lithology of ODP Site 1220 for the interval of interest is similar to that of ODP Site 1219. As with ODP Site 1219 the sampling resolution for this site was every 2cm. The samples run from Hole 1220B core 4, section 6, interval 26-28cm (33.5 Ma) to Hole 1220B core 4, section 6, interval 90-92cm (33.7 Ma). The total number of samples analysed was 33.

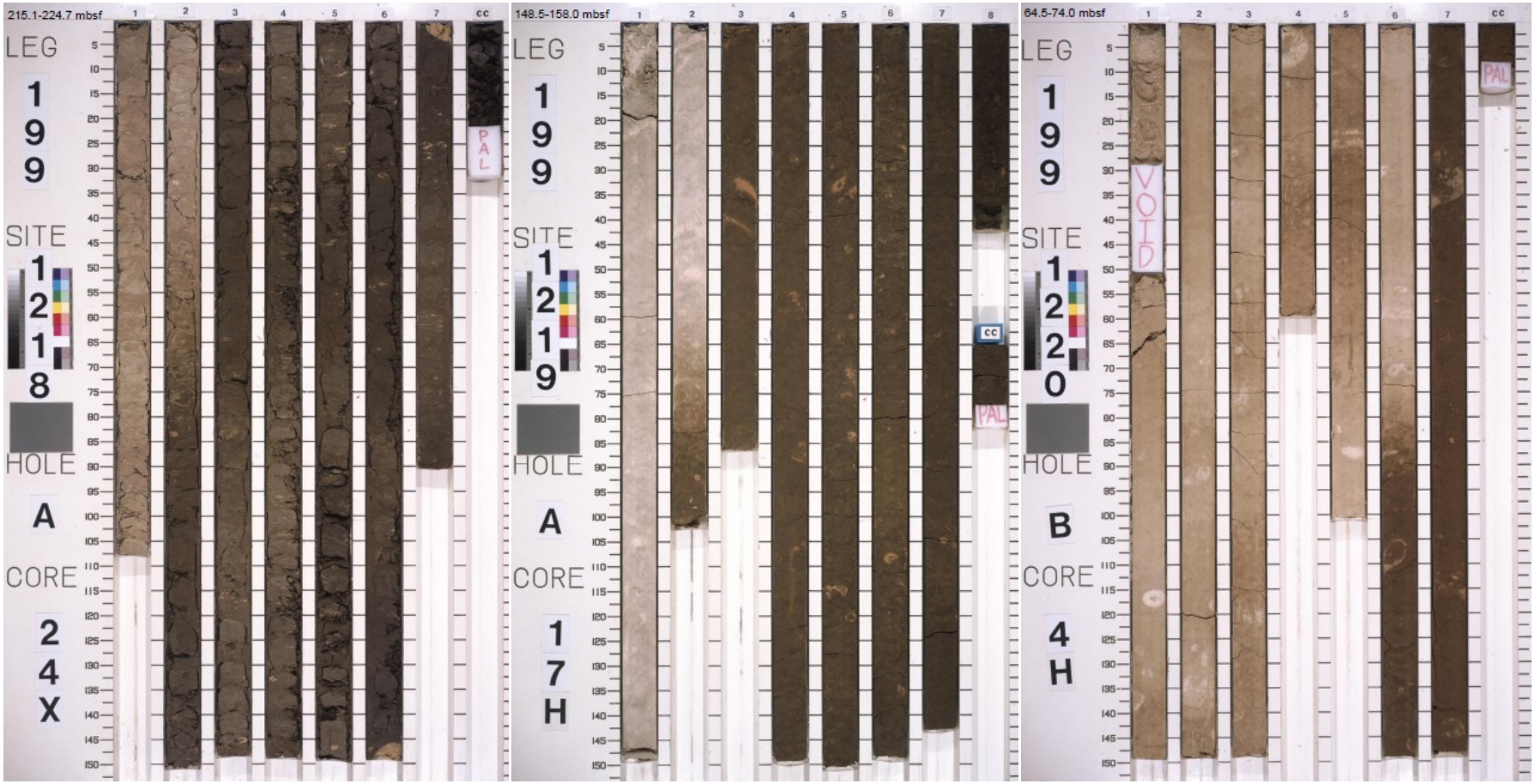

Figure 2-4 Core images from the interval used in this study from Leg 199, the change in colour records a shift from opal rich to calcium carbonate rich sedimentation (ODP Leg 199 Initial Reports, Shipboard Scientific Party, 2002b).

2.1.2 Oligocene-Miocene Boundary sites

ODP Leg 154 drilled on Ceara Rise which is located in the western equatorial Atlantic Ocean off the coast of South America (ODP Leg 154 Shipboard Scientific Party, 1995). This stretch of continental slope provides a depth transect through tropical Atlantic waters. ODP Site 929 was chosen because it was the deepest site drilled (water depth 4367m) and thus would provide the greatest contrast with shallower ODP Site 926 (water depth 3598m). Today, ODP Site 929 is positioned about 200 metres above the lysocline, within the mixing zone between North Atlantic Deep Water (NADW) and Antarctic Bottom Water (AABW) (ODP Leg 154 Shipboard Scientific Party, 1995). Its depositional history therefore should be very sensitive to changes in deep-water circulation and alkalinity. Shallower ODP Site 926 is bathed in NADW therefore any changes in water mass influence between these two sites should be seen in differences between benthic geochemical proxies. Another advantage of ODP Leg 154 sediments is their well developed cyclicity reflected in the lithological data (Wheedon et al., 1997) which has allowed the construction of an orbital age model.

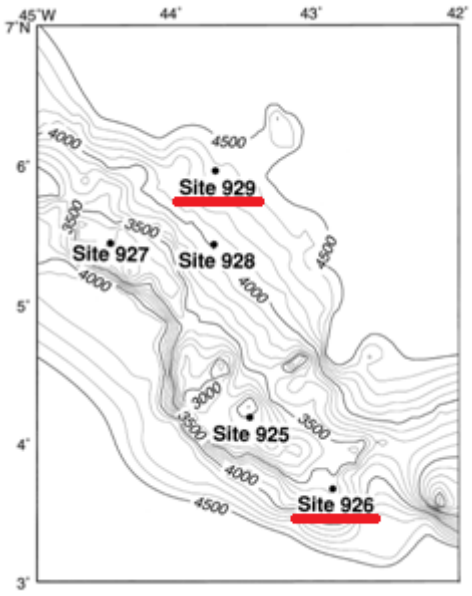

Figure 2-5 ODP Leg 154 Sites including those used in this study (underlined) from Curry et al. (1995).

ODP Hole 926B (3°43.148'N, 42°54.504'W)

The lithology of Hole 926B for the section sampled is described as clayey foraminiferal/nannofossil chalk with good preservation of benthic foraminifera across the study interval (ODP Leg 154 Shipboard Scientific Party, 1995). The sampling resolution for this site was approximately one sample every 10cm. The samples run from core 50, section 1, (22.8 Ma) to core 51, section 6 (23.6 Ma). The total number of samples analysed was 136. The interval of interest for this hole was drilled using XRB.

ODP Hole 929A (5°58.573'N, 43°44.394'W)

The lithology of Hole 929A over the sampled depth is very similar to that of 926B. The sampling resolution for this site was approximately one sample every 10cm. The samples run from core 34, section 4 (22.6 Ma) to core 36, section 1, (23.6 Ma). The total number of samples analysed was 157. The interval of interest for this hole was drilled using XRB.

2.1.3 Middle Miocene Climate Transition sites

ODP Sites 803 and 806 were drilled during ODP Leg 130 on the north eastern margin of the Ontong Java Plateau in the western equatorial Pacific. The geology and equatorial location of the Ontong Java Plateau through much of the Neogene has led to the accumulation/preservation of an extensive sequence of Miocene pelagic carbonate sediments (>1km in thickness) across the structure which is emplaced several thousand metres above the surrounding sea floor. The structure is a large igneous province. The sediments overlying the structure are undeformed in the central part of the plateau, as indicated by seismic stratigraphy and so are well suited to paleoclimate studies (ODP Leg 130, Shipboard Scientific Party, 1991). The two sites used here (ODP Sites 803 and 806) were chosen because they represent Miocene deposition at different water depths and thus likely experienced different degrees of carbonate saturation. The sites palaeowater depths have been estimated at 16 Ma as ~3550 m for ODP Site 803 and 2800 m for ODP Site 806 (Cramer et al., 2009).

As with Leg 199 two standard coring systems were used during Leg 130: both APC and XCB were used for the Site 803 study interval and XCB only for Site 806 study interval. Recovery for the whole sites was fair (76% for Hole 803D and 89% for Hole 806B.).

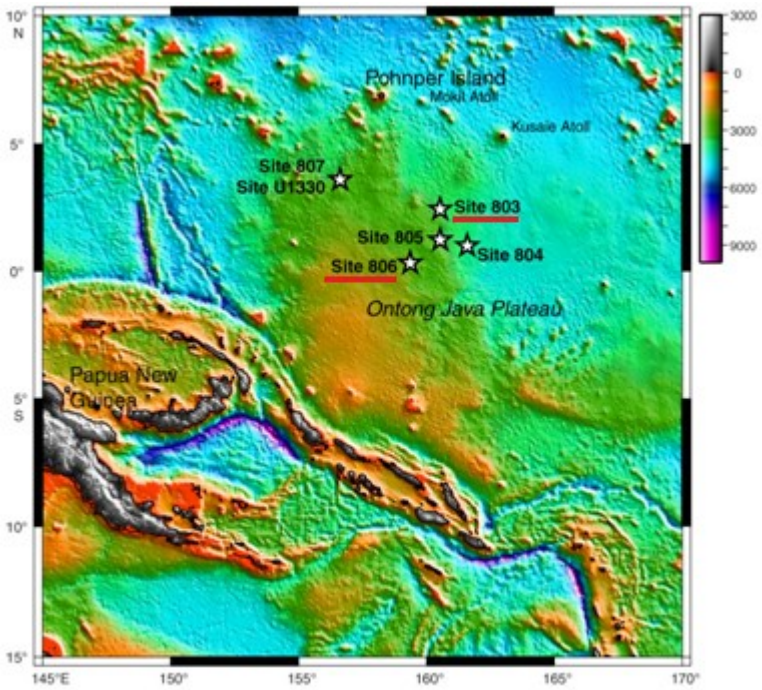

Figure 2-6 Site map of the Ontong Java Plateau region including sites used in this study (underlined).

ODP Hole 803D (2°25.98'N, 160°32.46'E)

Situated on the north eastern edge of the Ontong Java Plateau, ODP Site 803 is the deeper of the two western equatorial Pacific sites (modern water depth = 3412 m) and is approximately at the same depth as the modern lysocline (~3400m). ODP Site 803 is overlain by Pacific Bottom Water. The lithology of the interval used in this study is initially nannofossil ooze but transitions downwards into nannofossil chalk (Shipboard Scientific Party, 1991). The sampling resolution for this site was approximately 1 sample every 3m.

ODP Hole 806B (0°l9.11 'N, 159°21.69'E)

ODP Site 806 is situated on top of the Plateau in shallower water (modern water depth = 2520 m) and is presently bathed in Pacific Deep Water well above the lysocline (~3400 m). The sampling resolution for this site was approximately 1 sample every 5m. The lithology of the interval used in this study is initially foraminiferal nannofossil ooze but transitions downwards into foraminiferal nannofossil chalk (ODP Leg 130 Shipboard Scientific Party 1991). The description “foraminiferal nannofossil” indicates that there is a higher level of foraminifera at Site 806 than 803.

2.2 Age models

2.2.1 ODP Leg 199: Sites 1218, 1219, 1220

The age model used in this study for Leg 199 sites is the orbital chronology of Pälike et al. (2006a). The age model builds on a shipboard stratigraphy derived from physical property

records (bulk density, colour reflectance and magnetic susceptibility) collected during ODP Leg 199 using a multi-sensor track core scanner (ODP Leg 199; Shipboard Scientific Party, 2002). These data were used to generate an aligned and stacked revised composite depth scale between Sites 1218 and 1219 (Pälike et al., 2005). The detailed chronology was then generated by matching the benthic stable isotope data from ODP Site 1218 with the astronomical template of Lasker et al. (2004). This orbital integration has been shown to fit geological data better than previous solutions (Pälike and Shackleton, 2000). The Pälike et al. (2006a) age model data is stored within the Pangaea database: (doi.pangaea.de/10.1594/PANGAEA.547797). This thesis uses the version calibrated manually to the astronomical timescale to be consistent with Lear et al. (2004) and Coxall et al. (2005). Site 1219 is correlated to Site 1218 using the stacked records of lithologic proxy measurements (Pälike et al., 2005). The tie points between these two sites can be found in Table 2 of Pälike et al. (2005). Tie points between Sites 1218 and 1220 were produced using GRAPE (Gamma ray attenuation porosity evaluator) bulk density records and magnetic susceptibility data. However this correlation results in an apparent temporal offset in the bulk isotope and $CaCO_3$ data between ODP Site 1220 and ODP Sites 1218/1219 at the critical Step 2 region. To look in detail at this small window of time additional tie points were required. As bulk oxygen isotope data are less likely to be subject to regional variability this was used in “Analyseries” (Paillard et al., 1996) to produce two tie points across the studied interval. The new age model improves correlation in the record beyond the area of interest indicating that this new correlation is more appropriate and is discussed further in chapter 3). These highly detailed age models suggest average sedimentation rates of 8.01, 5.65 and 3.24 m/m.y for Sites 1218, 1219 and 1220 respectively, across the time intervals studied.

2.2.2 ODP Leg 154: Sites 926/929

The age model used for the Leg 154 sites is the orbital chronology of Pälike et al. (2006b) which is based upon cyclic variability in benthic foraminiferal stable isotope and sediment percent coarse fraction data.

The data sets used for the ODP Site 926 age model are available in the NOAA database; (http://www.ncdc.noaa.gov/oa/ncdc.html), ODP Site 929 data were received by personal communication from H. Pälike. The latter are an extension of the Pälike and Shackleton (2004) time series which involved adjustment of a previously produced astronomically tuned age model based on lithological characteristics (Shackleton et al., 1999) to the orbital solution of Laskar et al. (2004) (as with the Leg 199 age model). This detailed age model suggests average sedimentation rates of 16.45 m/m.y. for Hole 929A and 25.96 m/m.y. for Hole 926B across the time intervals studied.

2.2.3 ODP Leg 130, Holes 803D and 806B

Hole 806B ages were calculated using the biostratigraphic age model of Lear et al. (2003) which is based on nannofossil, radiolarian and planktonic foraminiferal biostratigraphical events within the ODP Leg 130 cores. Hole 803D ages were generated using the same method in this study. Using benthic foraminiferal $\delta^{13}C$ as a tuning target, the Hole 806B and 803D ages were then adjusted to the equivalent middle Miocene record from ODP Site 761, by adding 500 kyr. This greatly improved the site to site correlations.

2.3 Sample preparation

Once the samples were received from IODP repositories they were weighed, placed in glass jars and dried overnight in the oven at 40˚C. Samples were covered in 15 MΩ deionised water and the samples were gently disaggregated by automatic shaking for approximately 48 hours. The disaggregated samples were washed through a 63 µm sieve using 15 MΩ deionised water. Samples that still contained lithified fragments after this step were placed in the oven overnight and then rewashed the following day. Once the samples were completely disaggregated they were dried in the oven at 40˚C prior to weighing and picking. The <63 µm size fraction was also retained, dried and weighed and the % coarse fraction was determined using the relative weights of both size fractions.

The benthic foraminifera required for analysis were then picked from the 150-355 µm size fraction (Holes 929A, 926B, 806B, 803D) or the 250-355 µm size fraction (Holes 1218A/B, 1219A, 1220B) depending on benthic abundance.

2.4 Species Selection

Trace metal analysis

For trace metal analysis the species primarily used was *Oridorsalis umbonatus*. This is a desirable species for trace metal analysis due to several factors;

(i) Wide geographic distribution (the species is present in all sites in this study).

(ii) Easily indentified, thus avoiding issues with separating morphotypes (Rae et al., 2010)

(iii) Relatively high absolute Mg/Ca, (effectively enabling smaller temperature signals to be reconstructed).

(iv) Long stratigraphic range (Cenozoic to Recent).

(v) Extant species so modern core-top calibrations can be applied (Lear et al., 2002).

The other species used in trace metal analysis was *Cibicidoides mundulus*. This species was chosen to supplement the data produced from *Oridorsalis umbonatus* as it was found during this study that *Oridorsalis umbonatus* B/Ca ratios are approximately four times lower than those of *Cibicidoides* species (Yu & Elderfield, 2007). In addition *Oridorsalis umbonatus* is shallow/semi infaunal whereas *Cibicidoides mundulus* is epifaunal, therefore *Cibicidoides mundulus* may be more sensitive to changes in bottom water saturation state. Like *Oridorsalis umbonatus, Cibicidoides mundulus* is an extant species with a long stratigraphic range (Oligocene – Recent) thus making core-top calibrations possible.

Stable Isotope analysis

For stable isotopes analyses either *Cibicidoides mundulus* or *Cibicidoides wuellerstorfi* were used. *Cibicidoides* species are commonly used for producing stable isotope records

as they have been shown to have consistent and predictable offsets from equilibrium values (e.g. Katz et al., 2003).

2.5 Stable isotope analysis

For each trace metal sample, a paired set of carbon and oxygen stable isotope measurements were made if these data had not previously been produced by other researchers.

2.5.1 Sample Cleaning

Between 4 and 12 specimens of the benthic foraminiferal species *Cibicidoides mundulus* were used from the 150 -250 μm size fraction for the stable isotope analysis. To remove contaminants and chamber infill, the samples were gently crushed between two glass plates to open all chambers. The visible contaminants were then removed using a fine paintbrush. The crushed samples were then transferred into a sample pot and a few drops of 3% hydrogen peroxide added to each sample to oxidise any residual organic carbon on the fragments. After 30 minutes a drop of methanol was added and the samples were ultrasonicated for a few seconds. Immediately following this all excess solution was drawn off the samples. The samples were then dried in the oven at 40ºC before being transferred to glass vials for analysis.

2.5.2 Sample analysis

The carbon dioxide gas produced by sample dissolution (using phosphoric acid) was analysed to determine the $\delta^{18}O$ and $\delta^{13}C$ values. The samples were analysed on a ThermoFinnigan MAT252 with online sample preparation using an automated Kiel III carbonate device at Cardiff University that acidifies samples in individual reaction vials. Stable isotope results were calibrated to the PDB scale by international standard NBS-19. Long term analytical error is based on repeat analysis of standard NBS-19 is ± 0.08 ‰ for $\delta^{18}O$ and ± 0.05 ‰ for $\delta^{13}C$ (2σ).

2.6 Trace metal analysis

2.6.1 Sample cleaning

A minimum of 3 specimens of *Oridorsalis umbonatus/Cibicidoides mundulus* were gently crushed between two glass plates and visible contaminants were removed using a fine paintbrush. The fragments then underwent a modified version of the cleaning procedure first described by Boyle and Keigwin (1985/1986). This includes; (i) the removal of clay by ultrasonication of the fragments in both 18.2 MΩ deionised water and methanol, (ii) a reductive step to remove any metal oxides using a solution of hydrous hydrazine and citric acid in ammonia, (iii) an oxidative step using a solution of hydrogen peroxide in sodium hydroxide to remove any remaining organic matter, and (iv) an acid leach step using

Optima pure nitric acid. Between the mechanical clay removal step and the reductive step the samples were examined under a binocular microscope to remove any obvious non carbonate particles, as described by Barker et al (2003). Full details of the method and reagents used are provided in Appendix 8.2.1.

2.6.2 Sample dissolution and analysis

120 µl of 0.065 M Optima nitric acid was added to each cleaned sample. The samples were then agitated using a vortex mixer and centrifuged to facilitate dissolution. Once dissolved, 10 µm aliquot and 100 µl aliquots were removed from each solution and placed in new acid cleaned tubes. This provided subsamples for two analyses, the first to determine the calcium concentration ([Ca]) and the second to determine the trace metal ratios. On the day of the calcium analysis 190 µl of 0.5 M Optima nitric acid was added to the 10 µl of solution. These aliquots were then analysed on a Thermo Element XR Inductively Coupled Plasma Mass Spectrometer (ICP-MS) at Cardiff University. The [Ca] of each of the aliquots was then determined by comparing drift- and blank corrected intensity data (counts per second using the Ca43 isotope) for the samples to that of an analytical standard with a Ca concentration of 80 ppm. Samples were analysed in blocks of five, separated by a blank and a standard (Figure 2-7).

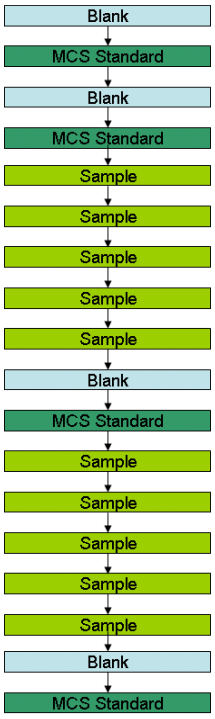

Figure 2-7 Schematic representation of typical analysis sequence for determining Ca concentration in dissolved foraminiferal samples. MCS is the "Multi-Element Cardiff Standard" used during trace metal analysis.

On the day of analysis for trace metal ratios 250 µl of 0.5 M Optima nitric acid was added to the 100 µl of sample solution. This dilution was performed on the day of analysis in order to minimise exchange of metals from or into the micro centrifuge tubes. The samples were then analysed on the Thermo Element XR HR-ICP-MS. Two independent consistency standards (CS1 and CS2) (Table 2-2) were analysed against the analytical standard (MCS) at the start and end of each run in order to calculate long-term accuracy and precision. Acid blanks (0.5M HNO_3) were analysed every 2 samples. Each sample analysis was followed by analysis of a standard with the same [Ca] as the sample to avoid matrix effects (see section 2.3.5) (Figure 2-8). This method is preferable to applying a single matrix effect correction to all data in a run (e.g. Lear et al., 2002), as matrix effects appear to vary slightly throughout a run. A more efficient method of analysis would be to dilute all samples down to a common concentration, but this was not feasible with the small sample sizes used in generating these benthic foraminiferal trace metal records.

Count data were recorded for ^{6}Li, ^{7}Li, ^{11}B, ^{24}Mg, ^{25}Mg, ^{27}Al, ^{43}Ca, ^{46}Ca, ^{48}Ca, ^{47}Ti, ^{55}Mn, ^{87}Sr, ^{88}Sr, ^{111}Cd, ^{138}Ba, ^{146} Nd and ^{238}U. The counts for each isotope were 'blank corrected' using the previous blank in the sequence. Intensity ratios were then calculated between Ca^{43} and the other elements. The blank corrected intensity isotope ratios were then used to calculate elemental ratios using each sample's matrix matched standard.

Trace metal ratios	units	CS1	CS2	MCS
Li/Ca	µmol/mol	5.77	46.2	11.1
B/Ca	µmol/mol	13.4	222	182
Mg/Ca	mmol/mol	1.21	7.26	2.33
Al/Ca	µmol/mol	2.97	89.1	41.22
Mn/Ca	µmol/mol	29.2	204	97.7
Sr/Ca	mmol/mol	0.46	1.74	1.41
Cd/Ca	µmol/mol	0.02	0.36	0.044
Nd/Ca	µmol/mol	0.11	2.22	1.06
U/Ca	nmol/mol	4.04	26.9	9.24
Ti/Ca	µmol/mol	0.84	5.02	1.00
Fe/Ca	µmol/mol	57.4	1005	129
Zn/Ca	µmol/mol	0.25	24.5	1.9

Table 2-2 Known trace metal ratio values for the consistency standards (CS1 and CS2) and the Multi-element Cardiff standard (MCS) used during trace metal analysis by ICP-MS. The neat standards are approximately 1000ppm [Ca].

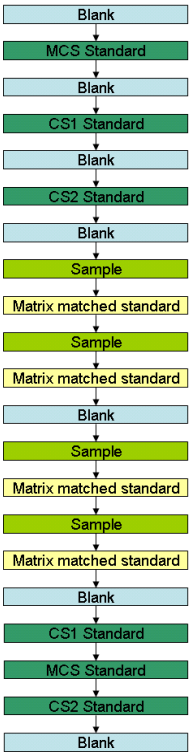

Figure 2-8 Schematic representation of typical analysis sequence for determining Trace metal/Ca ratios in dissolved foraminiferal samples. CS1 and CS2 are the two different consistency standards used at the beginning and end of a run, MCS is the "Multi-element" Cardiff Standard.

2.6.3 ICP-MS

This section briefly outlines how the Thermo Element Sector Field ICP-MS works. Dissolved samples are fed via capillary to a nebuliser which generates a fine spray aerosol. This is then filtered through a spray chamber before being directed into the plasma torch where high temperatures (up to 8000K) atomise and ionise the sample. A pressure gradient draws ions away from the plasma which is at atmospheric pressure, through the interface region (10^{-4}mbars) and into the mass spectrometer (10^{-7}mbars). Beyond the interface, ions are electrostatically focused and passed through a magnetic field. The magnetic field disperses the ions according to their mass and charge. Once deflected ions enter an electrostatic field where they are further focused according to their energy. This combination of magnetic and electric fields is known as a "double focusing" mass analyser. Upon leaving the mass analyser, ions enter the detection system. In counting or analogue detection modes used for the samples in this study, ions collide with a dynode, generating an electrical signal which may be measured as discrete pulses (counting mode) or charge (analog mode). In faraday mode the ion beam passes directly into a faraday cup from which accumulated charge is measured. Pulses and charges are converted into intensities in counts per second (cps) for each isotope analysed. Isotope

intensities are then ratioed to a gravimetric standard to yield quantitative results. Long term precision and accuracy determined by analysing CS1 and CS2 are found in Table 2-3.

Trace metal ratio	CS1 Long term precision (RSD)	CS1 Long term accuracy (%)
Li/Ca	8.0	4.7
B/Ca	9.7	8.4
Mg/Ca	0.7	3.2
Al/Ca	20.9	25.2
Mn/Ca	2.8	5.1
Sr/Ca	1.6	1.2
Cd/Ca	7.5	6.3
Nd/Ca	4.7	13.1
U/Ca	9.9	7.3
Ti/Ca	6.9	8.0
Fe/Ca	3.2	4.5
Trace metal ratio	**CS2 Long term precision (RSD)**	**CS2 Long term accuracy (%)**
Li/Ca	6.0	4.6
B/Ca	6.4	6.6
Mg/Ca	0.9	1.1
Al/Ca	31.4	11.1
Mn/Ca	1.8	1.1
Sr/Ca	1.4	0.9
Cd/Ca	8.3	8.7
Nd/Ca	3.0	2.6
U/Ca	9.9	7.8
Ti/Ca	6.1	24.8
Fe/Ca	3.1	9.4

Table 2-3 Long term precision and accuracy for standards CS1 and CS2 measured by ICP-MS at Cardiff University.

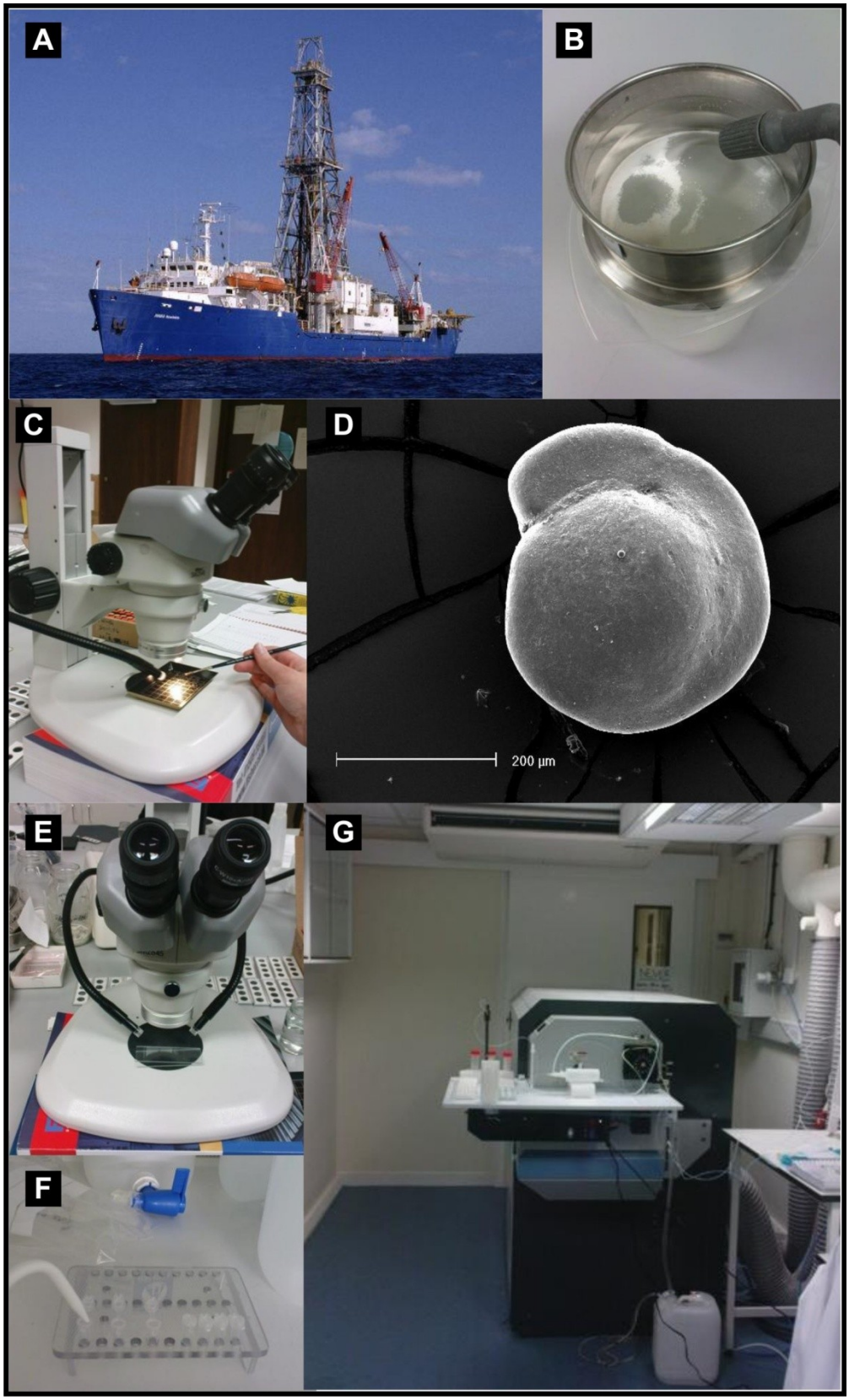

Figure 2-9 From drilling to data, (A) *JOIDES Resolution* drill ship used to collect all samples, (B) Washing material through 63µm sieve, (C) Picking benthics using a light microscope (D) *Oridorsalis umbonatus* (E) Crushing using glass slides, (F) Chemical cleaning of samples (G) analysis by ICP-MS.

2.6.4 Precision/accuracy and detection limits

Good laboratory practice dictates that precision and accuracy need to be known in order to establish the error within the data produced. The Cardiff University Palaeoceanography and Climate Systems (PACS) group determines long-term accuracy and precision by analysing two consistency standards every day of analysis. However due to low benthic foraminiferal abundance, many of the samples analysed in this study were less concentrated than the consistency standards. Therefore an experiment was performed in order to determine the relationship between precision, accuracy and sample size. CS1 was analysed at varying concentrations ([Ca] = 0.25, 0.5, 0.75, 1, 1.33, 2 and 4 mMol). A corresponding MCS standard was analysed immediately following each CS1. This was then repeated 6 times and the precision and accuracies were calculated using the 6 replicates.

Discussion of results

(i) Mg/Ca: At the concentrations measured in this study variations in [Mg] do not significantly affect the precision or accuracy of the analyses. (Figure 2-10). This experiment demonstrates that the errors associated with Mg/Ca analysis are similar across a range of sample concentrations between 0.0012 mMol [Mg] and 0.0048 mMol [Mg] indicating data from smaller samples are as reliable as that from larger samples. As all the samples analysed in this research are greater than the smallest [Mg] measured in this study and the Mg blank was stable over the course of the study the long term precision (0.7%) and accuracy (3.2%) determined in the laboratory by measurement of two consistency standards at the start and end of each run is applicable to all the Mg/Ca data in this study.

(ii) Li/Ca: The precisions of the 6 replicates analysed at [Li] = 1.42×10^{-3} and 2.83×10^{-3} µMol are significantly worse (14.38 and 4.31%) compared to standards analysed at higher concentrations (RSD values of approximately 1%). Therefore if a precision of better than 5% is required, the samples need to contain at least 2.83×10^{-3} µMol of lithium under these operating conditions. The Li/Ca RSD values are about twice as high as those for Mg/Ca. This is due to the fact that the magnesium is much more abundant in the standard (Mg/Ca = 1.16 mmol/mol, Li/Ca = 5.66 µmol/mol) as is also the case in benthic foraminiferal calcite. The accuracy of the Li/Ca analyses at [Li] ≥ 2.83×10^{-3} µmol was better than 8%. This is with the exclusion of an outlier at 0.0113 µMol [Li] (due to contamination of the MCS standard as indicated by unusually high aluminium concentration). If this standard was treated as a sample it would be removed in the routine data screening process (see section 2.5.7). There was no trend between accuracy and [Li] indicating that as long as samples analysed have a concentration of 2.83×10^{-3} µMol or above better than 8% accuracy should be achieved. At lower

concentrations the sample intensities are less than 5 x the blank values and thus would be discarded as part of the laboratory's routine screening process.

(iii) B/Ca: Of all the elements analysed B/Ca shows the most consistent trend between increasing standard concentration and improved precision and accuracy. The B/Ca data indicate that to get accuracy of ~± 9% then samples need to have a boron concentration of at least 0.052 µMol under these operating conditions. To determine the threshold concentration required to achieve 5% accuracy this test would need to be rerun using higher concentration standards. However since this experiment was performed, the boron blank in the laboratory has been significantly reduced, and thus a better criteria for determining a threshold for obtaining reasonable accuracy would be concentration relative to blank.

Results

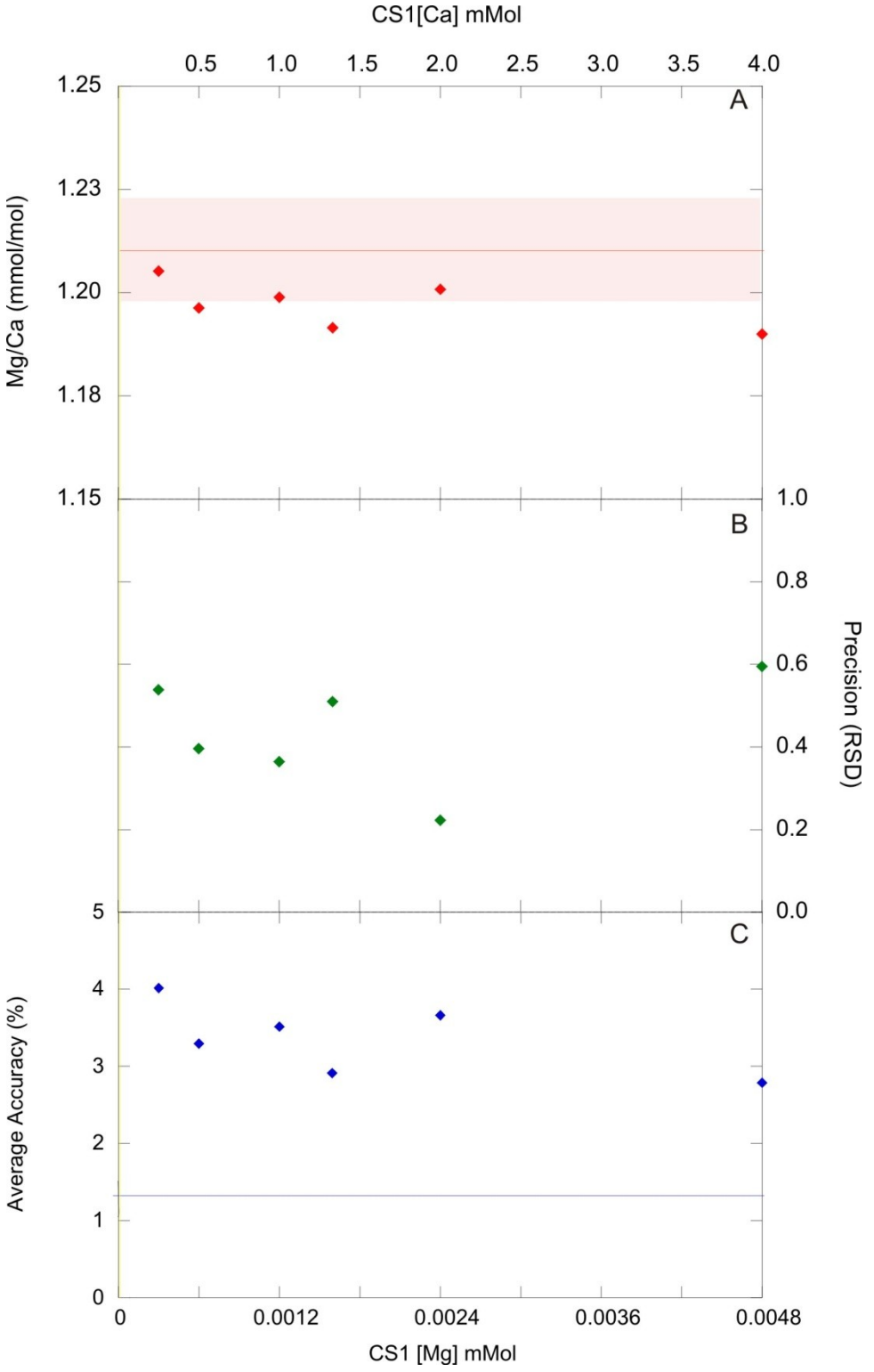

Figure 2-10 (A) Calculated average ratio (B) intra-run precision and (C) average accuracy of CS1 standard for Mg/Ca versus Ca and Mg concentration. The red line in panel A indicates the known standard ratio, with the shaded error indicating ± the long term accuracy based on replicate measurements. The blue line in panel C indicates the long term accuracy for the PACS laboratory and the yellow shaded area indicates the region between 0 and 5 times the magnesium concentration in the blank during this analysis.

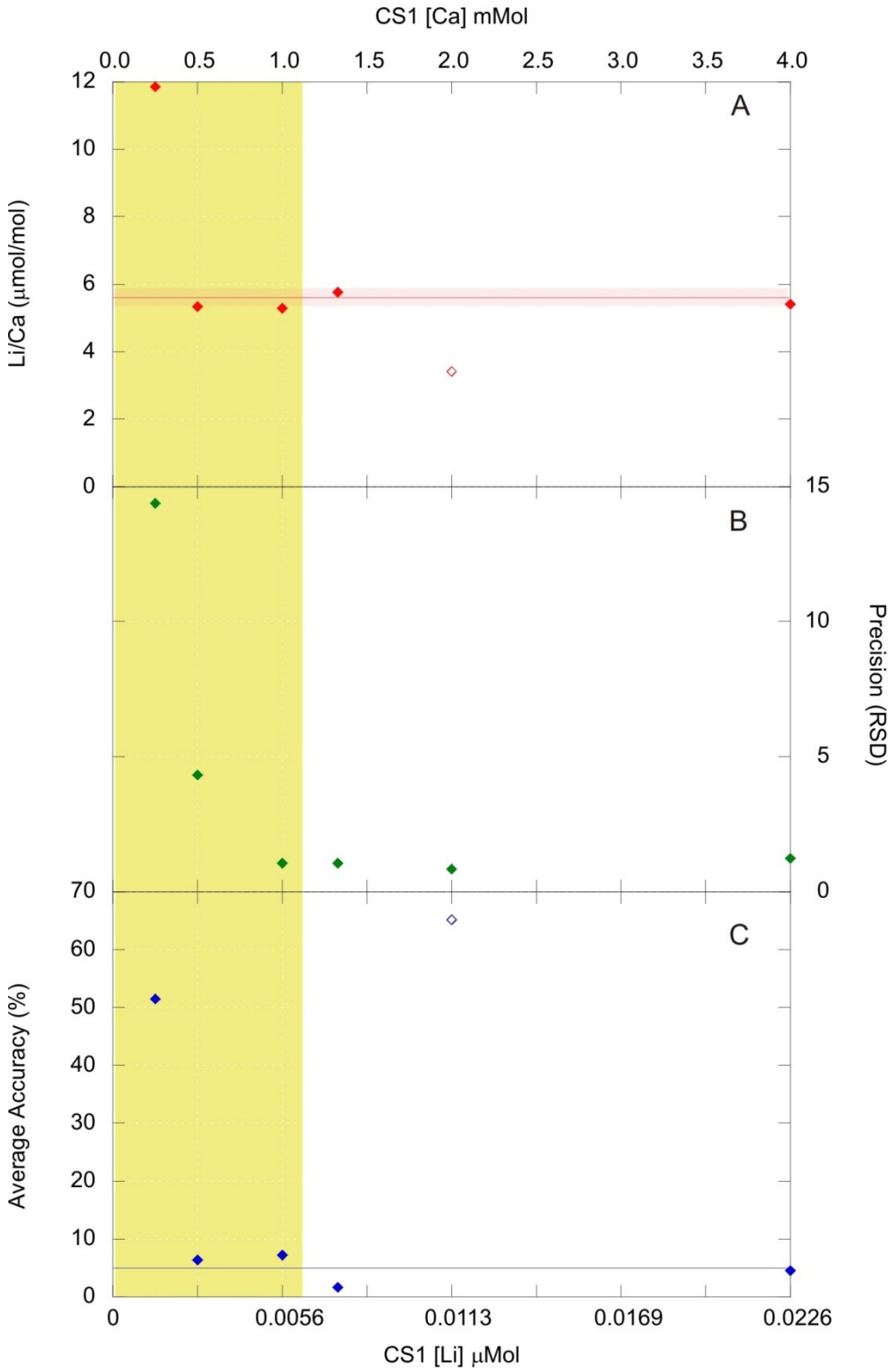

Figure 2-11 (A) Calculated average ratio (B) intra-run precision and (C) average accuracy of CS1 standard for Li/Ca versus Ca and Li concentration. The red line in panel A indicates the known standard ratio with the shaded error indicating ± the long accuracy based on replicate measurements.. The blue line in panel C indicates the long term accuracy for the PACS laboratory. and the yellow shaded area indicates the region between 0 and 5 times the lithium concentration in the blank during this analysis. The open symbols indicate a sample set which may have been contaminated. (see text for details).

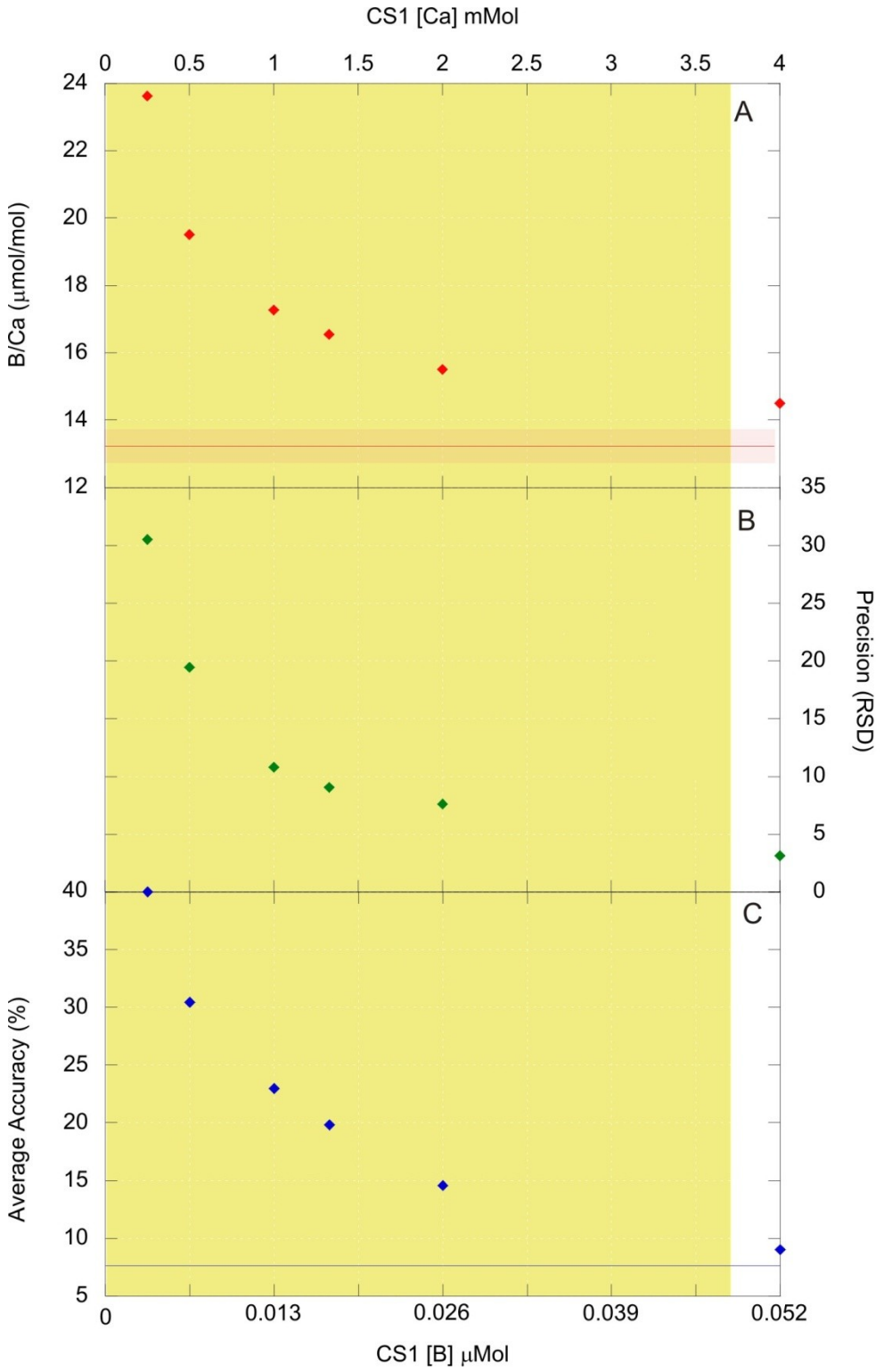

Figure 2-12 (A) Calculated average ratio (B) intra-run precision and (C) average accuracy of CS1 standard for B/Ca versus Ca and B concentration. The red line in panel A indicates the known standard ratio with the shaded error indicating ± the long term accuracy based on replicate measurements.. The blue line in panel C indicates the long term accuracy for the PACS laboratory. and the yellow shaded area indicates the region between 0 and 5 times the boron concentration in the blank during this analysis. The laboratory blank has significantly reduced since this experiment was performed.

Precision and accuracy relative to the blank

In order to accurately determine foraminifera trace metal/Ca values any component of the analyte signal from the acid in which the foraminifera are dissolved needs to be removed. This is achieved by analysing a vial blank every two samples and subtracting the blank's intensities (cps) from the samples and standard intensities (this is done automatically by the online system). If the blank is stable then the blank subtraction will be more accurate and thus the calculated ratios will be more accurate. If there is a large blank relative to the sample the sample will be more affected by noise in the blank signal. Part of the Cardiff University ICP-MS facility screening process is that any sample below 5 x the blank intensity is removed. As seen from Figure 2-10 magnesium has a very low blank relative to the analyte signal (standard or samples) and thus none are removed by this process. The relative standard deviation of the blank in this study for magnesium is also very low (0.0055%) demonstrating low variability. The lithium and boron blanks contribute a much higher proportion of the analysed standard (Figure 2-11 and Figure 2-12). Their relative standards deviations are also significantly higher (Table 2-4). The limit at which the analyte can be quantified is often taken as 10 times the standard deviation of the blank. However this value is not much higher than the blank itself in this study (Table 2-4) and returns a predicted precision and accuracy of >50% accuracy and better than 15% precision for lithium, and >40% accuracy and 40% precision for boron. This level of precision and accuracy is inadequate for the purpose of this study so in this thesis any samples less than 5 times the blank itself are removed (yellow shaded areas Figure 2-10, Figure 2-11 and Figure 2-12). Therefore the expected precision and accuracy for the data presented in this thesis using this method is better than 1.5% precision and 8% accuracy for Li/Ca and better than 3% precision and 9% accuracy for B/Ca.

Element	Average blank concentration (μmol)	10 times standard deviation of blank	Relative standard deviation of blank (%)
Mg	0.005837	3.24×10^{-6}	0.006
Li	0.00127	4.90×10^{-4}	3.858
B	0.00962	1.27×10^{-3}	13.20

Table 2-4 Blank concentrations, 10 x standard deviation and relative standard deviation (%) for the precision and accuracy study.

The graphs produced here (Figure 2-10, Figure 2-11 and Figure 2-12) serve as a useful guide for estimating errors on data spanning a range of trace metal concentrations. However it would be also be useful to know prior to analysis how many specimens are required in order to produce data to a required precision/accuracy. In order to do this several pieces of information are required.

(i) The level of precision and accuracy required.

(ii) The minimum abundance of the trace metal of interest expected in the foraminifera to be analysed.

(iii) Average weight of the individual foraminifera.

(iv) The volume of acid the samples are dissolved in.

(v) Blank composition on the day of analysis

Both the trace metal concentration and average weight of foraminiferal tests are quite variable. In addition, a significant proportion of calcite is lost during the cleaning process via fragmentation and dissolution [potentially up to 50% in planktonic foraminifera (Moffat-Sanchez, personal communication)]. Nevertheless, as an indication, a linear regression analysis of the ODP Leg 199 data generated during this study indicates that to achieve a <5% precision for *Oridorsalis umbonatus* B/Ca [i.e. sample [B] > 5 blank [B] (Figure 2-12)] requires ~8 benthic foraminifera from the 150-355 µm size fraction (Figure 2-13).

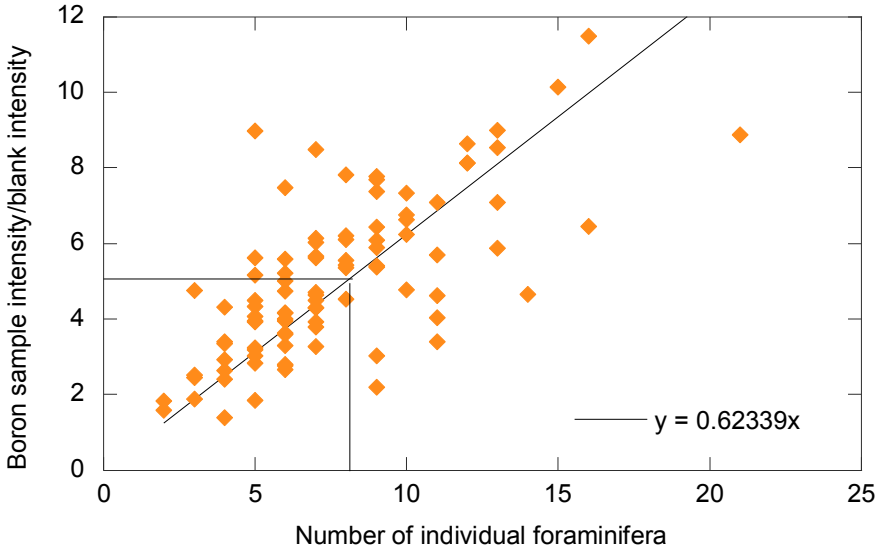

Figure 2-13 Number of individual *O. umbonatus* foraminifera used in analysis vs. boron sample intensity/blank intensity for ODP Leg 199 samples.

2.6.5 Matrix effects

Matrix effects cause inaccuracy in mass spectrometry by causing deviations of measured elemental ratios from the true ratios. Although the exact mechanism is not known, changes in the composition (matrix) of the sample affect the efficiency of ionisation or transmission of certain isotopes. Some ions are more sensitive to such matrix effects, one example being Mg^{2+} (Lear et al., 2002). Mg/Ca ratios measured by ICP-MS are dependent on the [Ca] of the sample with increasing [Ca] reducing apparent sensitivity to magnesium. This can prevent achieving a high level of accuracy using conventional calibration procedures. Therefore in this study individual standards with the same [Ca] are run after each sample to avoid any matrix effects.

Using individual matrix matched standards for each sample is a time-consuming and expensive procedure, effectively doubling the cost and analysis time. The goal of this study is to determine how necessary this procedure is by quantifying the variability in

intensity ratio with changing [Ca]. To quantify the variability the relationship between the raw intensity ratios and the calcium concentration of the matrix matched standards used to analyse the ODP Leg 199 samples is examined (Figure 2-14 - Figure 2-17).

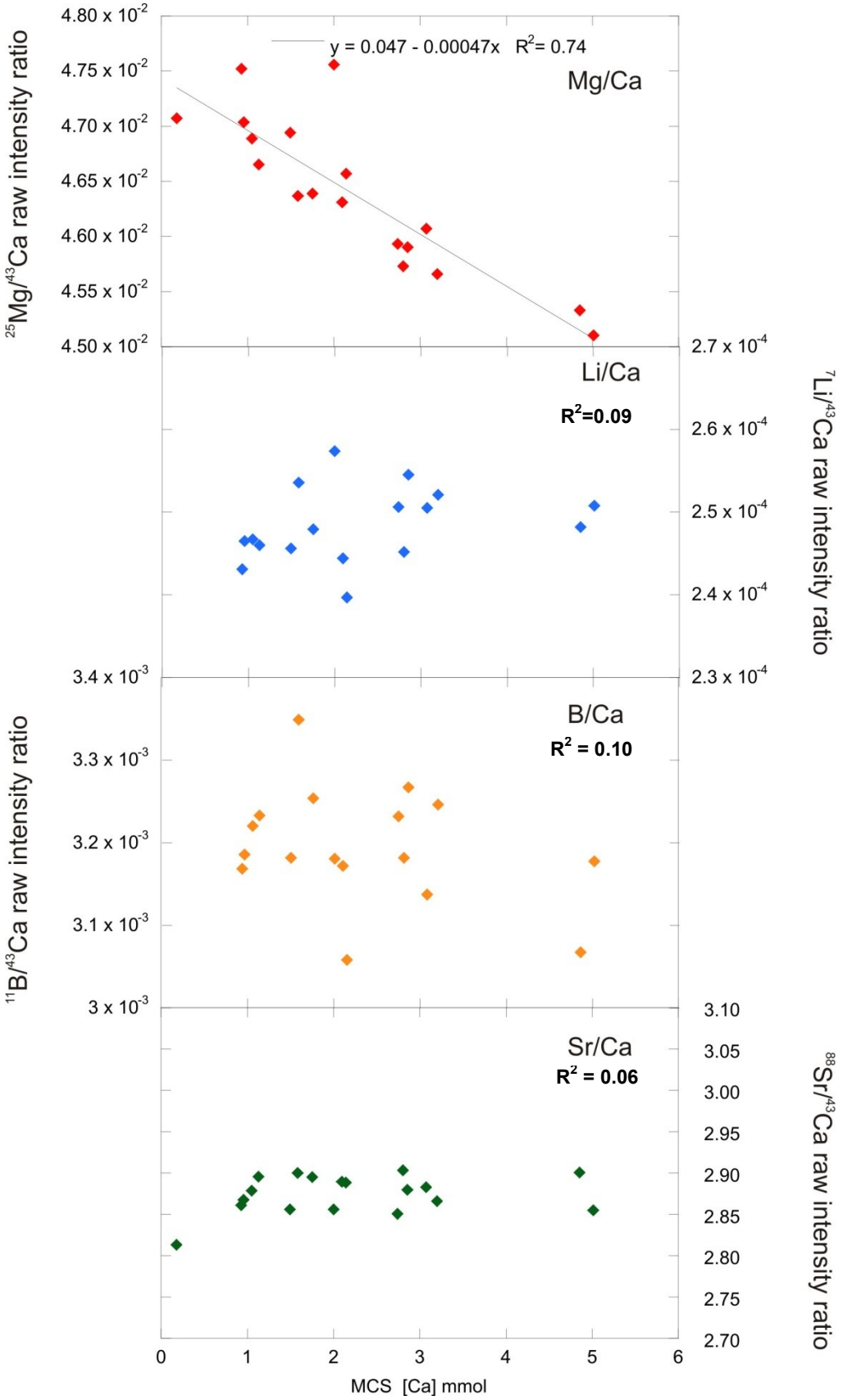

Figure 2-14 Relationship between raw isotope intensity ratio and calcium concentration for the matrix matched MCS standards used to analyse ODP Site 1218 samples. R^2 values are based on a linear fit equation.

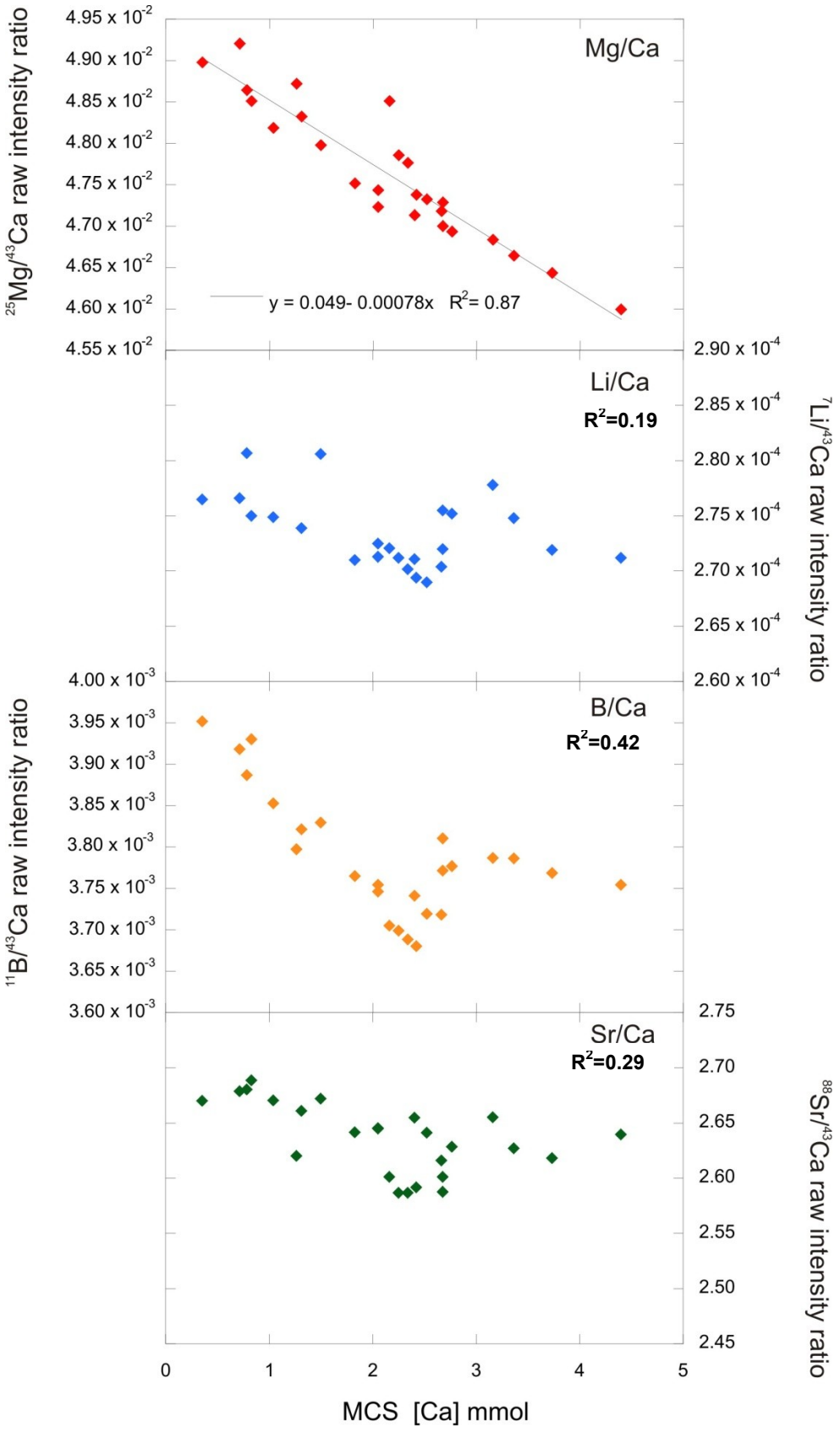

Figure 2-15 Relationship between raw isotope intensity ratio and calcium concentration for the matrix matched MCS standards used to analyse ODP Site 1219 samples. R^2 values are based on a linear fit equation.

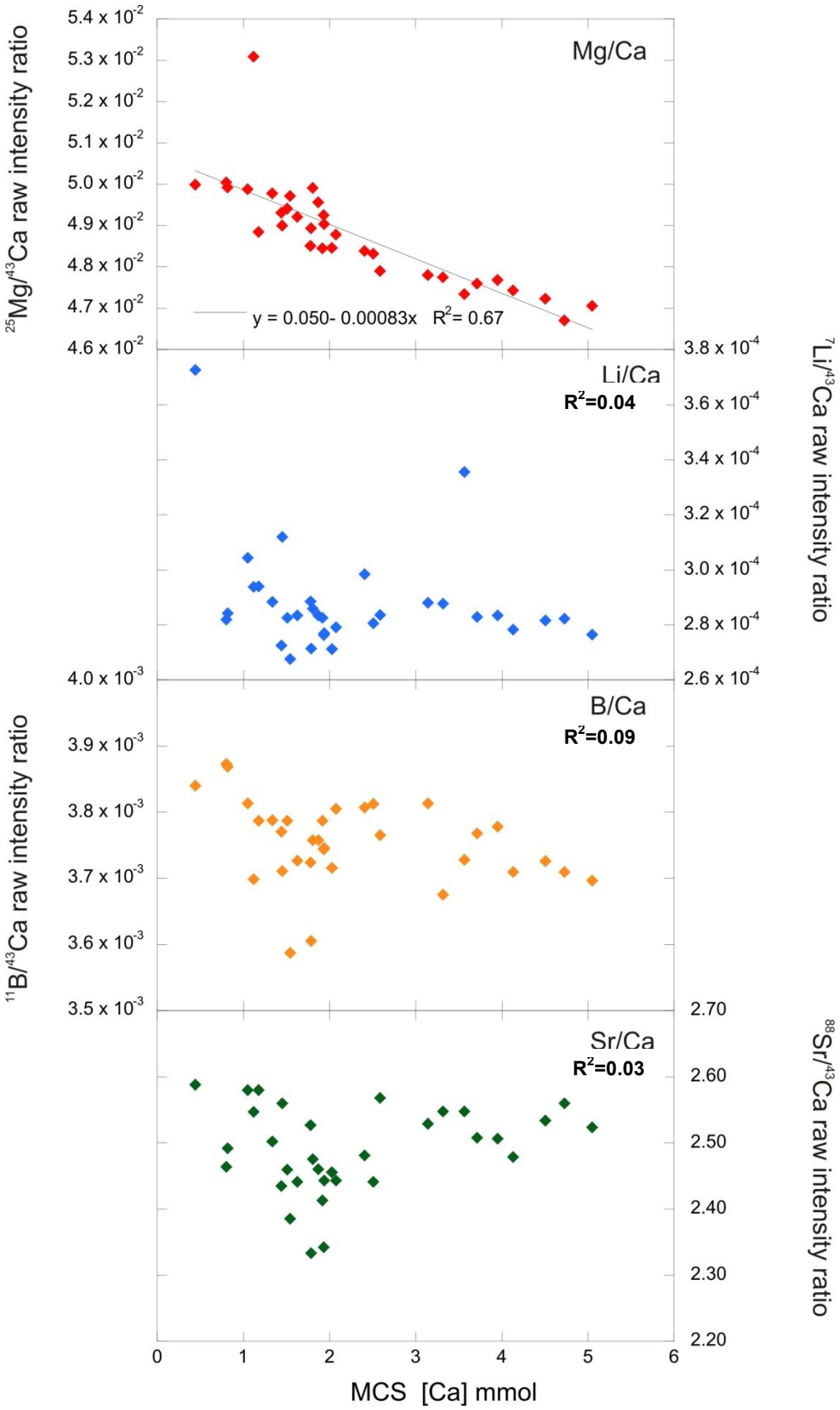

Figure 2-16 Relationship between raw isotope intensity ratio and calcium concentration for the matrix matched MCS standards used to analyse ODP Site 1220 samples. R^2 values are based on a linear fit equation.

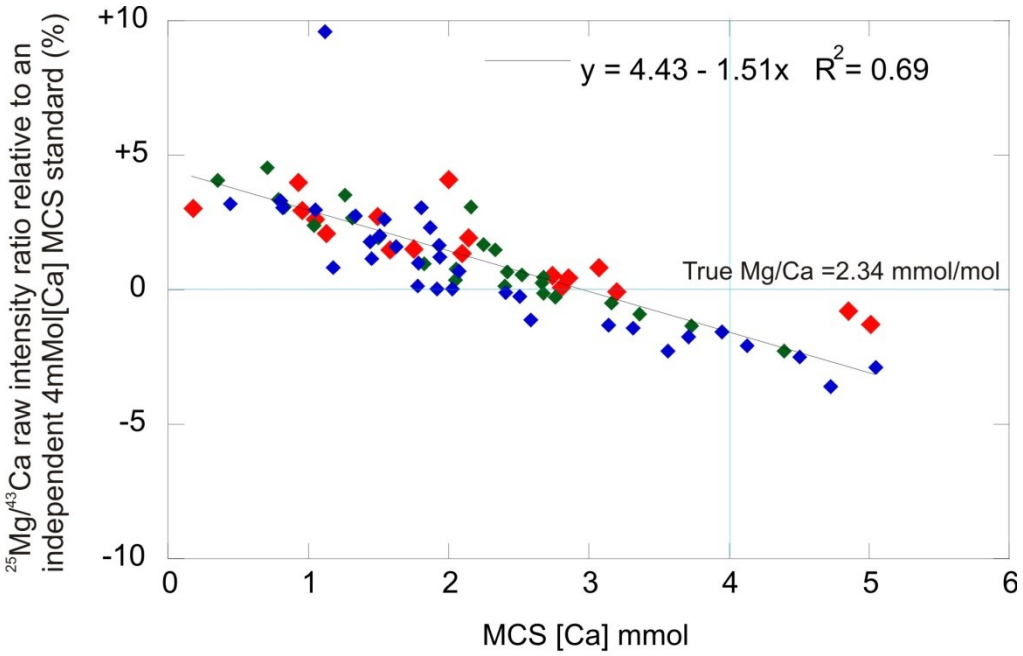

Figure 2-17 Relationship between raw isotope intensity ratio relative to a 4mmol [Ca] independent MCS raw intensity ratio and calcium concentration for the matrix matched MCS standards used to analyse Leg 199 Sites.

Discussion

Li/Ca, B/Ca and Sr/Ca matrix effects.

The data from these three trace metal ratios is relatively constant and do not indicate any particular trends with low R values for linear, exponential and polynomial trend fits.

Mg/Ca matrix effect.

The results of this study indicate that in these three runs the matrix effect is close to linear with an R^2 value of 0.69 for the three runs (Figure 2-14 - Figure 2-17). A polynomial fit also gives a similar fit of 0.69 which is suggestive that at calcium concentrations higher than those measured here the matrix effect is reduced. However sample size dictates that samples are rarely run over 4mmol [Ca]. The linear fit is in contrast to previous works (Lear et al., 2002; Burgess, unpublished PhD thesis) which suggest a greater rate of reduction in matrix effect at higher calcium concentrations. This suggests that the Mg/Ca matrix effect may not be constant through time. Over a range of between ~1 and 5 mMol calcium concentration the Mg/Ca matrix effect causes a bias in measured intensity ratios on the order of ± 5% (Figure 2-17). This potential error is significantly larger than the long-term analytical precision determined using matrix matched standards (CS1=3.2%, CS2 = 1.1%). Based on this study in order for the error associated with the Mg/Ca matrix effect to be less than the long-term precision for CS2 requires the matrix matched standard to be within 0.6 mMol calcium concentration of the standard. Therefore a more efficient means of analysing the foraminifera samples without compromising analytical accuracy or

precision is to group samples that are within 0.6 mMol [Ca] and analyse one matrix matched standard per group. However it may be advisable to run further studies to check the variability of the matrix effect before this procedure is adopted.

2.6.6 Effect of sample storage on analytical accuracy

Between sample dissolution and sample analysis there is an interval of time when the samples could potentially become contaminated by acid leaching of the polypropylene Eppendorf tubes in which they are contained. The tubes are guaranteed by Eppendorf to be chemical resistant and usable between -80 to 100ºC and are acid cleaned prior to use (Appendix 8.2.2). However one laboratory has reported an increase in pure acid magnesium concentration with increasing storage time (M. Greaves personal communication). Therefore to evaluate the impact of sample storage on analytical accuracy a simple test was devised which is described here. Two acid cleaned tubes were filled with acid, one with 120µl 0.065M Optima nitric acid to represent the sample dissolution step and the other with 350µl 0.5M Optima nitric acid to represent the pre-analysis dilution step, which normally occurs on the same day as analysis. This was repeated every two days with new acid cleaned tubes for approximately 2 months. On the day of analysis pairs of tubes were also filled 30 minutes, 1 hour and 1 hour 30 minutes before analysis. All the stored tubes from the two month interval were then analysed as "samples" as per the method described in section 2.5.2 with the 120µl 0.065M nitric acid being topped up to an analysis volume of 350µl with 0.5M nitric acid.

Results and discussion

There is no significant trend between the trace metal concentration of the acids and the length of storage in the microcentrifuge tubes (Figure 2-18 and Figure 2-19). This indicates that there was no significant long term leaching or adsorption of ions by the acids within the tubes. However the trace metal counts for the "samples" did not all fall within the range measured on the 0.5M nitric acid freshly poured into a Teflon vial. The potential causes for this are discussed below.

<u>0.5M Nitric acid</u>

The Mg intensities of the microcentrifuge tube acids are close to or within the range measured on the freshly poured acid. There are 2 outliers however they are less than 2.5 times the maximum blank value. In typical foraminiferal analysis Mg intensities are typically >100 times the blank and so these outliers are not considered significant. The microcentrifuge tubes Li intensities are mostly slightly below the blank values, indicating either a slight contamination of Li in the Teflon vial or that Li is being absorbed from the acid onto the microcentrifuge tube material. As the microcentrifuge tubes Li intensities do not decrease with increasing storage time the former explanation seems most likely. Three samples which were pipetted on the day of the run have significantly more Li although they are still within 25% of the blank. This potentially indicates sample

contamination with Li in these samples which may have also affected the vial blank. As these samples immediately followed a standard then this could also be attributed to a washout effect, however this trend is not seen in the blank. B is similar to Li in that the microcentrifuge tube intensities are close to or slightly below the minimum intensities measured from the Teflon vial. Sr remains within the blank range as expected (Figure 2-18).

0.065M Nitric acid

The Mg intensities of the microcentrifuge tube acids are lower than the freshly poured 0.5M nitric acid by up to 25%. Again this is not very significant in terms of typical foraminiferal analysis concentrations analysed or blank variability. Because there are no systematic changes associated with length of storage time this is not attributed to leaching, but suggests a difference in composition (purity) between the 0.5M nitric acid and the 0.065M nitric acid. The 0.065M nitric acid used here had slightly higher Li and B, similar Sr and slightly lower Mg concentrations than the 0.5M nitric acid. Although the difference in composition between the two acids is too small to affect analytical accuracy it does underline the general importance of using a blank that accurately reflects sample composition. The overall conclusion from this test is that samples can be stored for up to two months without significant leaching of trace metals from the tubes into the acid. Ideally this experiment should be repeated with standards to further test the efficacy of the microcentrifuge tubes in withstanding such leaching and adsorption processes.

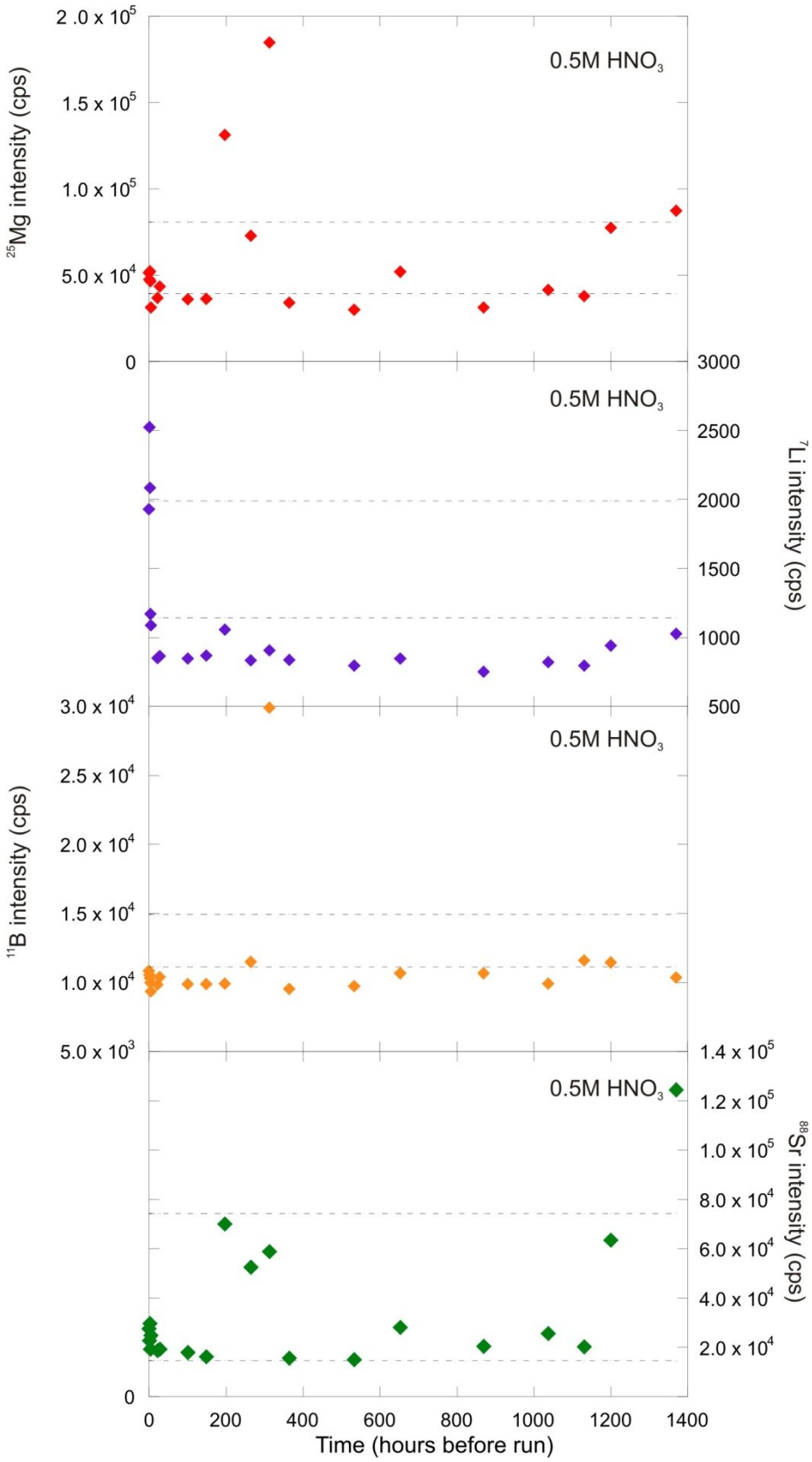

Figure 2-18 Relationship between trace metal content of 0.5M acid (indicated by measured isotope intensity) and storage time in microcentrifuge tube. Grey dashed lines indicate the minimum and maximum measured intensities of the 0.5M HNO_3 freshly poured into a Teflon vial.

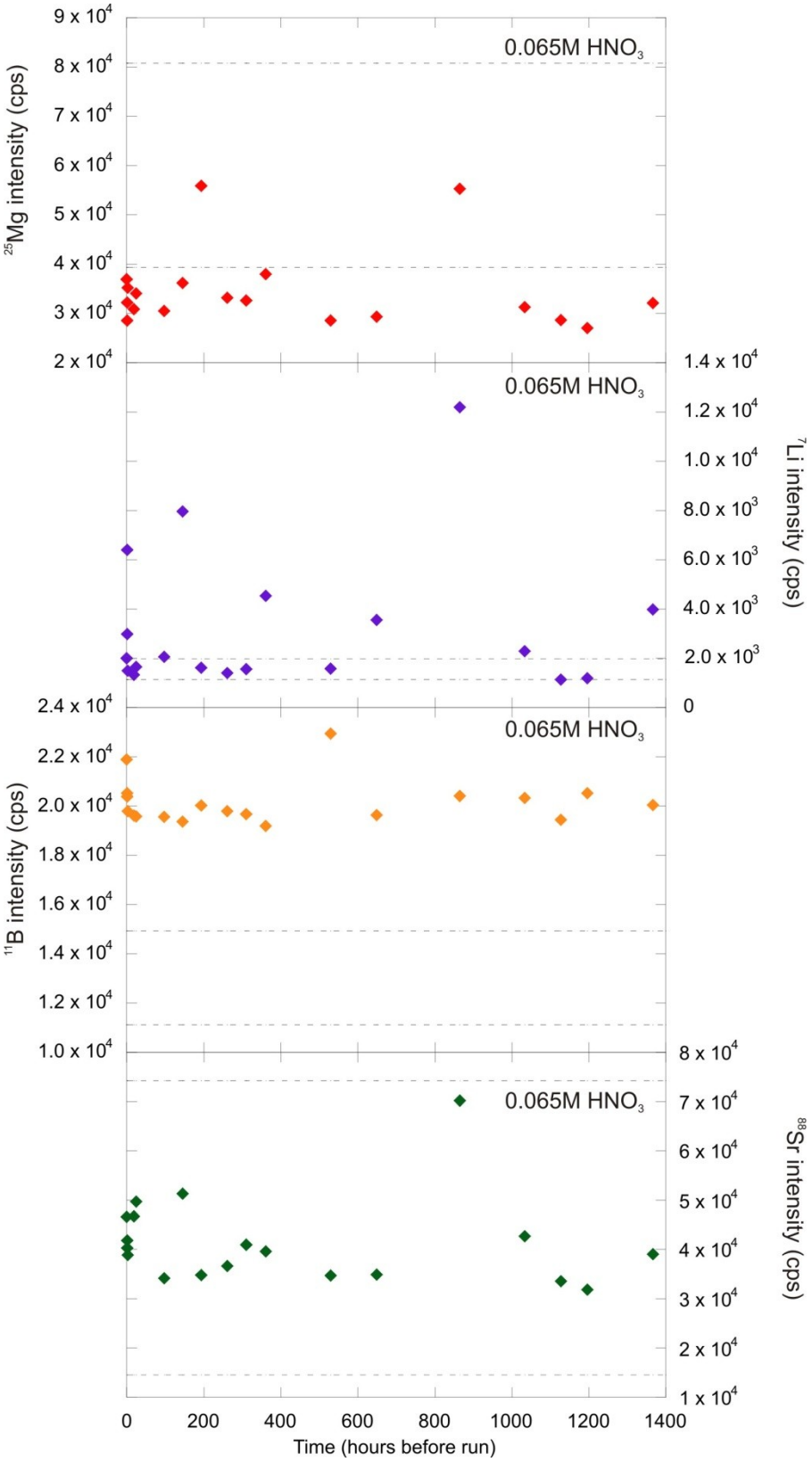

Figure 2-19 Relationship between trace metal content of 0.065M acid (indicated by measured isotope intensity) and storage time in microcentrifuge tube. Grey dashed lines indicate the minimum and maximum measured intensities of the 0.5M HNO3 freshly poured into a Teflon vial.

Boron washout test

The high sensitivity of ICP-MS analysis makes it possible to measure boron which is an ultra trace element in the samples analysed in this study. However there is a documented memory effect during ICP-MS analysis thought to be due to boron's tendency to volatilize as boric acid and stick to the spray chamber's inside surface (Al-Ammar et al., 1999). To reduce these memory effects a wash time between each sample is employed. The aim of the experiment described below was to determine the optimum wash time to reduce memory effect but not add too much additional run time to the analysis.

Consistency standard 2 (section 2.6.3) at a concentration of 4mmol [Ca] was analysed alongside the MCS standard also at a concentration of 4mmol [Ca]. The standards were analysed in triplicate using five different wash times (180, 150, 120, 90 and 60 seconds) (Figure 2-20).

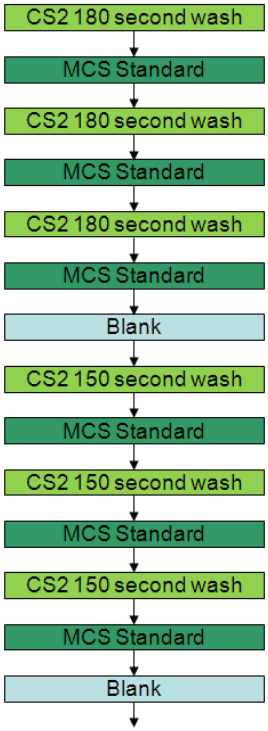

Figure 2-20 Section of ICP-MS sequence used to evaluate the effect of varying spray chamber wash time on B/Ca analysis.

Results and discussion

In general CS2 measured B/Ca decreases with increasing wash time which is likely due to a reduced memory effect as the spray chamber is washed out (Figure 2-21). There is no significant improvement in accuracy above ~120 s wash time suggesting that this is a reasonable length of wash time for a typical B/Ca analysis. This is double the length of the wash time typically used for a Mg/Ca analyses. For samples where B/Ca analysis is crucial, other means of reducing boron build up in the spray chamber could be explored, for example ammonia gas injection into the spray chamber (Al-Ammar et al., 1999)

Results

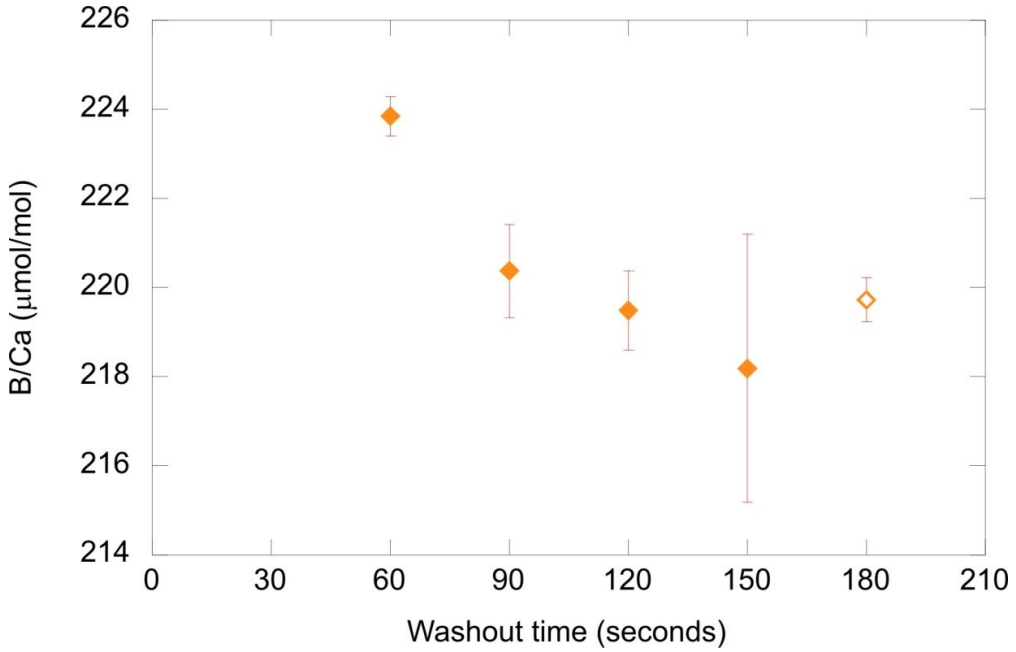

Figure 2-21 The relationship between B/Ca ratios and washout time for consistancy standard CS2. Error bars are ± 1 standard deviation of the three duplicates run for each washout time. The open diamond indicates a potentially contaminated result.

2.6.7 Data screening/Quality control

A critical evaluation of the data quality is essential in order to have confidence in the resulting interpretations. This is especially true for trace metal analysis of biogenic carbonates which are susceptible to contamination (due to factors such as diagenesis, preservation of organic matter and clay contamination) and low concentrations of analyte (for example, due to a lack of benthic foraminifera in some deeper site samples). The different types of data screening used in this study are described below.

Concentration of samples relative to blank

The samples are dissolved using ultra pure Optima nitric acid which is packaged in specially manufactured, precleaned fluoropolymer bottles to protect purity. However, the acid still contains some metal contaminants which are analysed by the mass spectrometer. To account for this “acid blanks” are run and subtracted from the samples and standards at regular intervals. If sample counts are low relative to the blank there may be a low signal to noise ratio. To account for this any samples with intensity signals less than 5 times the blank are removed.

Contamination indicated by the ratios of Fe/Ca, Al/Ca, and Mn/Ca

Although the cleaning steps outlined above are designed to remove contaminants such as silicates (clay removal step), organic matter (oxidising step) and Fe-Mn oxide coatings (reductive step) they may not always be entirely successful, (for example if the chambers are not fully opened by crushing or they have more contamination than the reagents can remove). These contaminants may produce an anomalously high result in the trace metal ratios of interest. For example work done by Barker et al., (2003) indicates that the clay removal step can reduce Mg/Ca by approximately 75%. This is because common clays can contain between 1 – 10% magnesium (Deer et al., 1992). This potential contamination can be screened for by looking at additional trace metal calcium ratios of metals known to be in the contaminants in high quantities. Barker et al (2003) define a point at which samples are significantly contaminated with silicate phases as Fe/Mg ratios >0.1mol/mol. However this threshold is potentially site specific and additionally Fe may be present in an oxide coating and/or pyrite, so if the reductive step is not undertaken Fe/Mg may be higher than the defined limit. Therefore in some situations Al/Ca may be a better indicator of clay contamination. For each site analysed during this study cross plots of Fe vs. Mg and Al vs. Mg were constructed to determine the Fe/Mg threshold above which data points should be discarded (Table 2-5). The threshold for ODP Leg 154 Sites is higher than the other sites due to the presence of pyrite which affects the Fe/Ca ratios but not the Mg/Ca ratios (this was determined by producing a cross plot of the two elemental ratios, no correlation was found).

ODP Leg	Fe/Mg threshold (mol/mol)
199	0.1
154	1*
130	0.1

Table 2-5 The Fe/Mg thresholds used in this study to determine clay contamination in benthic foraminiferal calcite samples. Asterix denotes ODP leg samples where a higher Fe/Mg threshold was used.

3 The Eocene/Oligocene Climate Transition (EOT)

The purpose of this chapter is to more closely explore the interplay of depth related carbonate saturation state and changing bottom water chemistry with respect to benthic foraminiferal composition during the Eocene/Oligocene transition, which represents one of the largest shifts in the ocean-climate system of the Cenozoic. This has been achieved by measuring trace metal concentrations in benthic foraminiferal calcite from three late Eocene to early Oligocene ODP sections of differing palaeowater depth (Table 3-1) in the Eastern Equatorial Pacific (EEP) (Figure 3-1). These sites were all recovered during ODP Leg 199 and comprise of ODP Sites 1218, 1219 and 1220.

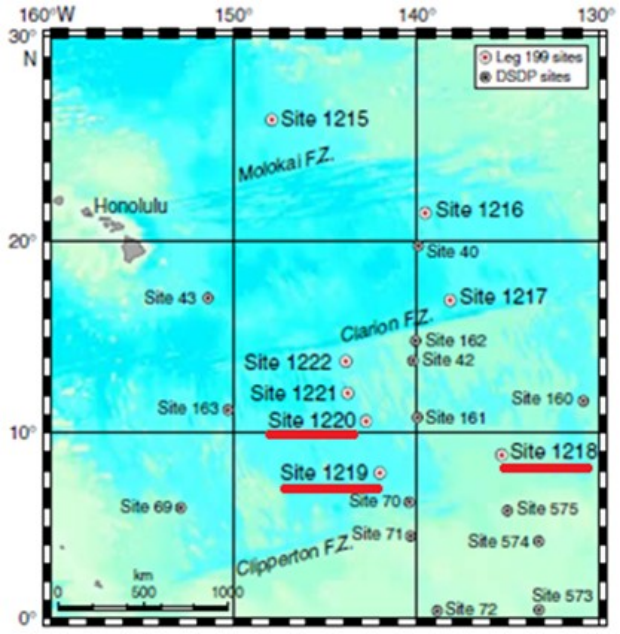

Figure 3-1 Map of the Equatorial Pacific region including ODP Leg 199 Sites used in this study (underlined) (ODP Leg 199 Shipboard Scientific Party, 2006).

ODP Site	Estimated palaeowater depth across the EOT (m)
1218	3700
1219	4200
1220	4300

Table 3-1 Estimated palaeowater depths of the Eocene-Oligocene ODP Sites used in this study (Shipboard Scientific Party, 2006).

3.1 Introduction

3.1.1 The Eocene/Oligocene Transition and ODP Sites 1218, 1219 and 1220

As discussed in the introduction (section 1.2.1), the EOT is thought to be a period of ice sheet expansion on Antarctica with an accompanying decrease in global temperatures. The classic isotope record for this event is the high resolution ODP Site 1218 benthic foraminiferal oxygen isotope record ($\delta^{18}O$) (Coxall et al., 2005; Figure 3-2) which reveals a >1.5‰ increase across the EOT that occurred in two steps in the Equatorial Pacific. The two steps, defined by rapidly increasing $\delta^{18}O$ are separated by a period of approximately 200kyrs. The deep sea cooling that is thought to have accompanied ice growth interpreted from this isotope excursion is not apparent in all benthic foraminiferal Mg/Ca records. Shallow continental margin/slope sites such as those recovered in Tanzania by the Tanzanian Drilling Project (TDP) (palaeowater depth ~500 metres, Lear et al., 2008) and St Stephens Quarry (SSQ) (palaeowater depth ~100 metres, Katz et al., 2008) do show a cooling. Yet most deep sea Mg/Ca records display either an increase (e.g. ODP Site 1218) or no change across the EOT. The coincident deepening of the CCD by ~1200 meters from ~3200 to 4400 metres (Rea and Lyle, 2005) is thought to be a complicating factor which has prevented the accurate assessment of deep sea temperature changes (Lear et al., 2004). Recent work attempting to correct the ODP Site 1218 benthic foraminiferal Mg/Ca record for the saturation state change using Li/Ca data, which is thought to be a proxy for carbonate saturation state and temperature, was unsuccessful (Lear et al., 2010). However an attempt to correct the DSDP Site 522 Mg/Ca data using the same Li/Ca based method did produce cooling (Lear et al., 2010). Atlantic DSDP Site 522 was at a shallower palaeowater depth than Pacific ODP Site 1218 during the EOT (~3000 m). This suggests that while the paired Mg/Ca-Li/Ca methodology shows promise, there is still an unresolved issue with the ODP Site 1218 Mg/Ca record. It seems that the EOT Mg/Ca record from this classic site was not only affected by temperature and saturation state but also other factor(s).

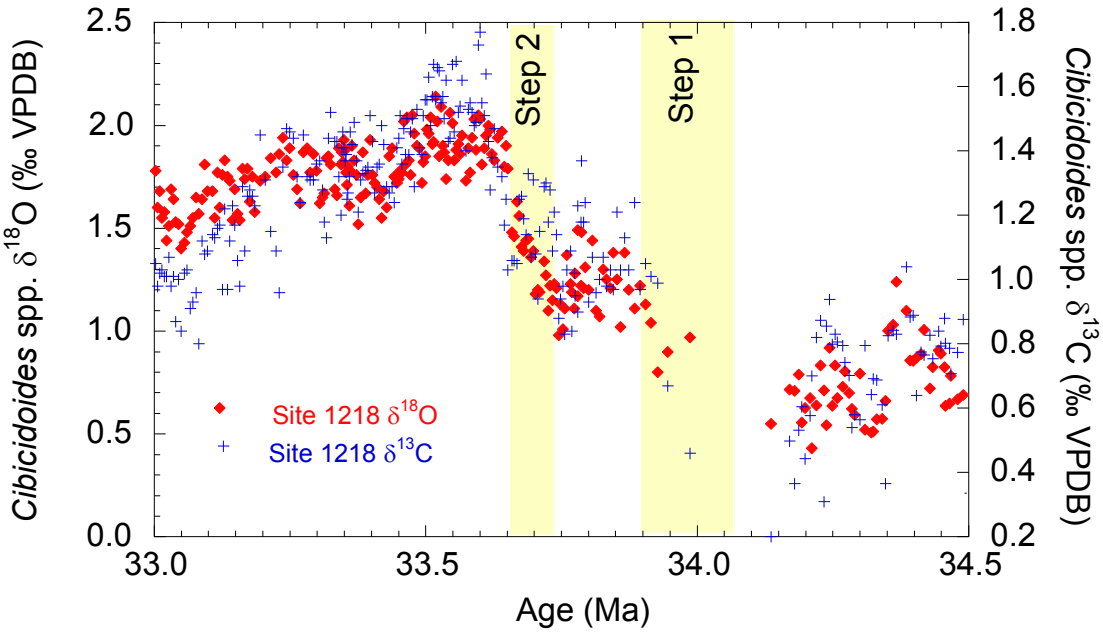

Figure 3-2 Benthic foraminiferal oxygen and carbon stable isotope records for the epifaunal genus *Cibicidoides* spp. from ODP Site 1218 (Coxall et al., 2005). Sample ages are on the orbitally tuned Leg 199 timescale (Coxall et al., 2005).

3.1.2 Resolving the ODP Site 1218 Mg/Ca record: Proposed hypothesis

The hypothesis proposed here is that in very deep undersaturated waters, the trace metal content of benthic foraminiferal calcite is affected by post burial calcite dissolution. I propose that the decrease in the extent of dissolution, associated with the CCD deepening ~1200 m (Rea and Lyle, 2005) contributed to the unexpected increasing foraminiferal Mg/Ca in ODP Leg 199 sites through the EOT.

3.1.3 Rationale for the dissolution hypothesis

Dissolution is the process by which a solid, liquid or gas forms a solution in a solvent. In these terms the material dissolving is the foraminiferal calcite and the solvent is seawater (or pore water).

Dissolution in planktonic foraminifera

Early core top studies found that planktonic foraminiferal Mg/Ca is correlated with the water depth at which they were deposited rather than the temperature of the overlying sea surface temperatures where the calcite was precipitated. This is highly suggestive of post-depositional dissolution at the sediment water interface (e.g. Lorens et al., 1977; Savin and Douglas, 1973). This systematic decrease in Mg/Ca with increasing water depth could be attributed to preferential dissolution of Mg-rich calcite (Brown and Elderfield, 1996). Various approaches have been offered to correct for dissolution effects in planktonic foraminiferal Mg/Ca such as using the size normalised test weight – dissolution

relationship (Rosenthal and Lohmann, 2002). Furthermore it is well documented that the corrosive cleaning procedures used prior to foraminiferal calcite analysis result in lowered Mg/Ca (e.g. Barker et al., 2003, Yu et al., 2007).

Dissolution in benthic foraminifera

It is thought that benthic foraminiferal calcite is less prone to the effects of dissolution than planktonic foraminifera for several reasons: they have a less variable habitat, thicker tests and sometimes form in poorly saturated bottom waters. However it has been suggested that dissolution may also preferentially remove metals from the calcite tests of benthic foraminifera (McCorkle et al., 1995). A potential example of a dissolution effect is found in data from deep water depth transects in the Atlantic Ocean where benthic foraminiferal Mg/Ca decreases with depth significantly beyond the changes expected from global temperature calibrations (Martin et al., 2002). However this trend can be accounted for by a secondary effect on Mg uptake related to carbonate saturation state and therefore is not necessarily caused by dissolution (Elderfield et al., 2006). It is thought that Mg is more homogeneously distributed in the calcite of benthic foraminifera than planktonic foraminifera and, as such, should be less susceptible to selective loss of Mg-rich portions of the test. Curry and Marchitto (2008) found that Mg distribution within the test walls of *Cibicidoides pachyderma* is Gaussian, suggesting magnesium is present in a single phase. This is just one species however, and other species may exhibit more variable test composition. Analysis of core-top living (Rose Bengal stained) and dead (unstained) benthic foraminifera indicates that there is no consistent difference in Mg/Ca between the two which points away from a dissolution effect (Lear et al., 2002). However the samples from this study were not from undersaturated waters (depths ranged from 194 to 2682 m in the Pacific) and thus may not have undergone dissolution. In summary it seems that in most cases there is no evidence of a significant dissolution effect on the trace metal composition of benthic foraminifera. However there is one line of evidence that suggests that in the deepest, least saturated waters dissolution may influence benthic foraminiferal Mg/Ca. A study of core-top benthic foraminifera from New Zealand indicates that in undersaturated waters ($\Delta CO_3^{2-}<0$) Mg/Ca values are lower than expected for the locations temperature and carbonate saturation state potentially hinting at a dissolution effect (Jordan, unpublished thesis). This is restricted to two data points (Figure 3-3) and clearly more data are needed to support this observation. However it will be difficult to obtain such data as few foraminifera live in such undersaturated waters.

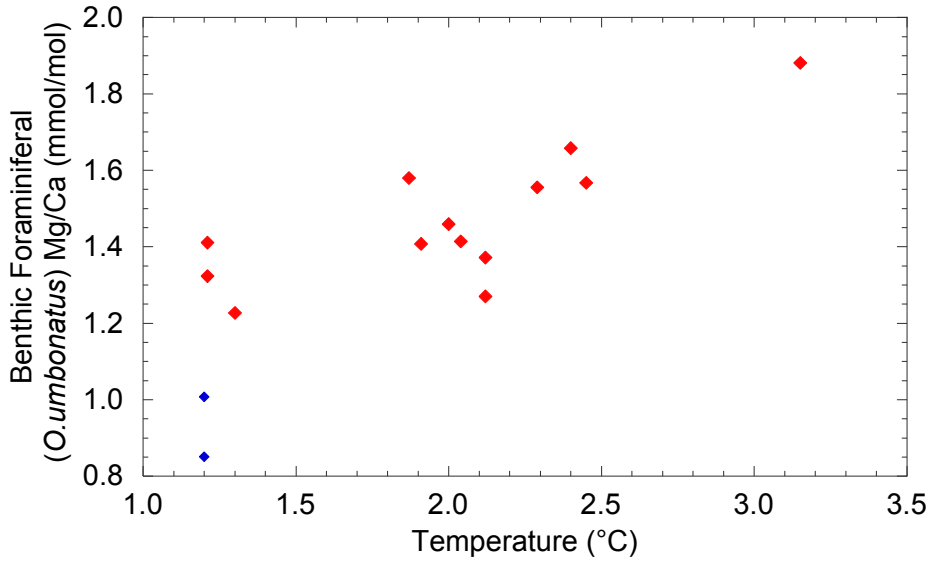

Figure 3-3 Core-top benthic foraminiferal (*Oridorsalis umbonatus*) Mg/Ca vs. temperature from the Pacific Ocean in the region of New Zealand (K.Jordan, unpublished thesis). The blue diamonds represent sites with ΔCO_3^{2-} of less than 0, red diamonds represent sites with ΔCO_3^{2-} of greater than 0.

3.1.4 Testing the dissolution hypothesis using ODP Leg 199 sites

To test the dissolution hypothesis outlined in section 3.1.2 I have produced a suite of trace metal analyses on benthic foraminiferal calcite across the EOT from ODP Sites 1218, 1219 and 1220. These sites were chosen for analysis because the level of dissolution at the three sites studied here is high causing virtually all of the planktonic foraminifera to be dissolved, and there is an absence of benthic foraminifera in many of the samples. In addition, ODP Site 1218 is the source of the classic ($\delta^{18}O$) record (Coxall et al., 2005) and yet interpretation of the ODP Site 1218 Mg/Ca record (Lear et al., 2004) is unresolved. As the sites are geographically close together and all below 3500 m palaeowater depth the inter-site temperature differences are minimal and thus would have no effect on the Mg/Ca ratio.

As described in the previous section there is no evidence for a dissolution control on the Mg/Ca of benthic foraminifera in saturated ocean waters. However the limited core-top data available for undersaturated waters suggests that dissolution in these corrosive conditions may lower benthic foraminiferal Mg/Ca. If so it would be expected that more extensive dissolution at deeper sites would reduce Mg/Ca further. Therefore I predict a larger increase in Mg/Ca across Step 2 of the EOT at ODP Sites 1219 and 1220 (paleo water depths 4200 m and 4300 m respectively) than at ODP Site 1218 (paleo water depth 3700 m). The Mg/Ca records produced to test this prediction are also accompanied by a suite of trace metal data including B/Ca and Li/Ca with the eventual aim being to use all

trace metal records synchronously to reconstruct temperature and carbonate saturation state changes across the EOT.

3.1.5 ODP Leg 199 site to site correlation

Accurate stratigraphic correlation between the ODP Leg 199 sites is crucial for assessing intersite offsets in the proxy. ODP Site 1218 is the most extensively studied site of the ODP Leg 199 depth transect and has an astronomically tuned age model based on variations in down-core physical properties and benthic foraminiferal stable isotope stratigraphy (see section 2.2.1). ODP Sites 1219 and 1220 have bulk carbonate isotope stratigraphies but no benthic foraminiferal isotope stratigraphy (due in part to the absence of sufficient foraminifera for analysis). ODP Site 1218 and ODP Site 1219 were correlated using the increased signal to noise ratio in stacked records (Pälike et al., 2005). This method appears to be robust as the bulk isotopes and % calcium carbonate data, which exist for both sites appear to be in phase (Figure 3-4, Figure 3-5 and Figure 3-6).

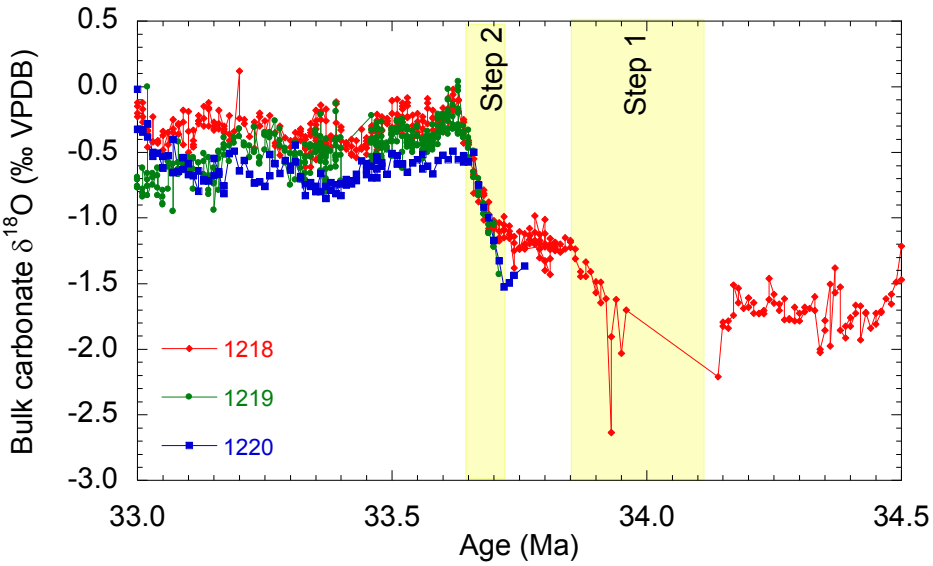

Figure 3-4 ODP Leg 199 bulk sediment calcium carbonate oxygen isotope record. ODP Site 1218 data from Pälike et al. (2006), ODP Site 1219 and ODP Site 1220 data H. Pälike personal communication. Sample ages are on the orbitally tuned timescale of Coxall et al. (2005). Steps 1 and 2 are defined in section 3.1.1.

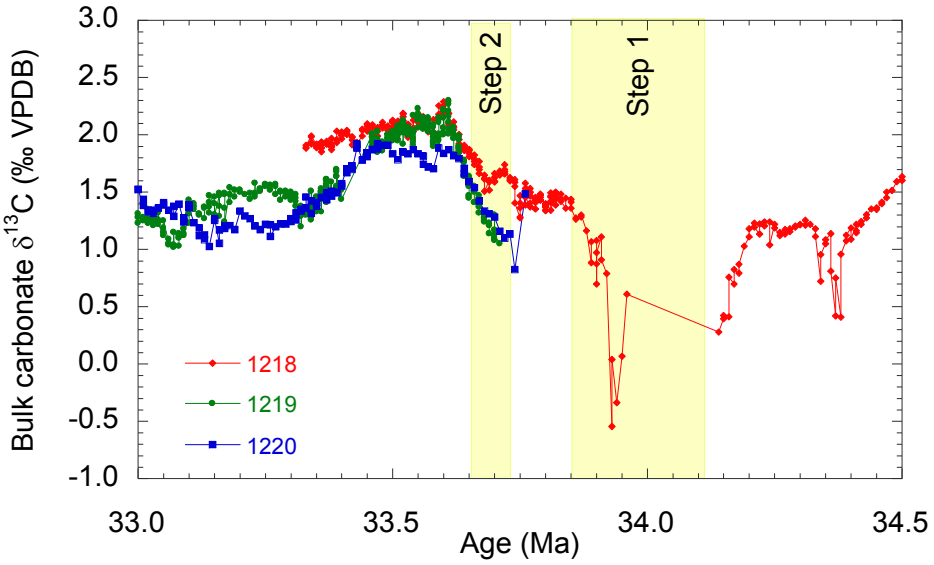

Figure 3-5 ODP Leg 199 bulk sediment calcium carbonate carbon isotope record. ODP Site 1218 data from Pälike et al. (2006), ODP Site 1219 and ODP Site 1220 data H. Pälike personal communication. Sample ages are on the orbitally tuned timescale of Coxall et al. (2005).

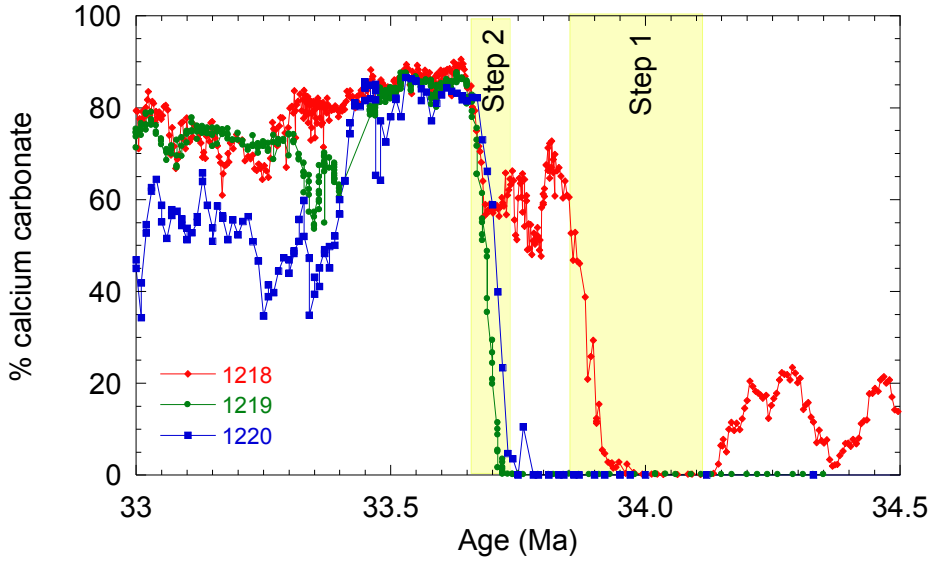

Figure 3-6 Leg ODP Leg 199 % calcium carbonate record. ODP Site 1218 data from Coxall et al., (2005), ODP Site 1219 and ODP Site 1220 data H. Pälike personal communication. Sample ages are on the orbitally tuned timescale of Coxall et al. (2005).

ODP Site 1220 was originally correlated to ODP Site 1218 using down-core variations in GRAPE (gamma ray attenuation porosity evaluator), bulk density and magnetic susceptibility data (H.Pälike personal communication). Detailed inspection of this 1220-

1218 correlation as part of this study, however, reveals an apparent temporal offset in the critical region of Step 2, between ODP Site 1220 (bulk $\delta^{18}O$ peaks at 33.66Ma) and ODP Sites 1218 and 1219 (peak simultaneously at 33.62Ma) (Figure 3-4). This apparent temporal offset is also apparent in the % calcium carbonate data (Figure 3-6) and indicates a 40 kyr miscorrelation between ODP Site 1220 and the other two sites. To improve the ODP Site 1220 to 1219/1218 correlation across Step 2 of the EOT the Site 1220 E-O sequence was rescaled to Site 1218 by correlating over Step two of the isotopic shift in the ODP Site 1220 and ODP Site 1218 bulk $\delta^{18}O$ records where they overlapped (Table 3-2). This was achieved using the 'lineage' function in AnalySeries 2.0.42 (Paillard et al., 1996) (Table 3-2). This new age model improves correlation in the record beyond the area of interest indicating that this new correlation is more fitting.

depth in 1218 (mcd)	depth in 1220 (mcd)	Age (Ma)
239.22	76.70	33.6192
240.34	76.85	33.7080

Table 3-2 Table of new tie-points between ODP Sites 1218 and 1220 within Step 2 of the EOT (this study).

3.2 Results; ODP Leg 199 trace metal records across the EOT

Trace metal data have been produced for ODP Site 1218 across the whole EOT, supplementing the previously published Mg/Ca and Li/Ca records (Lear et al., 2004, Lear & Rosenthal 2006). This has been undertaken in order to increase the resolution of the data across the EOT in this exceptional sequence, confirm lack of inter-laboratory offsets and to attempt to collect data for previously unmeasured trace metals such as boron.

Trace metal data have been produced for ODP Sites 1219 and 1220 across Step 2 (Figure 3-7) of the EOT only, as prior to this ODP Sites 1219 and 1220 were below the CCD and thus the sediment samples from this interval do not contain sufficient foraminifera for analysis.

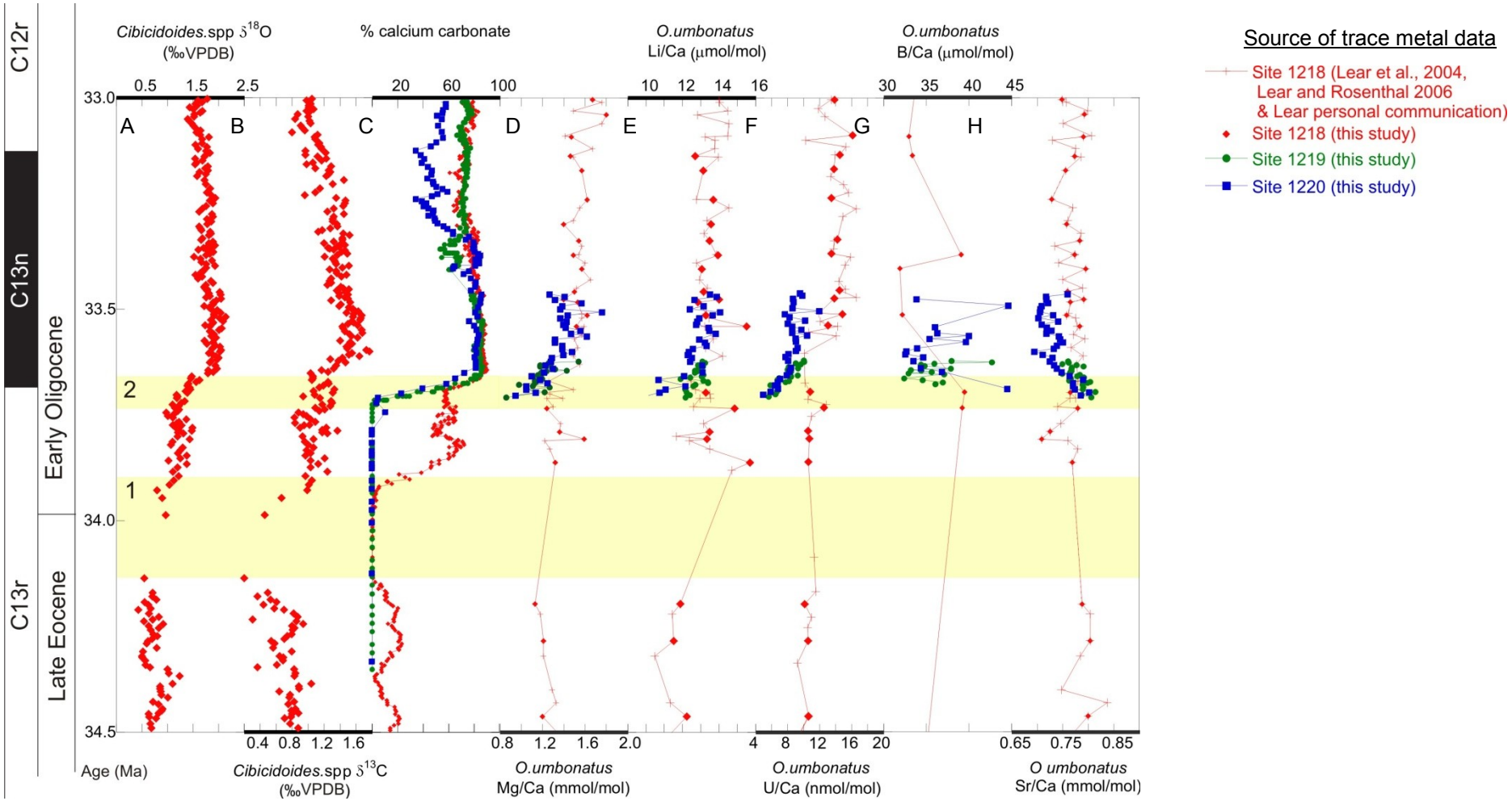

Figure 3-7 New and existing late Eocene to Early Oligocene carbonate based geochemical data from Equatorial Pacific ODP Leg 199 sites. A and B *Cibicidoides* spp. $\delta^{18}O$ and $\delta^{13}C$ (Coxall et al., 2005); C, bulk sediment % calcium carbonate (Coxall et al., 2005, H.Pälike, personal communication); D-H benthic foraminiferal trace metal data new (this study), published and unpublished data (see key).

3.2.1 Leg 199 Benthic foraminiferal trace metal records across "Step 2" of the EOT

All the trace metal records produced show a change across Step 2 of the EOT (Figure 3-7). The change across the step is defined by comparing mean values at the start of Step 2 (33.74 Ma) to those at the end of Step 2 (33.65 Ma). The start and end of Step 2 are constrained from the minimum and maximum in benthic foraminiferal $\delta^{18}O$ values (Figure 3-2). The overall changes in trace metal ratios across Step 2 are summarised in Table 3-3 and described in more detail below.

ODP Site	Palaeowater depth (m)	Step 2 Mg/Ca change (mmol/mol)	Step 2 Li/Ca change (µmol/mol)	Step 2 U/Ca change (nmol/mol)	Step 2 Sr/Ca change (mmol/mol)
1218	3700	0.16	0.00	0.00	0.00
1219	4200	0.28	1.01	3.63	0.05
1220	4300	0.29	2.90	3.53	0.06

Table 3-3 Overall change in trace metal ratios across Step 2 of the EOT. B/Ca is excluded as no data across this interval was obtained for this trace metal.

3.2.2 Mg/Ca

Across the E/O transition

ODP Site 1218 data supplementing that published by Lear et al., (2004) confirms an increase in Mg/Ca values from 1.2 mmol/mol to 1.6 mmol/mol across the entire EOT (Figure 3-7). The data prior to the EOT is sparse due to insufficient material however overall the Mg/Ca values are lower. There are insufficient data to quantify the change in Mg/Ca across Step 1 of the EOT (Figure 3-8). Benthic foraminiferal Mg/Ca increases in all sites across Step 2 of the EOT: ODP Site 1218 shows an increase of approximately 0.16 mmol/mol, ODP Site 1219 an increase of 0.28 mmol/mol and ODP Site 1220 an increase of 0.29 mmol/mol (Table 3-3). The Mg/Ca values continue to increase after the Step 2 benthic foraminiferal isotope excursion in ODP Site 1218 and ODP Site 1220; this is not observed in ODP Site 1219 due to insufficient data after the second isotope excursion. The ODP Site 1218 Mg/Ca increase after Step 2 is approximately 0.20 mmol/mol which is a similar magnitude to that across Step 2. This increasing trend ends at approximately 33.5 Ma. The ODP Site 1220 Mg/Ca increase after Step 2 is approximately 0.27 mmol/mol, which again is a similar change to that across Step 2 of the EOT. This increasing trend also ends at approximately 33.6 Ma. This is similar to the $\delta^{13}C$ increase which also extends beyond the $\delta^{18}O$ step to ~33.6 Ma (Figure 3-5).

Between Sites

In order to assess the intersite Mg/Ca differences the average values within Step 2 of the EOT were calculated to provide approximate offsets between the three sites (Table 3-4.) ODP Site 1218 has the highest mean Mg/Ca value within Step 2 (1.30 mmol/mol) followed

by ODP Site 1219 (1.12 mmol/mol). ODP Site 1220 has the lowest mean Mg/Ca values across the EOT (1.10 mmol/mol) but this is quite similar to that of ODP Site 1219).

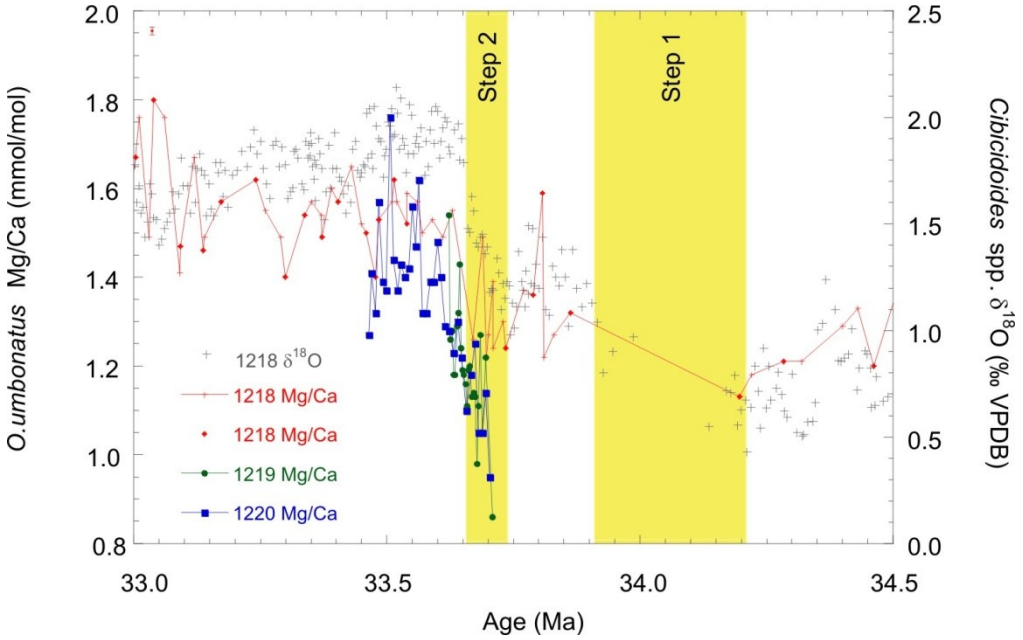

Figure 3-8 Benthic foraminiferal Mg/Ca and $\delta^{18}O$ across the EOT for ODP Leg 199 sites. Red crosses represent Mg/Ca data from ODP Site 1218 from Lear et al. (2004). $\delta^{18}O$ data from Coxall et al. (2005). Age model Pälike et al. (2006) with ODP Site 1220 adjustment (see text for details). Error bars = ± 1 s.d of Mg/Ca based on long term replicate analysis of consistency standards (CS1 and CS2, see Methods chapter).

ODP Site	Average Mg/Ca across EOT Step 2 mmol/mol	Intersite differences		
		1218	1219	1220
1218	1.30 ± 0.01	x	0.18	0.20
1219	1.12 ± 0.01	0.18	x	0.02
1220	1.10 ± 0.01	0.20	0.02	x

Table 3-4 Mean Mg/Ca ± 1 s.d for ODP Leg 199 sites within Step 2 of the EOT and the difference in values between sites.

3.2.3 Li/Ca

Across the E/O Transition

At ODP Site 1218 benthic foraminiferal Li/Ca increases from ~11.9 to ~14.1 μmol/mol across the EOT (Figure 3-9). Although there is a paucity of Li/Ca data, ODP Site 1218 appears to show a large increase across Step 1 followed by a decrease across the intermediate interval prior to Step 2. Across Step 2 ODP Site 1218 Li/Ca does not appear to increase although after Step 2 ODP Site 1218 Li/Ca increases by approximately 1.3

µmol/mol by 33.6 Ma. Many of the ODP Site 1219 samples were below the detection limit for Li/Ca (see section 2.6.4 in methods chapter) The remaining samples show a similar trend to ODP Site 1220; an increase across Step 2 of the transition. However the total magnitude of this increase cannot be determined as the ODP Site 1219 data do not cover the entire step. The minimum increase in Li/Ca across Step 2 at ODP Site 1219 is 1.01 µmol/mol. The increase in Li/Ca for ODP Site 1220 across Step 2 is ~2.9 µmol/mol and as with ODP Site 1218 the increase continues beyond Step 2 with a further increase of 2.0 µmol/mol prior to levelling out at ~13.3 µmol/mol by 33.6 Ma.

Between Sites

Benthic foraminiferal Li/Ca ratios from ODP Sites 1218 and 1219 are within analytical error. However the Li/Ca ratios from the deepest site (ODP Site 1220) are ~1.9 µmol/mol lower than the other two sites in the middle of Step 2. The ODP Site 1220 Li/Ca ratios subsequently increase such that by the end of Step 2 the Li/Ca ratios from all three sites are within error.

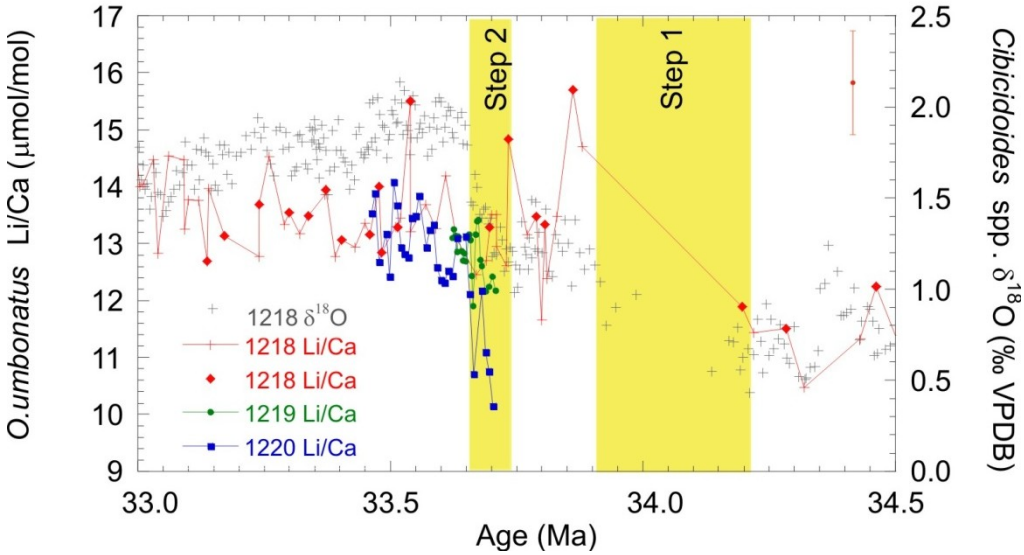

Figure 3-9 Benthic foraminiferal Li/Ca and $\delta^{18}O$ across the EOT for ODP Leg 199 sites. Red crosses represent ODP Site 1218 Li/Ca data from Lear and Rosenthal (2006). $\delta^{18}O$ data from Coxall et al. (2005). Age model Pälike et al. (2006) with ODP Site 1220 adjustment (see text for details). Error bars = ± 1 s.d of Li/Ca based on long term replicate analysis of consistency standards (CS1 and CS2, see Methods chapter).

3.2.4 B/Ca

Across the E/O transition

The high boron blank during the analysis of Leg 199 ODP sites (on average three times the normal operating value) coupled with the low boron content of the foraminifera species analysed (*O. umbonatus*) meant that much of the boron data collected was discarded (see methods section 2.5.4). ODP Site 1218 B/Ca shows high variability and no clear trend although this may be due to the extremely low resolution data. ODP Sites 1219 and 1220 B/Ca data mostly cover the post Step 2 interval. Both ODP Sites 1219 and 1220 hint at an increase following Step 2 but it is hard to define as it is on the same magnitude as the analytical precision.

Between Sites

ODP Site 1218 data is too sparse to be meaningfully compared with that of ODP Sites 1219 and 1220. ODP Site 1219 and ODP Site 1220 B/Ca ratios appear to encompass a similar range (between 35 and 40 µmol/mol).

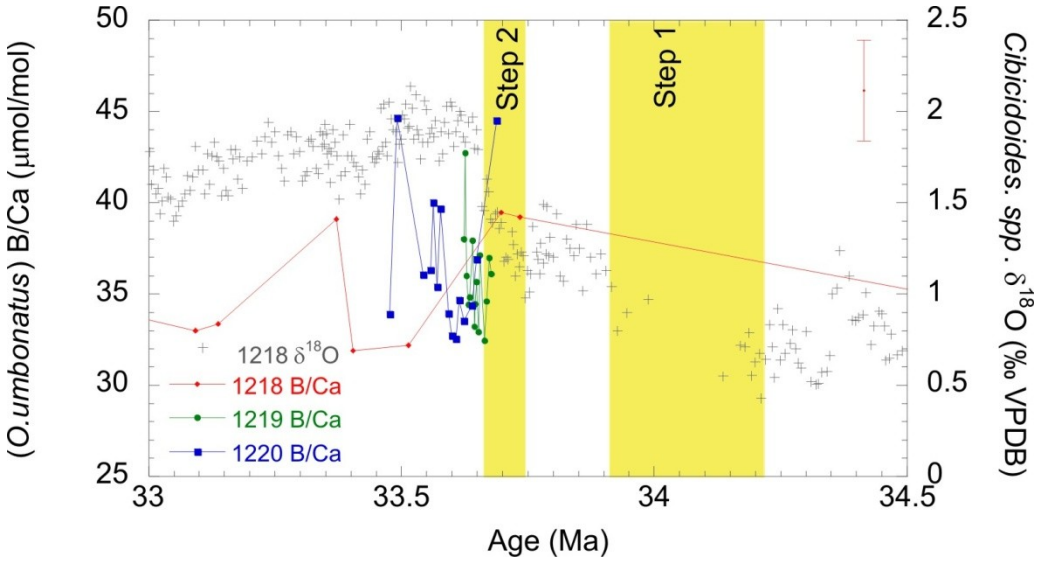

Figure 3-10 Benthic foraminiferal B/Ca and $\delta^{18}O$ across the EOT for ODP Leg 199 sites. $\delta^{18}O$ data from Coxall et al. (2005). Age model Pälike et al. (2006) with ODP Site 1220 adjustment (see text for details). Error bars = ± 1 s.d of B/Ca based on long term replicate analysis of consistency standards (CS1 and CS2 see Methods chapter).

3.2.5 U/Ca

Across the transition

Prior to the EOT, ODP Site 1218 *Oridorsalis umbonatus* U/Ca is relatively constant at ~10 nmol/mol. There is a brief transient increase on the order of 2nmol/mol at the start of Step 2 (33.7Ma), and a larger more permanent increase on the order of 4 nmol/mol at or just after the end of Step 2. Post EOT values at ODP Site 1218 are around 14 nmol/mol and exhibit a potentially cyclic variability on the order of ± 2 nmol/mol. ODP Site 1219 U/Ca values increase from approximately 5.0 nmol/mol in Step 2 to 10.0 nmol/mol after. Across Step 2 of the EOT ODP Site 1220 U/Ca values increase from 4.8 nmol/mol, to ~8 nmmol/mol. U/Ca increases slightly post Step 2 to values around 9 nmmol/mol at 33.6 Ma.

Between Sites

ODP Site 1218 U/Ca is ~5 nmol/mol higher than ODP Sites 1219 and 1220 for the majority of the record. At ~33.6 Ma this gradient appears to collapse but this is based only upon two samples from ODP Site 1218.

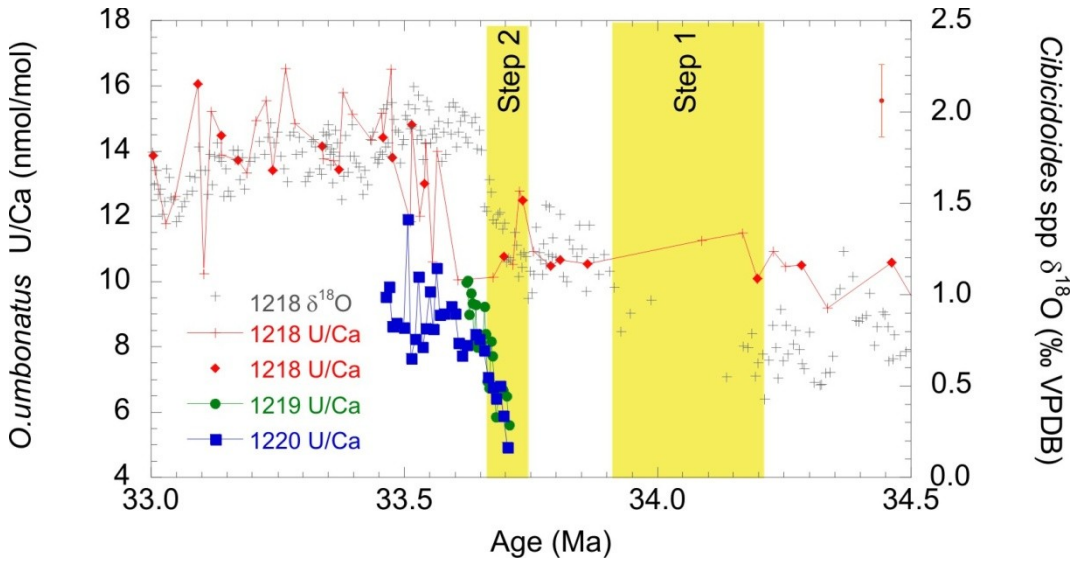

Figure 3-11 Benthic foraminiferal U/Ca and $\delta^{18}O$ across the EOT for ODP Leg 199 sites. Red crosses represent unpublished U/Ca data from ODP Site 1218 (C.H. Lear personal communication). $\delta^{18}O$ data from Coxall et al. (2005). Age model Pälike et al. (2006) with ODP Site 1220 adjustment (see text for details). Error bars = ± 1 s.d of U/Ca based on long term replicate analysis of consistency standards (CS1 and CS2 see Methods chapter).

3.2.6 Sr/Ca

Across the E/O transition

There is no detailed ODP Site 1218 Sr/Ca record across Step 1 of the EOT. However Sr/Ca prior to the transition (~34-34.5 Ma) is similar (~0.8 mmol/mol) to the Sr/Ca after

(~0.77 mmol/mol). There is a possible minimum in the plateau region between the two steps. Sr/Ca remains stable until ~33.50 Ma then gradually decreases by ~0.04mmol/mol between 33.50 and 33.35 Ma while $\delta^{18}O$ also decreases.

ODP Sites 1219 and 1220 Sr/Ca records decrease across Step 2 by ~0.05 mmol/mol. After Step 2 ODP Site 1220 continues to decrease by another 0.06 mmol/mol by 33.6 Ma to a minima of 0.69 mmol/mol.

Between sites

There is no consistent offset between the ODP Site 1218, ODP Site 1219 and ODP Site 1220 Sr/Ca records. At the start of Step 2 (~33.7 Ma), ODP Site 1219 and ODP Site 1220 Sr/Ca values (0.8 mmol/mol) are higher than ODP Site 1218 Sr/Ca (0.77 mmol/mol). However ODP Sites 1219 and 1220 Sr/Ca decrease across Step 2 causing ODP Site 1218 Sr/Ca to be 0.76 mmol/mol higher than ODP Sites 1219 and 1220 after 33.6 Ma.

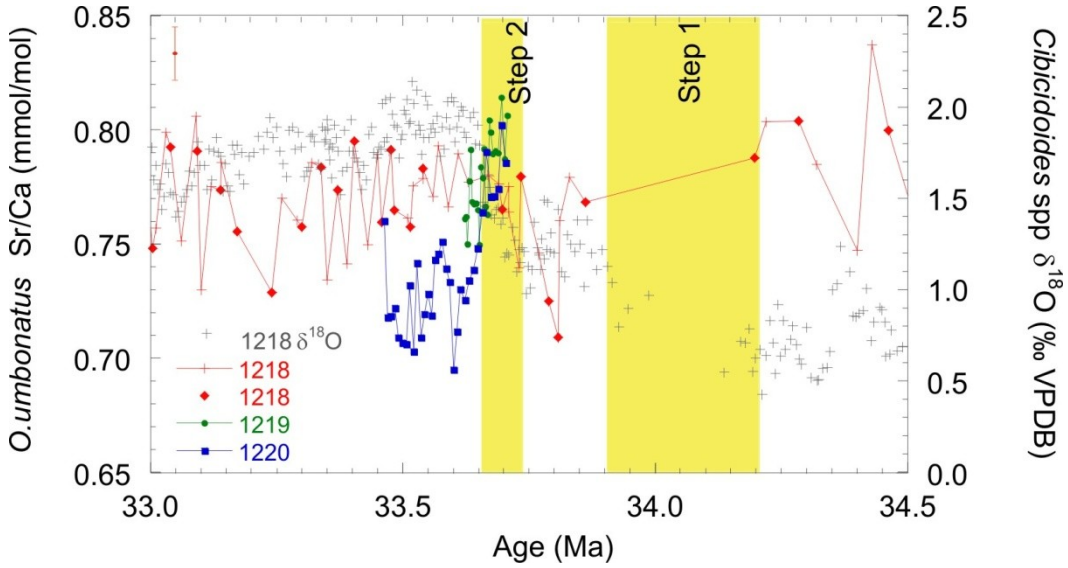

Figure 3-12 Benthic foraminiferal Sr/Ca and $\delta^{18}O$ across the EOT for ODP Leg 199 sites. Red crosses represent unpublished Sr/Ca data from ODP Site 1218 (C.H. Lear personal communication). $\delta^{18}O$ data from Coxall et al. (2005). Age model Pälike et al. (2006) with ODP Site 1220 adjustment (see text for details). Error bars = ± 1 s.d of Sr/Ca based on long term replicate analysis of consistency standards (CS1 and CS2 see Methods chapter).

3.3 Discussion of ODP Leg 199 EOT trace metal records

3.3.1 Mg/Ca

Across the EOT interval

The increase observed in benthic foraminiferal Mg/Ca across the EOT in all three Leg 199 sites (a change of between 0.16-0.29 mmol/mol across Step 2 (Table 3-3)) could be considered to indicate a temperature or saturation state increase. Temperature increase across this interval seems improbable as planktonic and benthic Mg/Ca records from other sites have shown a temperature decrease across the EOT (e.g. Lear et al., 2008; Katz et al., 2008). The 1.2 km CCD deepening recorded by these sites may potentially account for the observed Mg/Ca increase. This can be assessed by comparison with core-top calibrations, as set out using a new combined Mg/Ca and Li/Ca approach (Lear et al., 2010) This new method combines the assumed temperature and carbonate ion sensitivities of Li/Ca and Mg/Ca (Table 5-1) to determine temporal variations in temperature and saturation state rather than determining absolute values (Equations 1-4).

	T (°C)	ΔCO_3^{2-}
Mg/Ca	[a] 0.12 mmol/mol/°C	[b] 0.0086 mmol/µmol/kg
Li/Ca	[c] -0.74 µmol/mol/°C"	[d] 0.047 µmol/µmol/kg

Table 3-5 Trace metal sensitivities to temperature and carbonate saturation state used in the Lear et al. (2010) method. a) Marchitto et al. (2007), b) Elderfield et al. (2006), c) Lear et al., 2010, d) Lear et al. (2010) (adapted from Lear and Rosenthal (2006).

$\Delta Mg = 0.0086.\Delta CO_3^{2-} + 0.12.\Delta T$

Equation 11

$\Delta Li = 0.047.\ \Delta CO_3^{2-} - 0.74.\Delta T$

Equation 12

$\Delta T = (\Delta Mg - 0.183.\Delta Li) / 0.225$

Equation 13

$\Delta CO_3^{2-} = (\Delta Mg + 0.162.\Delta Li) / 0.0162$

Equation 14

Equations combining known sensitivities of Mg/Ca and Li/Ca to temperature and carbonate saturation state to determine relative changes in these variables (Lear et al., 2010).

The application of this method to ODP Site 1218 Li/Ca and Mg/Ca records indicates a cooling across the EOT of 0.3°C and a saturation state change of 36μmol/kg (Lear et al., 2010). Compared to other data sets from other global sites this is a small temperature change and likely to be an underestimate. The change in $\delta^{18}O$ across the EOT is greater than that from the TDP site (Lear et al., 2008). The global ice volume increase associated with the EOT should cause the same magnitude increase in the $\delta^{18}O$ record at each site. Therefore the cooling at ODP Site 1218 should have been of a greater magnitude than at the TDP site. Using the TDP calculated cooling of 2.5°C (Lear et al., 2008) as a conservative estimate of cooling at ODP Site 1218 the expected decrease in Mg/Ca for *O. umbonatus* would be between ~0.3 mmol/mol (using the sensitivity of Lear et al. (2010) which is based on the calibration of Marchitto et al. (2007) and ~0.4mmol/mol (based on the calibration of Lear et al. (2002). Adding this to the 0.3 mmol/mol observed increase in ODP Site 1218 across the EOT (Lear et al. 2004, this study) produces a net Mg/Ca change of 0.6mmol/mol. Using the *C.wuellerstorfi* sensitivity of Elderfield et al. (2006) (0.0086 mmol/mol/μmol/kg) therefore indicates a saturation state increase of ~70 μmol/kg. Using the carbonate saturation state sensitivity estimated for *C.mundulus* (Raitzsch et al., 2008) would imply a saturation state increase of ~35 μmol/kg. This change is much larger than 19 μmol/kg which is an estimate for the change across the EOT using the equation of Broecker and Peng (1982) (Equation 15) assuming constant carbonate ion concentration with depth in the deep ocean and modern temperature and seawater chemistry. The degree to which equation 5 should be modified by taking into account differences in Palaeogene seawater chemistry (e.g. seawater Mg/Ca) is outside the scope of this project but is acknowledged as a limitation for comparing Palaeogene depth dependent sensitivities to the modern. However, warmer bottom water temperatures and lower seawater Mg/Ca would act to reduce the $[CO_3^{2-}]_{sat}$ -depth gradient and thus the calculated ΔCO_3^{2-} offsets here can be considered as maximum estimates.

$[CO_3^{2-}]_{SAT} = 90 \exp[0.16(z - 4)]$.

Where z = depth in kilometres

Equation 15

There are three potential factors that may have caused the benthic foraminiferal Mg/Ca increase across the EOT at the ODP Leg 199 sites: temperature, a (precipitation) carbonate saturation effect or dissolution. The large increase in $\delta^{18}O$ strongly argues against a temperature increase. A precipitation saturation state effect would imply a surprisingly high Mg/Ca-ΔCO_3^{2-} sensitivity for this semi-infaunal species. Furthermore it is difficult to account for the significantly larger Mg/Ca change observed in the deeper sites using this mechanism alone. Therefore it seems likely that an additional factor - dissolution - caused part of the Mg/Ca shift. Dissolution of foraminifera affects tests Mg/Ca as higher

magnesium calcite is preferentially dissolved (Brown & Elderfield, 1996). At the start of the EOT the CCD was shallower and thus the ODP Leg 199 sites would have been subject to the effects of dissolution working to reduce Mg/Ca of sedimented foraminiferal tests below the ratios expected for the temperature and carbonate saturation state conditions at the time. As the EOT progressed the CCD deepened which would have reduced the intensity of dissolution and thus led to an increase in Mg/Ca at these sites. The Mg/Ca records indicate that that the overall increase in Mg/Ca is largest for the deeper sites, ODP Site 1220 and ODP Site 1219 with a change in Mg/Ca of ~0.29 mmol/mol across Step 2 vs. 0.16 mmol/mol for ODP Site 1218 (Table 3-3). This supports a dissolution mechanism as the deeper sites will have been less saturated with respect to carbonate. In addition, benthic foraminiferal Mg/Ca continues to increase after the second isotope until ~33.6 Ma. Although the % carbonate records are relatively constant between Step 2 and 33.6 Ma (Figure 3-6), the carbonate mass accumulation rate appears to increase following Step 2 (Coxall et al., 2005) (Figure 3-13) perhaps supporting a saturation related mechanism for this later Mg/Ca increase.

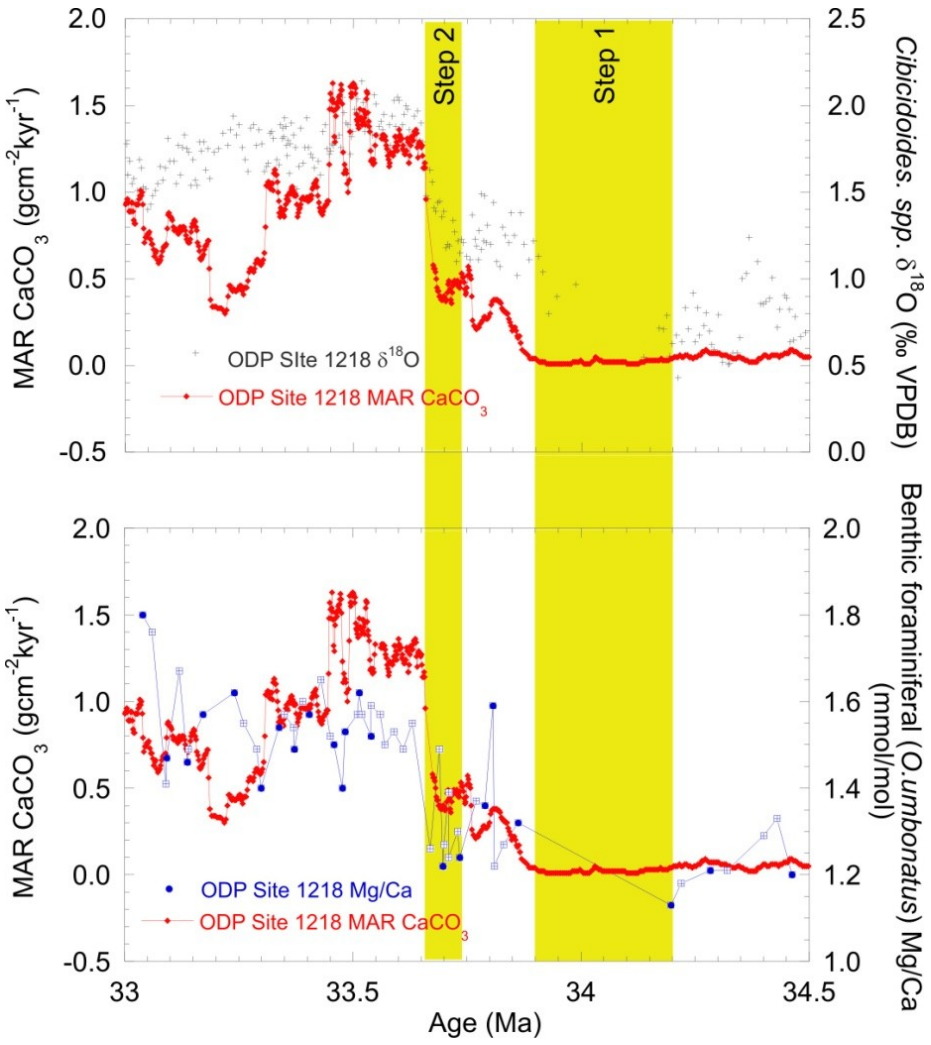

Figure 3-13 A) Mass accumulation rate of calcium carbonate across the EOT at ODP Site 1218 and benthic foraminiferal $\delta^{18}O$ from *Cibicidoides* spp. (Coxall et al., 2005). B) Mass accumulation rate of calcium carbonate across the EOT at ODP Site 1218 and ODP Site 1218 benthic foraminiferal Mg/Ca (Lear et al. (2004) and this study).

Intersite comparison

Mg/Ca is positively correlated with saturation state (Elderfield et al., 2006). Therefore there should be a negative relationship between Mg/Ca and palaeowater depth of the Leg 199 sites. This is due to the pressure effect on the solubility of $CaCO_3$, whilst temperatures at these depths are more or less constant.

Equation 15 can be used to estimate the decrease in calcite saturation state with depth if it is assumed that the carbonate ion concentration was constant below ~3.5 km (this is approximately the case in the modern (Figure 3-14).

If this assumption is correct then the saturation state differences between sites would be as follows; ODP Site 1220 and ODP Site 1219 have an estimated palaeowater depth difference of 100 metres and their ΔCO_3^{2-} difference should be 1.5 μmol/kg, ODP Site 1220 and ODP Site 1218 have an estimated palaeowater depth difference of 600 metres

and their ΔCO_3^{2-} difference should be 8.6 μmol/kg, ODP Site 1219 and ODP Site 1218 have a palaeowater depth difference of 500 metres and their ΔCO_3^{2-} difference should be 7.1 μmol/kg.

The sensitivity of Mg/Ca to ΔCO_3^{2-} determined using core top calibrations (Elderfield et al., 2006; Raitzsch et al., 2008) can then be used to predict the difference in Mg/Ca values between sites of differing palaeowater depth (Table 3-6).

	Difference in $\Delta[CO_3^{2-}]$ (μmol/kg)	Calculated ΔMg/Ca (Elderfield et al., 2006) (mmol/mol)	Calculated ΔMg/Ca (Raitzsch et al., 2008) (mmol/mol)	Measured offset in Mg/Ca (within step 2) (mmol/mol)
1218-1219	7.1	0.06	0.12	0.12
1218-1220	8.6	0.07	0.15	0.13
1219-1220	1.5	0.01	0.03	0.01

Table 3-6 Theoretical inter-site differences in carbonate saturation state based solely on pressure effects assuming modern seawater chemistry (Broecker and Peng, 1982) and associated Mg/Ca offsets based on core-top calibrations.

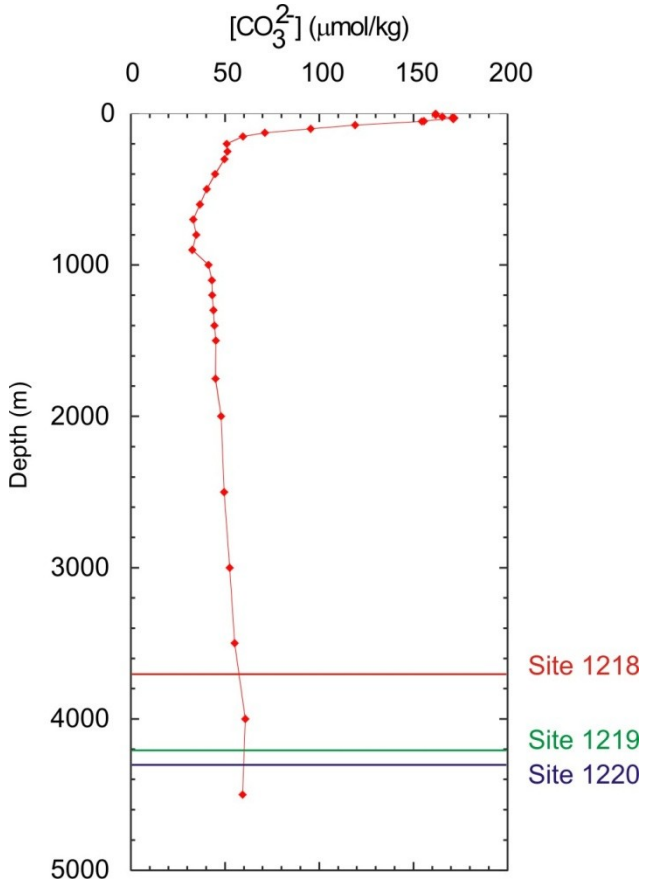

Figure 3-14 Modern day carbonate ion- depth profile from the Pacific Ocean with the ODP Leg 199 sites used in this study palaeowater depths indicated (data from WOCE station 70C Schlitzer, R, Ocean Data View, (2002).

The observed intersite Mg/Ca offsets are similar to those using the ΔCO_3^{2-}-Mg/Ca relationship of *C.mundulus*, an epifaunal species. However the applicability of this sensitivity to *O. umbonatus* is uncertain (Rathmann and Kuhnert, 2008). Conversely, using the observed Sites 1218-1219 and 1218-1220 Mg/Ca offsets and the estimated pressure related changes in carbonate saturation state (Table 3-6) results in a calculated ΔCO_3^{2-} – Mg/Ca sensitivity of 0.015 mmol/mol/μmol/kg for *O. umbonatus*. Interestingly, if this sensitivity is applied to the published Mg/Ca record from DSDP Site 522, which is assumed to be unaffected by dissolution, the assumed ~19 μmol/kg increase in saturation state associated with CCD deepening could potentially mask a 2.4°C cooling, in excellent agreement with the TDP records (Lear et al., 2008). However, this should be treated as a "ball park estimate" due to uncertainties in the nature of the $[CO_3^{2-}]$ depth profiles through time, and the simplified approach taken here which uses the modern ΔCO_3^{2-}-depth relationship of Broecker and Peng (1982).

A global synthesis of published benthic foraminiferal Mg/Ca EOT records is discussed in detail in section 4.4.

3.3.2 Li/Ca

Across the EOT interval

The increase in Li/Ca of 3 μmol/mol observed across the EOT at ODP Site 1218 can be interpreted as an increase in carbonate saturation state (Lear and Rosenthal, 2006) and/or a decrease in temperature as temperature and Li/Ca are inversely correlated (Marriott et al., 2004). Assuming no temperature change the Li/Ca change indicates a saturation state increase of 46μmol/kg. This is much larger than the theoretical value of 19 μmol/kg indicating that temperature change is also a factor. Conversely, if a saturation state change of 19μmol/kg is assumed, the Li/Ca-ΔCO_3^{2-} and Li/Ca-temperature sensitivities of Lear et al. (2010) predicts a temperature decrease of 2.9°C across the EOT. This is close to the expected magnitude of cooling at ODP Site 1218 and implies that calcite dissolution may not compromise Li/Ca-palaeothermometry to the same extent as Mg/Ca-palaeothermometry.

Intersite comparison

The predicted Li/Ca differences between the Leg 199 ODP sites are relatively small (Table 3-7). Because the sensitivity of Li/Ca to carbonate saturation state is small (0.047 μmol/mol/μmol/kg, Lear et al., 2010), the predicted offsets between ODP Sites 1219 and 1220 are not resolvable with current analytical capability. However, at the start of Step 2 there is a large (~2μmol/mol) offset between ODP Site 1220 and the other two sites. As this is much larger than the calculated offset (Table 3-7) it may potentially be caused by dissolution at the deeper site working to reduce Li/Ca values although such an effect would also be expected to affect the ODP Site 1219 record.

	Intersite difference in $\Delta[CO_3^{2-}]$ (µmol/kg)	Theoretical difference in Li/Ca Between sites using *Oridorsalis umbonatus* sensitivity. (µmol/mol)
1218-1219	7.1	0.33
1218-1220	8.6	0.40
1219-1220	1.5	0.07

Table 3-7 Predicted Li/Ca differences between ODP Leg 199 sites using the Li/Ca - ΔCO_3^{2-} sensitivity of Lear et al. (2010) for *Oridorsalis umbonatus*.

3.3.3 B/Ca

Across the EOT interval

The B/Ca data of ODP Site 1218 are too sparse to determine any trends across the EOT (Figure 3-10). The large change in saturation state that took place over the whole EOT with a theoretical bottom water increase in $[CO_3^{2-}]$ of 19 µmol/kg (using Equation 5 and assuming similar $[CO_3^{2-}]$ profiles) should have caused an increase in benthic foraminiferal B/Ca values. The predicted change is dependent upon the sensitivity used for example using the Yu and Elderfield (2007) sensitivities for *Cibicidoides wuellerstorfi* of 1.14 µmol/mol *per* µmol/kg and *Cibicidoides mundulus* of 0.69 µmol/mol per µmol/kg would produce B/Ca increases of 21 µmol/mol and 13 µmol/mol. Using the lower sensitivity of the shallow infaunal *Uvigerina* spp. (0.28 µmol/mol per µmol/kg) produces a change of 5.32 µmol/mol. A limited core-top data set suggests that *O. umbonatus* B/Ca is relatively insensitive to carbonate saturation state changes (Brown et al., 2011). Although the ODP Leg 199 B/Ca data are relatively noisy across the EOT, it is clear that the variability in all 3 records is only on the order of ~5-10 µmol/mol. This supports the proposed low sensitivity for *Oridorsalis umbonatus*.

Intersite comparison

The Leg 199 benthic foraminiferal B/Ca values are similar (~30-40 µmol/mol) across Step 2 of the EOT. Core-top B/Ca - ΔCO_3^{2-} sensitivities (Yu and Elderfield, 2007) may be used to calculate predicted intersite differences in B/Ca (Table 3-8).

	Intersite difference in $\Delta[CO_3^{2-}]$ (µmol/kg)	Theoretical difference in B/Ca Between sites using *Cibicidoides mundulus* sensitivity (µmol/mol)	Theoretical difference in B/Ca Between sites using *Uvigerina spp.* sensitivity (µmol/mol)
1218-1219	7.1	4.93	1.92
1218-1220	8.6	5.96	2.32
1219-1220	1.5	1.03	0.41

Table 3-8 Predicted B/Ca differences between ODP Leg 199 sites using the sensitivities of Yu and Elderfield (2007) for *Cibicidoides mundulus* and *Uvigerina* spp.

The predicted changes in B/Ca between ODP Sites 1219 and 1220 are smaller than the error associated with measuring B/Ca. This explains why ODP Site 1219 and ODP Site 1220 data are very similar. There is a larger saturation state difference between these two sites and ODP Site 1218 due to its much shallower palaeowater depth. The 1218 B/Ca record is too low resolution to calculate intersite offsets. However the limited data do not suggest a consistent offset of ~5 µmol/mol as predicted by the *Cibicidoides mundulus* calibrations. As discussed above therefore, it seems likely that *O. umbonatus* B/Ca has a relatively low sensitivity to ΔCO_3^{2-}.

3.3.4 U/Ca

Across the EOT interval

As discussed in the introduction (section 1.2.4) U/Ca in two species of benthic foraminifera (*Cibicidoides wuellerstorfi* and *Cibicidoides mundulus*) has been documented to have an inversely proportional relationship with carbonate saturation state (Raitzsch et al., 2011). If this is also the case for *Oridorsalis umbonatus*, then the U/Ca data indicates that carbonate saturation state is decreasing (Figure 3-11) across the EOT. Other evidence from these sites such as increasing carbonate mass accumulation rate,CCD deepening, % calcium carbonate and improved nannofossil preservation (Blaj et al., 2009) provide indisputable evidence that the saturation state of the eastern equatorial Pacific region increased across the EOT. If the U/Ca increases at the ODP Leg 199 sites were reflecting temperature, which is the case for some planktonic foraminifera (Yu et al., 2008) then the data would reflect a warming across the EOT. This seems unlikely across a glacial event and cooling has now been shown to have occurred in several other sites (Lear et al., 2008; Liu et al., 2010). Therefore a factor other than saturation state or temperature must be influencing the U/Ca values. Changes in oxygen levels in the pore waters can affect U/Ca levels in pore waters locally as lower oxygen levels lead to an increase in precipitation of uranium bearing authigenic material. However there is no other evidence to support changing levels in oxygenation at the seafloor across the EOT. It is proposed here that a dissolution effect reducing across the EOT is occurring. Prior to the EOT carbonate saturation state was low and thus the benthic foraminifera in this study were subject to higher levels of dissolution. Dissolution appears to preferentially remove high U/Ca (Russell et al., 2004; Yu et al., 2008). The decrease in element/Ca ratios is thought to be caused by heterogeneous distributions of elements in shells and preferential dissolution of parts of the shell enriched with these elements (Brown and Elderfield, 1996; Yu et al., 2008).

As the saturation state increased across the EOT dissolution would be reduced and so U/Ca values would increase. This is not a mechanism that is easily quantified. Further work beyond the scope of this project is required to better understand this process and this is discussed in more detail in Chapter 6. U/Ca could potentially be used as a proxy for

dissolution if more evidence to support preferential removal of U/Ca in undersaturated waters can be found.

Intersite comparison

ODP Site 1218 has higher U/Ca than ODP Sites 1219 and 1220 (Figure 3-11). If the Raitzsch et al. (2011) calibration is followed then this would imply that ODP Site 1218 has a lower saturation state than ODP Sites 1219 and 1220. However this is inconsistent with carbonate and microfossil evidence. Dissolution may explain this if areas of high U/Ca calcite dissolve preferentially. It is unlikely that there are O_2 concentration differences large enough between the sites to cause ODP Site 1218 to have higher U/Ca than ODP Sites 1219 and 1220, thus supporting a dissolution mechanism as a control on U/Ca values.

3.3.5 Sr/Ca

Across the E/O transition

ODP Site 1218 Sr/Ca data are similar in value before and after the EOT. This indicates that either Sr/Ca is not greatly affected by saturation state and temperature changes across the interval or that the effects of these parameters have cancelled each other out. However between Step 1 and Step 2 ODP Site 1218 Sr/Ca decreases by 0.07 mmol/mol. This change is not observed in other proxies. Across Step 2 and beyond a rapid decrease is seen in ODP Site 1219 and ODP Site1220 Sr/Ca. This trend is not observed at ODP Site 1218 ruling out changing seawater Sr/Ca as a causal mechanism. The negative change in ODP Site 1219 and ODP Site 1220 is unlikely to be caused by dissolution as this should cause a positive trend across the EOT as saturation state increased. This trend in Sr/Ca cannot be explained from currently known geochemical/oceanographic effects.

Intersite comparison

Modern and Eocene depth transects display a clear empirical relationship between increasing water depth and decreasing Sr/Ca on the order of 0.1 mmol/mol/km (e.g. Lear et al., 2003). The exact causal mechanism for this is unknown, although pressure-related effects have been implicated. The Sr/Ca records in the interval immediately following Step 2 conform to this expected relationship, however within Step 2 the ODP Site 1219 and 1220 Sr/Ca ratios are higher than the ODP Site 1218 ratios. This points to an additional unknown factor operating in this time window at deeper sites.

3.4 Comparison of ODP Leg 199 geochemical records across the EOT to those of other sites.

3.4.1 Discussion of Mg/Ca data from other sites across the EOT

The EOT has been proven to be a global event documented at many marine and terrestrial sites. Isotope data from these sites are in general agreement with Coxall et al. (2005).

Mg/Ca data from other sites may be of use when interpreting data from Leg 199 in terms of temperature change across the EOT. The primary aim of this section is to discuss the published Mg/Ca data from other sites in terms of paleoceanographic setting and draw comparisons to ODP Leg 199 data. The sites with benthic foraminiferal trace metal data across the EOT are illustrated on a global map for reference (Figure 3-15) and their palaeowater depths are listed in Table 3-9. Not all sites are discussed. The shallower shelf-slope sites (Tanzania and St Stephens Quarry) are not included as these records are not directly comparable with the other sites due to their paleoceanographic setting and the benthic foraminiferal species used. Records considered too low resolution to compare to other records (e.g. ODP Site 757 from Billups and Schrag, 2003) are also excluded.

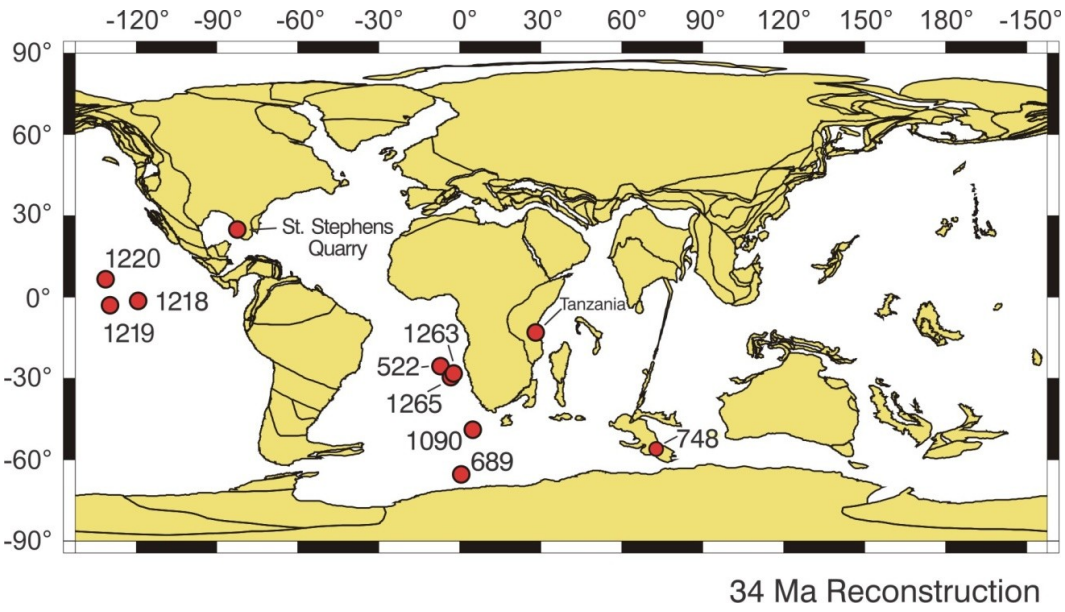

Figure 3-15 ODP/DSDP Site locations of the EOT sections compared in this study with their approximate positions at 34Ma plotted on a palaeogeographic reconstruction from the Ocean Drilling Stratigraphic Network (Bohaty et al., 2012). The two shallow slope-shelf sites TDP; (Lear et al., 2008) and St Stephen Quarry (Katz et al., 2008) are not compared in this discussion due to their shallow setting but are included on this map.

DSDP/ODP Leg	Site	location	Paleodepth (m)	Reference for Mg/Ca data	Reference for Li/Ca data	Reference for $\delta^{18}O$ data	Reference for $\delta^{13}C$ data	Species used for Mg/Ca
199	1220	Eq. Pacific	4300	This study		n/a	n/a	*O.umbonatus*
199	1219	Eq. Pacific	4200	This study		n/a	n/a	*O.umbonatus*
199	1218	Eq. Pacific	3700	This study/Lear et al. (2004)	Lear and Rosenthal (2006)	Coxall et al. (2005)	Coxall et al. (2005)	*O.umbonatus*
177	1090	South Atlantic	3200	Pusz et al. (2011)		Pusz et al. (2011)	Pusz et al. (2011)	*Cibicidoides* spp.
73	522	South Atlantic	3100	Lear et al. (2000)		Lear et al. (2000)	Lear et al. (2000)	*O.umbonatus*
208	1265	South Atlantic	2400	Pusz et al. (2011)		Pusz et al. (2011)	Pusz et al. (2011)	*Cibicidoides* spp.
208	1263	South Atlantic	2100	Peck et al. (2010)	Peck et al. (2011)	Reisselman et al. (2007)	Peck et al. (2010)	*O.umbonatus*
113	689	Weddell Sea	1500	Bohaty et al. (2012)		Bohaty et al. (2012)	n/a	*Cibicidoides* spp.
120	748	Southern Ocean	800	Bohaty et al. (2012)		Bohaty et al. (2012)	n/a	*Cibicidoides* spp.

Table 3-9 ODP sites with published records across the EOT assessed in this study with their palaeowater depths and published references.

3.4.2 Stable isotope data

Differences in global climate (Zachos et al., 2001), continental configuration (Figure 3-16) and ocean circulation (e.g. Cramer et al., 2009; Via and Thomas, 2008) preclude the use of modern bottom water temperatures to estimate inter-basinal temperature gradients. Therefore it is preferable to use the $\delta^{18}O$ records available for each site. The global ice volume component of the $\delta^{18}O$ signal should be equal at all sites. Inter-basinal salinity variations are assumed to be minimal although it is worth noting that today Antarctic Bottom Water (AABW) and North Atlantic Deep Water (NADW) impart a similar $\delta^{18}O$ signal despite their 2^{o}C temperature contrast. The potential presence of "warm saline deep water" in the Palaeogene further complicates interpretation of the EOT $\delta^{18}O$ records (Woodruff and Savin, 1989; Cramer et al., 2009). Nevertheless this is a worthwhile exercise to obtain a first order interpretation of the Mg/Ca records. The differences in temperature indicated by the $\delta^{18}O$ should also be reflected in the Mg/Ca data. Therefore a comparison of the available geochemical records from benthic foraminifera across the EOT provides a good test for the Mg/Ca paleotemperature proxy with the potential advantage of also reconstructing water masses properties. Differences in carbon isotope values between the sites may provide further insights into water mass chemistry.

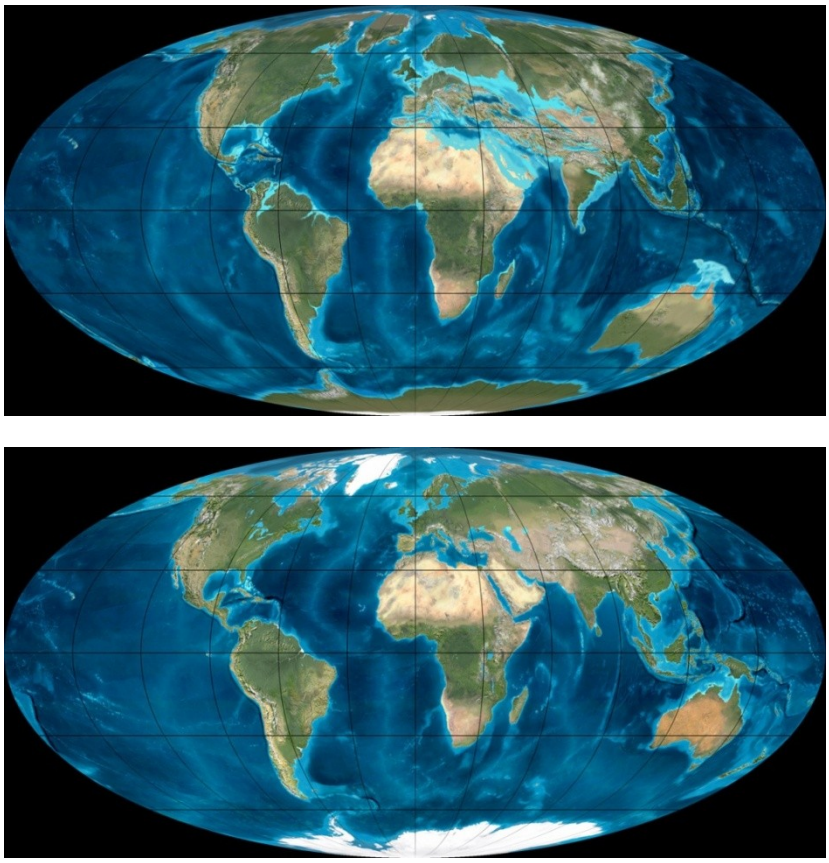

Figure 3-16 Palaeogeography of Earth in the early Oligocene (top) and present day (bottom) Maps from Ron Blakey, Colorado Plateau Geosystems, Inc.

3.4.3 $\delta^{18}O$ records

Between Sites

Benthic foraminiferal $\delta^{18}O$ values range by approximately 1‰ between the deep water sites (Figure 3-17). The $\delta^{18}O$ values vary with water depth and site location. The $\delta^{18}O$ of the sites at 33.25 Ma are compared in Table 3-10. This age was chosen as it is after the EOT and thus small offsets caused by imperfect site to site correlations will not be affected by large $\delta^{18}O$ changes over small intervals. The 33.25 Ma interval will be used below as a point of reference for comparison of Mg/Ca records assuming the $\delta^{18}O$ differences between the sites primarily reflect the inter-site temperature differences. Using this logic the sites in order of temperature from low to high are; ODP Site 748, ODP Site 689, ODP Site 522, ODP Site 1090, ODP Site 1265, ODP Site 1263 and ODP Site 1218. This is not directly related to paleowater depth as may be expected (Table 3-10) and therefore must be also related to geographical location. ODP Site 748 and ODP Site 689 are high latitude Southern Ocean sites (Figure 3-16) and therefore it may be expected that these sites would have colder deep water temperatures. The sites from the South Atlantic (ODP Site 1090, ODP Site 1265, DSDP Site 522 and ODP Site 1263 have similar $\delta^{18}O$ values and seem to follow a general trend of decreasing $\delta^{18}O$ with decreasing palaeowater depth (Figure 3-16). ODP Site 1263 $\delta^{18}O$ value is 0.5‰ lower than the DSDP Site 522 which has the highest $\delta^{18}O$ in the South Atlantic sites. This can be explained by ODP Site 1263's shallower palaeowater depth. ODP Site 1218 has the lowest $\delta^{18}O$ values indicating that it is the warmest and/or freshest despite its deep palaeowater depth. ODP Site 1263 and ODP Site 1218 have very similar $\delta^{18}O$ values despite having different water depth. This makes them ideal for comparison of trace metal records.

ODP/DSDP site	$\delta^{18}O$ at 33.25 Ma (‰)	Palaeowater depth (m)
748	2.6	800
689	2.4	1500
522	2.3	3100
1090	2.2	3200
1265	2.0	2400
1263	1.8	2100
1218	1.7	3700

Table 3-10 $\delta^{18}O$ values for deep water sites at 33.25 Ma. ODP Site 1263 is species corrected using the offset of Coxall et al. (2011) for *O. umbonatus*.

Across the EOT

Across the EOT the different sites have a similar trend in their $\delta^{18}O$ records which appear to be mostly in phase (ODP Site 689 and ODP Site 748 lag slightly across Step 1 but this

is attributed to be age model discrepancies rather than a regional signal). This indicates that the EOT was a global event and the deep water temperature changes which accompanied ice growth were similar in different ocean basins. The Step 1 $\delta^{18}O$ increase is ~0.6 ‰ and the Step 2 increase ~0.9 ‰ giving a total increase across the EOT of 1.5 ‰.

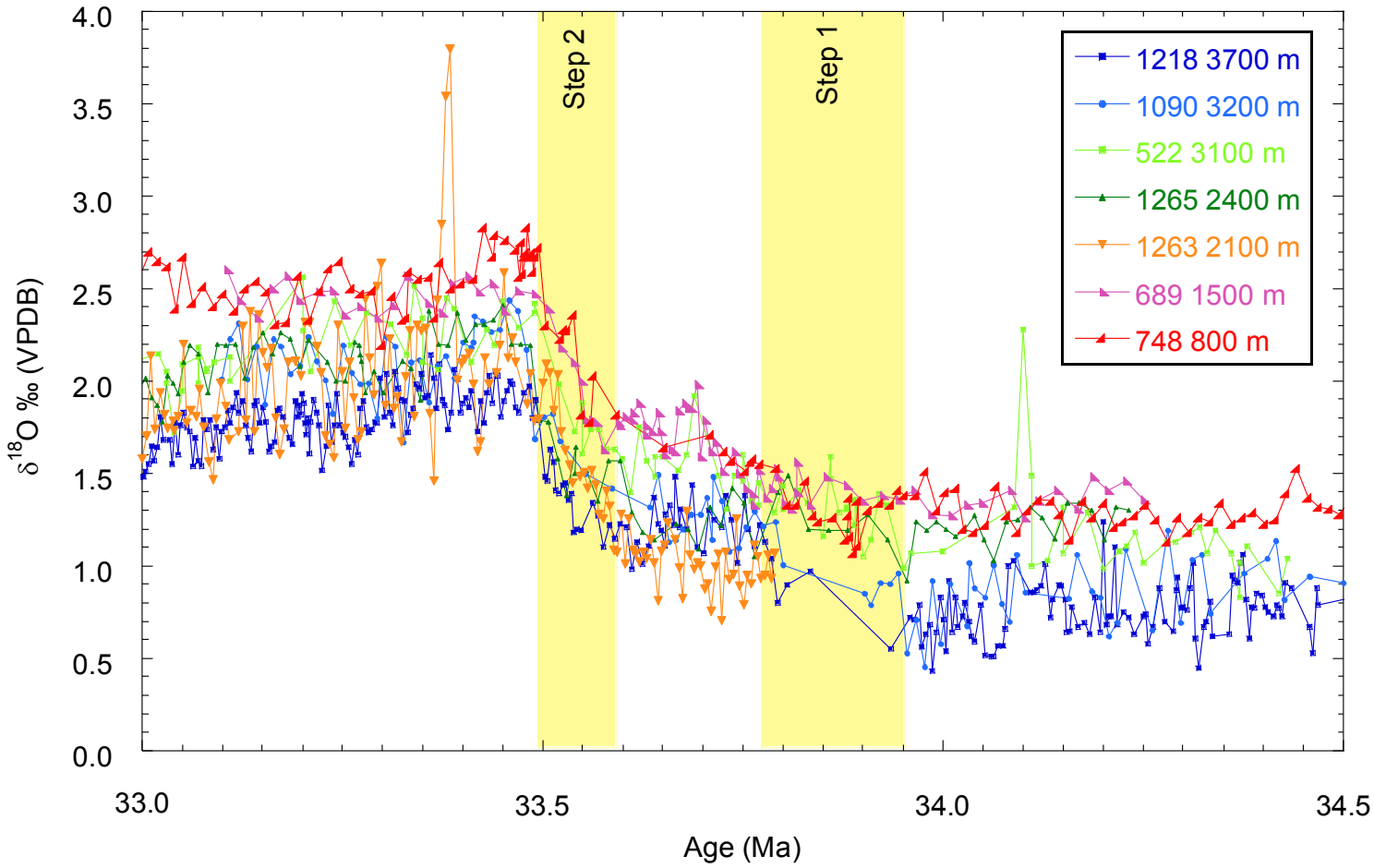

Figure 3-17 Benthic foraminiferal $\delta^{18}O$ records across the EOT (*Cibicidoides* spp. except ODP Site 1263 (*Oridorsalis umbonatus* which was corrected using the factors in Coxall et al. (2011)). Age scale is that of Cande and Kent (1995). Sources are given in Table 3-9.

δ^{13}C records

Between sites

Benthic foraminiferal δ^{13}C values range by approximately 1.2 ‰ between the deep water sites (Figure 3-18). The variability between sites is related to the water masses which overlay each site and differences in local productivity. The difference in δ^{13}C between sites is not directly relatable to changes in trace metal geochemistry yet they may provide an indication of water mass “ageing” and hence relative carbonate saturation state.

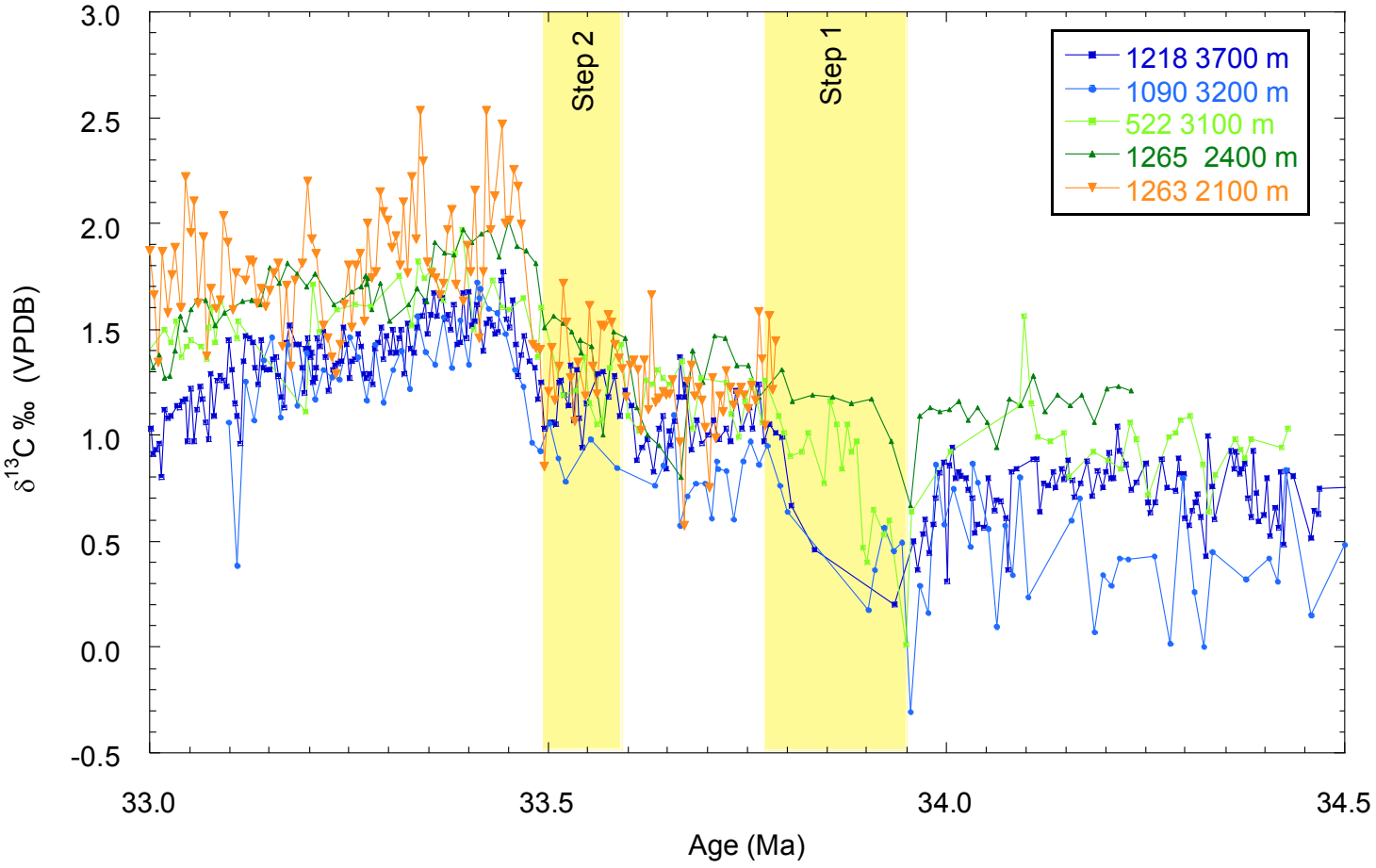

Figure 3-18 Benthic foraminiferal $\delta^{13}C$ records across the EOT (*Cibicidoides* spp. except ODP Site 1263 (*Oridorsalis umbonatus* which was corrected using the factors in Coxall et al. (2011)). Age scale is that of Cande and Kent (1995). Sources are given in Table 3-9.

Mg/Ca records

The Mg/Ca records from the various sites which cover the EOT are either from the benthic foraminiferal species *Oridorsalis umbonatus* or *Cibicidoides* spp. As these foraminifera likely have different sensitivities to temperature the Mg/Ca records will be considered separately. As discussed in section 3.3.1, the Mg/Ca records from the Leg 199 EOT palaeowater depth transect suggest that the *C.mundulus* (Raitzsch et al., 2008) Mg/Ca - ΔCO_3^{2-} sensitivity may be more appropriate than the *C.wuellerstorfi* sensitivity (Elderfield et al., 2006) for *O. umbonatus.* The (Raitzsch et al., 2008) sensitivity is therefore used in the following discussion on inter-site Mg/Ca offsets. As noted in section 3.3.1 this sensitivity was assessed using the modern $[CO_3^{2-}]_{SAT}$-depth relationship (Broecker and Peng, 1982). Nevertheless because the $[CO_3^{2-}]_{SAT}$-depth relationship can be assumed to be constant for different ocean basins (i.e. relatively small temperature contrasts and constant seawater Mg/Ca), this provides a useful tool for assessing intersite differences in relative carbonate saturation state.

Oridorsalis umbonatus

The sites for which *O.umbonatus* Mg/Ca data are available comprise of two regional water depth transects: the equatorial Pacific (ODP Sites 1218, 1219 and 1220) and Walvis Ridge (ODP Sites 522 and 1263) (Figure 3-19). There are large offsets in the Mg/Ca records between the sites (Figure 3-19). Briefly both Walvis ridge sites have higher Mg/Ca than the equatorial Pacific sites, and there is a larger Mg/Ca offset between the shallower Walvis Ridge sites than the deep equatorial Pacific sites. The extent to which these Mg/Ca offsets can be interpreted in terms of temperature and carbonate saturation state is explored below, with implications for the proposed “dissolution mechanism”.

Walvis Ridge Sites

Benthic foraminiferal $\delta^{18}O$ at the shallowest Walvis Ridge Site, ODP Site 1263, is about 0.5 ‰ lighter than the deepest Walvis Ridge Site, DSDP Site 522 (Table 3-10). This can be interpreted as a ~2-3 ^{o}C temperature offset between the sites. Using the *O. umbonatus* Mg/Ca temperature sensitivity used by Lear et al. (2010) results in an expected Mg/Ca offset of 0.28 mmol/mol, leaving a residual offset of 0.22 mmol/mol between these two Walvis Ridge sites. The Mg/Ca-ΔCO_3^{2-} sensitivity of shallow infaunal *C. mundulus* (Raitzsch et al., 2008) translates this Mg/Ca residual offset into a saturation state difference of ~13 μmol/kg. Put into context, in the modern day, assuming constant $[CO_3^{2-}]$, pressure effects alone would cause a saturation state difference of ~12 μmol/kg between these two sites.

Equatorial Pacific Sites

As discussed in section 4.3.1 the Mg/Ca offsets between the Leg 199 sites are similar to those expected if the Raitzsch et al. (2008) *C. mundulus* Mg/Ca-ΔCO_3^{2-} sensitivity is used

and about twice as large as expected if the Elderfield et al. (2006) *C. wuellerstofi* Mg/Ca-ΔCO_3^{2-} sensitivity is used.

Walvis Ridge-Equatorial Pacific

ODP Sites 1218 and 1263 provide a useful comparison as they have a similar $\delta^{18}O$ despite a ~1600 m difference in water depth between the two sites. Mg/Ca at the shallow Walvis Ridge site is ~1.02 mmol/mol higher than that at the deepest Pacific site. Using the *C. mundulus* Mg/Ca-ΔCO_3^{2-} sensitivity of Raitzsch et al. (2008) translates this Mg/Ca offset into a carbonate saturation state difference of 60 μmol/kg between the two sites.

ODP Site 1263 *O.umbonatus* Li/Ca is approximately 2-3 μmol/mol higher than that at ODP Site 1218 (Figure 3-20) (Lear and Rosenthal, 2006; Peck et al., 2011). Using the Li/Ca-ΔCO_3^{2-} sensitivity derived from core-top *O. umbonatus* from the Norwegian Sea (Lear et al., 2006; Lear et al., 2010) implies a carbonate saturation state difference of ~40-60 μmol/kg. Although there are assumptions associated with this approach (e.g. the lack of a regional salinity component in the $\delta^{18}O$ records), the results nevertheless lend some support to the *O. umbonatus* Mg/Ca-ΔCO_3^{2-} being similar to the *C. mundulus* Mg/Ca-ΔCO_3^{2-} sensitivity determined by Raitzsch et al. (2008) (0.017 mmol/mol/μmol/kg). Interestingly the magnitude of the interbasinal difference in saturation state estimated here implies a difference in water mass chemistry, such that the water mass bathing ODP Site 1218 had a lower [CO_3^{2-}] than that bathing Walvis Ridge. This is consistent with the interbasinal offsets in $\delta^{13}C$, as the more negative values at ODP Site 1218 imply an "older" water mass. The implication of this interpretation is that no "dissolution mechanism" is required to explain the large offset between the ODP Site 1263 and 1218 Mg/Ca records. By extension, this means that the "dissolution mechanism" proposed here to explain the overall Mg/Ca increase across the entire EOT at ODP Site 1218 must affect only the early part of the climate transition. The dissolution hypothesis would therefore predict a larger offset in Mg/Ca between ODP Site 1263 and ODP Site 1218 records prior to the transition. Although there are no trace metal data from Site 1263 prior to Step 2 of the EOT, the ODP Site 1218 Mg/Ca record can instead be compared to the other Walvis Ridge site, DSDP Site 522. This does support the dissolution hypothesis as the magnitude of the ODP Site 1218-522 Mg/Ca offset just prior to the EOT is larger than that following Step 1 of the EOT (Figure 3-19).

Site	Palaeowater depth	Modern [CO_3^{2-}] required for saturation	$\delta^{18}O$ at 33.25	*Cibicidoides* spp. Mg/Ca at 33.25 Ma	*O.umbonatus* Mg/Ca at 33.25
1220	4300	94	-	-	-
1219	4200	93	-	-	-
1218	3700	86	1.7	-	1.52
1090	3200	79	2.2	0.78	-
522	3100	78	2.3	-	1.91
1265	2400	70	2.0	1.85	-
1263	2100	66	1.8	-	2.5
689	1500	60	2.4	1.59	-
748	800	54	2.6	1.37	-

Table 3-11 Deep ocean sites palaeowater depth, modern [CO_3^{2-}] required for the site to be at saturation (calculated using Broecker and Peng, 1982), $\delta^{18}O$ and Mg/Ca values at 33.25 Ma. Sources are given in Table 3-9.

***Cibicidoides* spp.**

The offsets between the different sites using *Cibicidoides* spp. are not as large as those observed in those using *O. umbonatus* with the marked exception of ODP Site 1090 which has much lower Mg/Ca than the other sites (Figure 3-21). The three sites with similar Mg/Ca values are ODP Site 689 (Maud Rise), ODP Site 748 (Kerguelen Plateau) and ODP Site 1265 (Walvis Ridge). ODP Site 689 and ODP Site 748 have $\delta^{18}O$ values approximately ~0.5‰ heavier than the deeper ODP Site 1265. The similar Mg/Ca ratios at these three sites despite the ~0.5 ‰ $\delta^{18}O$ offset likely reflects a relatively subtle combination of temperature and saturation state effects on the Mg/Ca ratio and salinity effects on the $\delta^{18}O$ record.

In marked contrast ODP Site 1090 Mg/Ca is lower than the other sites by approximately 0.6 mmol/mol. The $\delta^{18}O$ values do not indicate that this site is colder than ODP Sites 757 or 689 and it has only a slightly lower $\delta^{18}O$ than ODP Site 1265 (~0.2 ‰). Therefore it seems likely that the bottom water mass at ODP Site 1090 had a lower saturation state compared to the other sites (e.g. 35-70 μmol/kg using the Elderfield et al. (2006)/Raitzch et al. (2008) calibrations). Using Equation 15 suggests approximately 10 μmol/kg of this can be attributed to pressure effects. Therefore it seems that ODP Site 1090 was bathed by a water mass with significantly lower [CO_3^{2-}] than ODP Sites 1263, 689 and 748. At first this seems surprising given the geographical location of ODP Site 1090, lying between Maud Rise and Walvis Ridge. However, independent evidence in the form of neodymium isotopes supports this view (Scher and Martin, 2006). In their work they find that ε_{Nd} of fish teeth at ODP Site 1090 do not have intermediate values between their North Atlantic and Maud Rise sites. Instead Site 1090 appears to contain a “Pacific” type signal which strengthens with the apparent influx of waters through Drake Passage in the Eocene. Further support for ODP Site 1090 receiving a Pacific sourced water mass lies in the relatively negative $\delta^{13}C$ values which are more similar to equatorial Pacific ODP Site 1218 than the Walvis Ridge sites (Figure 3-18).

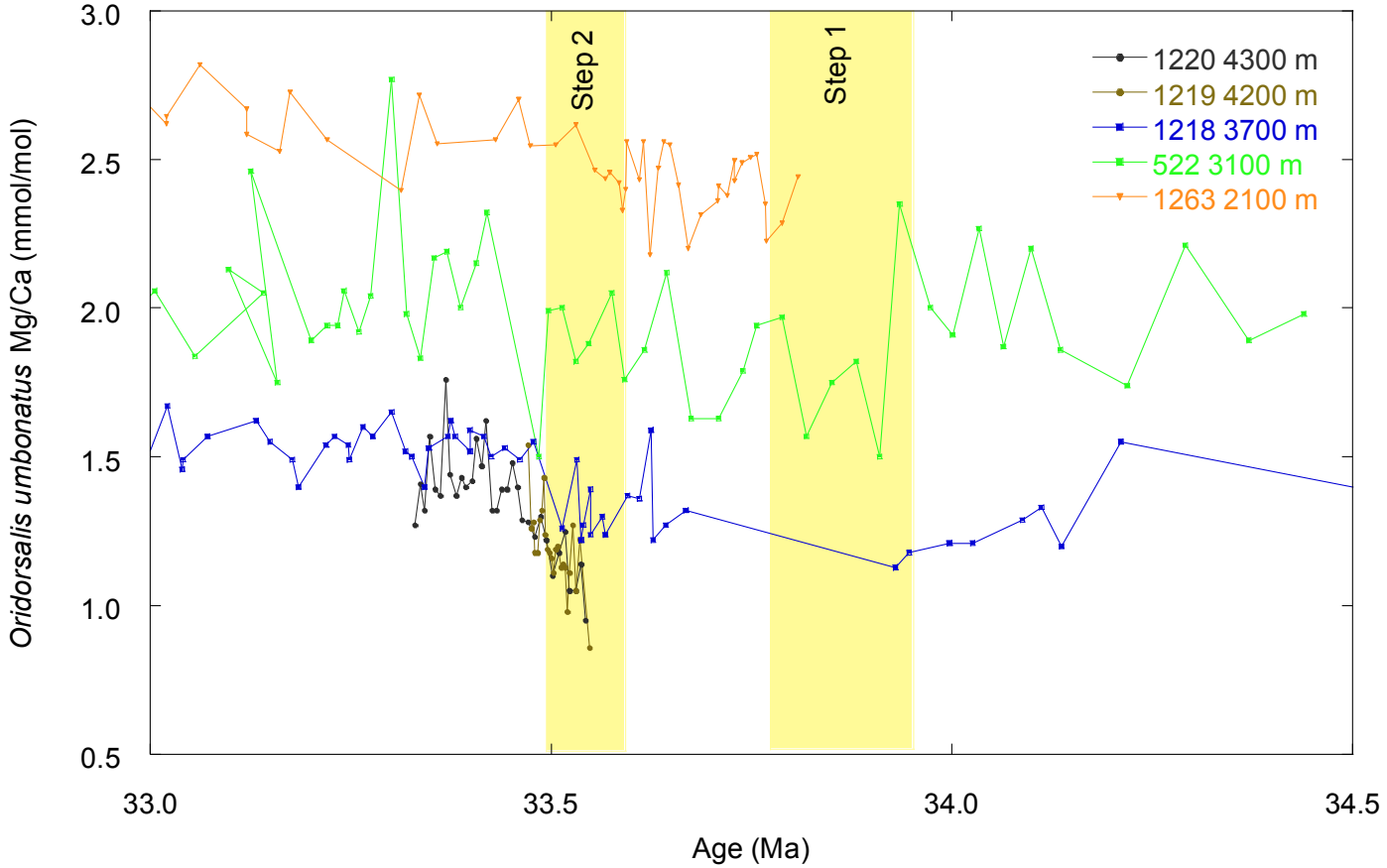

Figure 3-19 Benthic foraminiferal (*Oridorsalis umbonatus*) Mg/Ca records across the EOT. Age scale is that of Cande and Kent (1995). Sources are given in Table 3-9.

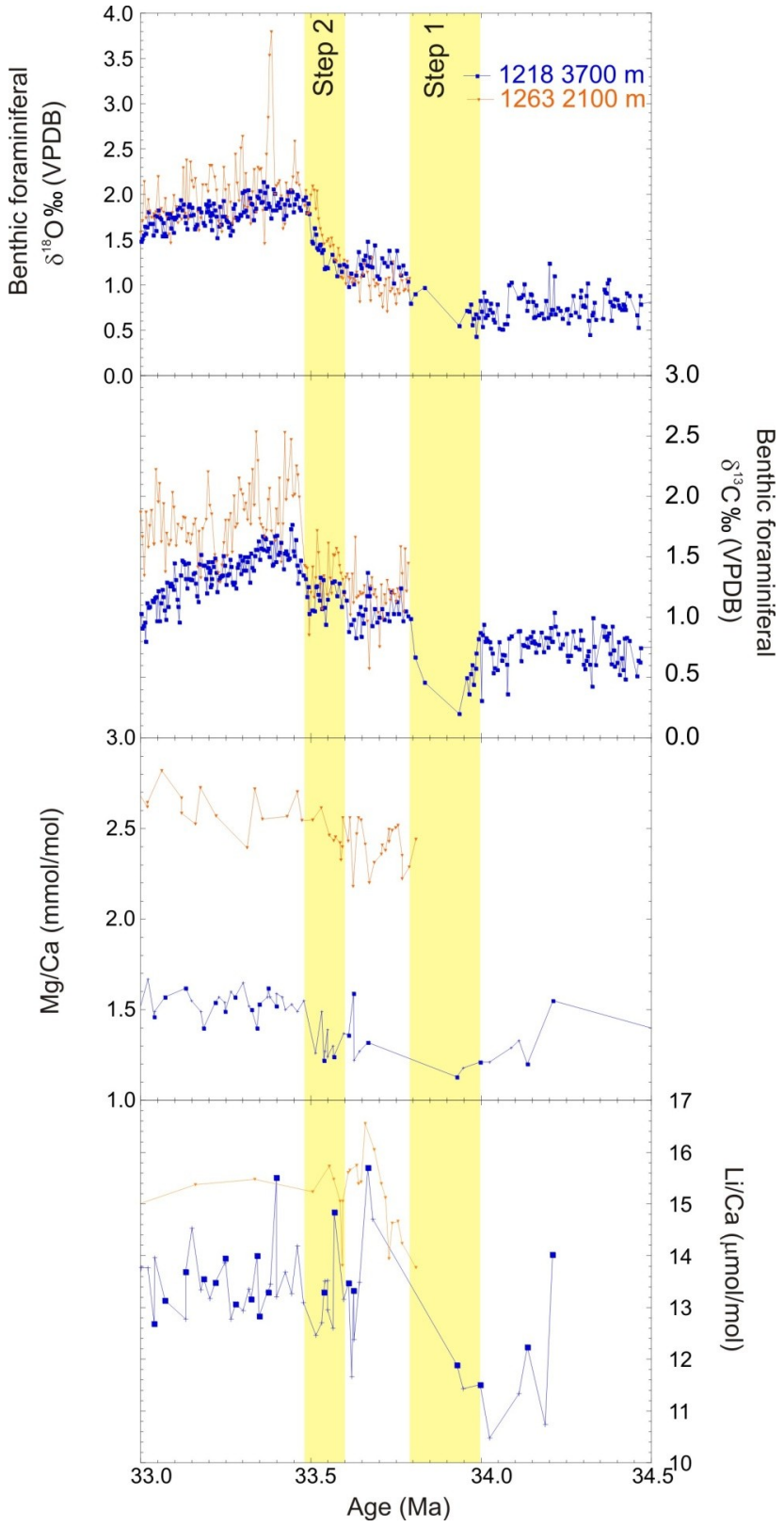

Figure 3-20 ODP Site 1218 and ODP Site 1263 comparison. Stable isotope data, ODP Site 1218 from *Cibicidoides* spp. (Coxall et al., 2005), ODP Site 1263 from *Oridorsalis umbonatus* (Reisselman et al., 2007), Mg/Ca and Li/Ca for both sites from *Oridorsalis umbonatus* (ODP Site 1218 this study and Lear and Rosenthal, 2006, ODP Site 1263 Peck et al., 2011). Age scale is Cande and Kent. (1995).

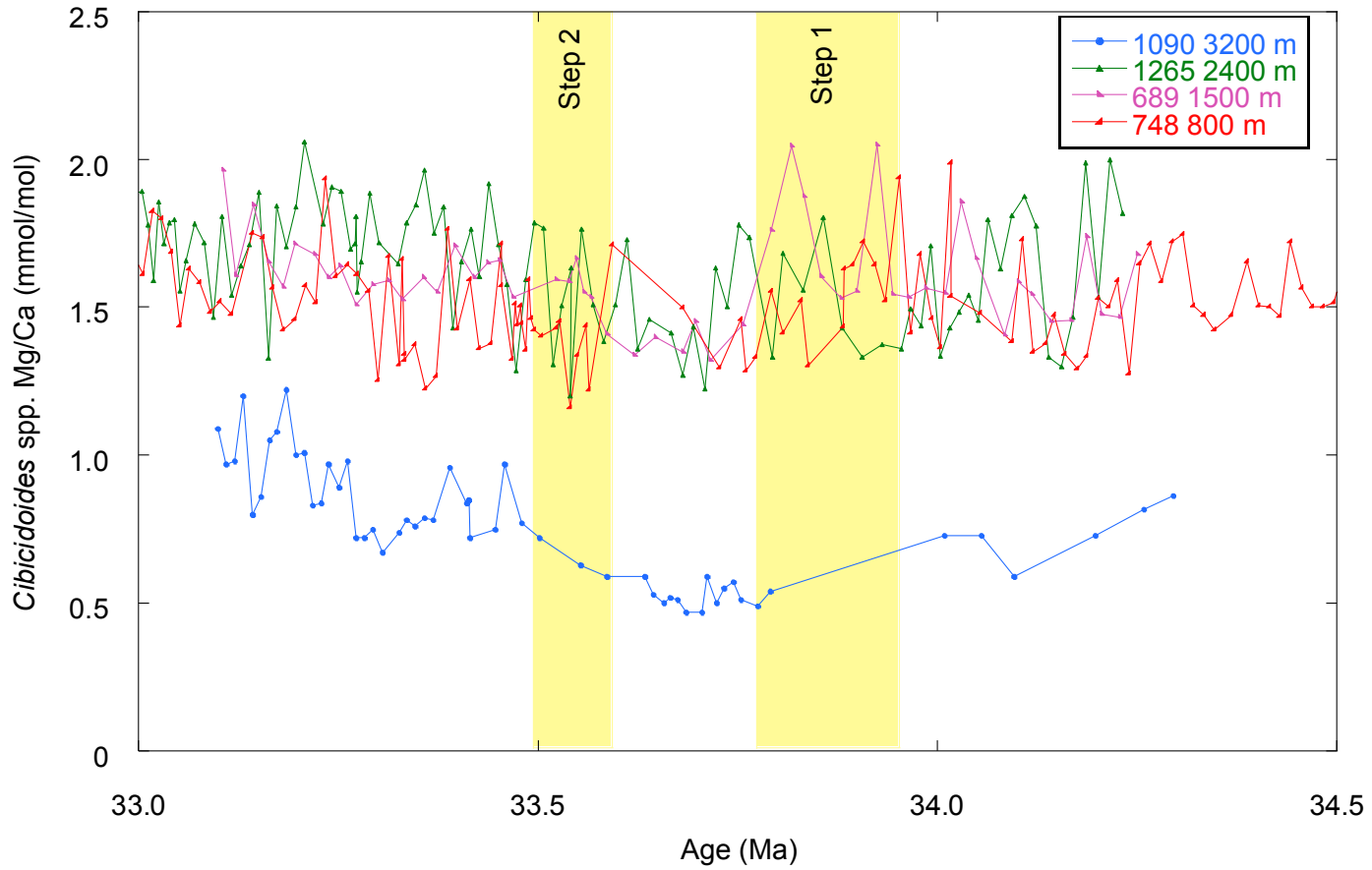

Figure 3-21 Benthic foraminiferal (*Cibicidoides* spp.) Mg/Ca records across the EOT Age scale is that of Cande and Kent (1995). Sources are given in Table 3-9.

3.5 Chapter conclusions

1. Eocene-Oligocene inter-site Mg/Ca offsets confirm a saturation state effect in *O. umbonatus* despite its assumed semi-infaunal habitat. One possibility is that at this time *O. umbonatus* may have had a more epifaunal habitat (Coxall and Wilson, 2011). This study suggests that the core-top Mg/Ca-ΔCO_3^{2-} calibration of *C. mundulus* (Raitzsch et al., 2008) is more appropriate than *C. wuellerstorfi* (Elderfield et al., 2006) for *O. umbonatus*.

2. The new Mg/Ca-ΔCO_3^{2-} relationship proposed here produces a ~2.5°C cooling at DSDP Site 522, which is in excellent agreement with the Tanzanian Drilling Project site cooling (Lear et al., 2008).

3. The saturation state sensitivity estimated here cannot explain the entire Mg/Ca increase at ODP Site 1218, leaving a residual (~0.4 mmol/mol) that may have been caused by a dissolution affect.

4. The dissolution affects ODP Site 1218 at Step 1 and ODP Site 1219 and 1220 at Step 2. The % calcium carbonate increased above 5% during Step 1 at ODP Site 1218 and during Step 2 at ODP Sites 1219 and 1220.

5. ODP Leg 199 records U/Ca across the EOT also support the dissolution hypothesis as U/Ca increases across the EOT despite being shown to be negatively correlated with saturation state (Raitzch et al., 2011). Further work using deeper core-top U/Ca values may establish whether U/Ca is affected by dissolution and enhance its ability to determine whether a site has undergone dissolution when coupled with other trace metal proxies.

6. Li/Ca changes across the EOT at ODP Site 1218 indicate bottom water cooling of ~3°C across the EOT. This value is consistent with shallow shelf-slope estimations. This indicates that ODP Site 1218 Li/Ca is not affected by dissolution in the same way as Mg/Ca which is potentially related to how the metals are incorporated into the test calcite.

7. Inter-site Mg/Ca offsets can be used to pick out water masses with significantly different carbonate chemistry. It appears that at the time of the EOT the equatorial Pacific was bathed by a water mass with a lower saturation state than the South Atlantic. This is the first time that the relative carbonate saturation state of different water masses has been examined using trace metal geochemistry beyond the Pleistocene.

8. Further work could also focus on applying the B/Ca proxy with other trace metals to new sites with more continuous sections such as those from the recent IODP PEAT (Pacific Equatorial Age Transect) cruise.

4 Mi-1

The primary aim of this chapter is to explore trace metal chemistry changes in benthic foraminiferal calcite across the major transient glaciation event close to the Oligocene/Miocene boundary. The secondary aim is to further explore the effect of depth related saturation state changes on two deep sea benthic foraminifera's chemistry. This has been achieved by measuring trace metal concentrations in late Oligocene to early Miocene benthic foraminifera from two sites of different paleodepths in the western tropical Atlantic.

4.1 Introduction

4.1.1 The Mi-1 event at the Oligocene-Miocene boundary

Mi-1 is an orbitally paced transient glacial event that occurs across the Oligocene/Miocene boundary as denoted by changes in $\delta^{18}O$ and $\delta^{13}C$ (Miller et al., 1991; Zachos et al., 1997; Paul et al., 2000; Pälike et al., 2006b) as discussed in Chapter 1. The highest resolution stable isotope record of this event is that from ODP Leg 154 drilled in the western tropical Atlantic on Ceara Rise (Pälike et al., 2006b) (Figure 4-1). These records show a ~1‰ increase in $\delta^{18}O$ (Figure 4-2) and ~0.8‰ increase in $\delta^{13}C$ (Figure 4-3) between 23.25 Ma and 23.02 Ma (Pälike et al., 2006b). The benthic foraminiferal $\delta^{13}C$ increase is preceded by an initial negative excursion that marks the base of the $\delta^{18}O$ rise. The excursions are followed by a recovery interval during which $\delta^{18}O$ values return to just above pre-event values (Figure 4-2). It is this $\delta^{18}O$ recovery that distinguishes Mi-1 from the EOT, the latter being characterised by a semi permanent increase in $\delta^{18}O$ and thus, global ice volume. Benthic foraminiferal $\delta^{13}C$ values recover, but similarly to $\delta^{18}O$, to a new baseline that is slightly higher than pre-Mi-1 event values (Figure 4-3). The records are against an astronomical age solution (Laskar et al., 2004). This results in a robust age model and simplified correlation between ODP Sites 926 and 929. High resolution stable isotope records have been produced for these two sites (Pälike et al., 2006b) and are used in this study.

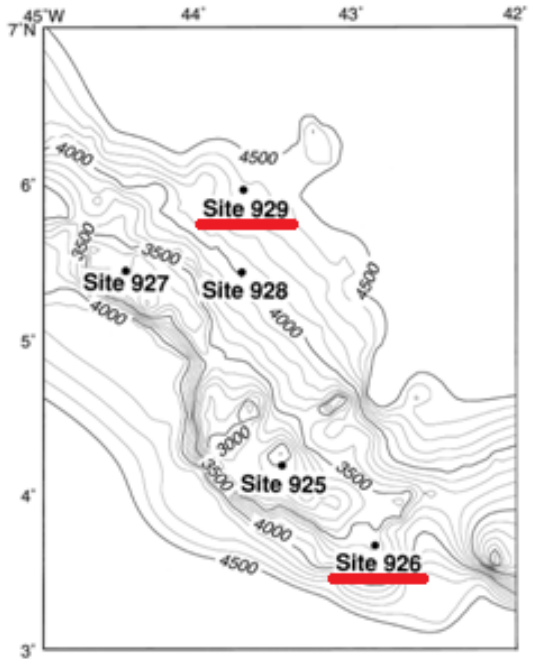

Figure 4-1 ODP Leg 154 sites drilled on Ceara Rise in the western tropical Atlantic (from ODP Leg 154 Shipboard Scientific party, 1995). Sites examined in this study are underlined.

ODP Site	Modern water depth (m)
926	3598
929	4356

Table 4-1 Modern water depths of the ODP sites used in this study across Mi-1 (after ODP Leg 154 Shipboard Scientific Party, 1995). The modern water depths are used as paleodepth estimates as Ceara Rise is thought to have undergone little subsidence from the late Oligocene to Present (Paul et al., 2000).

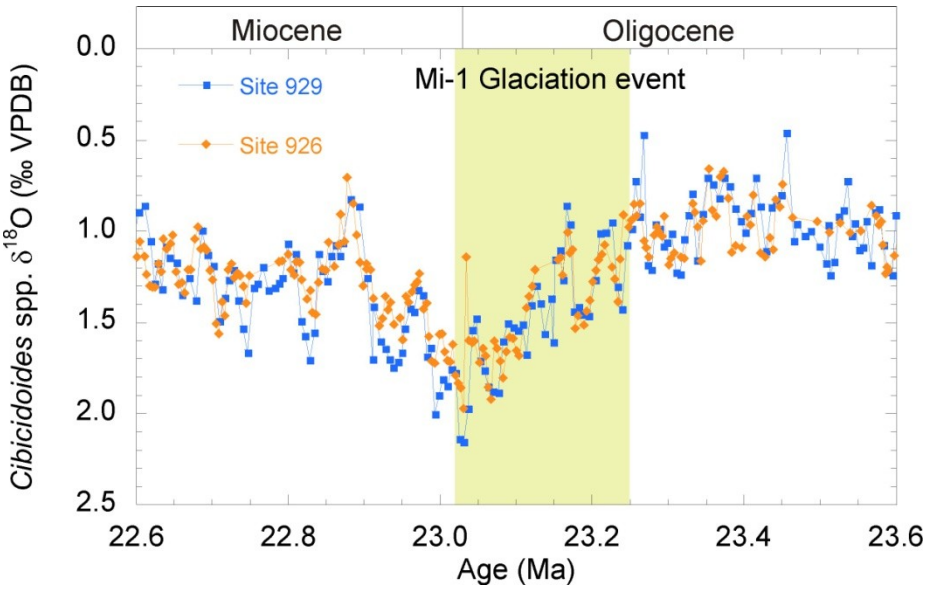

Figure 4-2 Benthic foraminiferal oxygen isotope records from *Cibicidoides* spp. for ODP Sites 926 and 929 (Pälike et al., 2006b). Age model Pälike et al. (2006b).

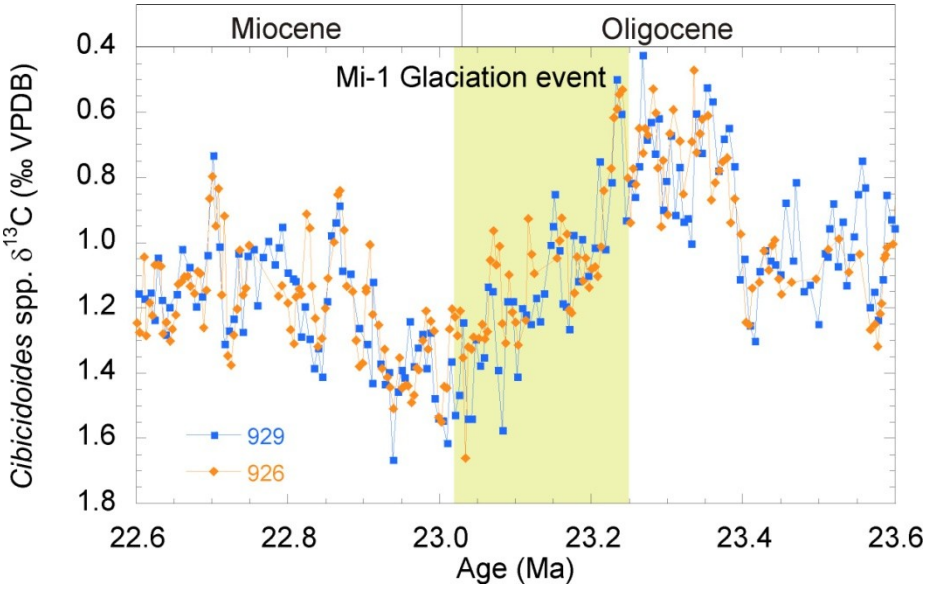

Figure 4-3 Benthic foraminiferal carbon isotope records from *Cibicidoides* spp. for ODP Sites 926 and 929 (Pälike et al., 2006b). Age model is based on Pälike et al. (2006b).

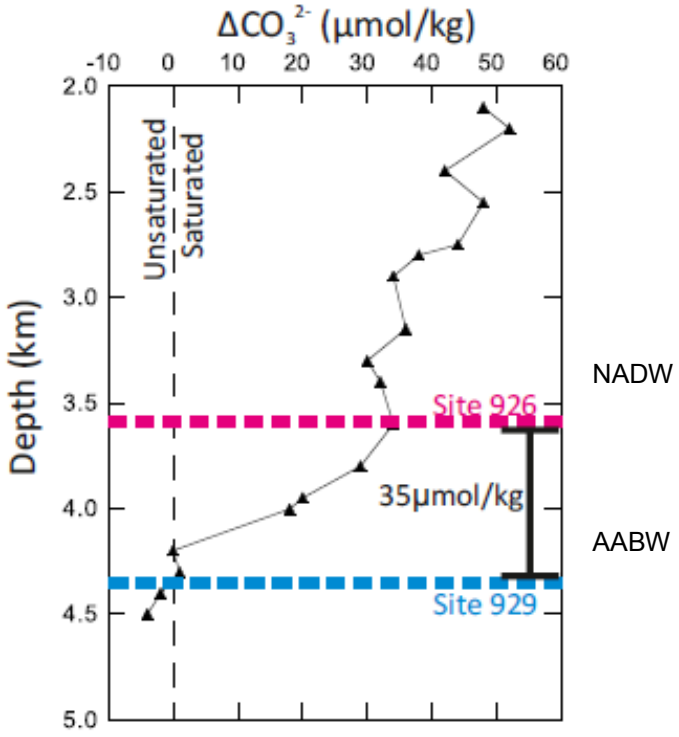

Figure 4-4 Profile of modern water column carbonate saturation state with water depths for ODP Sites 926 and 929. Original data produced at GEOSECS station 42 in the Western Atlantic (adapted from King et al., 1997). AABW = Antarctic Bottom Water, NADW = North Atlantic Deep Water.

Using the equation of Broecker and Peng (1982) (Equation 16) the difference in modern $[CO_3^{2-}]_{SAT}$ between ODP Sites 929 and 926 is calculated at approximately 10 µmol/kg. However using the empirical data of GEOSECS the difference is 35 µmol/kg (Figure 4-4). This is because there is a transition in water mass at 4100 metres between the NADW and AABW (King et al., 1997). This transition leads to a larger than expected saturation state difference between the two sites, which makes the region ideal to study of the effect of saturation state on trace metal geochemistry of benthic foraminifera. However changes in ocean circulation and deep water formation may have caused changes in the depth of the transition through time and this will be further explored in this study.

$[CO_3^{2-}]_{SAT} = 90 \exp [0.16(z - 4)]$.

Where z = depth in kilometres

Equation 16 (Broecker and Peng, 1982)

4.1.2 Proposed hypothesis for changes in trace metals across the Mi-1 event.

Unlike the EOT (see Introduction, Chapter 1) there are no significant changes in carbonate accumulation associated with Mi-1 indicative of major CCD deepening (Shipboard Scientific party, 1995). This is consistent with the more transient nature of this glacial event. The composite CCD curve of van Andel (1975) indicates a slight shallowing of the Atlantic CCD but this is after the Oligocene-Miocene boundary. Also the low resolution of van Andel (1975) would not be able to pick up a transient event such as Mi-1. It is hypothesised that if there are no large scale saturation state changes, then benthic foraminiferal Mg/Ca will decrease across the Mi-1 Ceara Rise records. This has the potential to shed new light on the extent of glaciation and temperature change. Between the two sites it is proposed that there may be significant differences in benthic foraminiferal trace metal records. This is based on the difference in carbonate saturation state of the two different subsurface water masses that today bathe the two sites (Figure 4-4). Despite having minimal differences in $\delta^{18}O$ (Figure 4-2) there may have been a temperature offset between the two sites due to being overlain by different water masses. The similar $\delta^{18}O$ but differing temperatures can be explained by the difference in salinity between the two water masses.

A further question to be answered in this study is whether there are different signals in trace metal records of epifaunal vs. infaunal species and whether these differences can be quantified. It has been suggested that as well as vital effects causing differences in trace metal response to oceanographic conditions between benthic foraminiferal species, the environment in which the benthic foraminifera lives may play a part (sediment-water interface or in sediment). For example it has been proposed that infaunal species may be less susceptible to the effects of seawater saturation state changes because the pore water from which they produce their tests is buffered (e.g. Elderfield et al., 2010). However, some infaunal species have shown a relationship between saturation state and B/Ca (Yu and Elderfield, 2007) suggesting this buffering effect may not hold true for all species or that potentially species which have been classified as infaunal may change their habitat depending upon environmental influences.

4.1.3 Testing the hypothesis for changes in trace metals across the Mi-1 event.

In order to address the research questions set out here I have produced a suite of trace metal records using benthic foraminiferal calcite across the Mi-1 event from ODP Leg 154 from ODP Sites 926 and 929. Records have been produced using the epifaunal species *Cibicidoides mundulus* and the infaunal species *Oridorsalis umbonatu*s (a long ranging species that also occurs at the EOT as well as having living counterparts). Compared to the EOT Equatorial Pacific records (chapter 3) high sediment carbonate content and good foraminiferal preservation have permitted larger sample sizes and ~4000 yr sampling resolution. These trace metal records cast new light on the temperature/ice volume

changes during this transient glaciation and the effect of carbonate saturation state on benthic foraminiferal trace metal proxies.

4.2 Results: Benthic foraminiferal trace metal records across the Mi-1 from ODP Leg 154.

4.2.1 Summary of Leg 154 trace metal results.

The Mi-1 event is defined from the $\delta^{18}O$ record as being between 23.25 Ma and 23.02 Ma and is shaded green in all figures. The post glacial warming event (PGW) is defined from the $\delta^{18}O$ as being between 23.02 and 22.88 Ma. *Oridorsalis umbonatus* and *Cibicidoides mundulus* trace metal records across the Mi-1 event at ODP Sites 929 and 926 show patterns of dynamic change including evidence for cyclic variability. Some of the trace metals show large changes across the Mi-1 event (Figure 4-5 and Figure 4-6) and others do not. There are also inter-site offsets observed in some of the trace metal records and offsets are observed between the two species analysed. Each metal is examined in more detail in the following sections.

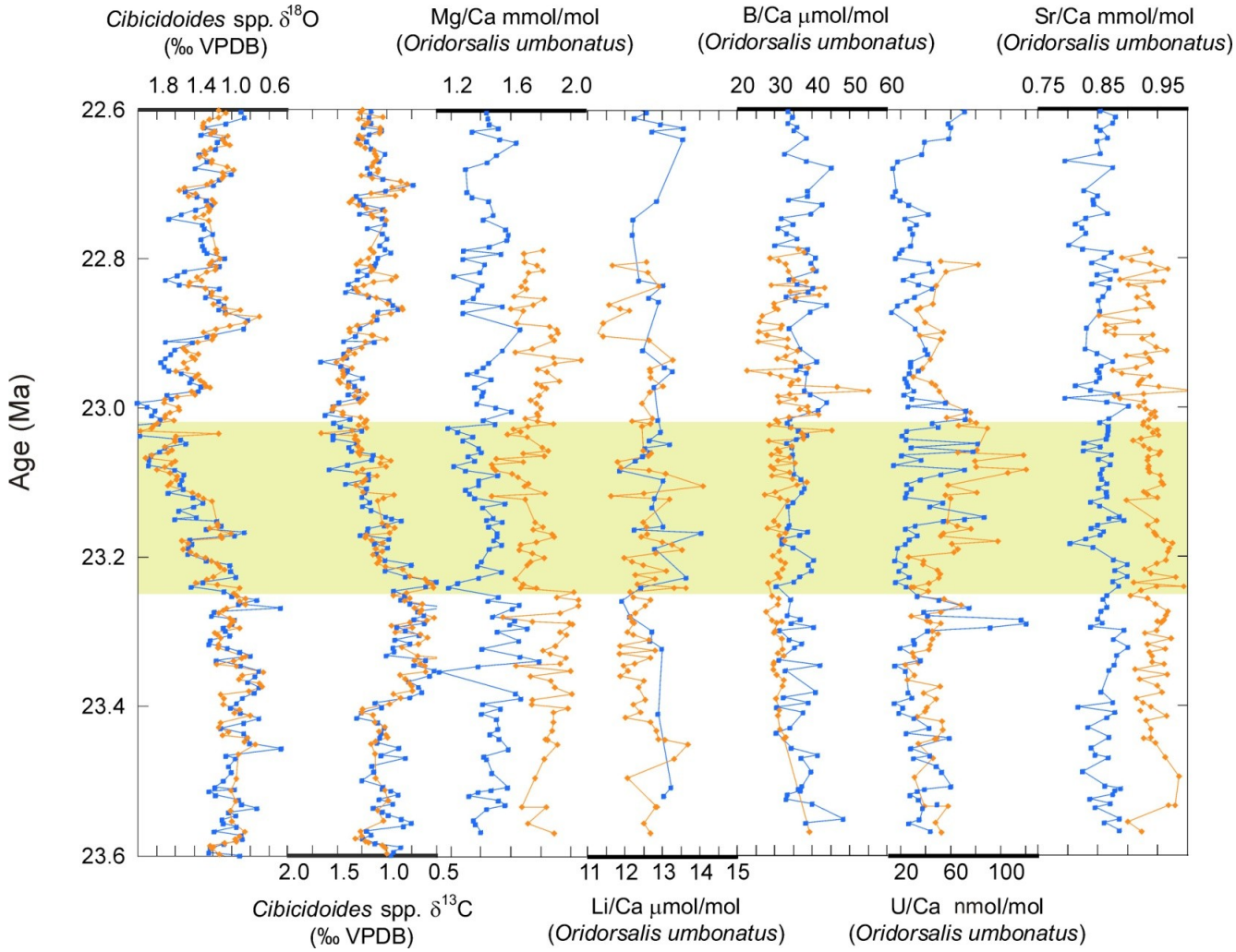

Figure 4-5 New trace metal data from benthic foraminifera *Oridorsalis umbonatus* from ODP Site 926 (orange diamonds) and ODP Site 929 (blue squares). Accompanying stable isotope data from Pälike et al. (2006b). Age model is from Pälike et al. (2006b).

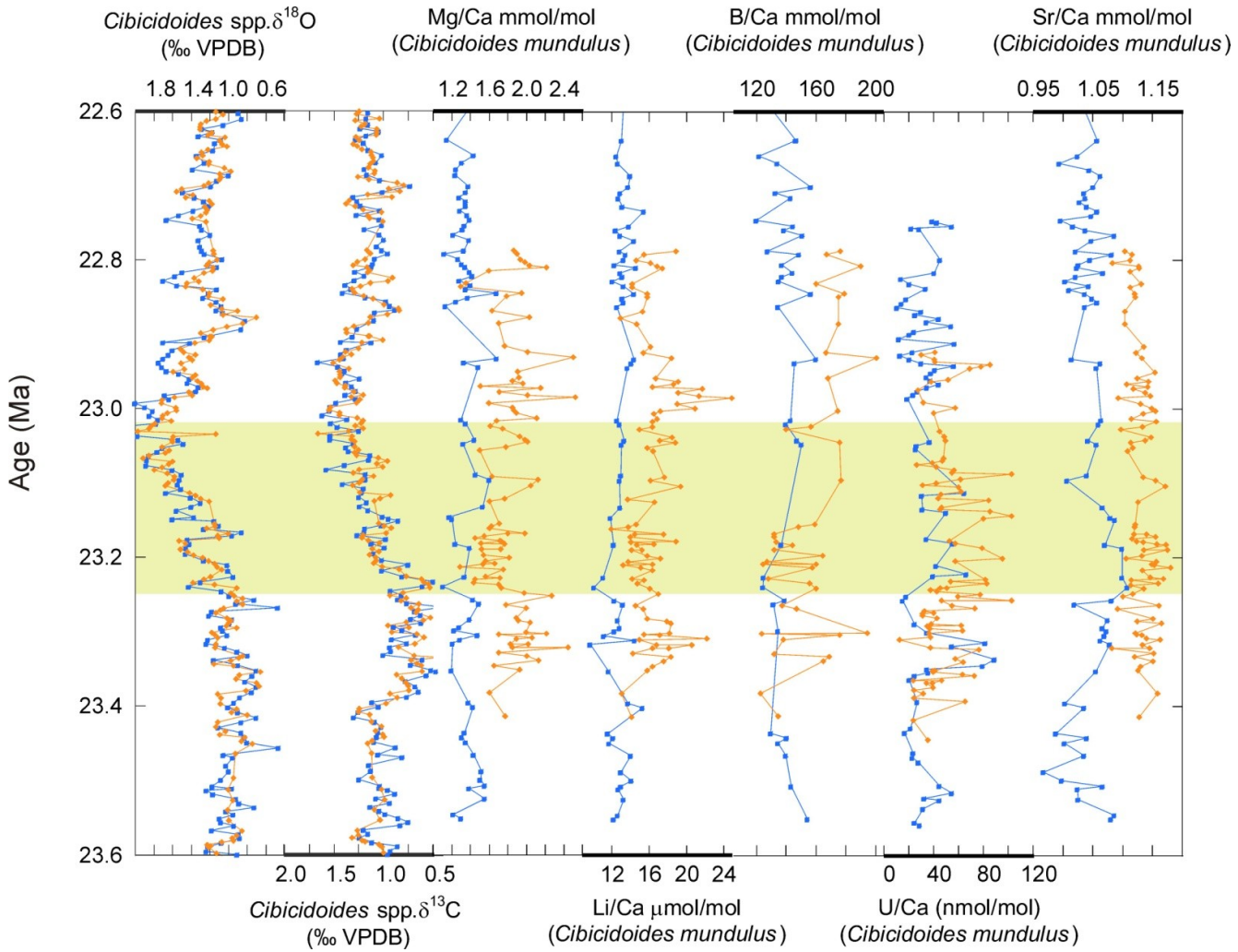

Figure 4-6 New trace metal data from benthic foraminifera *Cibicidoides mundulus* from ODP Site 926 (orange diamonds) and ODP Site 929 (blue squares). Accompanying stable isotope data from Pälike et al. (2006b). Age model is from Pälike et al. (2006b).

4.2.2 Mg/Ca

Across the Mi-1 event

Across the Mi-1 event (shaded in green in all figures) *Oridorsalis umbonatus* Mg/Ca values decrease in both ODP Sites 929 and 926 (Figure 4-7A). ODP Site 926 and 929 *Oridorsalis umbonatus* Mg/Ca decreases by ~0.5 mmol/mol. Following this decrease *Oridorsalis umbonatus* Mg/Ca increases at both sites with ODP Site 926 increasing to ~2 mmol/mol by 22.93 (an increase of ~0.4 mmol/mol) and ODP Site 929 increasing by ~0.46 mmol/mol by 22.89 Ma. This coincides with the minimum in stable isotopes (Figure 4-2 and Figure 4-3) which occurs at 22.88 Ma.

The *Cibicidoides mundulus* data are more variable and lower resolution than the *Oridorsalis umbonatus* data (Figure 4-7B). ODP Site 926 *Cibicidoides mundulus* Mg/Ca values decrease by approximately 0.50 mmol/mol across the Mi-1 event whereas ODP Site 929 shows no net change across Mi-1 but show ~0.3 mmol/mol decrease in Mg/Ca during the event before returning to pre-event values before the end of Mi-1. Following Mi-1 ODP Site 926 shows an increase in Mg/Ca of ~0.4 mmol/mol. ODP Site 929 shows no clear increase after Mi-1.

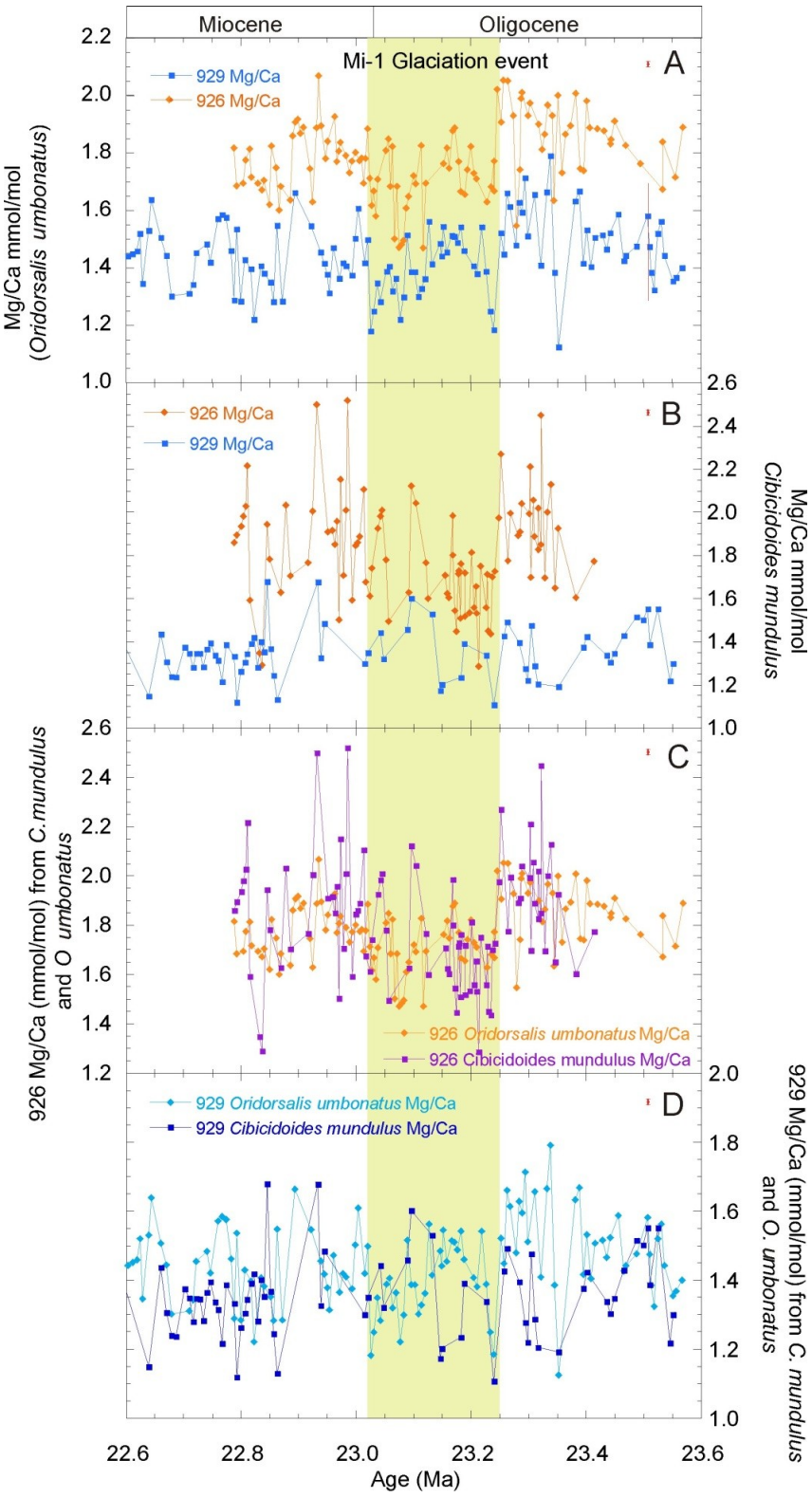

Figure 4-7 Benthic foraminiferal Mg/Ca across the Mi-1 glacial event and recovery for ODP Leg 154 sites. Age model is based on Pälike et al. (2006b). A = Mg/Ca *Oridorsalis umbonatus*, B = Mg/Ca *Cibicidoides mundulus*, C = ODP Site 926 Mg/Ca data for both species and, D = ODP Site 929 Mg/Ca data for both species. Error bars in top right hand corner of plots = ± 1 s.d of Mg/Ca based on long term replicate analysis of consistency standards (CS1 and CS2 see Methods chapter).

Offsets between ODP Sites 926 and 929

There is a distinct offset between ODP Site 926 and ODP Site 929 *Oridorsalis umbonatus* Mg/Ca values (Figure 4-7A). It is not always consistent due to noise within the data but the offset is on average, ~0.3 mmol/mol. This offset was calculated taking 10 different points in the record where data points were available for both sites, subtracting the ODP Site 929 Mg/Ca value from the ODP Site 926 value and then averaging. Also comparing an artificial record created by subtracting 0.3 mmol/mol from ODP Site 926 and overlaying onto ODP Site 929 indicates a good match (Figure 4-8).

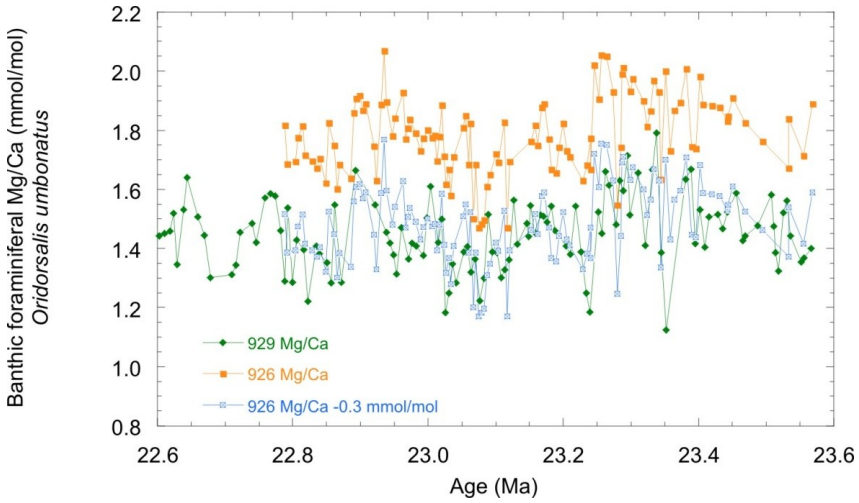

Figure 4-8 Benthic foraminiferal (*Oridorsalis umbonatus*) Mg/Ca for ODP Sites 926 and 929 and Site 926 Mg/Ca record -0.3 mmol/mol. Age model Pälike et al. (2006b).

The offset between the ODP Site 926 and ODP Site 929 Mg/Ca in *Cibicidoides mundulus* shows large variations and cannot be calculated. This is particularly obvious if the 0.3 mmol/mol offset derived from the *Oridorsalis umbonatus* data is applied to the *Cibicidoides mundulus* data (Figure 4-9).

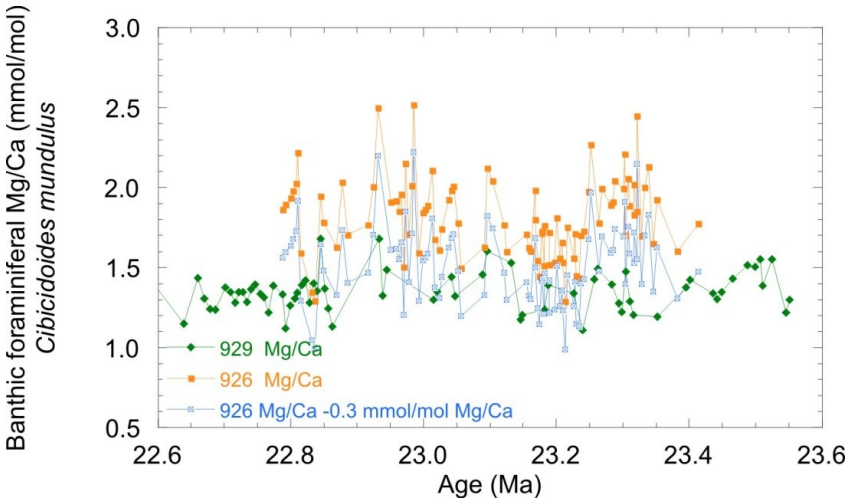

Figure 4-9 Benthic foraminiferal (*Cibicidoides mundulus*) Mg/Ca for ODP Sites 926 and 929 and Site 926 Mg/Ca record -0.3 mmol/mol. Age model is based on Pälike et al. (2006b).

Offsets between *Oridorsalis umbonatus* and *Cibicidoides mundulus* Mg/Ca values

There is no consistent offset in the Mg/Ca records of the two different species at either site (Figure 4-7C,D). There are offsets within the data set but they are not consistent and range from ~0 to ~0.4 mmol/mol. ODP Site 926 Mg/Ca from *Oridorsalis umbonatus* and *Cibicidoides mundulus* (Figure 4-7C) seem to be more in phase than ODP Site 929 *Oridorsalis umbonatus* and *Cibicidoides mundulus* Mg/Ca (Figure 4-7D).

4.2.3 Li/Ca

Across the Mi-1 event

There is much greater variability in the *Cibicidoides mundulus* records relative to the *Oridorsalis umbonatus* records. *Cibicidoides mundulus* Li/Ca at ODP Site 926 increases by ~2 μmol/mol across the Mi-1 event although there is not a steady increase and the Li/Ca values are quite variable. ODP Site 929 *Cibicidoides mundulus* Li/Ca increases by ~3 μmol/mol more gradually (Figure 4-10B). After Mi-1 the *Cibicidoides mundulus* Li/Ca values continue to increase until ~22.96 Ma.

Oridorsalis umbonatus Li/Ca increases at ODP Site 926 by ~0.8 μmol/mol (from 11.8 to 12.6 μmol/mol across the Mi-1 event. At ODP Site 929 there is an increase of ~0.9 μmol/mol (from 11.9 to 12.8 μmol/mol). The Li/Ca data are highly scattered which may be related to analytical error.

Offsets between Sites 926 and 929

The deeper site (ODP Site 929) *Oridorsalis umbonatus* record is of lower resolution. However the two sites show similar variability in measured Li/Ca with no clear or consistent inter-sites offset across Mi-1 (Figure 4-10A).

In contrast ODP Site 926 and ODP Site 929 *Cibicidoides mundulus* Li/Ca show a distinct offset throughout. However this offset varies in magnitude throughout the record from ~1.4 µmol/mol (e.g. at 23.26 Ma) to ~4 µmol/mol (e.g. at 23.00 Ma) (Figure 4-10B).

Offsets between *Oridorsalis umbonatus* and *Cibicidoides mundulus* Li/Ca values

ODP Site 926 *Oridorsalis umbonatus* and *Cibicidoides mundulus* have an offset at both ODP Site 926 and ODP Site 929. This offset is not constant but changes throughout the record (Figure 4-10C,D).

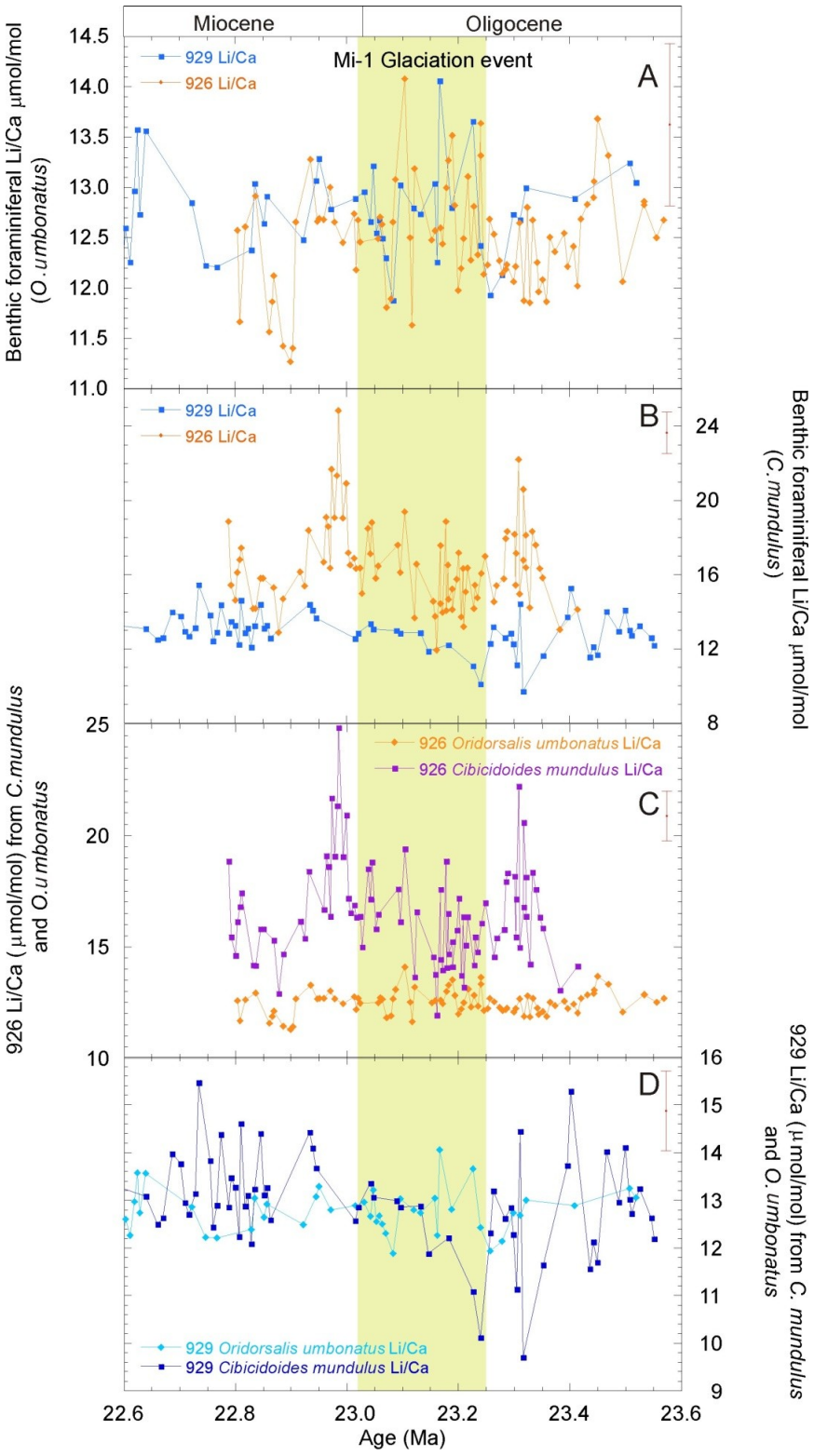

Figure 4-10 Benthic foraminiferal Li/Ca across the Mi-1 glacial event and recovery for ODP Leg 154 sites. Age model is based on Pälike et al. (2006b). A = Li/Ca from *Oridorsalis umbonatus*, B = Li/Ca from *Cibicidoides mundulus*, C = ODP Site 926 Li/Ca data from both species and D = ODP Site 929 Li/Ca data from both species. Error bars = ± 1 s.d of Li/Ca based on long term replicate analysis of consistency standards (CS1 and CS2 see Methods chapter).

4.2.4 B/Ca

Across the Mi-1 event

Oridorsalis umbonatus B/Ca values show no net change in the ODP Site 926 or 929 records across the Mi-1 event (Figure 4-11A). The ODP Site 926 *Oridorsalis umbonatus* record shows increased variability during Mi-1 between 22.97 and 22.86 Ma while post Mi-1 the B/Ca values follow a decreasing trend from a maximum of 55 μmol/mol to 25 μmol/mol coincident with the decrease in stable isotopes. This change is based on only a couple of data points at the start of the decease and requires further analyses for validation. Both sites B/Ca values range from approximately 25 μmol/mol to 45 μmol/mol. The 4000 yr sampling resolution suggests cyclicity in the *Oridorsalis umbonatus* B/Ca records for both sites.

Cibicidoides mundulus B/Ca data from ODP Site 926 are very variable (Figure 4-11B). However an increase in B/Ca in both sites can be seen with B/Ca values at ODP Site 926 increasing by ~30 μmol/mol and B/Ca values at ODP Site 929 increasing by ~10 μmol/mol.

Offsets between ODP Sites 926 and 929

Overall in the *Oridorsalis umbonatus* B/Ca data there appears to be a very slight offset between sites (Figure 4-11A), ODP Site 929 B/Ca data appear very slightly higher than 926 *Oridorsalis umbonatus* B/Ca data. Across the Mi-1 event this offset is calculated to be on average ~4 μmol/mol however this offset is very similar to the analytical uncertainty. In the *Cibicidoides mundulus* B/Ca data sets the offset cannot be calculated within Mi-1 due to the very high variability of the data. However ODP Site 926 *Cibicidoides mundulus* B/Ca values appear to be higher than at ODP Site 929 by ~20 μmol/mol through parts of the record (Figure 4-11B).

Offsets between *Oridorsalis umbonatus* and *Cibicidoides mundulus* B/Ca values

There is a large offset between *Oridorsalis umbonatus* and *Cibicidoides mundulus* B/Ca values (Figure 4-11 C,D). At ODP Site 926 the offset is approximately 120 μmol/mol and at ODP Site 929 the offset is approximately 105 μmol/mol. These values were calculated by taking 10 different points in the record where data points were available for both sites, subtracting the *Oridorsalis umbonatus* B/Ca value from the *Cibicidoides mundulus* value and then averaging.

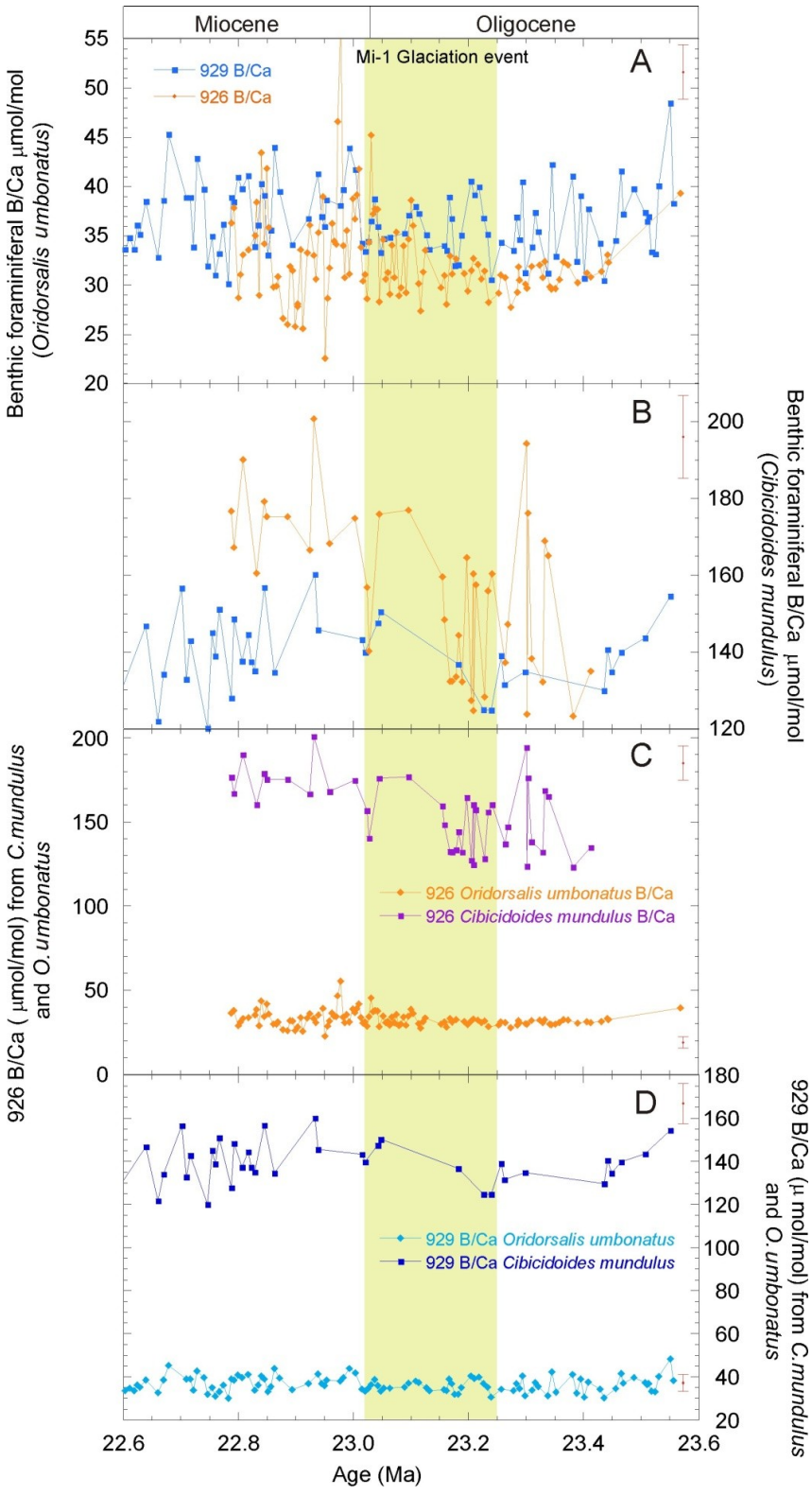

Figure 4-11 Benthic foraminiferal B/Ca across the Mi-1 glacial event and recovery for ODP Leg 154 sites. Age model is based on Pälike et al. (2006b). A = B/Ca from *Oridorsalis umbonatus*, B = B/Ca from *Cibicidoides mundulus*, C = ODP Site 926 B/Ca data from both species and D = ODP Site 929 B/Ca data from both species Error bars = ± 1 s.d of B/Ca based on long term replicate analysis of consistency standards (CS1 and CS2 see Methods chapter).

4.2.5 U/Ca

Across the Mi-1 event

Across the Mi-1 event ODP Site 926 *Oridorsalis umbonatus* U/Ca values increase by approximately 65 nmmol/mol (from 24 nmol/mol to 89 nmmol/mol) (Figure 4-12A). ODP Site 929 *Oridorsalis umbonatus* U/Ca data are more scattered but show an increase of ~58 nmol/mol across the Mi-1 event. After the Mi-1 event both sites *Oridorsalis umbonatus* U/Ca values decrease to a minimum of 33.5 nmol/mol (ODP Site 926) and 12.8 nmol/mol (ODP Site 929). This decrease terminates at 22.86 Ma which is coincident with the end of the decrease in $\delta^{18}O$.

Cibicidoides mundulus U/Ca also increases across Mi-1. Values peak slightly before the minimum $\delta^{18}O$ values. ODP Site 926 *Cibicidoides mundulus* U/Ca increases by ~78 nmol/mol and ODP Site 929 by ~30 nmol/mol (Figure 4-12B).

Offsets between ODP Sites 926 and 929

There is no consistent large offset between ODP Sites 926 and 929 for *Oridorsalis umbonatus* although Site 926 may be slightly higher (<5 nmol/mol difference) (Figure 4-12A). *Cibicidoides mundulus* U/Ca is similar to *Oridorsalis umbonatus* U/Ca in that there is no large offset between ODP Sites 926 and 929 although again ODP Site 926 may be slightly higher (<5 nmol/mol difference) (Figure 4-12B).

Offsets between *Oridorsalis umbonatus* and *Cibicidoides mundulus* U/Ca values

Although the two sites show different patterns of change, there is no discernable offset in U/Ca between the two species analysed at either ODP Site 926 or ODP Site 929 (Figure 4-12C,D).

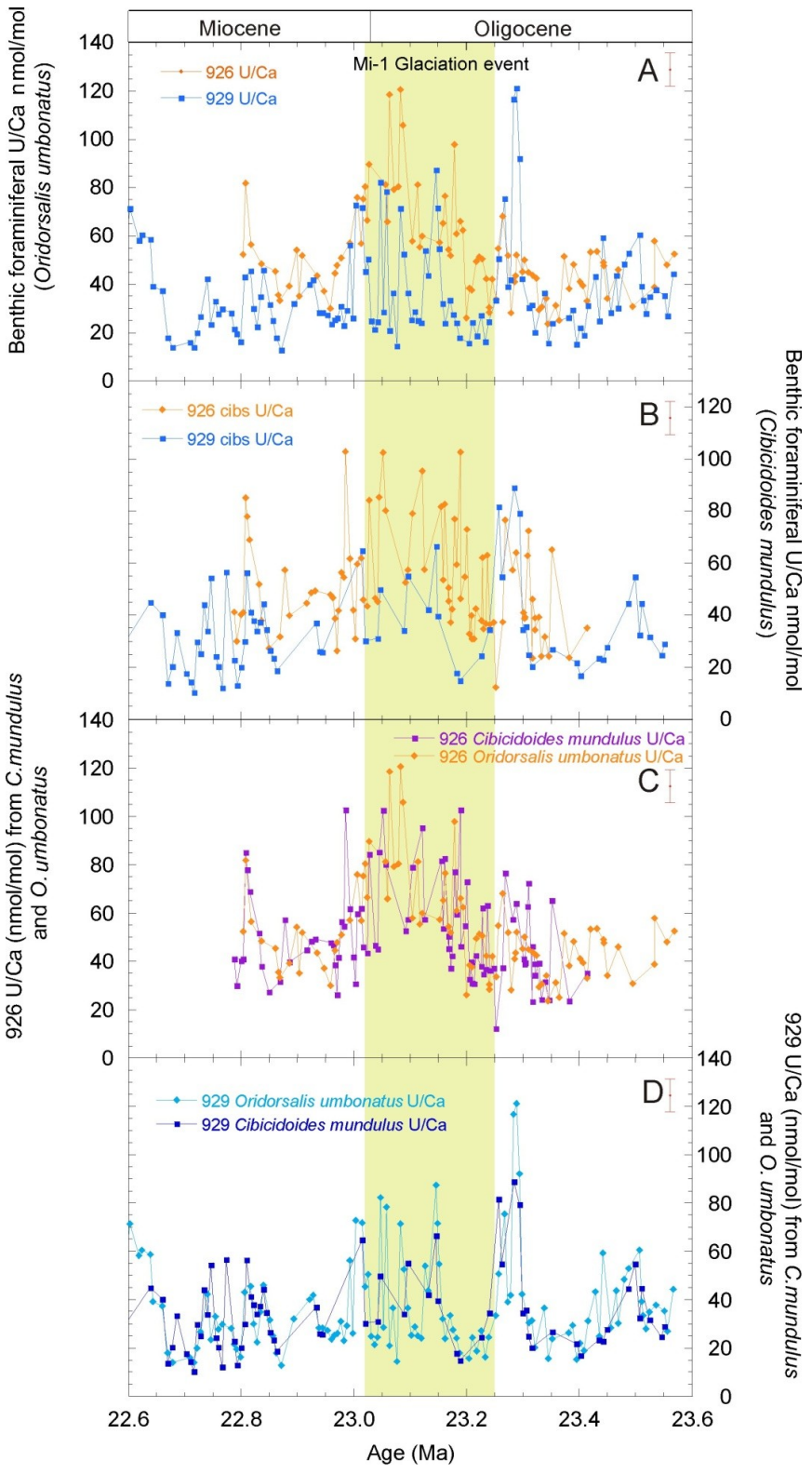

Figure 4-12 Benthic foraminiferal U/Ca across the Mi-1 glacial event and recovery for ODP Leg 154 sites. Age model is based on Pälike et al. (2006b). A = U/Ca from *Oridorsalis umbonatus*, B = U/Ca from *Cibicidoides mundulus*, C = ODP Site 926 U/Ca data from both species and D = ODP Site 929 U/Ca data from both species. Error bars = ± 1 s.d of U/Ca based on long term replicate analysis of consistency standards (CS1 and CS2 see Methods chapter).

4.2.6 Sr/Ca

Across the Mi-1 event

Sr/Ca values show no net change across Mi-1 at either site or for either species. ODP Site 929 *Cibicidoides mundulus*, however shows a trend of decreasing Sr/Ca in the late Oligocene followed by a temporary increase in the middle of Mi-1 (Figure 4-13).

Offsets between ODP Sites 926 and 929

There is a significant offset in benthic foraminiferal Sr/Ca values between ODP Site 926 and ODP Site 929 with ODP Site 926 Sr/Ca data values higher than ODP Site 929. The difference in average *Oridorsalis umbonatus* Sr/Ca between sites across the Mi-1 event is 0.08 mmol/mol (Figure 4-13A).. The difference in average *Cibicidoides mundulus* Sr/Ca across the Mi-1 event is 0.07 mmol/mol (Figure 4-13B).

Offsets between *Oridorsalis umbonatus* and *Cibicidoides mundulus* Sr/Ca values

There are large offsets in Sr/Ca values between the two species analysed in this study. For ODP Site 926 *Cibicidoides mundulus* Sr/Ca values are on average 0.19 mmol/mol higher than *Oridorsalis umbonatus* Sr/Ca values (Figure 4-13C). The offset for ODP Site 929 between *Oridorsalis umbonatus* and *Cibicidoides mundulus* is on average 0.20 mmol/mol again with *Cibicidoides mundulus* having the higher values (Figure 4-13D). These values were calculated taking 10 different points in the record where data points were available for both sites, subtracting the *Oridorsalis umbonatus* Sr/Ca value from the *Cibicidoides mundulus* value and then averaging.

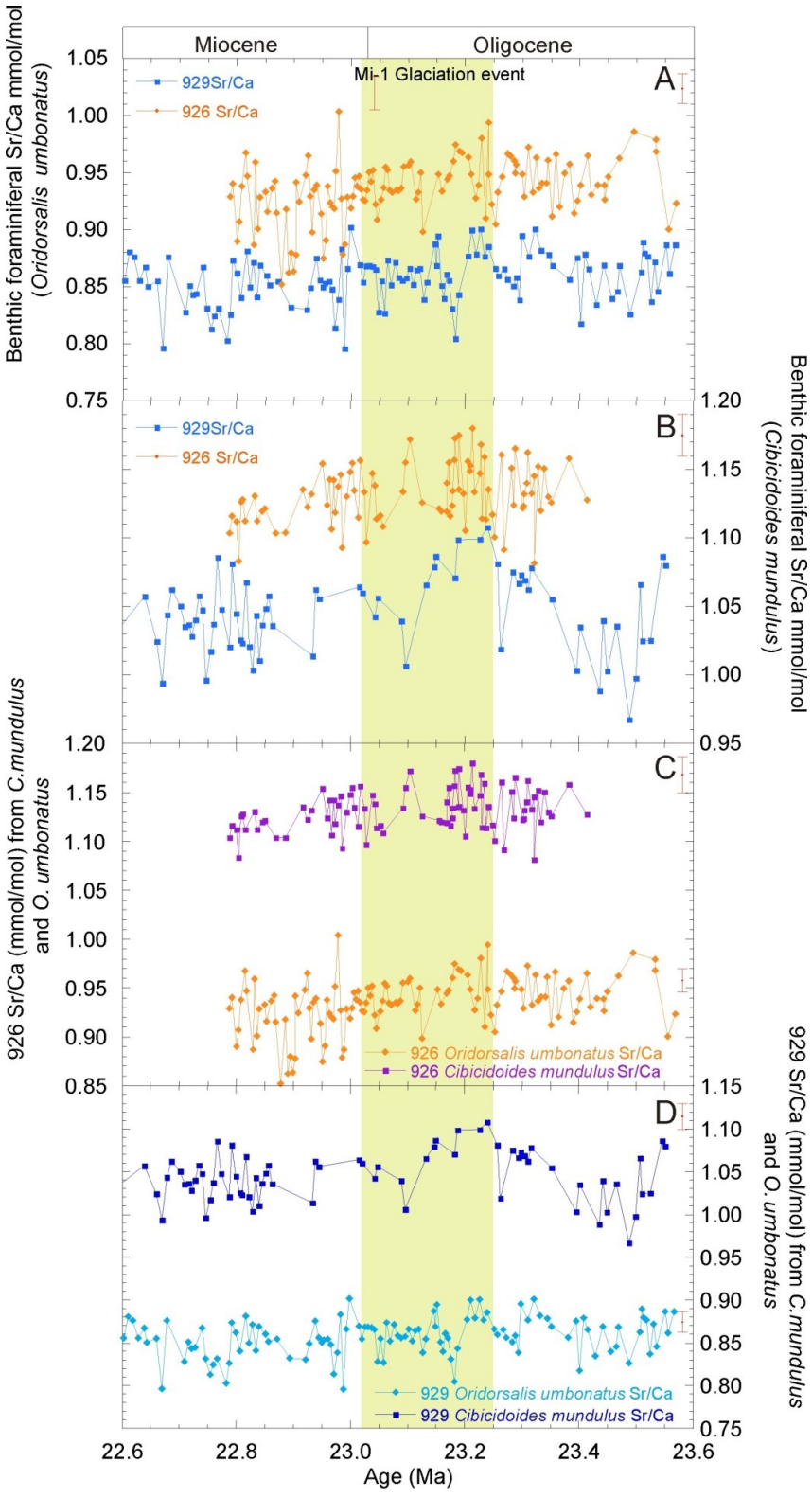

Figure 4-13 Benthic foraminiferal Sr/Ca across the Mi-1 Glacial event and recovery for ODP Leg 154 sites. Age model is based on Pälike et al. (2006b). A = Sr/Ca from *Oridorsalis umbonatus*, B = Sr/Ca from *Cibicidoides mundulus*, C = ODP Site 926 Sr/Ca data from both species and D = ODP Site 929 Sr/Ca data from both species. Error bars = ± 1 s.d of Sr/Ca based on long term replicate analysis of consistency standards (CS1 and CS2 see Methods chapter).

4.3 Discussion of ODP Leg 154 records

4.3.1 Epifaunal versus infaunal - microhabitat effects on trace metal composition

The *Cibicidoides mundulus* Mg/Ca records are very different to the *Oridorsalis umbonatus* Mg/Ca records across Mi-1 (Figure 4-7C+D) and this is attributed to the two species being affected to a different extent by carbonate saturation state of seawater due to their micro-environments. It can be seen clearly that regardless of temperature calibration used, the *Cibicidoides mundulus* ODP Site 926 record has larger amplitude changes than the *Oridorsalis umbonatus* record (Figure 4-14). Because both species must have experienced similar temperature histories, it is therefore proposed here that *Cibicidoides mundulus* is affected by both temperature and saturation state. This is due to it being epifaunal and thus exposed to variations in seawater saturation state.

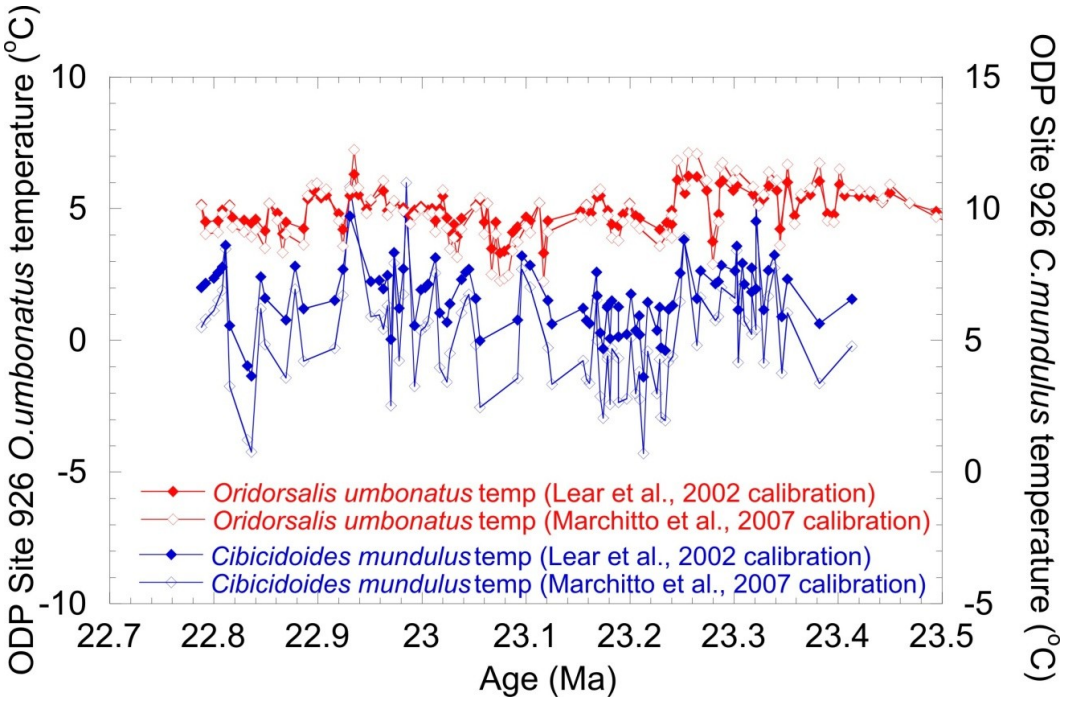

Figure 4-14 ODP Site 926 temperatures across Mi-1 for *Cicicidoides mundulus* and *Oridorsalis umbonatus* using the calibrations of Lear et al. (2002) and Marchitto et al. (2007).

As the *Cibicidoides mundulus* record is more variable than the *Oridorsalis umbonatus* record (Figure 4-14) then it indicates that there were some saturation state changes during Mi-1. It cannot be determined with absolute certainty whether the saturation state changes interpreted from the *Cibicidoides mundulus* Mg/Ca record reflect global changes in carbonate saturation state or if they reflect regional changes due to movement in the boundary between two water masses in the region (today these are AABW and NADW). In the modern ocean at the two current water depths AABW has a saturation state of ~0

µmol/kg and NADW a saturation state of ~35 µmol/kg (Figure 4-4). Therefore changes in the amount of production of these deep water masses and thus movement of the boundary between them may work to change saturation state at ODP Site 926. Movement of this boundary would also result in temperature change as the two water masses today have different absolute temperatures by ~2°C (Schlitzer, 2005, Ocean Data View, http://www.awi-bremerhaven.de/GEO/ODV). If the boundary changed and mixing occurred differently a temperature change would be expected in the *Oridorsalis umbonatus* Mg/Ca record. The similar timing but larger amplitude Mg/Ca variations seen in the *Cibicidoides mundulus* record compared to the *Oridorsalis umbonatus* record at ODP Site 926 hint at a water mass signal (Figure 4-7C). However the differing trends between the epifaunal and infaunal species at the deepest site, which presumably was not affected by such water mass mixing, implies also a change in whole ocean bottom water carbonate chemistry (Figure 4-7D).

If the Mi-1 glaciation produced a global saturation state increase in a similar way to the EOT (chapter 3) even if on a smaller scale, this would mean the *Cibicidoides mundulus* record would show less of an Mg/Ca decrease than the *Oridorsalis umbonatus* record. This can be seen in the cooling interval at ~23.1 Ma when *Oridorsalis umbonatus* Mg/Ca values are decreasing and *Cibicidoides mundulus* values are increasing thus indicating saturation state change (Figure 4-7D). This saturation state change could be caused by a change from shelf calcium carbonate deposition to basin calcium carbonate deposition due to sea level reduction (Merico et al., 2008).

The *Oridorsalis umbonatus* record is closely correlated with the $\delta^{18}O$ record which indicates that it is recording temperature only whilst *Cibicidoides mundulus* is recording both temperature and saturation state. The key difference between the Mg/Ca records produced by the two different foraminiferal species is that *Oridorsalis umbonatus* displays a constant offset between ODP Site 926 and ODP Site 929 of ~0.3 mmol/mol whereas the offset between ODP Site 926 and 929 Mg/Ca for the species *Cibicidoides mundulus* is variable and appears almost cyclic in nature (Figure 4-7 A,B). This indicates that the two species are being affected by different environmental parameters. A potential explanation for this is the micro-habits of the two species across the Mi-1 event. *Cibicidoides mundulus* is an epifaunal species and is often used in paleoceanographic stable isotope studies due to its consistent offsets from equilibrium values (Katz et al., 2003). *Oridorsalis umbonatus* on the other hand is a shallow infaunal species (Corliss, 1985). It has been suggested by some (e.g. Brown et al., 2011) that the effects of saturation state on the trace metal geochemistry of this species are reduced due to the foraminifera living in pore waters which are buffered against saturation state changes. However if this is the case then the Mg/Ca offsets observed between sites of differing palaeowater depth from ODP Leg 199 (chapter 3) would be hard to explain. Therefore, it is suggested here that the situation is more complex than infaunal vs. epifaunal. It has been shown that modern *Oridorsalis*

umbonatus has a variable habitat of 1-4 cm in the sediment (Rathburn and Corliss, 1994). The exact depth is probably related to food supply with the foraminifera migrating up and down the sediment depending on abundance of organic matter. If the pore-waters are buffered to different extents depending on depth then this may lead to varying apparent saturation state sensitivities of Mg/Ca. Alternatively *Oridorsalis umbonatus* may even have been epifaunal at times in the past. $\delta^{13}C$ gradients between *Oridorsalis umbonatus* and *Cibicidoides mundulus* across the EOT have been shown not to vary with productivity as would be expected if the $\delta^{13}C$ gradients were related to depth differences indicating they may be related to physiological rather than environmental differences (Coxall and Wilson 2011).

In this study *Cibicidoides mundulus* shows a large variability in offset between sites whereas *Oridorsalis umbonatus* has a constant offset. Therefore here *Oridorsalis umbonatus* Mg/Ca is interpreted as being due to temperature change only.

Due to this difference in *Oridorsalis umbonatus* and *Cibicidoides mundulus* Mg/Ca records, bottom water temperature changes will be calculated using two techniques: (i) *Oridorsalis umbonatus* Mg/Ca temperatures will be calculated using the Lear et al., 2002 calibration and (ii) *Cibicidoides mundulus* Mg/Ca temperatures will be calculated using the Lear et al., 2010 ΔMg-ΔLi technique (described in detail in chapter 3, section 3.3.1).

Bottom Water Temperature Variations through Mi-1

i) Temperature changes calculated using *Oridorsalis umbonatus* Mg/Ca

Temperature difference between ODP Site 926 and ODP Site 929

There is an offset in the *Oridorsalis umbonatus* calculated temperatures between the two sites (Figure 4-15) of approximately 2°C. This is in contrast to the $\delta^{18}O$ data (Figure 4-2) which indicates no offset between the two sites. However as the two sites today are bathed in different water masses, (NADW and AABW) this may be related to differences in salinity and also carbonate ion concentration which has been demonstrated to have an effect on $\delta^{18}O$ values (Spero et al., 1997).

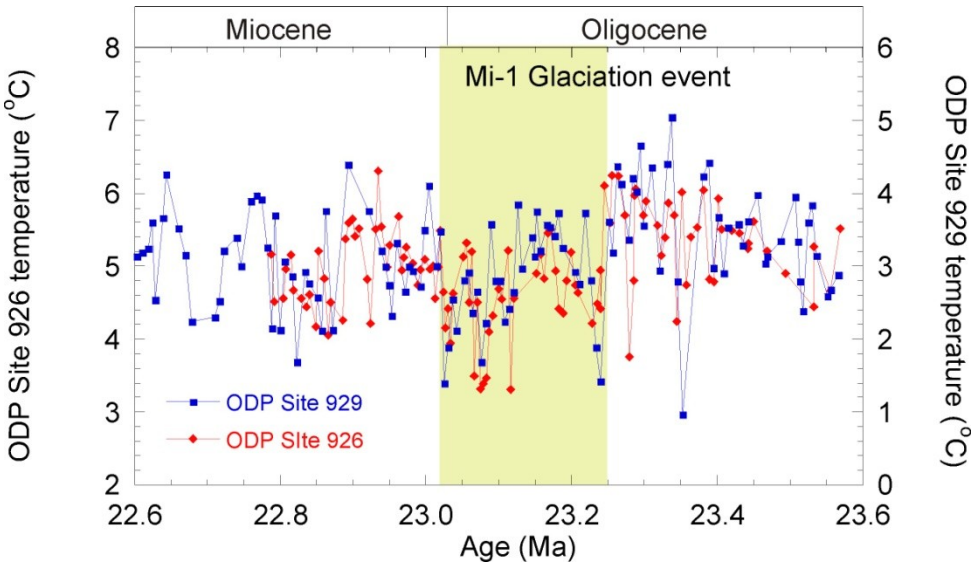

Figure 4-15 Temperature records for ODP Sites 926 and 929 from benthic foraminiferal Mg/Ca values of *Oridorsalis umbonatus* calculated using the calibration of Lear et al. (2002) assuming modern seawater Mg/Ca and assuming no saturation state effect. Note 2°C offset between the Y axes.

Temperature changes across Mi-1 and recovery

The Mg/Ca records from ODP Sites 926 and 929 indicate a decrease in Mg/Ca values in the benthic foraminifera *Oridorsalis umbonatus*. This is interpreted as a cooling signal. If the whole Mg/Ca decrease of ~0.5mmol/mol is attributed to temperature, this equals a cooling of ~2°C using the calibration of Lear et al. (2002) (Figure 4-15). That both sites indicate a similar Mg/Ca change and cooling is strong evidence that saturation state change does not affect *Oridorsalis umbonatus* values at these sites. This temperature change is also similar to that proposed by Paul et al. (2000) of 3°C. This was calculated using differences between planktonic and benthic $\delta^{18}O$ values to estimate the contribution of ice growth and temperature change to the total Mi-1 $\delta^{18}O$ change.

Temperature changes calculated using *Cibicidoides mundulus* and the ΔMg/Ca-ΔLi/Ca method

To process data for this method Mg/Ca and Li/Ca values from the same sample are required. As the ODP Site 926 *Cibicidoides mundulus* record is of higher resolution that is the record used in this method.

Temperature changes across Mi-1 and recovery

Across Mi-1 using the Lear et al. (2010) method on the ODP Site 926 *Cibicidoides mundulus* record produces a cooling of ~1.6°C (Figure 4-16). This is not a linear decrease across the transition as initially there is a temperature increase between ~23.25 and 23.15

Ma. Post glacial warming starts to occur at ~23.05 Ma but is terminated by a rapid cooling of ~3.5 °C and subsequent recovery at ~23.02 Ma.

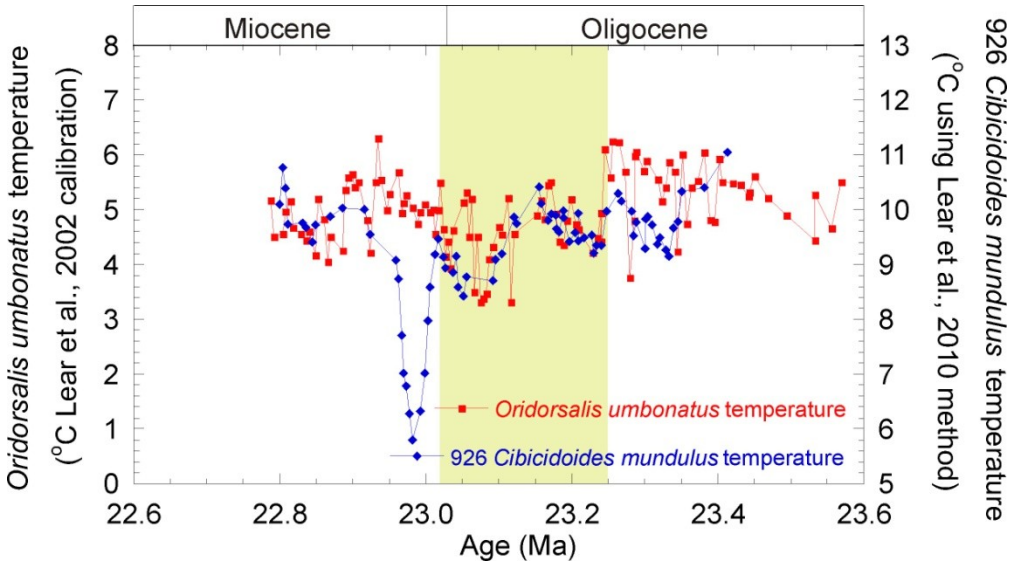

Figure 4-16 Temperature records for ODP Site 926 from *Oridorsalis umbonatus* (Lear et al., (2002) calibration) and *Cibicidoides mundulus* (using Lear et al., (2010) method). Note 5°C offset between Y axes.

Comparison of the two methodologies

There are broad similarities between the temperature records resulting from using the two different methodologies in that both produce a temperature decrease across Mi-1. However the magnitude of change in the *Cibicidoides mundulus* record is slightly smaller and the *Cibicidoides mundulus* temperature record deviates significantly during the post glacial warming where there is a dramatic short term cooling of 3.5°C. This rapid cooling is driven by the large, transient Li/Ca increase at ~23 Ma. This will now be referred to as the "23 Ma Li/Ca event". In order to shed light on this discrepancy between the two temperature reconstructions, the Mg/Ca and Li/Ca records will be compared with other trace metal records from ODP Site 926 and 929.

4.3.2 Additional Trace metal records

Li/Ca

Across the Mi-1 transition

Oridorsalis umbonatus

The *Oridorsalis umbonatus* Li/Ca records show much less variability than the *Cibicidoides mundulus* records (Figure 4-10C,D). This provides support to the argument that *Oridorsalis umbonatus* records are not affected by saturation state in this instance as Li/Ca is dependent on temperature and saturation state. Benthic foraminiferal Li/Ca has been

shown to be negatively correlated with temperature (Marriott et al., 2004). The Li/Ca sensitivity to temperature has been estimated to be -0.74 µmol/mol/°C (Lear et al., 2010). This sensitivity is based on the calibration of Bryan and Marchitto (2008) for *Cibicidoides pachyderma*, and corrected for saturation state using the saturation state sensitivity of *Oridorsalis umbonatus* (Lear et al., 2010). There are drawbacks to this approach; the first is that it mixes different species to determine the sensitivity, which ignores the influence of vital effects. Secondly, this approach to determining the sensitivity of benthic foraminiferal Li/Ca to temperature which represents the early stages of proxy development produces a good linear fit for warmer temperatures, but suggests a smaller sensitivity to temperature below 5˚C. This calibration sensitivity issue may be relevant here. However in the absence of alternative species specific constraints, the data from this study is interpreted using this available sensitivity. As we are assuming that *Oridorsalis umbonatus* is infaunal there is no saturation state component to the Li/Ca signal. This produces a temperature decrease of ~1.2˚C for ODP Site 926 and 929 *Oridorsalis umbonatus* from a ~0.9 µmol/mol increase in Li/Ca. Although the temperature change is not as large as that produced from Mg/Ca paleothermometry this is likely related to the sensitivity used and the error associated with the Li/Ca data.

Cibicidoides mundulus

Cibicidoides mundulus Li/Ca values across Mi-1 increase at both sites. The ODP Site 926 Li/Ca increase of ~2 µmol/mol produces a temperature decrease of ~1.5˚C and the ODP Site 929 Li/Ca increase of ~3 µmol/mol produces a temperature decrease of ~2.3˚C. These temperature changes are larger than those produced from *Oridorsalis umbonatus* changes. This is interpreted as a saturation state change increasing the Li/Ca signal.

Post glacial warming event

After Mi-1 the “post glacial warming” event indicated by the $\delta^{18}O$ is not observed in the Li/Ca data. ODP Site 926 *Cibicidoides mundulus* Li/Ca decreases by 2 µmol/mol between 22.9 and 22.86 Ma which could potentially indicate warming. This is not seen in the ODP Site 929 record due to the resolution of the record there are no Li/Ca values in this small interval (Figure 4-10A).

The Li/Ca *Cibicidoides mundulus* values increase after the Mi-1 event, which suggests a saturation state increase may be counteracting the negative Li/Ca warming signal at this time and there is a large Li/Ca peak at ~22.97 Ma. This is followed by a rapid decrease. The peak is much larger in ODP Site 926 (~7µmol/mol) than at ODP Site 929 (~2 µmol/mol) but this may either be related to the lower resolution of the ODP Site 929 data or differences in saturation state changes between the two sites. The peak is coincident with a U/Ca peak which indicates that it may be related to a mechanism other than temperature or saturation state change.

ODP Site 926/ODP Site 929 Comparison

Unlike all the other trace metal ratios studied here, benthic *Oridorsalis umbonatus* Li/Ca data do not show a consistent offset between ODP Site 926 and ODP Site 929. *Oridorsalis umbonatus* Li/Ca should be affected by the ~2°C difference in temperature (e.g. Lear et al., 2006; Lear et al., 2010) causing a Li/Ca offset of ~1.5 µmol/mol. However this is not observed. This may be related to the analytical error (long term precision 8%) with measuring Li/Ca.

In contrast, ODP Sites 926 and 929 *Cibicidoides mundulus* Li/Ca values display an inter-site offset although this offset is not constant (Figure 4-10B). This offset supports the suggestion that as today, ODP Site 929 is bathed by a more corrosive water mass than ODP Site 926. Periods where the intersite ΔLi/Ca offset is reduced (e.g. at 22.8 Ma) may indicate intervals of increased southern sourced water at the expense of a northern sourced water. Alternatively, changes in the intersite Li/Ca offset may reflect water mass changes in temperature of [CO_3^{2-}].

Leg 154 B/Ca records

Across the Mi-1 transition

Across the Mi-1 transition *Oridorsalis umbonatus* B/Ca does not show any significant change in either ODP Site 926 or ODP Site 929. This indicates that either there were no large scale saturation state changes across Mi-1 or that B/Ca *Oridorsalis umbonatus* B/Ca was insensitive to any changes due to its infaunal habitat across this event at Ceara Rise. Sedimentary records from ODP Site 926 and ODP Site 929 indicate an increase in % coarse fraction from the start of the event to 22.8 Ma from ~2% to 20% (Pälike et al., 2006b) (Figure 4-17). Taken at face value this could be interpreted as indicating reduced foraminiferal shell fragmentation and therefore, increased $CaCO_3$ preservation due to increased ΔCO_3^{2-} associated with the Mi-1 event (Zachos et al., 2007). However there could be other influences such as environmentally induced changes in biogenic carbonate production, and/or changes in dilution of coarse fraction by varying influxes of clays from the South American land mass (Shackleton and Crowhurst, 1997). Generally lower % coarse fraction at ODP Site 929 compared to ODP Site 926 across Mi-1 can be explained by the depth controlled saturation difference, that % coarse is significantly lower supports at least some saturation state control on the Mi-1 increase in B/Ca in the species *Cibicidoides mundulus*.

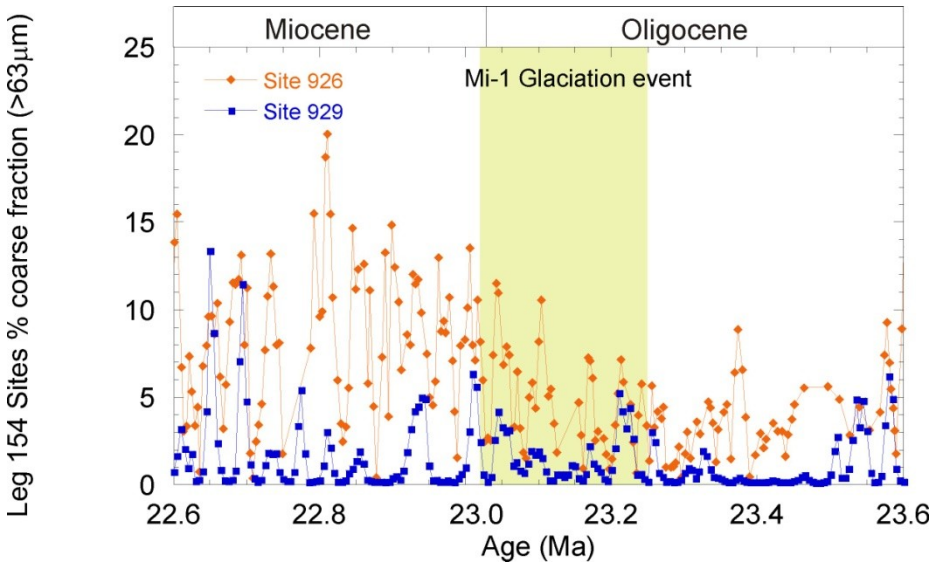

Figure 4-17 Percent coarse fraction (<63µm) from ODP Site 926 and 929, from Pälike et al. (2006b).

Cibicidoides mundulus B/Ca records could be interpreted as showing a small increase across the Mi-1 at both sites. There is large variability in the data. This may be related to the large difference in calcite B/Ca values that have been discovered between different benthic species and even different morphotypes of a single species, including the one studied here, *Cibicidoides mundulus* which has been shown to vary by up to 40 µmol/mol depending on morphotype. (Rae et al., 2011). Although every effort was made to use a single morphotype of *Cibicidoides mundulus* morphotypes are difficult to distinguish and its possible that accidental mixing of morphotypes may account for the high level of variability in the B/Ca data. The variability in the data is less likely to be related to analytical error as *Cibicidoides mundulus* has high absolute B/Ca concentrations, which makes the ratio measurements more accurate.

Inter-site comparison

There is no significant offset between ODP Site 926 and ODP Site 929 *Oridorsalis umbonatus* as the observed B/Ca offset (~4 µmol/mol) is very small, and it is less than the analytical uncertainty. This indicates that as suggested by the *Oridorsalis umbonatus* Mg/Ca record, *Oridorsalis umbonatus* is deep infaunal and therefore is unaffected by seawater saturation state changes. The *Cibicidoides mundulus* site-to-site offset varies. The variability in the B/Ca values is likely be related to a combination of saturation state changes caused by a shifting of the depth boundary between the two water masses and global saturation state changes as is thought to be the case for *Cibicidoides mundulus* Mg/Ca. The B/Ca variability can be loosely correlated to the Mg/Ca variability in the *Cibicidoides mundulus* record (Figure 4-18). This supports the idea that the variability in the *Cibicidoides mundulus* Mg/Ca data is related to saturation state.

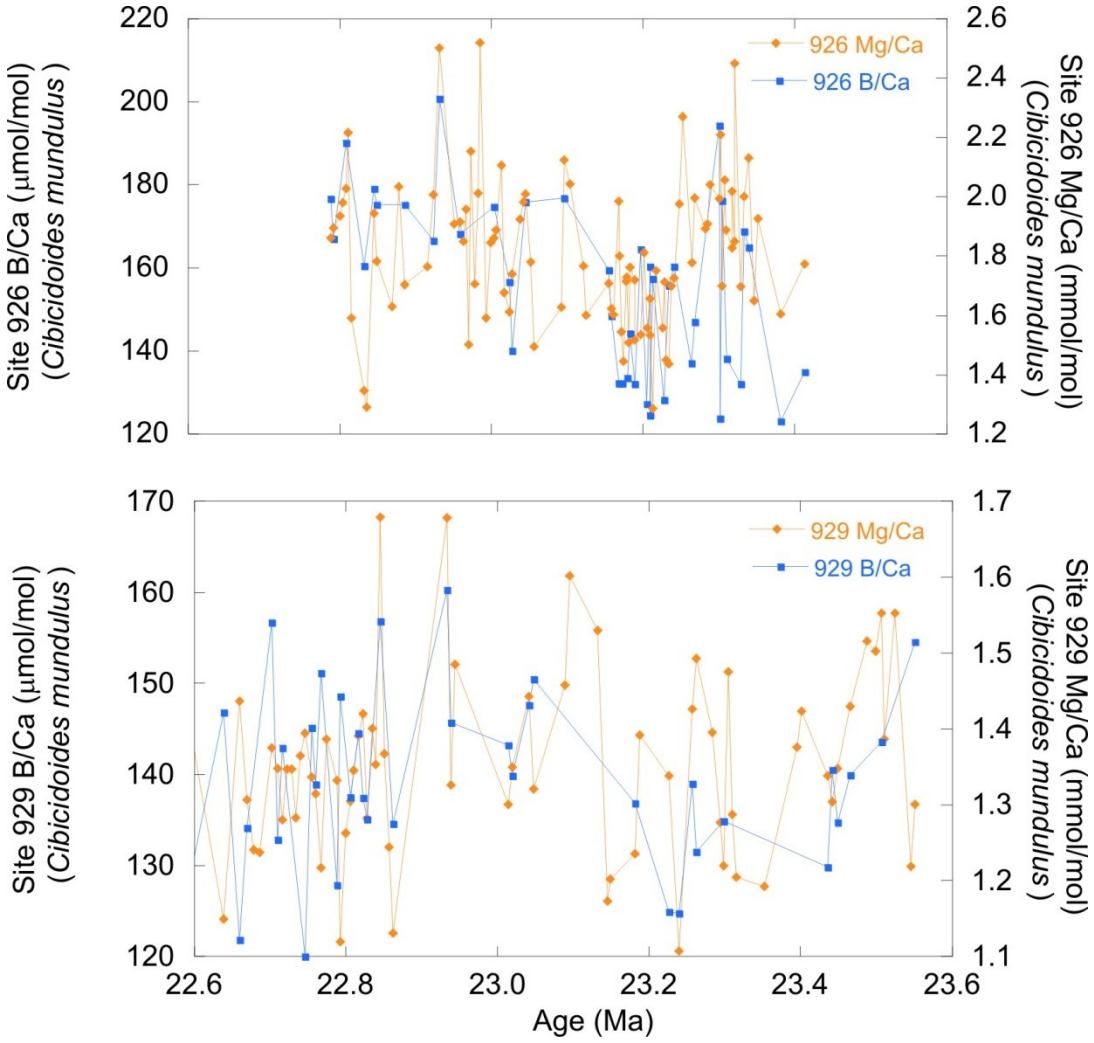

Figure 4-18 ODP Site 926 and 929 *Cibicidoides mundulus* B/Ca and Mg/Ca records across Mi-1.

B/Ca Species offsets

In both ODP Sites 926 and 929 B/Ca values in *Cibicidoides mundulus* are considerably higher than those of *Oridorsalis umbonatus*. This may be related to habitat differences; it seems that infaunal dwelling species may have lower absolute B/Ca values for example, *Uvigerina* spp. another infaunal taxon had been shown to also have low absolute B/Ca (Yu and Elderfield, 2007). In epifaunal species higher saturation state results in higher B/Ca values (Yu and Elderfield, 2007) likely a result of how the infaunal species incorporate B/Ca into their calcite (i.e. different vital effects).

Leg 154 U/Ca records

At Leg 154 sites U/Ca is unusual compared to other metals because the site-to-site contrast is larger than the species contrast. *Cibicidoides mundulus* and *Oridorsalis umbonatus* give the same trends (Figure 4-12C,D) but the Site 926 to Site 929 trends are different. (Figure 4-12A,B).

Across the Mi-1 transition

Overall U/Ca values increase in both species across the Mi1 event at both sites although the magnitude of change is different between sites. Recently U/Ca values in two species of benthic foraminifera (*Planulina wuellerstorfi* and *Cibicidoides mundulus*) have been shown from core-top data to be inversely correlated with carbonate saturation state (Raitzsch et al., 2011). However in this study it is assumed that saturation state does not have an effect on *Oridorsalis umbonatus* trace metal values due to its infaunal nature. Therefore the increase in *Oridorsalis umbonatus* U/Ca must be related to an alternative effect. Interpreting the *Cibicidoides mundulus* U/Ca increase with the U/Ca-ΔCO_3^{2-} relationship of Raitzsch et al. (2011) would imply that the carbonate saturation state decreased in both sites across the Mi-1 event, which is not supported by % coarse fraction records (Pälike et al., 2006b) (Figure 4-17) or B/Ca records (Figure 4-11B). Also, the U/Ca values measured in this study are much higher (~20-100 nmmol/mol) than those produced from the core-top benthic foraminifera calibration study (maximum ~20 nmmol/mol) and thus, the resulting transformations of the ODP Site 926 and 929 data cannot be interpreted with any confidence. Moreover, earlier observations from core-top studies (Russell et al., 1994) indicate that *Cibicidoides wuellerstorfi* U/Ca decreased with water depth at levels at and below the lysocline, which implies a positive relationship between saturation state and U/Ca values. Our understanding of the relationship between benthic U/Ca and ΔCO_3^{2-} therefore seems to be rather incomplete, and therefore, the use of U/Ca as a saturation state proxy should be approached with caution.

It is likely that temperature may also affect U/Ca in benthic foraminifera as has been demonstrated in planktonic foraminifera (Yu et al., 2008). However, use of existing planktonic foraminiferal U/Ca-temperature calibrations would produce unrealistically large temperature changes across Mi-1 and therefore if the decrease in U/Ca observed in the ODP Leg 154 sites is caused by temperature change this implies either a large sensitivity to temperature change or a large pre-exponential constant for any calibration.

A further factor which may affect U/Ca values is the availability of uranium for uptake by foraminifera. This could be related to detrital input (increased leaching of metals from clays in pore waters). However the slightly increasing coarse fraction across Mi-1 (Figure 4-17) would indicate decreasing and not increasing detrital input (Shackleton and Crowhurst, 1997). Uranium speciation in seawater may also be related to oxygen levels with increased oxygen levels leading to higher uranium availability for foraminiferal uptake. Under this scenario the transient peaks in benthic foraminiferal U/Ca would represent intervals of increased oxygenation of the bottom water mass. Interestingly, a positive relationship between test size and oxygenation of bottom waters has been demonstrated (Kaiho et al., 2006). If the increased test sizes reflect increased calcite precipitation rate then one may expect them to also have higher Li/Ca (Lear and Rosenthal, 2006). It is noteworthy that the “23 Ma Li/Ca event” does correspond to a transient increase in U/Ca

(Figure 4-12B) yet it is strange that the "23 Ma Li/Ca event" is only recorded by the epifaunal species. However if benthic foraminiferal U/Ca reflects oxygenation levels why do *Oridorsalis umbonatus* and *Cibicidoides mundulus* have similar U/Ca if they live at different depths in the sediment (Figure 4-12 C,D)? The effects of O_2, total organic carbon (TOC) and [CO_3^{2-}] interact in a non-straightforward way in the pore waters, meaning that as the changing U speciation works to increase foraminiferal U/Ca total [U] changes works to decrease foraminiferal U/Ca (Raitzsch et al., 2011). Therefore despite the steep O_2 profile in pore waters it is possible that U/Ca of foraminifera living at different depths may have similar absolute U/Ca (Raitzsch et al., 2011).

ODP Site 926 and ODP Site 929 comparison

There is no large consistent offset between ODP Site 926 and 929 for either *Oridorsalis umbonatus* or *Cibicidoides mundulus*, as would be expected if temperature (for *Oridorsalis umbonatus record*) or temperature/ΔCO_3^{2-} (for the *Cibicidoides mundulus* record) was the dominant control on U/Ca. Generally though ODP Site 926 benthic foraminiferal U/Ca is slightly higher than ODP Site 929. If ΔCO_3^{2-} was the dominant control then it would be expected that there would be an U/Ca offset with ODP Site 929 having higher values for U/Ca than ODP Site 926 due to the proposed negative relationship between U/Ca and ΔCO_3^{2-} (Raitzsch et al., 2011). Therefore it seems most likely that the U/Ca records reflect site specific parameters related either to sediment composition or bottom water chemistry.

Species offsets

No offset in U/Ca values is observed between *Oridorsalis umbonatus* and *Cibicidoides mundulus* data at either site. This suggests that the uptake of U/Ca into the biogenic calcite of these two foraminifera is not subject to different vital effects of living foraminifera. Another possibility is that the U/Ca is not of biogenic origin and instead represents contamination. As samples were vigorously cleaned as described in the methods chapter (chapter 2) it seems unlikely that this is the case. Moreover, if the U/Ca values were due to contamination then the data would likely be more scattered, and the two species would not show the same systematic trends seen here.

The use of U/Ca as a carbonate saturation state proxy in these records is inappropriate as there are several other potential influences which in these Ceara Rise records appear to have a dominant affect on U/Ca. Untangling these influences provides scope for further study.

Leg 154 Sr/Ca records

Across the Mi-1 transition/PGW

The Sr/Ca data across the Mi-1 event and into the PGW event does not show much variability at ODP Site 926 or ODP Site 929 for either benthic foraminiferal species. This suggests that Sr/Ca in benthic foraminifera does not directly record temperature or

saturation state in the way that Mg/Ca does. Sr/Ca in benthic foraminifera has been shown to have a negative linear relationship with depth (Lear et al., 2003). Whereas this could be interpreted as reflecting a temperature control or saturation state control, this new data suggests that another factor is the driving mechanism of Sr/Ca changes with water depth.

Inter-site comparison

Sr/Ca in *Oridorsalis umbonatus* is unique as unlike B/Ca and Li/Ca it displays a similar magnitude of intersite offset as *Cibicidoides mundulus* (~0.08 mmol/mol compared to 0.07 mmol/mol) indicating that Sr/Ca is affected by water depth differences. Using the *Oridorsalis umbonatus* sensitivity of Sr/Ca to water depth of 0. 095 mmol/mol/km (Lear et al., 2003) produces a suggested water depth difference of ~840 metres which is in good agreement with the modern water depth difference of 750 metres, considering the error associated with analysis (± 1.6%) and the calibration. Given the linear relationship between Sr/Ca and water depth it seems likely this is related to pressure effects in this instance.

Species Sr/Ca offsets

There is a Sr/Ca offset between the two species of ~0.2 mmol/mol with *Cibicidoides mundulus* having higher Sr/Ca than *Oridorsalis umbonatus*. This is probably either related to their habitat or vital effects.

4.3.3 Temperature and ice changes across the Mi-1 transition

The anomalous cooling associated with the "23 Ma Li/Ca event" in the *Cibicidoides mundulus* temperature record (Figure 4-16) is coincident with a transient U/Ca increase. This hints at a possibility that the benthic foraminiferal Li/Ca record may be compromised by an additional environmental parameter. Therefore the *Oridorsalis umbonatus* Mg/Ca temperature record is used in the following discussion and to calculate δ^{18}Osw. Note that all temperature and δ^{18}Osw calculations assume modern seawater Mg/Ca. Therefore interpretations will focus on temporal variations and not absolute values.

The *Oridorsalis umbonatus* Mg/Ca records from ODP Sites 926 and 929 indicate a decrease in Mg/Ca values across Mi-1. If the Mg/Ca decrease of ~0.5 mmol/mol is attributed solely to temperature this results in a cooling of ~2°C using the calibration of Lear et al. (2002) (Figure 4-15).

These Mg/Ca based temperature estimates can be used to calculate seawater (δ^{18}Osw) across the Mi-1 event by removing the temperature component. Using the palaeotemperature equation of Erez and Luz (1983) $\delta^{18}O_{sw}$ has been calculated across Mi-1 for both ODP Sites 926 and 929 using the *Oridorsalis umbonatus* derived temperatures (Figure 4-19). The change in $\delta^{18}O_{sw}$ across the Mi-1 glacial event is ~0.8 ‰ at both sites. Calculations for the Pleistocene estimate 0.08 - 0.11‰ δ^{18}O per 10 metres of sea level

change (Fairbanks and Matthews, 1978; Adkins et al., 2002). This has recently been used in computer model simulations of ice sheets for the middle Miocene (Langebroek et al., 2010) and to estimate sea level changes in the middle Miocene (Lear et al., 2010). Applied here, this produces a sea level fall in the range of ~70-100 metres associated with Mi-1. This is consistent with other published sea level estimates (e.g. Paul et al., 2000).

Across Mi-1 it is seen clearly that temperature leads ice volume growth as the temperature decrease starts to occur at ~23.25 Ma whereas the ice volume increase starts to occur at ~23.20 causing a lag between temperature and ice volume change of ~50 kyrs.

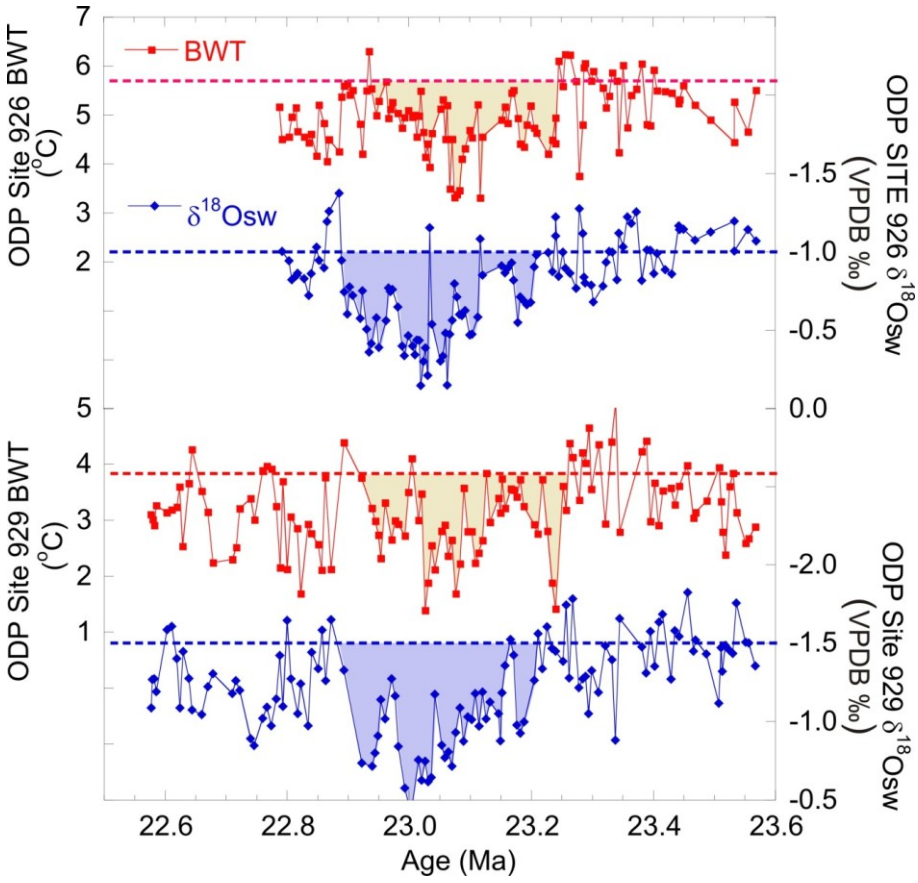

Figure 4-19 ODP Sites 926 and 929 bottom water $\delta^{18}O_{sw}$ calculated using the palaeotemperature equation of Erez and Luz (1983) and temperatures calculated from *Oridorsalis umbonatus* Mg/Ca values using the calibration of Lear et al. (2002).

Post glacial warming

After the Mi-1 event $\delta^{18}O$ values decrease (by approximately 0.82 ‰) to values similar to pre Mi-1 values by 22.9 Ma (Figure 4-19). As with the Mi-1 event there is a lag between temperature change (in this instance temperature increase) and ice volume change of ~50 kyrs. This excursion back to pre Mi-1 values (in approximately 200 ka) is why this event is classified as “transient” in contrast to the Eocene-Oligocene Climate Transition which represents a semi-permanent shift in $\delta^{18}O$ and therefore climate state (chapter 3). That the magnitude of the temperature and ice volume changes across the Mi-1 and subsequent

deglaciation are similar has implications for the sensitivity of ice sheet growth and decline to temperature. Ice sheet models have indicated that the decline of the Antarctic ice sheet requires a greater pCO_2 (and thus temperature) increase than the decrease required to produce the ice sheet (Pollard and Deconto, 2005). This hysteresis effect is in contrast to my data which that a similar temperature signal associated with the growth and decay of the ice sheet at Mi-1. Comparison with other sites may help determine whether the Ceara Rise temperature history reflects a regional or global signal. If confirmed at other sites, this may point to a more dynamic ice sheet than captured by current ice sheet models, or some component of northern hemisphere glaciation during Mi-1.

4.3.4 Equatorial Pacific ODP Site 1218; Stable isotope and trace metal records across Mi-1

Unlike the Eocene-Oligocene Climate Transition (Chapter 3) for which there are a number of records from around the world (Billups and Schrag, 2003; Lear et al., 2004; Lear et al., 2008; Katz et al., 2008; Pusz et al., 2010; Peck et al., 2010) the Mi-1 transient glaciation has remained relatively understudied. The Billups and Schrag (2003) Southern Ocean records have benthic trace metal data across the Mi-1 event but the data is not of sufficient resolution to record the details of the associated ocean physical and chemical changes (no data between 19.1 and 24.1 Ma). The only site with a trace metal record of sufficient resolution currently available is that of equatorial Pacific ODP Site 1218 which uses the species *Oridorsalis umbonatus*. This section aims to compare published and unpublished ODP Site 1218 trace metal data with that produced in this study to determine whether the changes observed in the western tropical Atlantic sites are also observed in the equatorial Pacific.

ODP Site 1218 benthic stable isotopes

Across the Mi-1 event ODP Site 1218 benthic $\delta^{18}O$ and $\delta^{13}C$ show similar patterns of transient isotopic increase to western tropical Atlantic ODP Sites 926 and 929 (Figure 4-20A). *Oridorsalis umbonatus* $\delta^{18}O$ show an increase of 0.95 ‰ and a $\delta^{13}C$ increase of ~0.8 ‰. The timing of the $\delta^{18}O$ increase at ODP Site 1218 is similar to ODP Sites 926 and 929.

ODP Site 1218 Mg/Ca

Across the Mi-1 event, *Oridorsalis umbonatus* Mg/Ca shows a clear decrease of ~0.4 mmol/mol (Figure 4-20B). This decrease is similar to the equivalent *Oridorsalis umbonatus* records at both ODP Site 926 (0.4 mmol/mol) and ODP Site 929 (0.5 mmol/mol). Following Mi-1 there appears to be a larger variability in the Mg/Ca values. The ODP Site 1218 Mg/Ca seems to slightly lead the ODP Site 926 Mg/Ca. Following Mi-1 ODP Site 1218 Mg/Ca values increase by ~0.4 mmol/mol.

ODP Site 1218 Li/Ca

ODP Site 1218 *Oridorsalis umbonatus* increases Li/Ca before and across the Mi-1 event. There seems to be little change across the post glacial warming (Figure 4-20C). Between 22.97 and 22.92 Ma there is a large increase in the Li/Ca data of ~3.3 µmol/mol. There is a rapid recovery from this excursion by ~22.8 Ma. This is an interesting excursion because it is exactly aligned with a negative excursion in Mg/Ca.

ODP Site 1218 Sr/Ca records

Across Mi-1 ODP Site 1218 *Oridorsalis umbonatus* Sr/Ca do not exhibit any obvious trends, following this event the *Oridorsalis umbonatus* Sr/Ca values appear to be more variable by a factor of ~ two.

ODP Site 1218 U/Ca records

Site 1218 *Oridorsalis umbonatus* U/Ca records across the Mi-1 event range between 10 and 18 nmol/mol. These absolute values are lower than those at ODP Site 926 or Site 929 (between 20-120 nmol/mol). Across the Mi-1 event U/Ca values increase by ~3.5 nmol/mol. After the Mi-1 event U/Ca values are variable but stable until 22.86 Ma when they start to decrease.

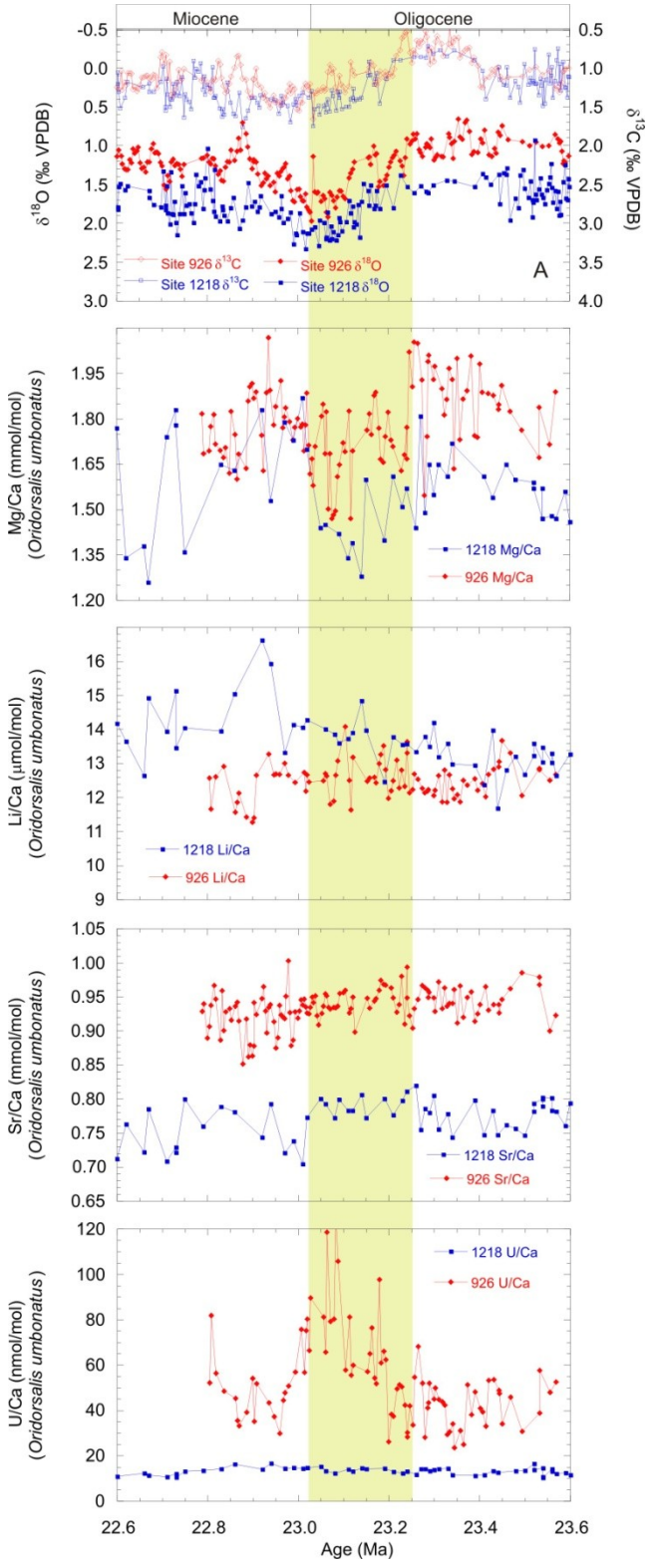

Figure 4-20 A) ODP Sites 1218 and 926 $\delta^{18}O$ and $\delta^{13}C$ (Lear et al., 2004; Pälike et al., 2006b) B) ODP Site 1218 (*O. umbonatus)* Mg/Ca (Lear et al., 2004) C) ODP Site 1218 (*O. Umbonatus)* Li/Ca (Lear and Rosenthal, 2006) D) unpublished ODP Site 1218 (*O. umbonatus*) U/Ca (C.H Lear, personal communication.) E) unpublished ODP Site 1218 (*O. umbonatus*) Sr/Ca (C.H Lear, personal communication).

4.3.5 Comparison of ODP Site 1218 records with ODP Site 926 and 929 records

Temperature and Ice volume

The magnitude of the increase in δ^{18}Osw and bottom water temperature decrease (~2°C) across the Mi-1 glaciation are similar at Ceara Rise (ODP Site 926) and the equatorial Pacific (ODP Site 1218) (Figure 4-21). ODP Site 1218 potentially shows more warming after the deglaciation (Figure 4-21) improving the resolution of the data may confirm this. The equatorial Pacific records are also similar to the Ceara Rise records in that temperature leads ice volume growth and decay. Unlike the Ceara Rise temperature record, the ODP Site 1218 record suggests that bottom water temperatures reached values perhaps 1 degree warmer than those pre Mi-1 just prior to glaciation.

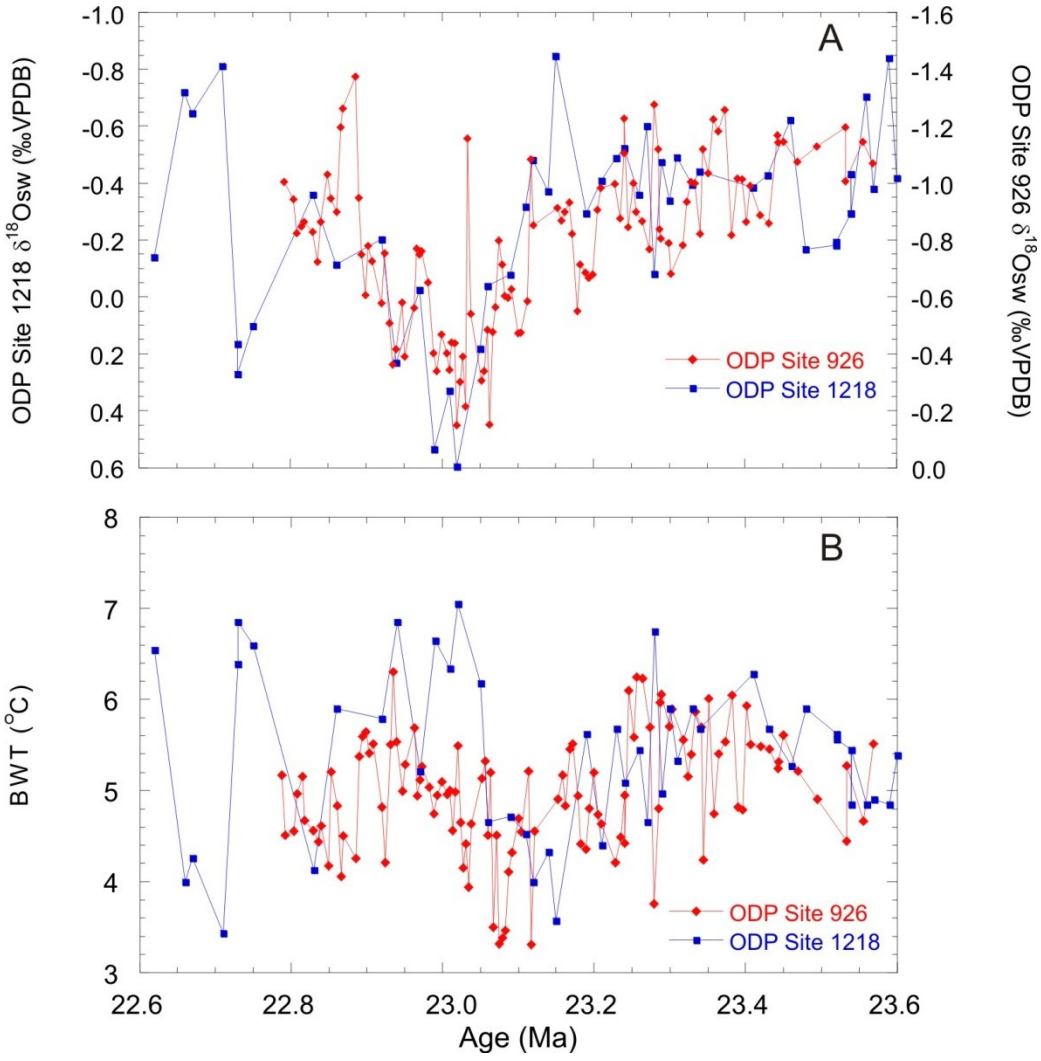

Figure 4-21 A) ODP Sites 1218 and 926 $\delta^{18}O_{SW}$ calculated using the palaeotemperature equation of Erez and Luz (1983) and B) ODP Sites 1218 and 926 bottom water temperatures calculated from *Oridorsalis umbonatus* Mg/Ca values using the calibration of Lear et al. (2002). Note 0.6 ‰ offset in the $\delta^{18}O_{sw}$ axes.

ODP Site 1218, other trace metals

Li/Ca

The increase in Li/Ca across Mi-1 (of ~1 µmol/mol) is smaller than the increase expected for a 2°C temperature decrease using the sensitivity of Lear et al., 2010 (expected increase ~1.5 µmol/mol). Also Li/Ca is increasing at a similar rate prior to the Mi-1 event at a similar rate (Figure 4-20C). This suggests that either the saturation state was decreasing at Site 1218 to counteract the temperature signal or Li/Ca changes may be related to other changes in palaeoceanographic conditions which compromises its use as a temperature/saturation state indicator. A way to test this hypothesis would be to produce B/Ca data at Site 1218 across this interval for using an epifaunal benthic foraminifera such as *Cibicidoides mundulus* to determine saturation state variability.

Sr/Ca

As with the ODP Leg 154 site records, ODP Site 1218 Sr/Ca does not show a strong trend across Mi-1. This agrees with the suggestion that Sr/Ca is influenced by a factor related to depth which is not temperature or saturation state. The depth difference between Site 1218 and Site 926 across Mi-1 was ~600 m. Using the Sr/Ca-water depth sensitivity of Lear et al., 2003 for *Oridorsalis umbonatus* this should cause a site-to-site offset of ~0.6 mmol/mol. This is comparable to the offset between the two sites indicating that this sensitivity is can be applied between ocean basins.

U/Ca

Compared to the ODP Leg 154 sites (ODP Sites 926 and ODP 929), the absolute U/Ca values from ODP Site 1218 *Oridorsalis umbonatus* benthic calcite are much lower by approximately a factor of 5. One possible explanation for the large differences between the ocean basins is that a non Mg bearing contaminant was not effectively removed by the cleaning method used here. A potential candidate for this is pyrite. This mineral was observed in some ODP Leg 154 samples and despite efforts to remove some may have remained. However benthic foraminiferal records from TDP samples rich in pyrite do not have increased U/Ca so this may not be the cause (C.H Lear. personal communication). Another possibility is that different levels of oxygenation between the two sites at the seafloor may have caused differences in uranium concentrations in seawater. Uranium is conservative in oxygenated ocean waters; it is sensitive to the redox conditions in environments and may become insoluble (McManus et al., 2005). An alternative way to explain *Oridorsalis umbonatus* being exposed to different redox conditions between the two sites would be if it was living at different depths in the sediment.

4.4 Conclusions

4.4.1 Global climate change in the late Oligocene to early Miocene (23.6 and 22.6 Ma)

1. The conclusions of this study based on new and existing trace metal and stable isotope records are that between 23.3 and 23.0 Ma a transient glacial event occurred that had global consequences for deep water temperature and chemistry. The estimated sea level change based on Mg/Ca and $\delta^{18}O$ records from this study is ~80 metres which is in agreement with the estimates of Paul et al. (2000).
2. At Ceara Rise in the western tropical Atlantic this glaciation was accompanied by a minimum deep water cooling of ~2°C across the Mi-1 event. The temperature change estimate from ODP Site 1218 in the Equatorial Pacific Mg/Ca also indicates a cooling of approximately 2°C and a similar change in $\delta^{18}Osw$. This indicates that the signal was global in nature. The post glacial warming temperature change at Ceara Rise is estimated from this study to be approximately ~2°C

4.4.2 Implications for trace metal proxies of this research

Mg/Ca

1. The late Oligocene-early Miocene benthic foraminiferal *Oridorsalis umbonatus* Mg/Ca data from the Equatorial Pacific and western tropical Atlantic produce estimates of deep water cooling within error of an independent estimate in the western tropical Atlantic across Mi-1 (Paul et al., 2000). This validates the use of Mg/Ca in benthic foraminifera as a palaeothermometer and indicates that in some oceanographic settings *Oridorsalis umbonatus* is unaffected by saturation state changes. The implications of this are that *Oridorsalis umbonatus* changes its habitat depending on environment conditions and this will be reflected in the trace metal signal produced.
2. *Cibicidoides mundulus* on the other hand is concluded here to reflect both saturation state and temperature change when below the saturation state threshold. Further work using core top calibrations from sites of similar temperature but differing saturation state would help determine the absolute sensitivity of *Cibicidoides mundulus* to saturation state changes.

Li/Ca

1. At ODP Sites 926 and 929 the cooling observed in the benthic *Oridorsalis umbonatus* Mg/Ca records is not observed to the same extent in the *Oridorsalis umbonatus* Li/Ca records. This may be explained by the use of an unsuitable Li/Ca-temperature sensitivity (as is based on temperatures above 5°C), or that a factor other than temperature was contributing towards the *Oridorsalis umbonatus* Li/Ca changes. Surprisingly there is no offset in *Oridorsalis umbonatus* Li/Ca between ODP Sites 926

and 929, as would be expected if Li/Ca is sensitive to temperature as the Mg/Ca data indicate a 2°C difference between the two sites.

2. In contrast a distinct inter-site offset is observed in *Cibicidoides mundulus* Li/Ca from ODP Sites 926 and 929. This offset may be attributed to both temperature and saturation state differences as *Cibicidoides mundulus* is affected by both these factors. Using the Lear et al. (2010) method for determining temperature changes using Li/Ca and Mg/Ca for ODP Site 926 causes an anomalous cooling due to a large Li/Ca peak at ~23 Ma. This peak is coincident with a large U/Ca peak which suggests that Li/Ca may be affected by a factor other than saturation state and temperature and caution should be applied when using this method.

B/Ca

1. The lack of any clear inter-site offset in B/Ca values across the ODP Site 926-929 depth transect for *Oridorsalis umbonatus* indicates that B/Ca in this species may not be a good proxy for carbonate saturation state as in this environment it is deep infaunal and thus buffered by pore waters. This is in agreement with core-top studies (Brown et al., 2011).
2. The large variability in *Cibicidoides mundulus* B/Ca which can be loosely correlated with *Cibicidoides mundulus* Mg/Ca indicates that *Cibicidoides mundulus* B/Ca may be used as a proxy for saturation state. However there is large scatter in the data which may be due to analysing different morphotypes, which have been recently shown to have different absolute B/Ca values (Rae et al., 2011). Also large analytical error makes interpretation difficult and efforts need to be made to improve B/Ca analysis (chapter 2).
3. The large offset in B/Ca values between *Oridorsalis umbonatus* and *Cibicidoides mundulus* supports the previously made observations that infaunal benthic foraminifera have lower absolute B/Ca values than epifaunal benthic foraminifera (Yu and Elderfield, 2007).

U/Ca

The benthic foraminiferal records studied here show the clearest signals. However the cause of the variability remains unknown. U/Ca does not appear to be suitable as a saturation state proxy during Mi-1 at Ceara Rise. Using the U/Ca – saturation state relationship and recent calibration of Raitzsch et al 2011 to interpret benthic U/Ca the ODP Site 926 and ODP Site 929 U/Ca records produced in this study indicate a very large saturation state decrease across the Mi-1 glaciation at ODP Sites 926 and 929. ODP Site 1218 Mi-1 U/Ca values and magnitude of change across Mi-1 are smaller than ODP Site 926 and ODP Site 929, however still indicate a saturation state decrease. This is inconsistent with other trace metal proxies and % coarse fraction data that allude to a saturation state increase. One possible explanation for the large

difference in uranium content between the western tropical Atlantic sites and the Equatorial Pacific is that Ceara Rise was receiving an external source of uranium from the adjacent Amazonian fluvial system. However this cannot easily explain the marked contrast in U/Ca records between the two Ceara Rise sites. Mg/Ca and U/Ca are not correlated suggesting that if the uranium is indeed sourced from a non-marine contaminant phase it has not affected the Mg/Ca signal. Alternatively the contrast between ODP Sites 926 and 929 U/Ca records perhaps hint at a water mass signal, whereby changing oxygen levels may have altered the availability of uranium for uptake by foraminifera.

Sr/Ca

1. The lack of change in the Sr/Ca values across the Mi-1 or PGW events indicate that Sr/Ca is not sensitive to temperature change and saturation state change.
2. The offsets in Sr/Ca values observed across the depth transect as well as at ODP Site 1218 suggest that Sr/Ca values in benthic foraminifera are controlled by depth. This is in agreement with previous work (e.g. Lear et al., 2003), which indicates a relationship between Sr/Ca and water depth.
3. An interesting parallel between Sr/Ca and B/Ca data is that the epifaunal species *Cibicidoides mundulus* has higher overall Sr/Ca and B/Ca values than shallow infaunal *Oridorsalis umbonatus*. This may be related to different vital effects caused by the two species living in different benthic environments.

4.5 Further Work

This study has provided independent geochemical proxy evidence that the Mi-1 event determined from $\delta^{18}O$ changes has both ice volume/sea level change and temperature components. The new trace metal data produced here has provided new insights into the magnitude of deep sea temperature change and therefore sea-level change. These data allude to possible changes in deep sea carbonate saturation, but highlight large holes in our understanding of the way in which proxies such as Mg/Ca, Li/Ca and Sr/Ca respond to saturation state change. To produce further constraints on this major global climatic event records are required from other ocean basins to compare and contrast differences in temperature change across the Mi-1 event. Also the sea level estimates provided here are approximate and ideally should be constrained further.

One of the most important findings of this work are the limitations to our understanding of trace metal based palaeoceanographic proxies. The trace metal data collected from ODP Site 926 and 929 has answered some questions with respect to trace metal proxies which are still in development. However, it has also thrown up several new questions which require further work. This includes refining the “cold-end” of the benthic foraminiferal Li/Ca-temperature calibration through core-top studies including undersaturated waters to

establish if there is a ΔCO_3^{2-} threshold below which a Li/Ca saturation state proxy will not work.

U/Ca does not appear to be suitable as a saturation state proxy during Mi-1 at Ceara Rise. Further work is required to establish the reasons for this, including the possibility that Leg 154 samples are influenced by terrestrial input to the sediment pile. This could be tested by analysing bulk sediment [U] from all 3 sites. Other U/Ca ground testing should include core-top calibrations from undersaturated sites or benthic culturing experiments involving saturation state, temperature and oxygen levels.

Building on the results presented here, such work will further advance knowledge on the suitability of benthic foraminiferal trace metal ratios as paleoclimate proxies and the potential caveats to be considered in their application.

5 Middle Miocene Climate Transition (MMCT)

5.1 Introduction

The aim of this chapter is to explore the interplay of depth related carbonate saturation state and changing bottom water chemistry with respect to benthic foraminiferal composition during the MMCT, and to shed new light on the temperature/sea level reconstructions for this event. The MMCT was a major glaciation event during the Cenozoic, representing the expansion of the Antarctic ice sheet and a shift towards today's more glaciated climate. The MMCT is indicated by a positive excursion in $\delta^{18}O$ records on the magnitude of ~1 ‰ (Miller et al., 1991; Flower and Kennett, 1993; Holbourn et al., 2004; Lear et al., 2010). To further understand this major climate transition ice volume/sea level change across the event need to be considered. A mismatch between $\delta^{18}O$ records (Holbourn et al., 2004) and sea level curves (Hardenbol et al., 1998) prompt the need for an independent temperature proxy to deconvolve the ice volume/sea level changes from the $\delta^{18}O$ signal.

The Mg/Ca proxy as a salinity independent temperature proxy has the potential to deconvolve bottom water temperature (BWT) and ice volume from the $\delta^{18}O$ signal (e.g. Lear et al., 2000). However a secondary saturation state control on Mg/Ca may affect the temperature signal (Lear et al., 2004; Chapter 3). In order to avoid this problem of a saturation state control on benthic foraminiferal Mg/Ca, recent work has explored the potential of using paired Mg/Ca and Li/Ca records to determine relative changes in temperature and saturation state using their known sensitivities to temperature and saturation state (Lear et al., 2010). This study used middle Miocene samples from ODP Site 761 as a case study. ODP Site 761 is situated at 2179 m water depth on the Wombat Plateau, off northwest Australia (16˚ 44.23' S, 115˚ 32.10' E) (Figure 5-1). Slow sedimentation rates have led to unusually shallow burial depths (<50 m) for the middle Miocene sequence, producing enhanced foraminiferal preservation. Modern day bottom water carbonate saturation state is ~30 µmol/kg (Lear et al., 2010). The palaeowater depth of the site during the middle Miocene is thought to be similar to today's water depth (Holbourn et al., 2004).

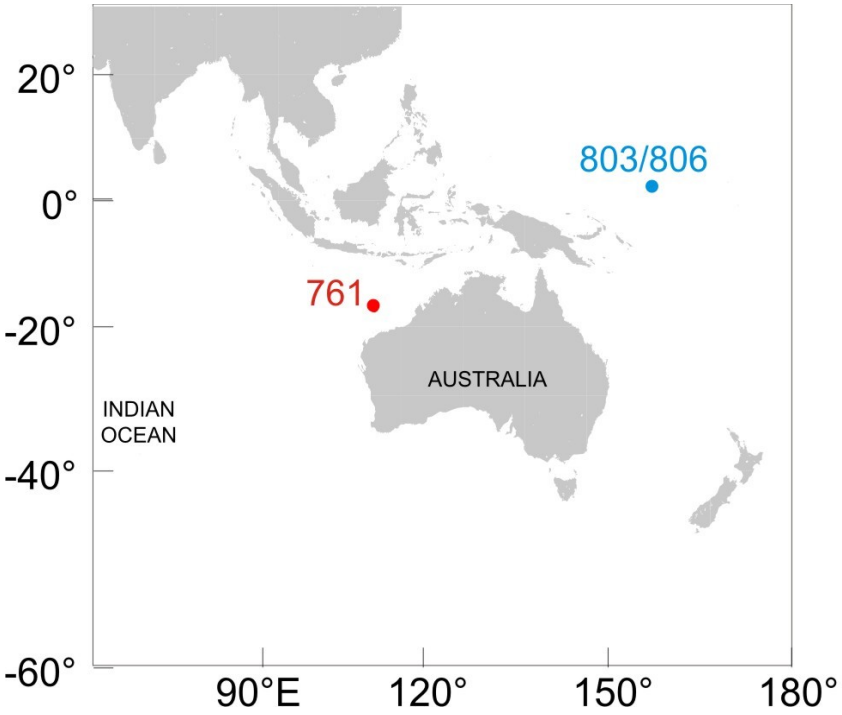

Figure 5-1 Locations of ODP Sites 761, 803 and 806.

The benthic foraminiferal *(O. umbonatus)* Mg/Ca record from ODP Site 761 displays an overall decrease through the MMCT, which may be interpreted at face value as a cooling (green diamonds in Figure 5.2). However, the benthic foraminiferal Li/Ca records suggest that the site experienced concomitant changes in bottom water saturation state through the climate transition. If ODP Site 761 lay above the Mg/Ca-carbonate saturation state threshold (proposed at ~25 µmol/kg (Elderfield et al., 2006)) then the uncorrected Mg/Ca-temperature variations are likely robust (green diamonds in Figure 5.2). However, if ODP Site 761 lay below the saturation state threshold (which may be higher than previously supposed (Chapter 3)) then the Mg/Ca record needs to be corrected for changes in saturation state (red diamonds in Figure 5.2). Because the authors of this study had no reason to favour either scenario they used both “corrected” and uncorrected” temperatures and ice volume histories in their reconstruction of the climate transition. Inevitably this increased the uncertainties of the estimated climate parameters, for example the maximum offset between the corrected and uncorrected temperature records is ~2.8°C which translates into a $\delta^{18}O_{sw}$ uncertainty of ~ 0.69 ‰ (Figure 5-1B). Put into perspective, this offset in calculated $\delta^{18}O_{sw}$ is similar to the expected change in $\delta^{18}O_{sw}$ (~-0.8 ‰) if the modern day Antarctic ice sheet were to melt (Cramer et al., 2011).

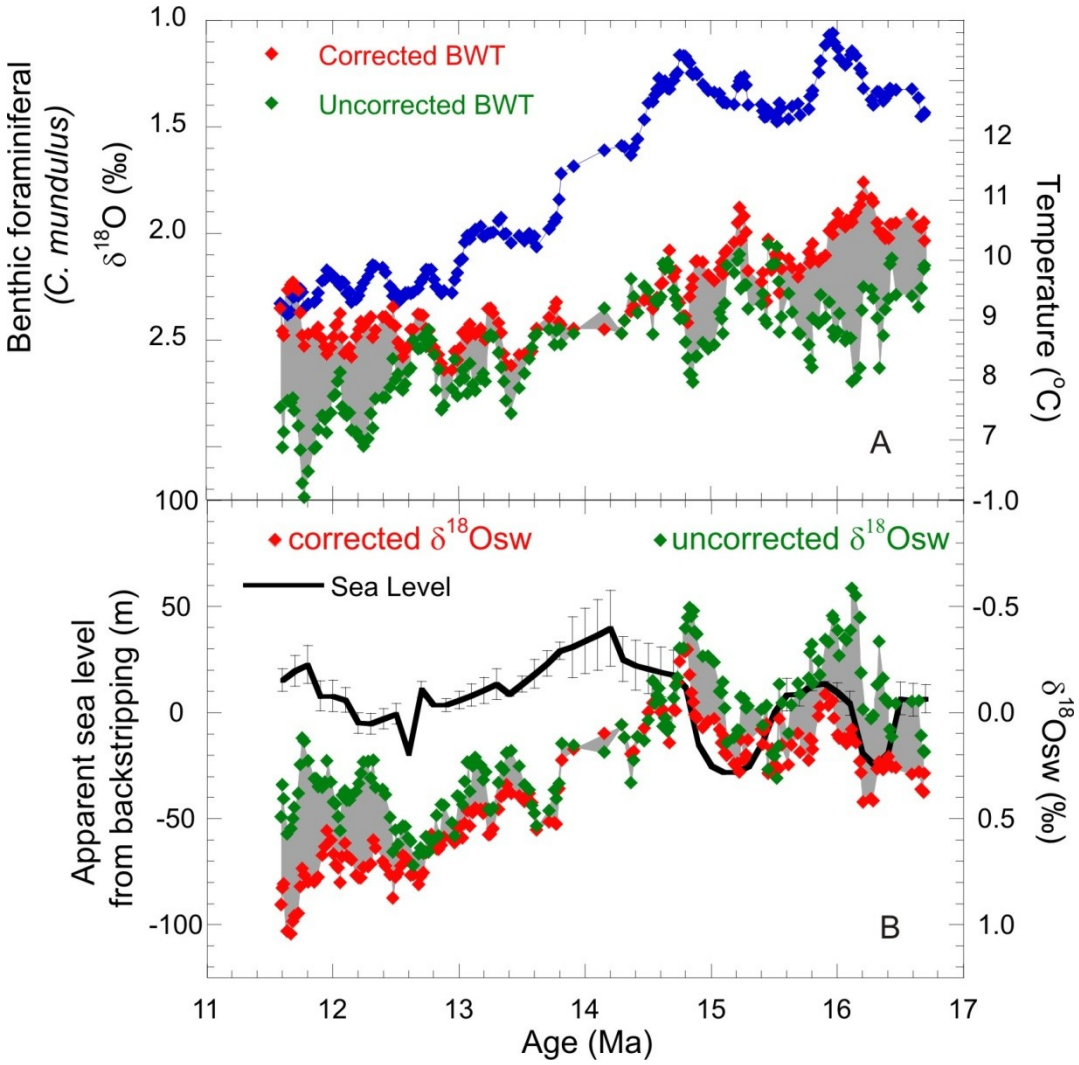

Figure 5-2 A) Benthic foraminiferal $\delta^{18}O$ and Mg/Ca-Li/Ca based temperatures across the MMCT (Lear et al., 2010). The grey shaded area is the range between the saturation state corrected and uncorrected temperatures (uncorrected assume that ODP Site 761 was above the saturation state threshold).

B) $\delta^{18}O_{sw}$ derived using the corrected and uncorrected temperature estimates of 5-2A (Lear et al., 2010) compared to apparent sea level from backstripping (Kominz et al., 2008).

Therefore, one of the goals of this work was to attempt to determine whether ODP Site 761 was above or below the Mg/Ca-saturation state threshold during the MMCT by comparison of the Site 761 Mg/Ca record with new Mg/Ca records from two different sites: ODP Site 806 and ODP Site 803.

5.1.1 Working hypothesis

The MMCT contains variations in both temperature and saturation state. Therefore, a benthic foraminiferal Mg/Ca record from a site lying above the saturation state threshold will be different (in terms of both absolute Mg/Ca and also Mg/Ca variations) from a site lying below the saturation state threshold. For this study therefore, the ODP Site 761 record is compared to two deeper sites, the deepest of which most probably lay below the saturation state threshold during the MMCT. The working hypothesis is that if all three Sites contain similar downcore variations in Mg/Ca it is likely that all three were situated below the saturation state threshold. Furthermore, inter-site Mg/Ca offsets should be consistent with inter-site $\delta^{18}O$ offsets if the sites lay above the threshold, but be larger than expected from the $\delta^{18}O$ records if the sites lay below the threshold. Finally, a change in the inter-site Mg/Ca offset that is not accompanied by a change in the inter-site $\delta^{18}O$ offset may reflect the transitioning of a site through the saturation state threshold.

5.1.2 Site Selection and Approach

In order to help determine whether ODP Site 761 lay above or below the carbonate saturation state threshold during the MMCT I have produced a suite of trace metal analyses and stable isotope analyses on benthic foraminiferal calcite across the MMCT from ODP Sites 803 and 806. These sites were chosen as the Ontong Java Plateau (OJP) setting provides good quality, continuous core sections from two deeper palaeowater depths. ODP Sites 806 and 803 (ODP Leg 130) are located on the north eastern margin of the OJP (Figure 5-1). Their modern water depths are 3400 m for ODP Site 803 and 2500 m for ODP Site 806. Palaeowater depths have been estimated at 16 Ma as ~3550 m for ODP Site 803 and 2800 m for ODP Site 806 (Cramer et al., 2009). The modern day saturation states for these sites are ~10 µmol/kg for Site 806 and ~3.5 µmol/kg for Site 803 (Figure 5-3).

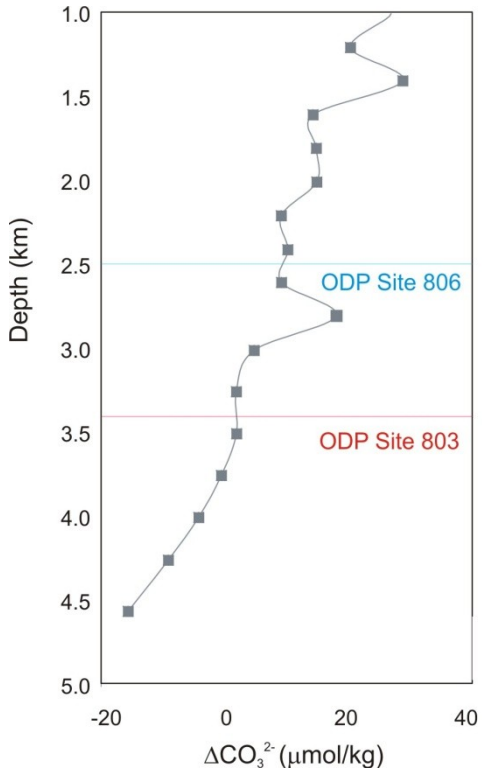

Figure 5-3 Saturation state profile for the OJP region (adapted from Dekens et al., 2002). Data from WOCE cruise P10, station 10 put into CO_2 System calculations (Lewis and Wallace, 1998).

Hole 806B ages were calculated using the biostratigraphic age model of Lear et al. (2003b), which is based on nannofossil, radiolarian and planktonic foraminiferal biostratigraphical events within the Leg 130 cores. Hole 803D ages were generated using the same method in this study. Using benthic foraminiferal $\delta^{13}C$ as a tuning target, the Hole 806B and 803D ages were then adjusted to the middle Miocene record from ODP Site 761, by adding 500 kyr (Appendix 8.5.1).

5.2 Results

The stable isotope and trace metal records produced in this study for ODP Sites 806 and 803 are presented here along with published ODP Site 761 records (Lear et al., 2010). The published ODP Site 761 records shown in Figure 5-2, Figure 5-11 and Figure 5-12 here are 5 point moving averages of the data, those in Figure 5-4 to Figure 5-9 are unsmoothed. The ODP Site 806 and ODP Site 803 data are all raw data.

5.2.1 ODP Legs 130 and 122 benthic foraminiferal stable isotope records

$\delta^{18}O$

The $\delta^{18}O$ values at all sites (ODP Sites 761, 803 and 806) increase by ~1.2‰ between ~14.7 and ~12.95 Ma (Figure 5-4). Due to the low resolution of the data at ODP Site 803

the onset of the $\delta^{18}O$ shift is not entirely clear, but it is widely assumed to be a global event. ODP Site 761 and ODP Site 806 have similar absolute $\delta^{18}O$ values indicating that they either have similar temperatures during the MMCT, or that any offset in temperature is compensated for in the $\delta^{18}O$ record by an offset in salinity. ODP Site 803 $\delta^{18}O$ values are approximately 0.3‰ higher than ODP Site 806 values, suggesting slightly colder (~1.5˚C) temperatures at the deepest site (Figure 5-4).

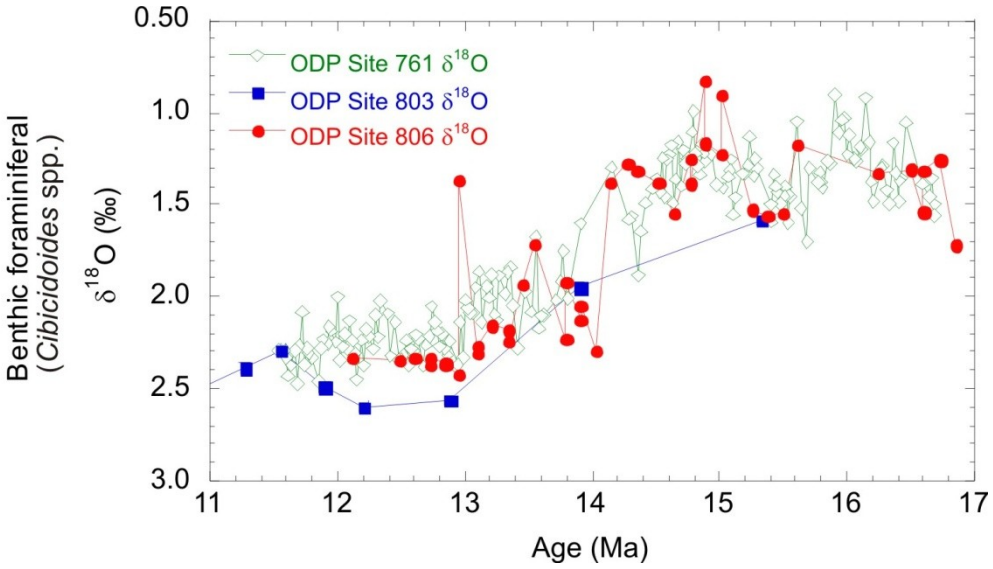

Figure 5-4 Benthic foraminiferal (*Cibicidoides* spp.) $\delta^{18}O$ records from ODP Sites 806 and 803 (this study) and ODP Site 761 (Lear et al., 2010).

$\delta^{13}C$

The benthic foraminiferal $\delta^{13}C$ records from ODP Sites 761, 803 and 806 follow the same trends across the MMCT. There are no offsets observed between the three sites (Figure 5-5).

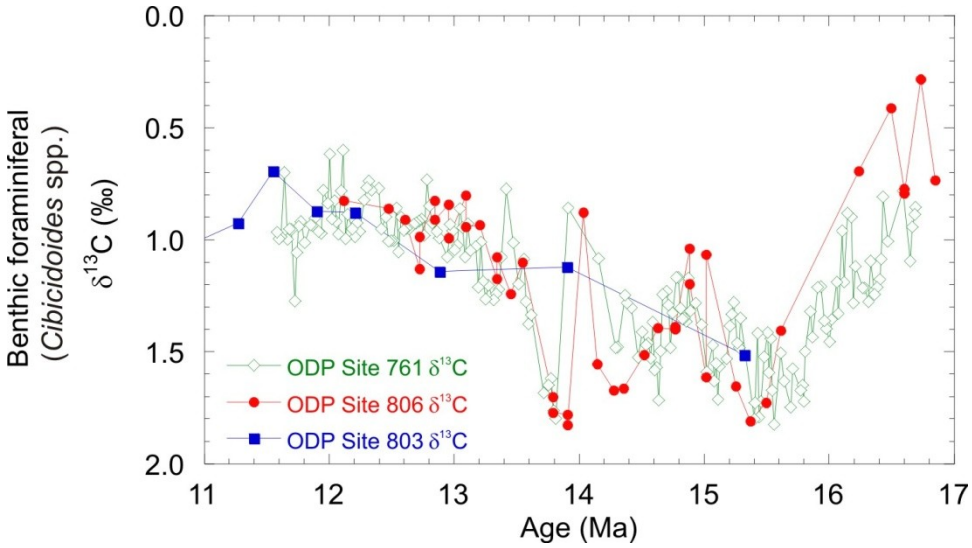

Figure 5-5 Benthic foraminiferal (*Cibicidoides* spp.) $\delta^{13}C$ records from ODP Sites 806 and 803 (this study) and ODP Site 761, (Lear et al., 2010).

5.2.2 ODP Leg 130 and Leg 122 benthic foraminiferal trace metal records

Mg/Ca

Both Mg/Ca records at ODP Site 761 and ODP Site 806 show a small decrease across the MMCT of ~0.3 mmol/mol (Figure 5-6). However there is a Mg/Ca offset between ODP Site 761 and ODP Site 806 which is not observed in the $\delta^{18}O$ records. The offset is ~0.5 mmol/mol. ODP Site 803 does not show as much variability as the other two sites or an overall decrease across the MMCT, but is much lower resolution. The offset between ODP Site 761 and ODP Site 803 is ~0.7 mmol/mol although this offset may not be constant through the record. While the 803 record is low-resolution, the 761-803 Mg/Ca offsets prior to the main $\delta^{18}O$ shift at ~13.8 Ma appear to be consistently larger (~0.9 mmol/mol) than those following the $\delta^{18}O$ shift.

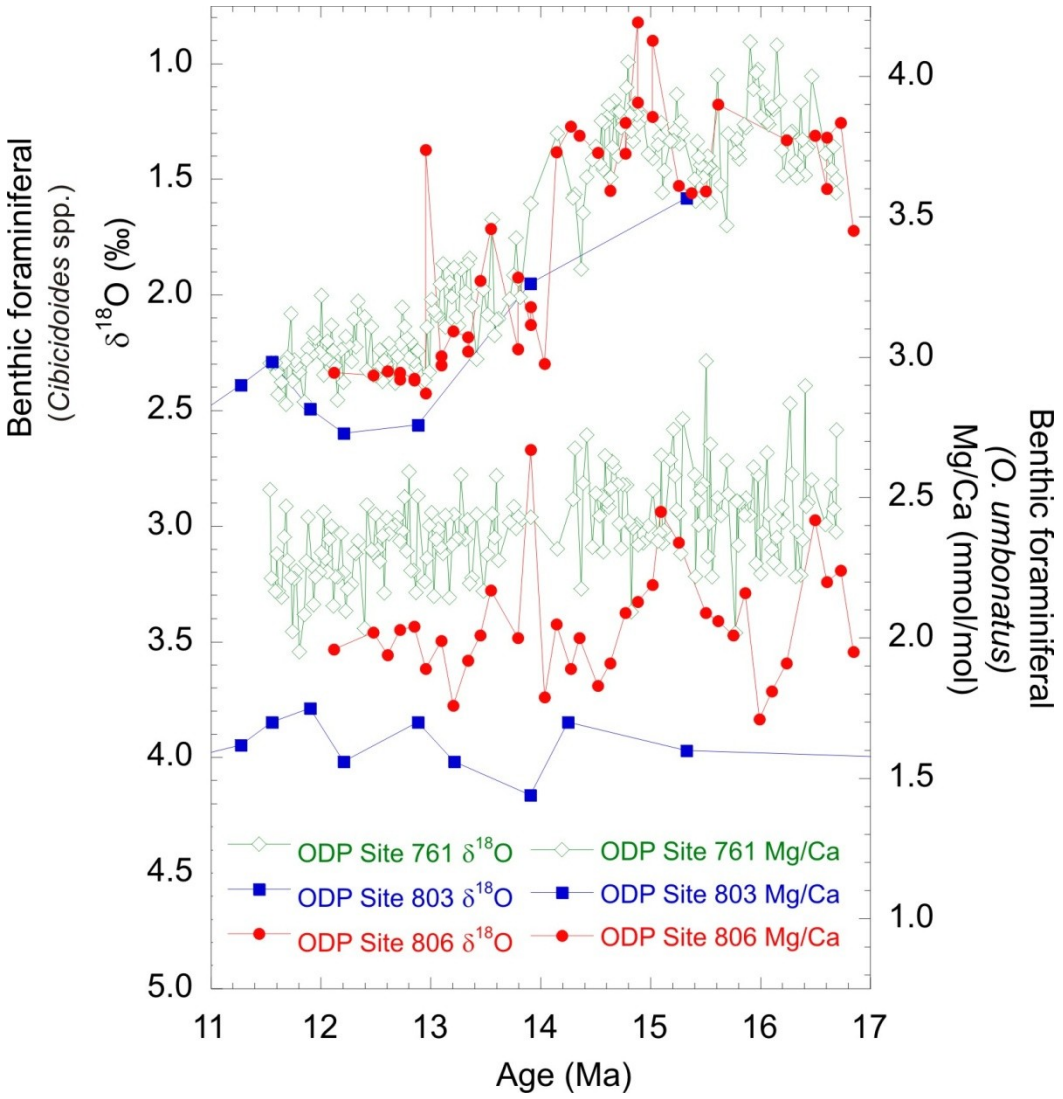

Figure 5-6 Benthic foraminiferal *(Oridorsalis umbonatus)* Mg/Ca records from ODP Sites 806 and 803 (this study) and ODP Site 761, Lear et al. (2010). Benthic foraminiferal *(Cibicidoides* spp.*)* $\delta^{18}O$ records from ODP Sites 806 and 803 (this study) and ODP Site 761, (Lear et al., 2010).

Li/Ca

ODP Sites 806 and 803 Li/Ca records show a general increase across the MMCT (Figure 5-7). This is the same trend seen in the ODP Site 761 record (Lear et al., 2010). The magnitude of the change is potentially lower at ODP Site 803 than the other sites. The Li/Ca offset between ODP Site 806 and ODP Site 761 increases from approximately 1 μmol/mol in the older part of the record to ~2 μmol/mol in the younger part of the record. ODP Site 803 Li/Ca values appear to lie between ODP Site 761 and ODP Site 806 values, around 0.5 μmol/mol lower than the Site 761 record (Figure 5-7).

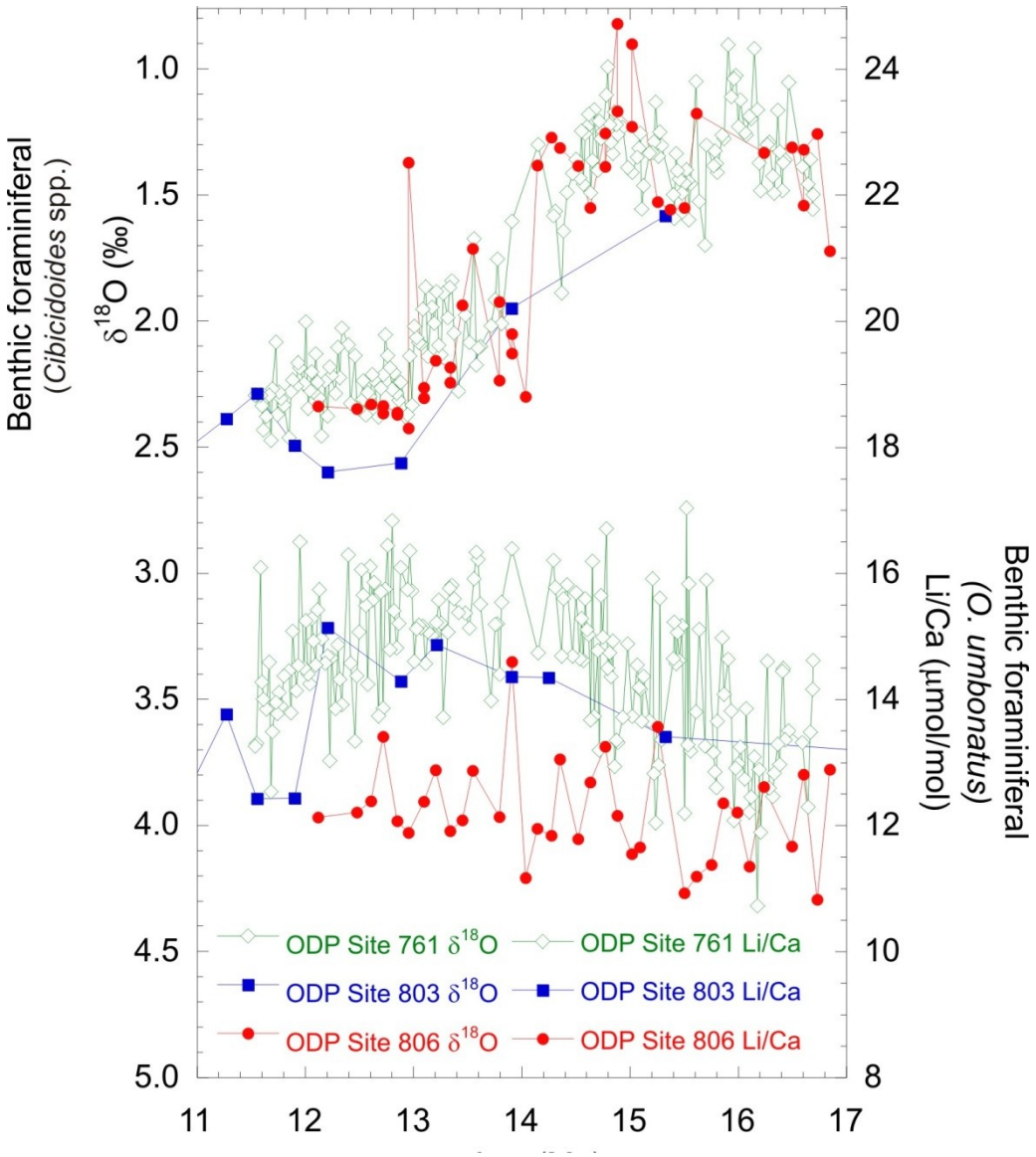

Figure 5-7 Benthic foraminiferal (*Oridorsalis umbonatus)* Li/Ca records from ODP Sites 806 and 803 (this study) and ODP Site 761, (Lear et al., 2010). Benthic foraminiferal (*Cibicidoides* spp.*)* $\delta^{18}O$ records from ODP Sites 806 and 803 (this study) and ODP Site 761, (Lear et al., 2010).

B/Ca

Across the MMCT both ODP Site 806 and ODP Site 803 B/Ca values increase (Figure 5-8) by ~6 µmol/mol. ODP Site 803 B/Ca values are slightly higher than those at ODP Site 806 in the middle of the transition. However the ODP Site 803 record is very low resolution. There are no published B/Ca records available from ODP Site 761 for comparison.

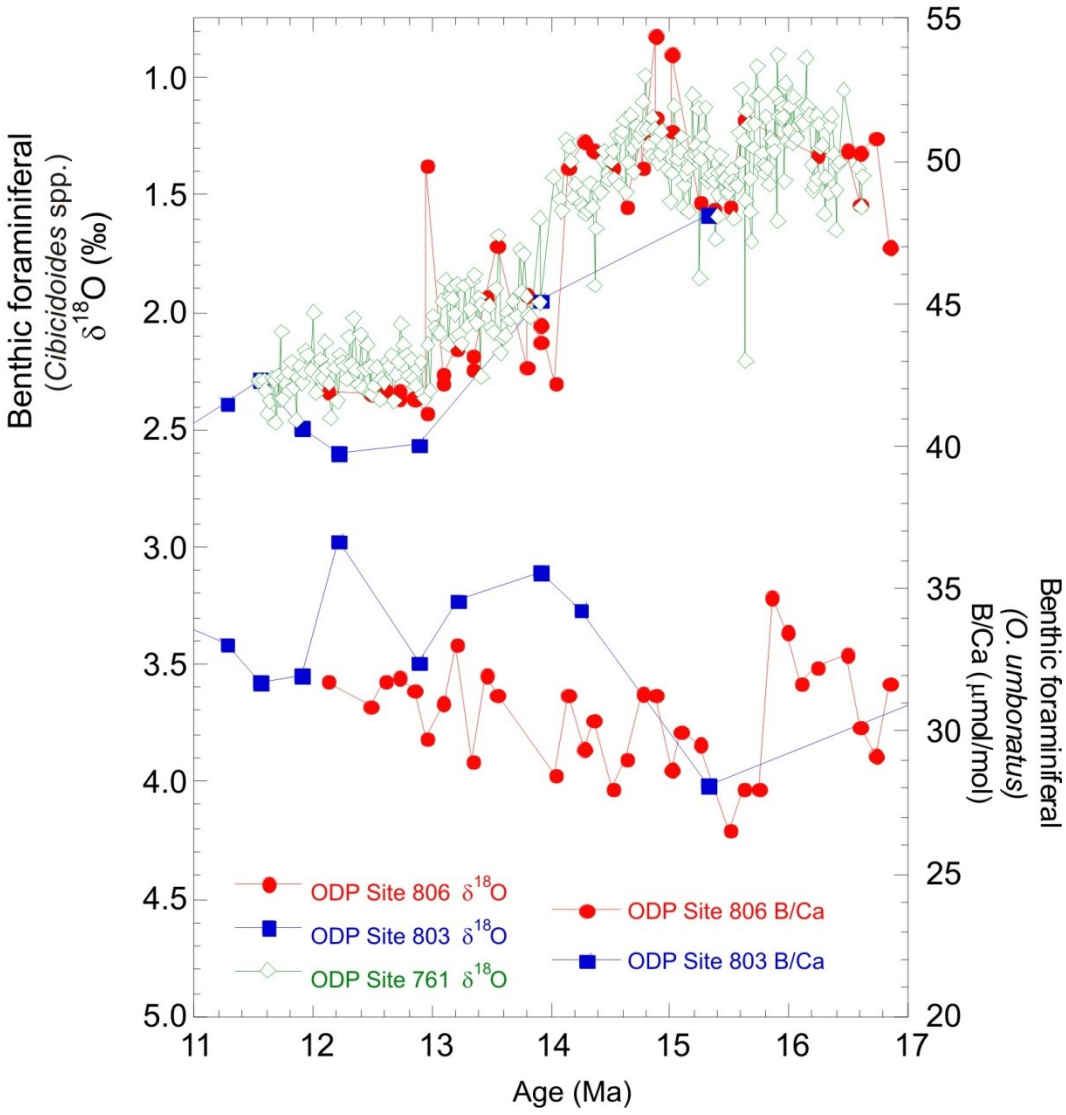

Figure 5-8 Benthic foraminiferal (*Oridorsalis umbonatus)* B/Ca records from ODP Sites 806 and 803 (this study) Benthic foraminiferal (*Cibicidoides* spp.) $\delta^{18}O$ records from ODP Sites 806 and 803 (this study) and ODP Site 761 (Lear et al., 2010).

5.3 Discussion

The Li/Ca records from ODP Sites 761, 803 and 806 all show a general increasing trend through the climate transition (Figure 5-7), supporting the interpretation of increasing saturation state across the MMCT (Lear et al., 2010). The overall increase in benthic foraminiferal B/Ca coincident with the increase in Li/Ca also supports a saturation state increase (Yu and Elderfield, 2007). However, the inter-site Li/Ca offset between ODP Site 806 and 761 appears to increase through the transition. There are two possible explanations for this. The first is that the Li/Ca-temperature sensitivity may decrease below ~5˚C (Lear et al., 2010). Therefore, if Site 806 cooled below ~5˚C whilst ODP Site 761 remained above 5˚C, the inter-site Li/Ca offset would be expected to increase. If this is the

case then a similar increase in the inter-site Li/Ca offset should be observed between ODP Sites 761 and 803. This is not apparent in the record (Figure 5-7). The second explanation is that ODP Site 806 witnessed a change in bottom water mass composition during the climate transition. Temperatures derived from the ODP Site 806 Mg/Ca record assuming no carbonate saturation state effect show similar trends and magnitude of overall decrease across the MMCT event as those derived from ODP Site 761 (Figure 5-10). Therefore, even considering the uncertainty surrounding the potential saturation state changes at both sites it seems that the Mg/Ca records provide a relatively robust broad-brush picture of MMCT temperature variations.

The difference in absolute Li/Ca values between ODP Site 803 and ODP Site 806 (ODP Site 803 Li/Ca is higher than ODP Site 806 Li/Ca) is at first sight surprising, as ODP Site 803 is the deeper site and thus likely had a lower carbonate saturation state. One interpretation of these data therefore is that the Li/Ca records are dominated by a temperature component, with the 803-806 inter-site offset reflecting a ~2-3˚C temperature offset and the overall Li/Ca increase through the transition reflecting a cooling of around 2-3˚C. Such a scenario might be expected if *O. umbonatus* had adopted an infaunal habitat for these samples, as proposed for the Mi-1 records presented in Chapter 4. If this was the case, the Li/Ca inter-site offsets would further imply that ODP Site 806 was bathed by a water mass approximately 3˚C warmer than Site 761. This is not supported by the inter-site Mg/Ca offsets, as ODP Site 806 Mg/Ca < ODP Site 761 Mg/Ca. Therefore it seems more likely that the Li/Ca records reflect a combination of temperature and saturation state, implying that *O. umbonatus* adopted an epifaunal or very shallow infaunal habitat in these sediments.

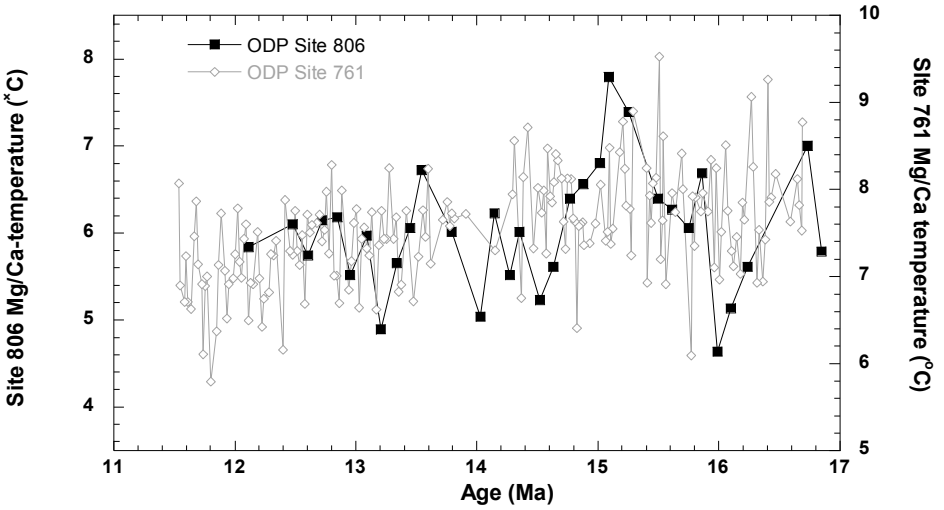

Figure 5-9 ODP Sites 806 (this study) and 761 (Lear et al., 2010) uncorrected Mg/Ca temperature records (calculated using Lear et al., 2002 *Oridorsalis umbonatus* calibration and assuming modern seawater Mg/Ca). Y axes have the same scale but are offset by 1.5°C.

The inter-site offsets in temperature and saturation state can be estimated using the assumed sensitivities of *O. umbonatus* Mg/Ca and Li/Ca to these parameters. Trace metal records across the Eocene-Oligocene Transition suggest that the sensitivity of *O. umbonatus* Mg/Ca to saturation state is more similar to that determined for *C. mundulus* by Raitzsch et al. (2008) (~0.017 mmol/mol/μmol/kg) than that determined for *C. wuellerstorfi* by Elderfield et al. (2006) (~0.0086 mmol/mol/μmol/kg) (Chapter 3). Sensitivities for the other parameters are given in Table 5-1. Therefore it can be assumed that when both sites lie below the Mg/Ca-saturation state threshold:

$\Delta Mg = 0.017 \times \Delta CO_3^{2-} + 0.12 \times \Delta T$

Equation 17

$\Delta Li = 0.047 \times \Delta CO_3^{2-} - 0.74 \times \Delta T$

Equation 18

Where delta (Δ) notation refers to the inter-site contrast. It follows that:

$\Delta CO_3^{2-} = (\Delta Li + 6.17 \times \Delta Mg)/0.152$ and

$\Delta T = (2.76 \times \Delta Mg - \Delta Li)/1.07$

For intervals where both sites of interest lie above the Mg/Ca-saturation state threshold:

$\Delta Mg = 0.12 \times \Delta T$ and

Equation 19

$\Delta Li = 0.047 \times \Delta CO_3^{2-} - 0.74 \times \Delta T$

Equation 20

Such that

$\Delta T = \Delta Mg/0.12$ and

$\Delta CO_3^{=} = (\Delta Li + 6.17 \times \Delta Mg) / 0.047$

	T (°C)	ΔCO_3^{2-}
Mg/Ca	0.12 ± 0.11 mmol/mol/°C [a]	0.017 ± 0.004 mmol/μmol/kg [b]
Li/Ca	-0.74 ± 0.98 μmol/mol/°C [c]	0.047 ± 0.58 μmol/μmol/kg [d]

Table 5-1 Trace metal sensitivities to temperature and carbonate saturation state used in the Lear et al. (2010) method. a) Marchitto et al. (2007), b) Raitzsch et al. (2008), c) Lear et al. (2010), d) Lear et al. (2010) (adapted from Lear and Rosenthal, 2006).

Assuming all three Sites lay above the Mg/Ca-carbonate saturation state threshold results in unrealistic temperature and saturation state offsets (e.g., ~7˚C and 129 μmol/kg between Sites 761 and 803) that cannot be reconciled with the oxygen isotope records. Therefore ODP Site 803 must have lain below the saturation state threshold. The question remaining is whether ODP Site 761 lay above or below the threshold. The observation that the 803-761 inter-site Mg/Ca offset appears to be larger prior to the main ice growth step, when overall levels of saturation state were lower, may help answer this question (Figure 5-10).

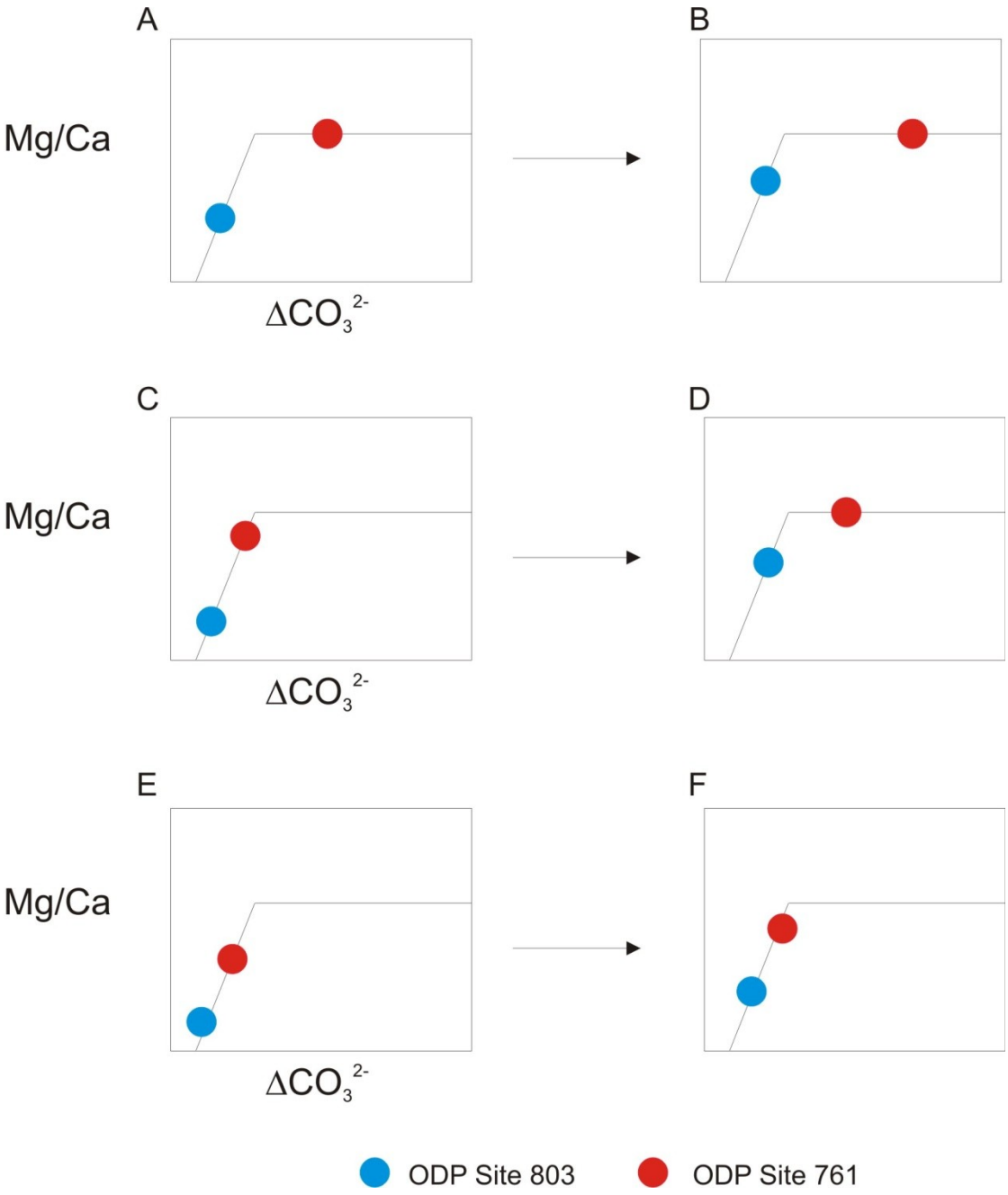

Figure 5-10 Schematic diagram to show how an increase in bottom water saturation state may affect inter-site Mg/Ca offsets (vertical offset between the two coloured spots) for a range of scenarios discussed in the text. Not to scale.

In this schematic diagram the X-axis is bottom water saturation state (ΔCO_3^{2-}), and the Y-axis is benthic foraminiferal Mg/Ca. When the line becomes horizontal this indicates where the threshold has been reached as Mg/Ca is no longer affected by carbonate saturation state. The three different scenarios in Figure 5-10 all represent the expected qualitative change in Mg/Ca caused by an increase in bottom water saturation state and assuming zero temperature change. The differences between the scenarios are explained below:

Scenario A to B represents an increase in saturation state across MMCT, with ODP Site 803 below and ODP Site 761 above the carbonate saturation state threshold at the start of the MMCT. After the climate transition, 803 is still below, and ODP Site 761 is still above the saturation state threshold, but the saturation state increase has resulted in a smaller inter-site Mg/Ca offset by the end of the MMCT.

Scenario C to D represents an increase in saturation state across MMCT, where both ODP Site 803 and ODP Site 761 are below the threshold at start of transition. At end of transition ODP Site 761 is above the threshold, but ODP Site 803 is still below threshold. This scenario also produces a Mg/Ca offset that is smaller at the end of the transition than at the start.

Scenario E to F is an increase in saturation state across the MMCT, where both ODP Site 803 and ODP Site 761 are below the saturation state threshold at the start and end of the climate transition. This scenario does not result in a change in the inter-site Mg/Ca offset through time.

Therefore scenarios A to B or C to D best fit the observation of a decreasing inter-site Mg/Ca offset associated with the increasing saturation state through the Middle Miocene Climate Transition. For both of these scenarios ODP Site 761 lay above the Mg/Ca-saturation state threshold following the climate transition. Determining whether ODP Site 761 lay above or below the threshold at the start of the climate transition is not as straightforward. If ODP Site 761 lay below the saturation state threshold at the start of the climate transition then the equations set out above may be used to calculate the inter-site offsets in temperature and saturation state prior to the glaciation (Table 5-1).

Site Comparison	ΔMg (mmol/mol)	ΔLi (μmol/mol)	ΔTemperature	ΔSaturation state
803-761	0.9	0.5	1.9˚C	40 μmol/kg
806-761	0.5	1.0	0.4˚C	27 μmol/kg

Table 5-1: Calculated inter-site offsets in temperature and saturation state (see text for details).

This suggests that of the three sites studied here, the shallowest site (ODP Site 761) was the warmest and most saturated, while the deepest site (ODP Site 803) was the coldest and least saturated. Given the uncertainties in this approach, the calculated temperature offsets are remarkably consistent with the observed inter-site offsets in $\delta^{18}O$ (Figure 5-4).

If ODP Site 761 lay above the saturation state threshold at the start of the climate transition, then only some portion of the inter-site ΔCO_3^{2-} contrast would impact the inter-site ΔMg. This would have the same effect as reducing the Mg/Ca sensitivity to ΔCO_3^{2-}. If the above calculation is repeated using the same Li/Ca sensitivities, but a halved Mg/Ca-ΔCO_3^{2-} sensitivity, then an 803-761 inter-site temperature contrast of 2.3˚C and saturation state contrast of 42 μmol/kg is obtained. It is harder to reconcile this temperature offset with the observed inter-site δ^{18}O offset of ~0.3 ‰. Therefore on balance it seems more likely that ODP Site 761 lay below, or at least near, the saturation state threshold immediately prior to the MMCT.

5.3.1 Implications for MMCT temperature and δ^{18}Osw reconstructions

The uncorrected Mg/Ca temperature history from ODP Site 761 (green diamonds in Figure 5-1) assumes that scenario A to B in Figure 5-12 is correct, whereas the corrected Mg/Ca temperature history (red diamonds in Figure 5-1) assumes that scenario E to F is correct. As discussed above, comparison of the Site 761 Mg/Ca record to the new records presented here suggests that the most likely scenario is C to D in Figure 5-12. In other words, on balance it seems most likely that ODP Site 761 lay beneath the Mg/Ca-carbonate saturation state threshold prior to the MMCT and above the Mg/Ca-carbonate saturation state threshold following the MMCT. The saturation state increase associated with the glacial climate transition could be attributed to a change from shelf carbonate deposition to deep-sea carbonate deposition resulting from the global sea level fall (Berger and Winterer, 1974; Merico et al., 2008). If this assumption is right then the corrected record should be used until ~14.8 Ma, which marks the initiation of the δ^{18}O increase. The uncorrected record should be used following the climate transition. The low-resolution benthic foraminiferal B/Ca record from ODP Site 803 suggests that bottom water saturation state had increased by ~14 Ma (Figure 5-8). In any case, there is only a small difference between the corrected and uncorrected temperature records in the 13.6-14.8 Ma window. Therefore, the new preferred temperature history follows the red diamonds in Figure 5-13 and the new preferred δ^{18}Osw history follows the red diamonds in Figure 5-14. The similarity between the form of the δ^{18}O record and the new preferred temperature record (Figure 5-13), and the form of the apparent sea level record and the new preferred δ^{18}Osw record (Figure 5-14) is encouraging.

When describing the overall climatic change across the MMCT, Lear et al. (2010) compared the ~15.3 and ~12.5 Ma intervals. These intervals were chosen because there was less difference between the corrected and uncorrected temperatures at these times. However, this meant that the authors did not describe the overall climatic change between peak conditions of the Miocene Climatic Optimum and the glacial maximum following the MMCT. The new preferred temperature and δ^{18}Osw reconstructions allow such a comparison. For example between 16.2 Ma and 11.6 Ma the calculated temperature

change from the Mg/Ca using the scenario denoted by the red symbols (Figure 5-11) is ~4.5°C and the calculated $\delta^{18}O_{sw}$ increase is ~0.8 ‰, which is consistent with the corresponding sea level fall estimated by backstripping (Figure 5-12) (Kominz et al., 2008).

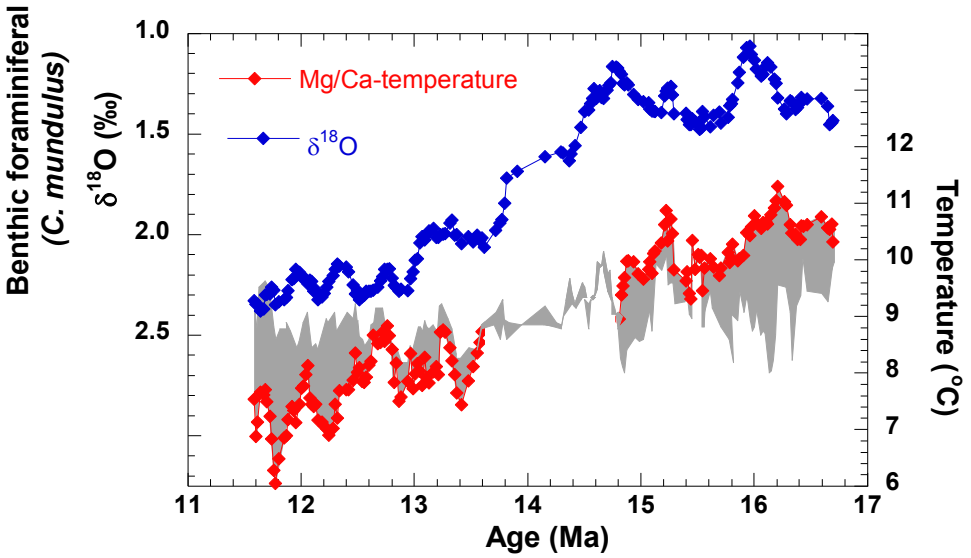

Figure 5-11 ODP Site 761 temperature and benthic foraminiferal $\delta^{18}O$ records (Lear et al., 2010). The red diamonds represent the new preferred temperature scenario.

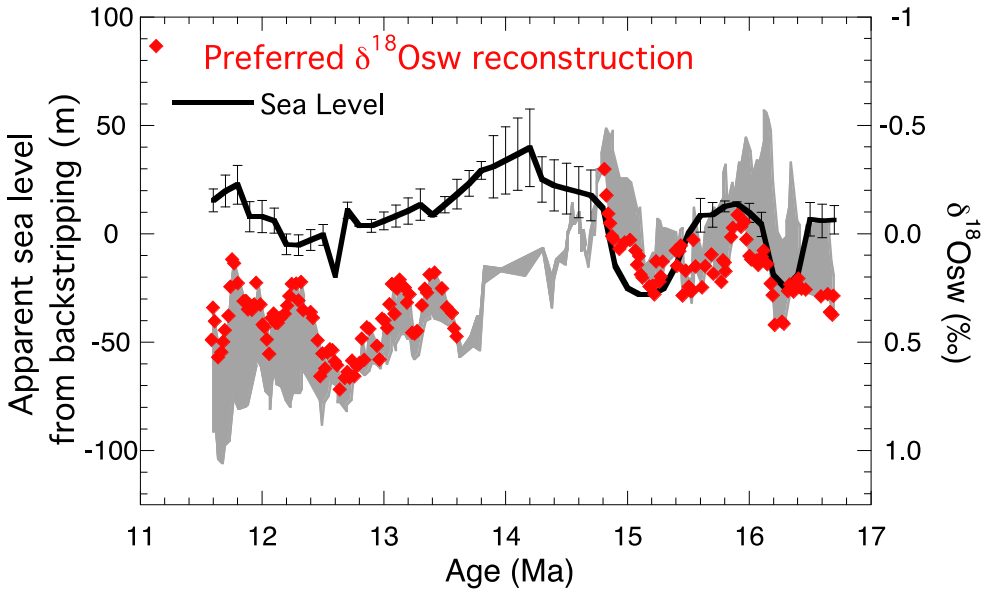

Figure 5-12 $\delta^{18}O_{sw}$ reconstruction (Lear et al., 2010) with apparent sea level from backstripping (Kominz et al., 2008). The red diamonds represent the new preferred reconstruction derived from the improved temperature reconstruction.

This increase in $\delta^{18}O_{sw}$ is equivalent to the growing the modern day Antarctic ice sheet (Cramer et al., 2011), and implies either minimal continental ice volume at peak warm intervals during the Miocene Climatic Optimum, and/or some degree of Northern Hemisphere Glaciation associated with the MMCT. Minimal ice volume during the MCO would imply that the Antarctic ice sheet has been more sensitive to pCO_2 than currently assumed, as peak MCO pCO_2 levels appear to have been ~400-500 ppmV (Kürschner et al., 2008), whereas ice-sheet models suggest a required threshold of ~1000 ppmV for Antarctic deglaciation (Pollard and DeConto, 2005). Recent drilling on the Antarctic margin does indicate a surprisingly dynamic Antarctic ice-sheet, but does not support complete deglaciation in the climatic optimum (Passchier et al., 2011). Therefore, in addition to Antarctic ice sheet retreat during the Miocene Climatic Optimum, the temperature and δ^{18}Osw records produced here imply some degree of Northern Hemisphere Glaciation approximately 11 my prior to the conventional date for NHG inception. This may not be unreasonable, as drilling in Fram Strait has found middle Miocene IRD fluxes comparable to those recovered from the Pliocene (Thiede et al., 1998).

5.4 Conclusions and future directions

1. The temperature and saturation histories derived from ODP Leg 130 Sites from the Ontong Java Plateau are similar to those at ODP Site 761 thus confirming that the ODP Site 761 record is not just a local signal. However to truly determine whether this record represents a global signal it would be worthwhile to produce records from sites from other ocean basins.

2. The depth transect approach taken here suggests that ODP Site 761 crossed above the Mg/Ca-carbonate saturation state threshold at the MMCT. This has enabled the previous temperature and seawater δ^{18}O records to be refined.

3. The new preferred temperature and seawater δ^{18}O records suggest a cooling of 4.5°C and a $\delta^{18}O_{sw}$ change of 0.8 ‰ between the Miocene Climatic Optimum and peak middle Miocene glacial conditions.

4. The overall cooling from the Miocene Climatic Optimum through the Middle Miocene Climate Transition is thought to have resulted from declining levels of pCO_2 (Kürschner et al., 2008). Therefore the middle Miocene presents a possible candidate for estimating Earth System Sensitivity in the deep past (e.g., Lunt et al., 2008, Pagani et al., 2009). This study demonstrates the potential that the “depth transect” approach has in helping refine interpretation of Mg/Ca-temperature records and brings us one step closer to achieving this goal.

6 Synthesis

6.1 Conclusions and new questions

6.1.1 Interpreting trace metals in benthic foraminifera

This study has demonstrated that benthic foraminiferal trace metal ratios have great potential to provide information about oceanographic conditions in the past. In particular the benthic foraminiferal Mg/Ca bottom water temperature proxy has been shown to produce reliable temperature data (Chapters 4 and 5). The results of this study show that the trace metal composition of benthic foraminiferal calcite may be subject to influences other than temperature and carbonate saturation state. These may include post-mortem dissolution, deepwater oxygenation levels and benthic foraminiferal microhabitat. These insights have led to three specific recommendations that should be considered when constructing Cenozoic benthic foraminiferal trace metal records, which are outlined below.

1) Dissolution

The Eocene-Oligocene Transition (EOT) sections strongly suggest a dissolution influence on benthic foraminiferal trace metal composition that is difficult to quantify. This influence is only apparent during Step 1 of the EOT at ODP Site 1218 and Step 2 of the EOT at Sites 1219 and 1220. The lack of calcareous planktonic foraminifera in these samples points to the undersaturated nature of the bottom waters. It is therefore recommended that quantitative temperature reconstructions using benthic foraminiferal trace metal records are not attempted from Sites where bottom waters were undersaturated with respect to calcite.

2) Evaluation of microhabitat

The extant benthic foraminiferal species *Oridorsalis umbonatus* is widely used in Cenozoic palaeoceanography due to its cosmopolitan nature and presence in core-top sediments, which enables modern calibrations to be constructed. Typically considered to be shallow – infaunal in its benthic habitat, this study suggests that the longevity of this species may reflect a somewhat opportunistic ecology, involving major fluctuations in test size and the ability to live in different microhabitats under different oceanographic conditions. This is supported by the observation that modern *Oridorsalis umbonatus* has been found between 1 and 4 cm depth in the sediment (Rathburn and Corliss, 2004). Such vertical migration through the upper seafloor sedimentary layers is likely to be related to food supply, which is dependent upon overlying surface ocean productivity and sedimentation rate. *Oridorsalis umbonatus* may occupy a more epifaunal microhabitat (for example as proposed in Chapter 3 for the Leg 199 EOT sections) or a more infaunal microhabitat (for example as proposed in Chapter 4 for the Leg 154 Mi-1 sections). This is important for the interpretation of the trace metal records because foraminifera adopting an epifaunal

lifestyle (at/near sediment/water interface) will experience changes in both bottom water temperature and saturation state, whereas foraminifera adopting an infaunal lifestyle, i.e. living deeper within the sediment, will primarily experience changes in bottom water temperature, while being buffered from saturation changes by pore water. It is therefore recommended that trace metal records of *O. umbonatus* are paired with those of a known epifaunal species. In particular, comparison of B/Ca records might be particularly useful as this is thought to be an independent proxy for saturation state. If there is low variability in *O. umbonatus* Mg/Ca and B/Ca records relative to the epifaunal records then it is more likely that *O .umbonatus* is recording temperature only.

3) Correcting Mg/Ca records for changes in carbonate saturation state

Core-top studies have suggested that a carbonate saturation state influence on benthic foraminiferal Mg/Ca is confined to deep, cold waters (e.g., Elderfield et al., 2006). However, this conclusion in part reflects modern day ocean hydrography, specifically the relationship of the relative influences of temperature and saturation state with water depth. The results presented in Chapter 3 suggest that in the early Cenozoic the saturation state effect on benthic foraminiferal Mg/Ca extended upwards into intermediate water depths. Therefore, the requirement for a means of "correcting" benthic foraminiferal Mg/Ca becomes even more pressing. This study has demonstrated that once the proposed "dissolution effect" is accounted for, paired Mg/Ca and Li/Ca records may be used to reconstruct variations in both temperature and seawater saturation state (e.g., for the EOT (Chapter 3) and the MMCT (Chapter 5)). This approach however did not produce a reasonable temperature history from the Ceara Rise Mi-1 records. A recent core-top study suggested that benthic foraminiferal U/Ca may provide a useful alternative proxy for estimating bottom water carbonate saturation state (Raitzsch et al., 2011). Yet, benthic foraminiferal U/Ca records generated from Mi-1 cannot be interpreted in terms of saturation state but instead point to an additional, site-specific environmental parameter. Nevertheless, the U/Ca may yet be useful in this regard, as excursions in the U/Ca record coincide with the anomalous temperatures derived from the Li/Ca records. Therefore it is recommended here that benthic foraminiferal U/Ca is used to assess the reliability of the Li/Ca records as a saturation state proxy. In addition, further core-top calibrations may enable the use of B/Ca as a means of validating the Mg/Ca-Li/Ca method for correcting Cenozoic Mg/Ca records for a saturation state influence.

6.1.2 Potential new proxy for oxygenation levels

In both species examined in this study, U/Ca in benthic foraminifera does not behave in a way that indicates it is inversely correlated with saturation state as suggested by recent core-top studies (e.g., Raitzsch et al., 2011). Leg 199 U/Ca increases across the EOT suggesting that it is subject to the same dissolution effect as Mg/Ca (Chapter 3). Benthic foraminiferal U/Ca displays significant inter-site contrasts across Mi-1 (Chapter 4). These

variations are interpreted as reflecting either terrestrial input / sediment composition or changes in oxygenation levels. Future work could be directed at further examination of this potential new proxy using a two-pronged approach. Firstly, modern (core-top and cultured) benthic foraminifera from a range of oxygen levels could be analysed for U/Ca. Secondly, the sections presented here (e.g., in Chapter 4) could be examined in more detail, for example by analysing U/Ca of bulk sediment, or assessing downcore benthic foraminiferal assemblage changes.

6.1.3 Temperature histories across Cenozoic glacial events

The benthic foraminiferal trace metals records used in this study have provided insights into the temperature and ice volume changes across both semi-permanent and transient glaciation events.

Using the Leg 199 depth transect across the EOT, it was determined that the Raitzsch et al. (2008) *Cibicidoides mundulus* Mg/Ca- ΔCO_3^{2-} sensitivity was a better fit for *Oridorsalis umbonatus* than the *Cibicidoides wuellerstorfi* sensitivity of Elderfield et al. (2006). Applying this new sensitivity to previously published DSDP Site 522 records produces a cooling of 2.5°C, which is in excellent agreement with the slope-shelf sites of the Tanzanian Drilling Project (Lear et al., 2008). The majority of the cooling occurred during the first step of the climate transition, accompanied by limited ice growth, whilst the second step of the climate transition was dominated by ice sheet growth. This is in good agreement with ice sheet models, which predict that internal mechanisms (e.g., coalescence of small, upland glaciers) may produce stepped increases in ice volume (DeConto and Pollard, 2003).

Due to the inferred infaunal nature of *Oridorsalis umbonatus* at Ceara Rise across the transient Mi-1 glaciation event it was possible to estimate temperature and sea level changes across both the glaciation and subsequent deglaciation (Chapter 4). It was estimated that bottom water temperatures cooled by ~2°C at Ceara Rise and there was a sea level decrease of 60-80 metres. Temperatures increased during the deglaciation by ~2°C and the sea level increase approximately equalled the decrease caused by the Mi-1 glaciation. The symmetrical nature of this temperature-ice volume history is not predicted by ice sheet models due to the hysteresis effect (Pollard and DeConto, 2003), and may imply either an incomplete understanding of Antarctic ice sheet dynamics, some component of Northern Hemisphere Glaciation during Mi-1, or that the Ceara Rise bottom water temperature records do not reflect a global temperature signal. Clearly, more records across this major climate event are required.

The temperature and sea level changes across the Middle Miocene Climate Transition have previously been estimated using changes in benthic foraminiferal Mg/Ca and Li/Ca at

ODP Site 761 (Lear et al., 2010). However there are relatively large uncertainties in the reconstructed temperatures and ice volumes as it was unknown whether ODP Site 761 lay above or below the saturation state threshold for the Mg/Ca-ΔCO_3^{2-} effect. Comparison with trace metal records from a deeper site indicate that ODP Site 761 crossed the saturation state threshold during the MMCT and helps constrain the temperature change at ODP Site 761 between 16.2Ma and 11.6Ma as being ~4.5°C (Chapter 5). Although supported by estimates of sea level change derived from sequence stratigraphy, the magnitude of ice growth between the Miocene Climatic Optimum and the end of the MMCT is surprisingly large (similar to modern day Antarctic ice volume). This implies either a more dynamic Antarctic ice sheet than previously thought, or the presence of Northern Hemisphere ice in the Miocene.

6.2 Future directions

6.2.1 Benthic foraminiferal trace metal proxies

This study has confirmed that there is great potential in benthic foraminiferal trace metal proxies but that there are complexities in these methods. In order to improve benthic foraminiferal trace metal proxy knowledge and application there are several avenues of investigation which are outlined here:

Core-top studies: To attempt to quantify the dissolution effect that is observed in ODP Leg 199 sites it is suggested that core-top studies be carried out in oceanographic regions of low bottom water saturation state and contrasted with those of high saturation state.

Culturing studies: Culturing studies may help determine the effects of temperature, saturation state and oxygen levels on Mg/Ca, Li/Ca, B/Ca and U/Ca in benthic foraminifera. This is because these conditions may be more easily controlled and quantified in a culturing study than from a core-top study.

Further down-core studies in combination with other proxies

As new bottom water temperature proxies are developed (e.g. clumped isotopes in calcium carbonate (Ghosh et al., 2007)) it may be possible to compare results from different proxies as a method of validation and a new means of deconvolving trace metal records.

Analytical methodology improvement

Mg/Ca in benthic foraminifera has now become routinely measurable using mass spectrometry (or other methods) and high levels of precision are readily achieved (<1% r.s.d.) (Chapter 2). Other metals such as lithium and boron which are less abundant in benthic foraminiferal calcite are not measured to the same level of precision. This may lead to increased noise in the data or to data being discarded due to not being analytically sound, resulting in lower resolution records. Either larger sample sizes need to be

analysed (which may not be possible due to the low abundance of benthic foraminiferal species in samples) or analytical techniques need to be improved. Methodological improvements could include lowering the concentrations of these trace metals in the blank and a reduction in sample volume to increase measured concentration in the sample. Improvements in machine sensitivity would also improve the viability of these records.

6.2.2 Cenozoic climate change history

Although the trace metal records produced in this study have provided information about the timing and absolute changes in temperature and ice volume across the three Cenozoic climate events in question, further information is required in order to be able to make assertions with respect to the causes of the climate change events. For example from the Mi-1 event it is now clear that deep sea temperature cooling preceded ice volume growth and warming preceded ice sheet decline. However it is unknown from these trace metal records whether the cooling was initiated by changes in ocean circulation, orbital configuration or decline in pCO_2 levels. Additional studies could be done using trace metal proxies to try and answer these questions about the causes of these Cenozoic climate changes. For example higher resolution studies may reveal cyclicity within the Mg/Ca data indicating temperature was driven by orbital cycles, also studies of one interval at several sites may provide information about water mass changes and ocean circulation across the climate events. As more proxies are being developed these can also be used in conjunction with saturation state proxies to provide information about pCO_2 and the global carbon cycle (e.g. boron isotopes). It may be through the combination of other proxies with trace metal proxies that climate change events during the Cenozoic and potentially future climate changes will be more fully understood.

7 References

Al-Ammar, A., Gupta, R. K. and Barnes, R. M. (1999) Elimination of boron memory effect in inductively coupled plasma-mass spectrometry by addition of ammonia. *Spectrochimica Acta Part B: Atomic Spectroscopy* 54 (7), 1077-1084.

Baker, P. A., Gieskes, J. M. and Elderfield, H. (1982) Diagenesis of carbonates in deep-sea sediments-Evidence from Sr/Ca ratios and interstitial dissolved Sr data. *J. Sediment. Petrol* 52 71-82.

Barker, S., Greaves, M. and Elderfield, H. (2003) A study of cleaning procedures used for foraminiferal Mg/Ca paleothermometry. *Geochemistry Geophysics Geosystems* 4 (9), 1.

Bemis, B., Spero, H., Bijma, J. and Lea, D. (1998) Reevaluation of the oxygen isotopic composition of planktonic foraminifera: Experimental results and revised paleotemperature equations. *Paleoceanography* 13 (2), 150-160.

Bender, M. L., Lorens, R. B. and Williams, D. F. (1975) Sodium, magnesium and strontium in the tests of planktonic foraminifera. *Micropaleontology,* 21 448-459.

Bentov, S. and Erez, J. (2006) Impact of biomineralization processes on the Mg content of foraminiferal shells: A biological perspective. *Geochemistry Geophysics Geosystems* 7 (1), Q01P08.

Berger, W. H. and Winterer, E. L. (1974) Plate stratigraphy and the fluctuating carbonate line. *Pelagic Sediments: on Land and under the Sea* 11-48.

Billups, K. and Schrag, D. P. (2003) Application of benthic foraminiferal Mg/Ca ratios to questions of Cenozoic climate change. *Earth and Planetary Science Letters* 209 (1-2), 181-195.

Blaj, T. (2009) *Late Eocene Through Oligocene Calcareous Nannofossils from the Paleo-equatorial Pacific Ocean: Taxonomy, Preservation History, Biochronology and Evolution*. Department of geology and geochemistry, Stockholm University.

Bohaty, S. M., Zachos, J. C. and Delaney, M. L. (2012) Foraminiferal Mg/Ca evidence for Southern Ocean cooling across the Eocene–Oligocene transition. *Earth and Planetary Science Letters* 317 251-261.

Boyle, E. and Keigwin, L. (1987) North Atlantic thermohaline circulation during the past 20, 000 years linked to high-latitude surface temperature. *Nature* 330 (6143), 35-40.

Boyle, E. A. and Keigwin, L. D. (1985) Comparison of Atlantic and Pacific paleochemical records for the last 215,000 years: changes in deep ocean circulation and chemical inventories. *Earth and Planetary Science Letters* 76 (1-2), 135-150.

Broecker, W. S., Peng, T. H. and Beng, Z. (1982) *Tracers in the Sea*. Lamont-Doherty Geological Observatory, Columbia University.

Brown, R. E., Anderson, L. D., Thomas, E. and Zachos, J. C. (2011) A core-top calibration of B/Ca in the benthic foraminifers Nuttallides umbonifera and Oridorsalis umbonatus: A proxy for Cenozoic bottom water carbonate saturation. *Earth and Planetary Science Letters* 310 (3), 360-368.

Brown, S. J. and Elderfield, H. (1996) Variations in Mg/Ca and Sr/Ca ratios of planktonic foraminifera caused by postdepositional dissolution: Evidence of shallow Mg-dependent dissolution. *Paleoceanography* 11 (5), 543-552.

Bryan, S. and Marchitto, T. (2008) Mg/Ca–temperature proxy in benthic foraminifera: New calibrations from the Florida Straits and a hypothesis regarding Mg/Li. *Paleoceanography* 23 (2).

Burton, E. A. and Walter, L. M. (1987) Relative precipitation rates of aragonite and Mg calcite from seawater: Temperature or carbonate ion control? *Geology* 15 (2), 111.

Cande, S. C. and Kent, D. V. (1995) Revised calibration of the geomagnetic polarity time scale for the Late Cretaceous and Cenozoic. *Journal of Geophysical Research,* 100 6093–6096.

Chaisson, W. P., and Leckie, R.M., (1993) High-resolution Neogene planktonic foraminifer biostratigraphy of Site 806, Ontong Java Plateau (western equatorial Pacific). *In Berger, W.H., Kroenke, L.W., Mayer, L.A., et al., Proc. ODP, Sci. Results, 130: College Station, TX (Ocean Drilling Program),* 137–178.

Chilingar, G. V. (1962) Dependence on temperature of Ca/Mg ratio of skeletal structures of organisms and direct chemical precipitates out of sea water. *Bull. South. Calif. Acad. Sci* 61 (1), 45-61.

Coggon, R. M., Teagle, D. A. H., Smith-Duque, C. E., Alt, J. C. and Cooper, M. J. (2010) Reconstructing past seawater Mg/Ca and Sr/Ca from mid-ocean ridge flank calcium carbonate veins. *Science* 327 (5969), 1114.

Corliss, B. (1985) Microhabitats of benthic foraminifera within deep-sea sediments.

Coxall, H. K., Wilson, P. A., Palike, H., Lear, C. H. and Backman, J. (2005) Rapid stepwise onset of Antarctic glaciation and deeper calcite compensation in the Pacific Ocean. *Nature* 433 (7021), 53-57.

Coxall, H. K. and Pearson, P. N. (2007) The Eocene-Oligocene transition. *Deep Time Perspectives on Climate Change: Marrying the Signal From Computer Models and Biological Proxies* 351-387.

Coxall, H. K. and Wilson, P. A. (2011) Early Oligocene glaciation and productivity in the eastern equatorial Pacific: Insights into global carbon cycling. *Paleoceanography* 26 (2), PA2221.

Cramer, B. S., Toggweiler, J. R., Wright, J. D., Katz, M. E. and Miller, K. G. (2009) Ocean overturning since the Late Cretaceous: Inferences from a new benthic foraminiferal isotope compilation. *Paleoceanography* 24 (4), PA4216.

Cramer, B. S., Miller, K. G., Barrett, P. J. and Wright, J. D. (2011) Late Cretaceous–Neogene trends in deep ocean temperature and continental ice volume: Reconciling records of benthic foraminiferal geochemistry ($\delta^{18}O$ and Mg/Ca) with sea level history. *Journal of Geophysical Research* 116 (C12), C12023.

Curry, W. B. and Marchitto, T. M. (2008) A secondary ionization mass spectrometry calibration of *Cibicidoides pachyderma* Mg/Ca with temperature. *Geochem. Geophys. Geosyst* 9 (4), Q04009.

DeConto, R. and Pollard, D. (2003) A coupled climate-ice sheet modeling approach to the early Cenozoic history of the Antarctic ice sheet. *Palaeogeography, Palaeoclimatology, Palaeoecology* 198 (1-2), 39-52.

DeConto, R., Pollard, D., Wilson, P., Pälike, H., Lear, C. and Pagani, M. (2008) Thresholds for Cenozoic bipolar glaciation. *Nature* 455 (7213), 652-656.

Deer, W. A., Howie, R. A. and Zussman, J. (1985) *An introduction to the rock-forming minerals*. Longman London.

Delaney, M. L., Wh Be, A. and Boyle, E. A. (1985) Li, Sr, Mg, and Na in foraminiferal calcite shells from laboratory culture, sediment traps, and sediment cores. *Geochimica et Cosmochimica Acta* 49 (6), 1327-1341.

Demicco, R. V., Lowenstein, T. K., Hardie, L. A. and Spencer, R. J. (2005) Model of seawater composition for the Phanerozoic. *Geology* 33 (11), 877-880.

Elderfield, H., Bertram, C. J. and Erez, J. (1996) A biomineralization model for the incorporation of trace elements into foraminiferal calcium carbonate. *Earth and Planetary Science Letters* 142 (3-4), 409-423.

Elderfield, H., Yu, J., Anand, P., Kiefer, T. and Nyland, B. (2006) Calibrations for benthic foraminiferal Mg/Ca paleothermometry and the carbonate ion hypothesis. *Earth and Planetary Science Letters* 250 (3-4), 633-649.

Elderfield, H., Greaves, M., Barker, S., Hall, I. R., Tripati, A., Ferretti, P., Crowhurst, S., Booth, L. and Daunt, C. (2010) A record of bottom water temperature and seawater $\delta^{18}O$ for the Southern Ocean over the past 440 kyr based on Mg/Ca of benthic foraminiferal Uvigerina spp. *Quaternary Science Reviews* 29 (1-2), 160-169.

Eldrett, J., Harding, I., Wilson, P., Butler, E. and Roberts, A. (2007) Continental ice in Greenland during the Eocene and Oligocene. *Nature* 446 (7132), 176-179.

Emiliani, C. (1955) Pleistocene temperatures. *Journal of Geology* 63 538–578.

Engebretson, D. C., Cox, A. and Gordon, R. G. (1985) Relative motions between oceanic and continental plates in the Pacific basin, Spec. *Pap.-Geol. Soc. Am* 206 1–59.

Epstein, S., Buchsbaum, R., Lowenstam, H. and Urey, H. (1951) Carbonate-water isotopic temperature scale. *Geological Society of America Bulletin* 62 (4), 417.

Erez, J. and Luz, B. (1983) Experimental paleotemperature equation for planktonic foraminifera. *Geochimica et Cosmochimica Acta* 47 (6), 1025-1031.

Erez, J. (2003) The source of ions for biomineralization in foraminifera and their implications for paleoceanographic proxies. *Reviews in mineralogy and geochemistry* 54 (1), 115.

Ferguson, J., Henderson, G., Kucera, M. and Rickaby, R. (2008) Systematic change of foraminiferal Mg/Ca ratios across a strong salinity gradient. *Earth and Planetary Science Letters* 265 (1-2), 153-166.

Flower, B. P. and Kennett, J. P. (1993) Middle Miocene ocean-climate transition: high-resolution oxygen and carbon isotopic records from Deep Sea Drilling Project Site 588A, southwest Pacific. *Paleoceanography* 8 (6), 811-843.

Garrels, R. M. and Christ, C. L. (1965) *Solutions, minerals, and equilibria*. Harper & Row New York.

Ghosh, P., Eiler, J., Campana, S. E. and Feeney, R. F. (2007) Calibration of the carbonate [] clumped isotope'paleothermometer for otoliths. *Geochimica et Cosmochimica Acta* 71 (11), 2736-2744.

Graham, D. W., Bender, M. L., Williams, D. F. and Keigwin Jr, L. D. (1982) Strontium-calcium ratios in Cenozoic planktonic foraminifera. *Geochimica et Cosmochimica Acta* 46 (7), 1281-1292.

Hall, J. and Chan, L. (2004) Li/Ca in multiple species of benthic and planktonic foraminifera: thermocline, latitudinal, and glacial-interglacial variation 1. *Geochimica et Cosmochimica Acta* 68 (3), 529-545.

Hall, J. M., Chan, L. H., McDonough, W. F. and Turekian, K. K. (2005) Determination of the lithium isotopic composition of planktic foraminifera and its application as a paleo-seawater proxy. *Marine Geology* 217 (3-4), 255-265.

Haq, B., Hardenbol, J. and Vail, P. (1987) Chronology of fluctuating sea levels since the Triassic. *Science* 235 (4793), 1156.

Hardenbol, J., Thierry, J., Farley, M. B., Jacquin, T., De Graciansky, P. C. and Vail, P. R. (1998) Mesozoic and Cenozoic sequence chronostratigraphic framework of European basins. *SPECIAL PUBLICATION-SEPM* 60 3-14.

Holbourn, A., Kuhnt, W., Simo, J. A. and Li, Q. (2004) Middle Miocene isotope stratigraphy and paleoceanographic evolution of the northwest and southwest Australian margins

(Wombat Plateau and Great Australian Bight). *Palaeogeography, Palaeoclimatology, Palaeoecology* 208 (1-2), 1-22.

Holbourn, A., Kuhnt, W., Schulz, M. and Erlenkeuser, H. (2005) Impacts of orbital forcing and atmospheric carbon dioxide on Miocene ice-sheet expansion. *Nature* 438 (7067), 483-487.

Hoogakker, B. A. A., Klinkhammer, G. P., Elderfield, H., Rohling, E. J. and Hayward, C. (2009) Mg/Ca paleothermometry in high salinity environments. *Earth and Planetary Science Letters* 284 (3), 583-589.

Horita, J., Zimmermann, H. and Holland, H. D. (2002) Chemical evolution of seawater during the Phanerozoic: Implications from the record of marine evaporites. *Geochimica et Cosmochimica Acta* 66 (21), 3733-3756.

Huh, Y., Chan, L. H., Zhang, L. and Edmond, J. M. (1998) Lithium and its isotopes in major world rivers: implications for weathering and the oceanic budget. *Geochimica et Cosmochimica Acta* 62 (12), 2039-2051.

Izuka, S. K. (1988) Relationship of magnesium and other minor elements in tests of Cassidulina subglobosa and C. oriangulata to physical oceanic properties. *The Journal of Foraminiferal Research* 18 (2), 151.

Jordan, K. (2008) Evaluating carbonate saturation effects on magnesium calcium core top calibration in benthic foraminifera. *unpublished masters thesis*. Graduate School-New Brunswick Rutgers, The State University of New Jersey

Katz, A. (1973) The interaction of magnesium with calcite during crystal growth at 25-90 C and one atmosphere. *Geochimica et Cosmochimica Acta* 37 (6), 1563-1578.

Katz, M., Katz, D., Wright, J., Miller, K., Pak, D., Shackleton, N. and Thomas, E. (2003) Early Cenozoic benthic foraminiferal isotopes: Species reliability and interspecies correction factors. *Paleoceanography* 18 (2), 1024.

Katz, M., Miller, K., Wright, J., Wade, B., Browning, J., Cramer, B. and Rosenthal, Y. (2008) Stepwise transition from the Eocene greenhouse to the Oligocene icehouse. *Nature Geoscience* 1 (5), 329-334.

Keith, M. L. and Weber, J. N. (1964) Carbon and oxygen isotopic composition of selected limestones and fossils. *Geochimica et Cosmochimica Acta* 28 (10-11), 1787-1816.

Kennett, J. P. and Shackleton, N. J. (1976) Oxygen isotopic evidence for the development of the psychrosphere 38 Myr ago. *Nature* 260, 513–515.

King, T. A., Ellis, W. G., Murray, D. W., Shackleton, N. J. and Harris, S. (1997) Miocene evolution of carbonate sedimentation at the Ceara Rise: A multivariate data/proxy approach. *Ocean Drilling Program. Proc. Ocean Drill. Program Sci. Results*, 154, pp. 349-365

Kisakurek, B., Eisenhauer, A., Bohm, F., Garbe-Schonberg, D. and Erez, J. (2008) Controls on shell Mg/Ca and Sr/Ca in cultured planktonic foraminiferan, Globigerinoides ruber (white). *Earth and Planetary Science Letters* 273 (3-4), 260-269.

Kominz, M. A., Browning, J. V., Miller, K. G., Sugarman, P. J., Mizintseva, S. and Scotese, C. R. (2008) Late Cretaceous to Miocene sea-level estimates from the New Jersey and Delaware coastal plain coreholes: An error analysis. *Basin Research* 20 (2), 211-226.

Koziol, A. M. and Newton, R. C. (1998) Experimental determination of the reaction; magnesite+ enstatite= forsterite+ CO 2 in the ranges 6-25 kbar and 700-1100 degrees C. *American Mineralogist* 83 (3-4), 213.

Ku, T. L., Knauss, K. G. and Mathieu, G. G. (1977) Uranium in open ocean: concentration and isotopic composition. *Deep Sea Research* 24 (11), 1005-1017.

Kürschner, W. M., Kvaček, Z. and Dilcher, D. L. (2008) The impact of Miocene atmospheric carbon dioxide fluctuations on climate and the evolution of terrestrial ecosystems. *Proceedings of the National Academy of Sciences* 105 (2), 449.

Laskar, J., Robutel, P., Joutel, F., Gastineau, M., Correia, A. and Levrard, B. (2004) A long-term numerical solution for the insolation quantities of the Earth. *Astronomy and Astrophysics* 428 (1), 261-285.

Lear, C. H., Elderfield, H. and Wilson, P. A. (2000) Cenozoic Deep-Sea Temperatures and Global Ice Volumes from Mg/Ca in Benthic Foraminiferal Calcite. *Science* 287 (5451), 269.

Lear, C. H., Rosenthal, Y. and Slowey, N. (2002) Benthic foraminiferal Mg/Ca-paleothermometry: a revised core-top calibration. *Geochimica et Cosmochimica Acta* 66 (19), 3375-3387.

Lear, C. H., Elderfield, H. and Wilson, P. A. (2003) A Cenozoic seawater Sr/Ca record from benthic foraminiferal calcite and its application in determining global weathering fluxes. *Earth and Planetary Science Letters* 208 (1-2), 69-84.

Lear, C., Rosenthal, Y. and Wright, J. (2003b) The closing of a seaway: ocean water masses and global climate change. *Earth and Planetary Science Letters* 210 (3-4), 425-436.

Lear, C. H., Rosenthal, Y., Coxall, H. K. and Wilson, P. A. (2004) Late Eocene to early Miocene ice sheet dynamics and the global carbon cycle. *Paleoceanography* 19 (4), 1029-1039.

Lear, C. H. and Rosenthal, Y. (2006) Benthic foraminiferal Li/Ca: Insights into Cenozoic seawater carbonate saturation state. *Geology* 34 (11), 985-988.

Lear, C. H. (2007) Mg/Ca palaeothermometry: a new window into Cenozoic climate change. *Deep Time perspectives of Climate Change: Marrying the Signal from Computer Models and Biological Proxies: The Geological Society of London* 313-322.

Lear, C. H., Bailey, T. R., Pearson, P. N., Coxall, H. K. and Rosenthal, Y. (2008) Cooling and ice growth across the Eocene-Oligocene transition. *Geology* 36 (3), 251.

Lear, C. H., E. M. Mawbey and Y. Rosenthal (2010) Cenozoic Benthic Foraminiferal Mg/Ca and Li/Ca Records: Towards Unlocking Temperatures and Saturation States. *Paleoceanography*, 25, PA4215,

Lemarchand, D., Gaillardet, J., Lewin, E. and Allegre, C. (2002) Boron isotope systematics in large rivers: implications for the marine boron budget and paleo-pH reconstruction over the Cenozoic. *Chemical Geology* 190 (1-4), 123-140.

Liu, Z., Pagani, M., Zinniker, D., DeConto, R., Huber, M., Brinkhuis, H., Shah, S., Leckie, R. and Pearson, A. (2009) Global cooling during the Eocene-Oligocene climate transition. *Science* 323 (5918), 1187.

Lorens, R. B., Williams, D. F. and Bender, M. L. (1977) The early nonstructural chemical diagenesis of foraminiferal calcite. *Journal of Sedimentary Research* 47 (4), 1602.

Lowenstein, T. K., Timofeeff, M. N., Brennan, S. T., Hardie, L. A. and Demicco, R. V. (2001) Oscillations in Phanerozoic Seawater Chemistry: Evidence from Fluid Inclusions. *Science* 294 (5544), 1086-1088.

Lunt, D. J., Haywood, A. M., Schmidt, G. A., Salzmann, U., Valdes, P. J. and Dowsett, H. J. (2009) Earth system sensitivity inferred from Pliocene modelling and data. *Nature Geoscience* 3 (1), 60-64.

Lyell, C. (1830) Principles of geology, being an attempt to explain the former changes of the Earth's surface, by reference to causes now in operation. London: John Murray. Volume 1.

Manley, G. (1974) Central England temperatures: monthly means 1659 to 1973. *Quarterly Journal of the Royal Meteorological Society* 100 (425), 389-405.

Marchitto, T., Curry, W. and Oppo, D. (2000) Zinc concentrations in benthic foraminifera reflect seawater chemistry. *Paleoceanography* 15 (3), 299–306.

Marchitto, T. M., Bryan, S. P., Curry, W. B. and McCorkle, D. C. (2007) Mg/Ca temperature calibration for the benthic foraminifer Cibicidoides pachyderma. *Paleoceanography* 22 (1).

Marriott, C., Henderson, G., Belshaw, N. and Tudhope, A. (2004) Temperature dependence of δ^7Li, δ^{44}Ca and Li/Ca during growth of calcium carbonate. *Earth and Planetary Science Letters* 222 (2), 615-624.

Marriott, C. S., Henderson, G. M., Crompton, R., Staubwasser, M. and Shaw, S. (2004) Effect of mineralogy, salinity, and temperature on Li/Ca and Li isotope composition of calcium carbonate. *Chemical Geology* 212 (1-2), 5-15.

Martin, W. R. and Sayles, F. L. (1996) CaCO3 dissolution in sediments of the Ceara Rise, western equatorial Atlantic. *Geochimica et Cosmochimica Acta* 60 (2), 243-263.

Martin, P. and Lea, D. (2002) A simple evaluation of cleaning procedures on fossil benthic foraminiferal Mg/Ca. *Geochem. Geophys. Geosyst* 3 (10), 8401.

Martin, P. A., Lea, D. W., Rosenthal, Y., Shackleton, N. J., Sarnthein, M. and Papenfuss, T. (2002) Quaternary deep sea temperature histories derived from benthic foraminiferal Mg/Ca. *Earth and Planetary Science Letters* 198 (1-2), 193-209.

McCorkle, D.C. Keigwin, L.D. Corliss, B.H. Emerson S.R. (1990), The influence of microhabitats on the carbon isotopic composition of deep-sea benthic foraminifera *Paleoceanography*, 5 pp. 161–185

McCorkle, D. C., Martin, P. A., Lea, D. W. and Klinkhammer, G. P. (1995) Evidence of a dissolution effect on benthic foraminiferal shell chemistry: $\delta^{13}C$, Cd/Ca, Ba/Ca, and Sr/Ca results from the Ontong Java Plateau. *Paleoceanography* 10(4), 699-714.

Merico, A., Tyrrell, T. and Wilson, P. (2008) Eocene/Oligocene ocean de-acidification linked to Antarctic glaciation by sea-level fall. *Nature* 452 (7190), 979-982.

Miller, K. G., Fairbanks, R. G. and Mountain, G. S. (1987) Tertiary oxygen isotope synthesis, sea level history, and continental margin erosion. *Paleoceanography* 2 (1), 1-19.

Miller, K. G., Wright, J. D. and Fairbanks, R. G. (1991) Unlocking the ice house: Oligocene-Miocene oxygen isotopes, eustasy, and margin erosion. *Journal of Geophysical Research* 96 (B4), 6829-6848.

Mucci, A. (1987) Influence of temperature on the composition of magnesian calcite overgrowths precipitated from seawater. *Geochimica et Cosmochimica Acta* 51 (7), 1977-1984.

Nürnberg, D., Bijma, J. and Hemleben, C. (1996) Assessing the reliability of magnesium in foraminiferal calcite as a proxy for water mass temperatures. *Geochimica et Cosmochimica Acta* 60 (5), 803-814.

ODP Leg 130, S. S. P. (1995) Introduction. *In Kroenke, L.W., Berger, W.H., Janecek, T.R., et al., Proc. ODP, Init. Repts., 130: College Station, TX (Ocean Drilling Program)* 5–13.

ODP Leg 154, S. S. P. (1995) Introduction. *In Curry, W.B., Shackleton, N.J., Richter, C., et al., 1995. Proc. ODP, Init. Repts, 154: College Station, TX (Ocean Drilling Program).*

ODP Leg 199 S.S.P (2002) Leg 199 summary. *In Lyle, M., Wilson, P.A., Janecek, T.R., et al., Proc. ODP, Init. Repts., 199: College Station, TX (Ocean Drilling Program),* 1-87.

O'Leary, M. H. (1988) Carbon isotopes in photosynthesis. *Bioscience* 38 (5), 328-336.

Oomori, T., Kaneshima, H., Maezato, Y. and Kitano, Y. (1987) Distribution coefficient of Mg2+ ions between calcite and solution at 10-50 C. *Marine Chemistry* 20 (4), 327-336.

Pagani, M., Liu, Z., LaRiviere, J. and Ravelo, A. C. (2009) High Earth-system climate sensitivity determined from Pliocene carbon dioxide concentrations. *Nature Geoscience* 3 (1), 27-30.

Paillard, D., Labeyrie, L. and Yiou, P. (1996) Analyseries 1.0: a Macintosh software for the analysis of geographical time-series. *Eos* 77 379.

Pälike, H., Moore, T., Backman, J., Raffi, I., Lanci, L., Parés, J.M., and Janecek, T. (2005) Integrated stratigraphic correlation and improved composite depth scales for ODP Sites 1218 and 1219. . *Proc. ODP, Sci. Results,199: College Station, TX (Ocean Drilling Program),* 1–41.

Pälike, H., Moore, T., Backman, J., Raffi, I., Lanci, L., Parés, J. M. and Janecek, T. (2005) Integrated stratigraphic correlation and improved composite depth scales for ODP Sites 1218 and 1219. In (Vol. 199, pp. 1–41).

Palike, H., Norris, R., Herrle, J., Wilson, P., Coxall, H., Lear, C., Shackleton, N., Tripati, A. and Wade, B. (2006) The heartbeat of the Oligocene climate system. *Science* 314 (5807), 1894.

Pälike, H., Frazier, J. and Zachos, J. (2006b) Extended orbitally forced palaeoclimatic records from the equatorial Atlantic Ceara Rise. *Quaternary Science Reviews* 25 (23-24), 3138-3149.

Pälike, H. and Shackleton, N. (2000) Constraints on astronomical parameters from the geological record for the last 25 Myr. *Earth and Planetary Science Letters* 182 (1), 1-14.

Party, O. L. S. S. (2002b) Site 1218. *In Lyle, M., Wilson, P.A., Janecek, T.R., et al., Proc. ODP, Init. Repts., 199: College Station, TX (Ocean Drilling Program),* .

Passchier, S., Browne, G., Field, B., Fielding, C. R., Krissek, L. A., Panter, K. and Pekar, S. F. (2011) Early and middle Miocene Antarctic glacial history from the sedimentary facies distribution in the AND-2A drill hole, Ross Sea, Antarctica. *Geological Society of America Bulletin* 123 (11-12), 2352-2365.

Patnaik, P. (2003) *Handbook of inorganic chemicals*. McGraw-Hill New York.

Paul, H., Zachos, J., Flower, B. and Tripati, A. (2000) Orbitally induced climate and geochemical variability across the Oligocene/Miocene boundary. *Paleoceanography* 15 (5), 471-485.

Pearson, P., McMillan, I., Wade, B., Jones, T., Coxall, H., Bown, P. and Lear, C. (2008) Extinction and environmental change across the Eocene-Oligocene boundary in Tanzania. *Geology* 36 (2), 179.

Pearson, P. and Palmer, M. (2000) Atmospheric carbon dioxide concentrations over the past 60 million years. *Nature* 406 (6797), 695-699.

Peck, V. L., Yu, J., Kender, S. and Riesselman, C. R. (2010) Shifting ocean carbonate chemistry during the Eocene-Oligocene climate transition: Implications for deep-ocean Mg/Ca paleothermometry. *Paleoceanography* 25 (4), PA4219.

Pfuhl, H. A. and McCave, I. N. (2005) Evidence for late Oligocene establishment of the Antarctic Circumpolar Current. *Earth and Planetary Science Letters* 235 (3-4), 715-728.

Pollard, D. and DeConto, R. M. (2005) Hysteresis in Cenozoic Antarctic ice-sheet variations. *Global and Planetary Change* 45 (1-3), 9-21.

Pusz, A. E., Thunell, R. C. and Miller, K. G. (2011) Deep water temperature, carbonate ion, and ice volume changes across the Eocene-Oligocene climate transition. *Paleoceanography* 26 (2), PA2205.

Rae, J. W. B., Foster, G. L., Schmidt, D. N. and Elliott, T. (2011) Boron isotopes and B/Ca in benthic foraminifera: Proxies for the deep ocean carbonate system. *Earth and Planetary Science Letters*. 302, 403-413.

Raitzsch, M., Kuhnert, H., Groeneveld, J. and Bickert, T. (2008) Benthic foraminifer Mg/Ca anomalies in South Atlantic core top sediments and their implications for paleothermometry. *Geochem. Geophys. Geosyst* 9 Q05010.

Raitzsch, M., Kuhnert, H., Hathorne, C., Groeneveld, J. and Bickert, T. (2011) U/Ca in benthic foraminifers: A proxy for the deep-sea carbonate saturation. *Geochemistry Geophysics Geosystems* 12 (6), Q06019.

Rathburn, A. and Corliss, B. (1994) The ecology of living (stained) deep-sea benthic foraminifera from the Sulu Sea. *Paleoceanography* 9 87-87.

Rea, D. and Lyle, M. (2005) Paleogene calcite compensation depth in the eastern subtropical Pacific: Answers and questions. *Paleoceanography* 20 (1).

Reuning, L., Reijmer, J. J. G., Betzler, C., Swart, P. and Bauch, T. (2005) The use of paleoceanographic proxies in carbonate periplatform settings--opportunities and pitfalls. *Sedimentary Geology* 175 (1-4), 131-152.

Rickaby, R., Elderfield, H., Roberts, N., Hillenbrand, C. and Mackensen, A. (2010) Evidence for elevated alkalinity in the glacial Southern Ocean. *Paleoceanography* 25 (1).

Rosenthal, Y., Boyle, E. A. and Slowey, N. (1997) Temperature control on the incorporation of magnesium, strontium, fluorine, and cadmium into benthic foraminiferal shells from Little Bahama Bank: Prospects for thermocline paleoceanography. *Geochimica et Cosmochimica Acta* 61 (17), 3633-3643.

Rosenthal, Y., Lear, C., Oppo, D. and Linsley, B. (2006) Temperature and carbonate ion effects on Mg/Ca and Sr/Ca ratios in benthic foraminifera: Aragonitic species Hoeglundina elegans. *Paleoceanography* 21 (1).

Rosenthal, Y., Lohmann, G., Lohmann, K. and Sherrell, R. (2000) Incorporation and preservation of Mg in Globigerinoides sacculifer: Implications for reconstructing the temperature and $^{18}O/^{16}O$ of seawater. *Paleoceanography* 15 (1), 135-145.

Rosenthal, Y. and Lohmann, G. P. (2002) Accurate estimation of sea surface temperatures using dissolution-corrected calibrations for Mg/Ca paleothermometry. *Paleoceanography* 17 (3), 1044.

Rosenthal, Y., Perron-Cashman, S., Lear, C., Bard, E., Barker, S., Billups, K., Bryan, M. and Delaney, M. (2004) Interlaboratory comparison study of Mg/Ca and Sr/Ca measurements in planktonic foraminifera for paleoceanographic research. *Geochemistry Geophysics Geosystems* 5 (4), Q04D09.

Russell, A. D., Emerson, S., Mix, A. C. and Peterson, L. C. (1996) The use of foraminiferal uranium/calcium ratios as an indicator of changes in seawater uranium content. *Paleoceanography* 11 (6), 649-664.

Russell, A. D., Emerson, S., Nelson, B. K., Erez, J. and Lea, D. W. (1994) Uranium in foraminiferal calcite as a recorder of seawater uranium concentrations. *Geochimica et Cosmochimica Acta* 58 (2), 671-681.

Russell, A. D., Hönisch, B., Spero, H. J. and Lea, D. W. (2004) Effects of seawater carbonate ion concentration and temperature on shell U, Mg, and Sr in cultured planktonic foraminifera. *Geochimica et Cosmochimica Acta* 68 (21), 4347-4361.

Savin, S. M. and Douglas, R. G. (1973) Stable isotope and magnesium geochemistry of Recent planktonic foraminifera from the South Pacific. *Bulletin of the Geological Society of America* 84 (7), 2327.

Scher, H. and Martin, E. (2006) Timing and climatic consequences of the opening of Drake Passage. *Science* 312 (5772), 428.

Schlitzer, R. (2005) Ocean Data View http://www. awi-bremerhaven. de/GEO. ODV.

Sexton, P. F., Wilson, P. A. and Pearson, P. N. (2006) Microstructural and geochemical perspectives on planktic foraminiferal preservation: “Glassy” versus “Frosty”. *Geochemistry, Geophysics, Geosystems* 7 Q12P19.

Shackleton, N. J. (1987b) The carbon isotope record of the Cenozoic: History of organic carbon burial and of oxygen in the ocean and atmosphere. *Geological Society, London, Special Publications* 26 (1), 423-434.

Shackleton, N. J. (1987) Oxygen isotopes, ice volume and sea level. *Quaternary Science Reviews* 6 (3-4), 183-190.

Shackleton, N. J. and Crowhurst, S. (1997) Sediment fluxes based on an orbitally tuned time scale 5 Ma to 14 Ma, Site 926. *Proc. Ocean Drill. Program Sci. Results*, 154, 69–82.

Shackleton, N.J, Crowhurst, S., Weedon, G. and Laskar, J. (1999) Astronomical calibration of Oligocene-Miocene time. *Philosophical Transactions: Mathematical, Physical and Engineering Sciences* 357 (1757), 1907-1929.

Shevenell, A. E., Kennett, J. P. and Lea, D. W. (2008) Middle Miocene ice sheet dynamics, deep-sea temperatures, and carbon cycling: A Southern Ocean perspective. *Geochem. Geophys. Geosyst* 9 Q02006.

Sigman, D. M. and Boyle, E. A. (2000) Glacial/interglacial variations in atmospheric carbon dioxide. *Nature* 407 (6806), 859-869.

Simon, L., Lécuyer, C., Maréchal, C. and Coltice, N. (2006) Modelling the geochemical cycle of boron: Implications for the long-term δ^{11}B evolution of seawater and oceanic crust. *Chemical Geology* 225 (1-2), 61-76.

Spero, H., Bijma, J., Lea, D. and Bemis, B. (1997) Effect of seawater carbonate concentration on foraminiferal carbon and oxygen isotopes. *NATURE-LONDON-* 497-499.

Spivack, A. J. and Edmond, J. M. (1987) Boron isotope exchange between seawater and the oceanic crust. *Geochim. Cosmochim. Acta* 51 (5), 1033–1043.

Takayama, T. (1993.) Notes on Neogene calcareous nannofossil biostratigraphy of the Ontong Java Plateau and size variations of Reticulofenestra coccoliths. *In Berger, W.H., Kroenke, L.W., Mayer, L.A., et al., Proc. ODP, Sci. Results, 130: College Station, TX (Ocean Drilling Program),* 179–229.

Thiede, J., Winkler, A., Wolf-Welling, T., Eldholm, O., Myhre, A. M., Baumann, K. H., Henrich, R. and Stein, R. (1998) Late Cenozoic history of the Polar North Atlantic: results from ocean drilling. *Quaternary Science Reviews* 17 (1-3), 185-208.

Toggweiler, J. R. and Bjornsson, H. (2000) Drake Passage and palaeoclimate. *Journal of Quaternary Science* 15 (4), 319-328.

Urey, H. (1947) The thermodynamic properties of isotopic substances. *Journal of the Chemical Society* 562-581.

van Andel, T. H. (1975) Mesozoic/Cenozoic calcite compensation depth and the global distribution of calcareous sediments. *Earth and Planetary Science Letters* 26 (2), 187-194.

Via, R. K. and Thomas, D. J. (2006) Evolution of Atlantic thermohaline circulation: Early Oligocene onset of deep-water production in the North Atlantic. *Geology* 34 (6), 441.

Vincent, E. and Berger, W. H. (1985) Carbon dioxide and polar cooling in the Miocene: the Monterey hypothesis. *The carbon cycle and atmospheric CO_2 Natural variations archean to present; Proceedings of the Chapman Conference on Natural Variations in Carbon Dioxide and the Carbon Cycle, American Geophysical Union*, 455-468.

Weedon, G. P., Shackleton, N. J. and Pearson, P. N. (1997) The Oligocene time scale and cyclostratigraphy on the Ceara Rise, western equatorial Atlantic. *Ocean Drilling Program. Proc. Ocean Drill. Program Sci. Results*, pp. 101-114.

Wilson, P. A. and Opdyke, B. N. (1996) Equatorial sea-surface temperatures for the Maastrichtian revealed through remarkable preservation of metastable carbonate. *Geology* 24 (6), 555-558.

Woodruff, F. and Savin, S. M. (1989) Miocene deepwater oceanography. *Paleoceanography* 4 (1), 87-140.

Yu, J. and Elderfield, H. (2007) Benthic foraminiferal B/Ca ratios reflect deep water carbonate saturation state. *Earth and Planetary Science Letters* 258 (1-2), 73-86.

Yu, J. and Elderfield, H. (2008) Mg/Ca in the benthic foraminifera Cibicidoides wuellerstorfi and Cibicidoides mundulus: Temperature versus carbonate ion saturation. *Earth and Planetary Science Letters* 276 (1-2), 129-139.

Yu, J., Elderfield, H., Greaves, M. and Day, J. (2007) Preferential dissolution of benthic foraminiferal calcite during laboratory reductive cleaning. *Geochemistry Geophysics Geosystems* 8 (6), Q06016.

Yu, J., Elderfield, H. and Hönisch, B. (2007) B/Ca in planktonic foraminifera as a proxy for surface seawater pH. *Paleoceanography* 22 (2), PA2202.

Yu, J., Elderfield, H., Jin, Z. and Booth, L. (2008) A strong temperature effect on U/Ca in planktonic foraminiferal carbonates. *Geochimica et Cosmochimica Acta* 72 (20), 4988-5000.

Zachos, J., Flower, B. and Paul, H. (1997) Orbitally paced climate oscillations across the Oligocene/Miocene boundary. *Nature* 388 (6642), 567-570.

Zachos, J., Pagani, M., Sloan, L., Thomas, E. and Billups, K. (2001) Trends, Rhythms, and Aberrations in Global Climate 65 Ma to Present. *Science* 292 (5517), 686.

Zachos, J., Shackleton, N., Revenaugh, J., Palike, H. and Flower, B. (2001b) Climate response to orbital forcing across the Oligocene-Miocene boundary. *Science* 292 (5515), 274.

Zachos, J. and Kump, L. (2005) Carbon cycle feedbacks and the initiation of Antarctic glaciation in the earliest Oligocene. *Global and Planetary Change* 47 (1), 51-66.

Zachos, J., Dickens, G. and Zeebe, R. (2008) An early Cenozoic perspective on greenhouse warming and carbon-cycle dynamics. *Nature* 451 (7176), 279-283.

8 Appendices

8.1 Chapter 1

8.1.1 Compiled published benthic foraminiferal Mg/Ca calibrations

	Species	B	A	Temperature range (°C)	Reference
Exponential equations	*C.pachyderma*	1.36	0.1	4.5-18	Rosenthal et al. (1997)
$Mg/Ca = B^*_{exp}(AT)$	*C.pachyderma*	0.85	0.11	0-18	Martin et al. (2002)
	C.wuellerstorfi				
	C.pachyderma	0.87	0.11	1-18	Lear et al. (2002)
	C.wuellerstorfi				
	C.compressus				
	Planulina Spp.	0.79	0.12	2-12	Lear et al. (2002)
	O.umbonatus	1.01	0.114	1-10	Lear et al. (2002)
	O.umbonatus	1.53	0.09	3-10	Rathmann et al. (2004)
	Melonis spp.	0.98	0.101	1-18	Lear et al. (2002)
	P. ariminensis	0.91	0.062	3-15	Lear et al. (2002)
	Uvigerina Spp.	0.92	0.061	2-18	Lear et al. (2002)
Linear equations	*C.pachyderma*	0.35	0.25	4-18	Marchitto & deMenocal. (2003)
Mg/Ca = B + (AT)	*C.pachyderma*	1.25	0.16	-1-18	Rosenthal et al. (2005)
	C.wuellerstorfi		0.12	6-19	
	C.pachyderma	1.2	0.14	6-19	Marchitto et al. (2007)
	C.pachyderma	0.7	2.22	10-25	Curry & Marchtto. (2005)
	Planoglabratella opercularis	89.7	2.9	10-25	Toyofuku et al. (2000)
	Quinqueloculina yabei	66	1.6	10-25	Toyofuku et al. (2000)
	Planoglabratella opercularis	81.5	0.034	2-18	Toyofuku & Kitazato. (2005)
	Hoeglundina elegans	0.96	0.06	2-18	Rosenthal et al. (2006)

8.2 Chapter 2

8.2.1 Cardiff University foraminifera cleaning and dissolving procedures

Foraminifera cleaning procedure

J. Riker, September 2008

This description is modified from the "Foram Procedure for Cadmium" recorded by Paula Rosener (1988), as updated to reverse the redox steps (1994). Our procedure differs in that the sample transfer is performed between reduction and oxidation. Our procedure is also expanded to include instructions specific to our lab. It is not necessary to perform Step III in all cases; please confirm the appropriate cleaning process before starting.

I. Before You Start

• Set your tubes of crushed forams in a clean, perspex rack. Ensure samples are clearly labelled with permanent ink and record a list or diagram of samples before starting. Randomize your samples prior to cleaning.

• Locate your reagents (remake or refill as necessary). All reagents should be prepared and stored in new, acid-leached PE bottles. You will need:

10% HCl or HNO_3 for rinsing pipette tips (250 mL; top up bottle from labelled dewars in the flow bench each day you clean)

DI H_2O for rinsing pipette tips (250 mL; rinse and refill bottle with fresh water each day you clean)

DI H_2O for foram cleaning (500 mL wash bottle; rinse and refill with fresh water each day you clean)

Trace grade methanol for foram cleaning (store in a 250 mL bottle; pour off a small amount into a 125 mL spray bottle just before use)

Empty 60 mL bottle for reducing reagent

Empty 60 mL bottle for rinsing reducing reagent

Empty 60 mL bottle for oxidizing reagent

DI H_2O for sample transfers (250 mL; rinse and refill bottle with fresh water each day you clean)

0.002 M HNO_3 for foram leaching (0.001 M for small samples) (250 mL; make fresh if old or contaminated)

• Turn on flow bench and allow to run for at least 15 minutes before using.

• Wipe down all work surfaces with DI water before starting (counter surfaces, interior of flow benches and fume cupboard, equipment surfaces).

• If floor has not been mopped recently, mop floor using DI water from the reservoir in Room 2.12.

II. Removal of Fine Clays

1. Drain the ultrasonic bath in the flow bench and refill with fresh DI H H_2O. Fill to the base of your perspex rack. Use the prop provided and never fill below the minimum fill line.

2. Tap your sample rack firmly on the bench to shake forams to the base of tubes.

3. Open tube tops slowly in case forams are stuck to the sides or lids.

4. Using your DI H_2O for foram cleaning, gently fill each tube most of the way.

5. If forams are visible in the tube lids, add a small amount of water to the lids as well. Close tubes.

6. Tap rack firmly on the bench to settle forams and get rid of any air bubbles. CHL: If forams will not settle or bubbles won't rise, tap the side or corners of the rack firmly on the edge of the flow bench.

7. Turn on siphon (switch is on the rear of the pump, on the right-hand side). Always make sure the siphon tip is in the flow bench when the pump is on.

8. If siphon waste beaker is full, empty into the labelled waste container beneath the water purifier. Check the waste level throughout the cleaning process and don't let it rise above the "max fill" line.

9. Rinse siphon tip in 10% HCl (3x) and then DI H_2O (3x) tip rinses. Don't siphon up too much tip rinse at once, as this can cause siphon waste to splash and contaminate the pump tubing.

10. Siphon off as much water as possible from the tubes. This works best if you avoid putting the siphon tip directly in the sample. Instead, rest the tip against the front of the tube, above water level, and siphon down gradually.

11. Open all tubes and fill ~1/3 full with water (not quite up to the rack base). Close tubes. CHL: The forams will agitate best in minimal H_2O.

12. Tap rack as necessary to remove air bubbles.

13. Ultrasonicate for 1 minute (set the bath to "hold"). Fine clays should now be dislodged and held in suspension.

14. Turn off bath and remove rack. Open all tubes and vigorously squirt DI H_2O for foram cleaning into each tube so as to agitate the sample and mix clays throughout. Close tubes.

15. Tap rack firmly on the bench, invert and shake, then wait for forams to settle. Don't wait too long, or suspended clays will also settle. If necessary, tap the rack again to encourage forams to settle.

16. Clean siphon tip (3x 10% HCl and 3x DI H_2O) while waiting for forams to settle.

17. Siphon off as much water as possible. Don't siphon off your forams.

18. Repeat steps 11-17 a total of 3x with DI H_2O. To avoid systematic variations in the effectiveness of clay removal: Begin siphoning at a different row and (or) side of the rack during each rinse step. Change the orientation of the rack in the sonic bath during each sonication.

19. Fill 125 mL spray bottle ~1/5 full with trace grade methanol. Loosen cap of spray bottle when not in use to keep methanol from dripping from the tip.

20. Repeat steps 11-17 1-2x with trace grade methanol, depending on the degree of clay contamination in your samples. Special instructions for methanol:

- Always wear goggles when working with methanol
- Fill tubes to the top of the rack with methanol (rather than just 1/3 full)
- Do not add additional methanol after ultrasonicating; simply siphon off existing methanol
- Methanol is less viscous than water, so take special care when siphoning; don't go to quite to the bottom of the tube

• When siphoning methanol, it may work better to press siphon tip against the rear of the tube (rather than the front)

• Dispose of any leftover methanol in the labelled waste container

21. Repeat steps 11-17 an additional 2x with DI H_2O.

22. Pipette off all remaining water using a clean (3x 10% HCl and 3x DI H_2O), 100 µL (yellow) pipette tip. It is not necessary to rinse the tip between samples.

III. Removal of Metal Oxides (Reducing Step)

1. Turn on power source for hotplate in the fume cupboard and set to 300 °C.

2. Rinse and fill the glass evaporating dish in the fume cupboard with DI H_2O from the ELGA tap. Fill to the base of your perspex rack. Set on hotplate.

3. Rinse and fill tall form beaker containing thermometer with DI H_2O from the ELGA tap. Set on hot plate. Use this to top up the evaporating dish as water evaporates.

4. Drain the ultrasonic bath in the fume cupboard and refill with fresh DI H_2O. Fill to the base of your perspex rack. Use the prop provided and never fill below the minimum fill line.

5. Prepare your reducing reagent in the labelled, empty 60 mL bottle. Please note that hydrous hydrazine is volatile, carcinogenic, and explosive. Always work in the fume cupboard and take care to minimize exposure. Dispose of all related waste (pipette tips, parafilm, gloves) in a plastic bag and seal bag before removing from fume cupboard.

• Pour 10 mLs ammonia solution and 10 mLs citric acid/ammonia solution (both stored in the fridge) into the empty bottle; pour these reagents directly from the bottles (no pipettes) and take care not to touch the lids of reagent bottles to any other surfaces.

• Prepare a waste bag, a fresh strip of parafilm, and a clean (3x 10% HCl and 3x DI H_2O) 1000 µL (blue) pipette tip

• Remove hydrous hydrazine from fridge

• Pipette 1200 µL hydrous hydrazine into the reducing reagent

• Dispose of pipette tip

• Cap reducing reagent and invert to mix

• Re-parafilm hydrous hydrazine and return to fridge

6. Before proceeding, ensure hot water bath is hot (on verge of boiling, 80-90 °C). This can take about 30 minutes.

7. Open tubes. Using a clean (3x 10% HCl and 3x DI H_2O) 100 µL pipette tip, add 100 µL reducing reagent to each tube. Be aware that the reagent has a low viscosity and tends to drip. Close tubes firmly.

8. Because ammonia has a high vapor pressure, tube caps will tend to blow open in the hot water both. To prevent this, clamp tubes shut by screwing a perspex plate to the top of your rack. Ensure your tubes are firmly closed and that they are in good contact with the plate surface.

9. Place racks in the hot water bath for a total of 30 minutes. Calcium carbonate is slightly soluble in ammonia, so avoid letting your foram fragments sit in the reducing agent for longer than the necessary 30 minutes. Every 2 minutes:

- Remove rack
- Tighten screws on perspex clamp
- Invert, shake, and tap rack to settle forams and remove bubbles
- Ultrasonicate rack for a few seconds (this will agitate the reagent into all parts of the sample and discourage dissolved oxides from re-precipitating)
- Tap rack firmly and return to hot water bath
- Top off the water bath as necessary using hot water from the beaker

10. After 30 minutes, remove rack and clamp and carefully open and close all tubes to release gas. Keep one finger on the top of the tube and use your thumb to open the tube in a peeling motion.

11. Pipette off as much reducing reagent as possible using a clean (3x 10% HCl and 3x DI H_2O) 100 µL pipette tip. Do not use siphon. Eject waste into the reducing reagent bottle. Eject tip into waste bag.

12. Fill tube caps and tubes (to top of rack or higher) with DI H_2O for foram cleaning. Close tubes. Tap rack firmly to settle forams.

13. Turn on the siphon in the fume cupboard using the labelled control knob on the left-hand panel. Rinse the siphon tip (3x 10% HCl and 3x DI H_2O). Siphon caps and then siphon off as much water as possible from tubes.

14. Repeat steps 12 and 13 two more times.

15. Fill tubes half full with DI H_2O for foram cleaning, close tubes, then set in the hot water bath for 5 minutes.

16. In the meantime, prepare a fresh strip of parafilm.

17. Remove hydrazine waste container (brown bottle) from fridge and place in fume cupboard.

18. Dump leftover reducing reagent into waste container.

19. Fill the empty 60 mL bottle for rinsing reducing reagent with DI H_2O from the ELGA tap.

20. Rinse the reducing reagent bottle 2-3x with DI H_2O, dumping rinse water into the waste container.

21. Re-parafilm waste container and return to fridge.

22. If 5 minutes have passed, remove rack from hot water bath, clean siphon tip (3x 10% HCl and 3x DI H_2O), siphon caps, and then siphon off as much water as possible from tubes.

23. Repeat steps 12 and 13 two more times.

24. Repeat step 15.

25. Repeat step 22. It is now safe to remove the rack from the fume hood.

26. Turn hotplate off or down as appropriate (you will need it again in Section V). Please remember to turn off the power source as well.

IV. Sample Transfer

1. In the flow bench, label a new set of acid-leached tubes for your samples.

2. Using a disposable scalpel, cut off ~1/4 of a 100 µL pipette tip.

3. Set the pipettor to 70 µL and thoroughly clean the pipette tip (6x 10% HCl and 6x DI H_2O).

4. If you haven't already, rinse and refill your DI H_2O for sample transfers.

5. Open an old tube. Hold pipette tip directly over foram fragments and pipette and expel fragments (±H_2O) into the new tube of the same sample number.

6. Add a small amount of DI H_2O for sample transfers to the old tube. Repeat transfer until no foram fragments are visible in the old tube and then again once more (usually 2-3x).

7. Between samples, rinse the pipette tip 2-3x in your DI H_2O for sample transfers.

8. Once all samples have been transferred into new tubes, turn on the siphon, clean the siphon tip (3x 10% HCl and 3x DI H_2O), and siphon off as much water as possible.

V. Removal of Organic Matter (Oxidizing Step)

1. In the fume cupboard, ensure hot water bath is hot (on verge of boiling, 80-90 °C) and filled to the base of your perspex rack.

2. Prepare your oxidizing reagent in the labelled, empty 60 mL bottle.

• Pour 15 mL 0.1 N NaOH (stored in the fridge) into the empty bottle; pour this reagent directly from the bottle (no pipettes) and take care not to touch the lid of the reagent bottle to any other surface

• Using a clean (3x 10% HCl and 3x DI H_2O) 100 µL pipette tip, add 50 µL H_2O_2; SB: please pour a small quantity of H_2O_2 into the H_2O_2 bottle cap, pipette from the cap, and dispose of cap contents before re-capping the bottle

• Cap reagent bottle and invert to mix

3. Open tubes and add 250 µL oxidizing reagent to each sample. Close tubes.

4. Set rack in hot water bath for 5 minutes.

5. Remove rack and invert, shake, and tap the rack to settle forams and remove bubbles. Ultrasonicate rack for a few seconds, then tap rack firmly and return to hot water bath.

6. Repeat steps 4 and 5.

7. Open tubes and top them off with DI H_2O for foram cleaning.

8. Turn on siphon, clean siphon tip (3x 10% HCl and 3x DI H_2O), and siphon off oxidizing reagent.

9. Repeat steps 7 and 8 two more times.

VI. Dilute Acid Leach

1. In the flow bench, clean a 1000 µL pipette tip (3x 10% HCl and 3x DI H_2O).

2. Add 250 µL 0.002 N HNO_3 to each tube. Because HNO_3 will dissolve carbonate, you may wish to use 0.001 N HNO_3 for small samples. You may also wish to skip ultrasonication and do fewer (or no) repetitions of the leach.

3. Tap the rack firmly and check for air bubbles. If necessary, tap some more.

4. Ultrasonicate the rack for 30 seconds.

5. Remove rack from bath. Invert, shake, and tap rack firmly to settle forams.

6. Open tubes. While waiting for forams to settle, turn on siphon and clean siphon tip (3x 10% HCl and 3x DI H_2O).

7. Once forams have settled, siphon off as much acid as possible.

8. Repeat steps 2-7 4x as quickly as possible to avoid dissolving your samples. To avoid systematic variations in the effectiveness of the acid leach: Begin siphoning at a different row and (or) side of the rack during each rinse step. Change the orientation of the rack in the sonic bath during each sonication.

9. Fill tubes and caps with DI H_2O for foram cleaning. Close tubes.

10. Tap rack firmly, check for bubbles, and ultrasonicate for a few seconds.

11. Remove rack from bath. Invert, shake, and tap rack firmly to settle forams.

12. Turn on siphon and clean siphon tip (3x 10% HCl and 3x DI H_2O). Once forams have settled, siphon caps and then siphon off as much water as possible from tubes.

13. Repeat steps 10-13.

14. Pipette off all remaining water using a clean (3x 10% HCl and 3x DI H_2O), 100 µL pipette tip. It is important to remove as much water as possible. Use a new, freshly-cleaned tip for each sample.

Your samples may be stored indefinitely at this point.

Dissolving and Diluting Benthic Forams for Trace Metal Analysis

J. Riker, May 2008

The following protocol describes how to dissolve and dilute cleaned benthic forams for trace metal analysis on the Element (using the FULL_FORAM_LMR method). This protocol assumes you have ~20 small tests per sample. If you have large or bulky samples, or if you are analyzing a different species, please consult with a lab manager to ensure that your final sample concentrations fall within the working range of the instrument.

Dissolving Cleaned Forams

1. Before starting, check to see that fluid was successfully siphoned from all tubes following the weak acid leach. Remove any excess fluid with a clean pipette tip (6x HNO_3 tip rinse, 6x H_2O tip rinse).
2. Add 120 µL 0.065 M Optima HNO_3 (see "Reagents," below) to each tube with a clean pipette tip (6x HNO_3 tip rinse, 6x H_2O tip rinse). Be aware that static may draw dry forams up the sides of the tubes; open tubes gently, one at a time, with the cleaned and acid-filled pipette tip ready to dispense.
3. After filling, close caps, invert each sample, and mix for a few seconds on the vortex tube stirrer. Centrifuge each tube for 3 minutes.
4. Leave overnight to dissolve. If samples do not dissolve overnight, try the following (in order):
    a. Release any built up CO_2 by gently opening and closing tube (trapped CO_2 will buffer the dissolution reaction).
    b. Invert and rotate tube (this should expose more of the foram surface area to the dissolution acid and disturb any buffered environment that may exist at the tube base). Watch to see if forams dissolve.

c. Ultrasonicate tubes (same effect as above). Check to see if forams have dissolved.
d. Place tubes in the fridge overnight (carbonate is more soluble at low temperature). Check to see if forams have dissolved.
e. As a last resort (if 10-20 forams remain undissolved), add an additional 50-100 μL 0.065 M HNO_3 to the tube. ***Transfer forams plus acid to a new, clean centrifuge tube before adding more acid.*** Never fill tubes used during the cleaning process above the 120 μL mark, as microfractures often form in these tubes during cleaning.

Splitting Dissolved Samples for Ratio and Ca Concentration Analysis

1. If your samples have been refrigerated, allow them to warm to room temperature before proceeding.
2. Once you have confirmed that samples are dissolved, label two sets of clean tubes with the appropriate sample numbers. Label one set of tubes with the letters "CC" (for Ca concentration analysis) and the other set with "TM" (for trace metal ratio analysis).
3. Invert, vortex, and centrifuge all samples.
4. Set pipettor to 100 μL and clean a pipette tip (6x HNO_3 tip rinse, 6x H_2O tip rinse). Open the first trace metal ratio tube you wish to fill.
5. Gently remove the corresponding sample tube from the centrifuge (always double check the sample number), taking care not to disturb the sediment pack at the tube base. Keep the tube in the same orientation it was sitting at in the centrifuge and walk slowly to the flow bench.
6. Gently open the tube and withdraw 100 μL of dissolved sample. Keep the pipette tip as close to the fluid surface as possible, moving the tip down as you pipette. This will help you to avoid sucking up solid contaminants at the tube base. Pipette the fluid into the opened empty tube.
7. Repeat with all tubes for trace metal analysis, using a new, cleaned pipette tip for each sample.
8. Re-centrifuge remaining dissolved samples.
9. Set pipettor to 10 μL and clean a pipette tip (3x HNO_3 tip rinse, 3x H_2O tip rinse). Open the first Ca concentration tube you wish to fill.
10. Using the same technique described above, pipette 10 μL of dissolved sample into each tube for Ca concentration analysis.
11. ***As a rule, always pipette off 100 μL of each dissolved sample for ratio analyses before pipetting off 10 μL for Ca analyses.*** This will help to minimize contamination of your ratio samples, which require more accurate analysis than your Ca samples, with particles or leachants concentrated at the tube base.
12. Discard (or label and store, if you prefer) the original dissolved sample tubes.

Diluting Dissolved Samples for Ca Concentration Analyses

1. ***On the day you plan to run your Ca concentration analyses,*** add 190 μL 0.5 M Optima HNO_3 (see "Reagents") to each Ca concentration sample tube using a clean pipette tip (6x HNO_3 tip rinse, 6x H_2O tip rinse), for a total sample volume of 200 μL.
2. Invert, vortex, and centrifuge sample tubes immediately prior to analysis.

Diluting Dissolved Samples for Ratio Analysis and Matrix-Matching Standards

1. Run Ca concentration analyses to determine the appropriate dilution of a matrix-matched standard (a standard of roughly equivalent Ca concentration) for each trace metal ratio sample. To calculate volumes of acid and standard to pipette, use the template spreadsheets provided by the lab manager.
2. Label a set of clean centrifuge tubes with the appropriate sample numbers and the letter "S" for standard. If you are planning to run your blanks in tubes (rather than in a vial), prepare an additional set of tubes for the blanks.
3. ***On the day you plan to run your ratio analyses,*** add 250 μL 0.5M Optima HNO_3 to each trace metal ratio sample tube using a clean pipette tip (6x HNO_3 tip rinse, 6x H_2O tip rinse), for a total sample volume of 350 μL.
4. Pipette each matrix-matched standard using your calculated volumes of standard and 0.5 M Optima HNO_3, for a total standard volume of 350 μL (same as your samples).
5. If necessary, pipette tube blanks (350 μL 0.5M Optima HNO_3).
6. Invert, vortex, and centrifuge sample tubes immediately prior to analysis. Stir standard tubes on the vortex, but it is not necessary to centrifuge them.

Reagents

Before preparing reagents, have a lab manager pour an aliquot of concentrated Optima HNO_3 into an acid-cleaned 60 mL Nalgene bottle. Pipette only out of this small bottle. ***Never handle the large Optima HNO_3 bottle stored in the fridge unless you have been given explicit permission.*** Your aliquot can be stored at room temperature in a plastic bag.

0.065 Molar Optima HNO3: Weigh out 249.35 g DI H_2O from the ELGA system in an acid-cleaned 250 mL Nalgene bottle (don't forget to zero the scale with the empty bottle first). Using a clean pipette tip, add 1036 μL 16 M Optima HNO_3.

0.5 Molar Optima HNO3: Weigh out 242.5 g DI H_2O from the ELGA system in an acid-cleaned 250 mL Nalgene bottle. Using a clean pipette tip, add 7750 μL 16 M Optima HNO_3.

8.2.2 Cardiff University tube cleaning procedure

General: Leave flow benches off overnight (extends life of filters), turn on for ~15min before starting work in them and wash well with D.I. water. Leave 10%HCl in the flow bench, but with the lid tightly closed, the nozzle (which falls off easily) wrapped in parafilm and bags over both the lid and nozzle. Fume cupboard needs turning on at the black switch under the cover, as well as the switch on the front at the left. Leave the lids to bottles upside down on the work bench, and avoid touching the rim of bottles when filling

1. Rinse the large beaker and watch glass well with D.I. water.
2. Fill the beaker (~3/4 full) with 10% HCl (remember to unscrew the top to the acid container).
3. Clean a disposable pipette with a few rinses of 10% HCl – remember to dilute to waste.
4. Squirt 10% HCl into the tubes, and remove any bubbles (either tap the tubes on the base or suck out bubbles with the pipette), fill the lids too.
5. Drop (tubes) into the beaker of acid.
6. Once you're done, check the tubes to see if any bubbles have got into the tubes, and remove as necessary.
7. Place the watch glass on the beaker, and the beaker on the hot plate, Set hot plate to:
    1) 100 for >1hr
    2) 150 for a further >1hr
    3) 200 – bubbles will start to form. Hold at this temperature until the end of the day and then **TURN THE HOTPLATE OFF**.
8. Leave the tubes in acid overnight (with the fume cupboard on).
9. Next day; clean flow benches again with D.I. water and leave on for ~15mins before starting work.
10. In the fume cupboard, decant the acid back into its container, taking care not to allow any tubes to follow the acid in (this is most easily achieved by holding the watch glass on top of the lid).
11. Fill the beaker with D.I. water and agitate (swirl around/shake gently/poke) the tubes in the diluting water.
12. Pour the dilute acid to waste
13. Repeat 11-12 times 3
14. Carefully pick up a tube, by the pointy end if possible (this is easiest if the beaker is ~3/4 full of water).
15. "flick" out the dilute acid in the bottom of the tube, and place between thumb and forefinger (or between fore and middle fingers).
16. Repeat 14-15 until you have 4-6 in your hand.
17. Using your "D.I. water for tubes" bottle squirt water into the tubes, lids, and rinse the hinge and around the cap.

18. Pour out the water and using a gangster hand gesture flick out the dregs in the bottom. Do this in the general vicinity of the sink, but not too close as there's a whole world of Mg in the sink (tapwater).
19. Repeat, 17-18 4-6 times, dependant on your current levels of paranoia
20. Place the now empty tubes on the flow bench, open end facing into the airflow to dry.
21. Repeat steps 14-20 until your beaker is empty.
22. When the tubes are dry (they don't take very long) carefully close the caps, avoiding touching the rim and inside of the lids.
23. Place them in a fresh ziplock bag, and label with your name, what they are, the date and the number in the bag.
24. Clean the flow bench, fume cupboard and work surface with D.I., rinse out the beaker and watch glass, switch off the flow bench, D.I. water and if safe to do so the fume cupboard.
25. Switch off all lights.
26. Retreat from the clean lab happy in the knowledge of a job well done, with the warm inner glow of a (wo)man who has some nice clean tubes.

MB

v1.1 23/10/06

8.3 Chapter 3

8.3.1 Data collected from ODP Leg 199 Sites.

Site	Hole	Section	Type	Interval	Top (cm)	Bottom (cm)	Depth (mbsf)	Age (Ma)	Li7/Ca43 μmol/mol	B11/Ca43 μmol/mol	Mg25/Ca43 mmol/mol	Sr88/Ca43 mmol/mol	U238/Ca43 nmol/mol
1218	B	23	X	1	0	4.5	204.10	32.700	13.68	33.83	1.55	0.776	12.74
1218	B	23	X	1	50	54.5	204.60	32.741	14.37	34.81	1.64	0.758	13.14
1218	B	23	X	1	100	104.5	205.10	32.784	12.58	31.32	1.52	0.769	15.54
1218	B	23	X	2	0	4.5	205.60	32.823	13.61	36.73	1.69	0.794	14.68
1218	B	23	X	2	50	54.5	206.10	32.859	13.15	43.90	1.67	0.777	15.86
1218	B	23	X	2	100	104.5	206.60	32.897	13.01	34.27	1.52	0.765	16.14
1218	B	23	X	3	0	4.5	207.10	32.931	12.99	32.07	1.52	0.766	12.49
1218	B	23	X	3	50	54.5	207.60	32.966	13.92	38.39	1.76	0.756	13.32
1218	B	23	X	3	100	104.5	208.10	33.004	14.01	34.98	1.67	0.752	13.87
1218	B	23	X	4	0	4.5	208.60	33.039	12.83	39.48	1.80	0.799	18.81
1218	B	23	X	4	50	54.5	209.10	33.092	13.25	32.98	1.47	0.792	16.07
1218	B	23	X	4	100	104.5	209.60	33.138	12.69	33.37	1.46	0.773	14.47
1218	B	23	X	5	0	4.5	210.10	33.172	13.14	32.76	1.57	0.758	13.73
1218	B	23	X	5	50	54.5	210.60	33.240	13.69	35.90	1.62	0.732	13.42
1218	B	23	X	5	100	104.5	211.10	33.299	13.55	37.53	1.40	0.760	14.87
1218	B	23	X	6	0	4.5	211.60	33.338	13.49	37.20	1.54	0.786	14.15

1218	B	23	X	6	50	54.5	212.10	33.371	13.95	39.09	1.49	0.775	13.43
1218	B	23	X	6	100	104.5	212.60	33.404	13.07	31.90	1.57	0.797	15.33
1218	B	23	X	7	0	4.5	213.10	33.458	13.16	32.00	1.50	0.765	14.41
1218	A	23	X	6	100	104.5	214.00	33.477	14.00	34.91	1.40	0.790	13.81
1218	B	23	X	7	40	44.5	213.50	33.483	12.84	31.68	1.53	0.765	23.42
1218	A	23	X	7	0	4.5	214.50	33.514	13.29	32.19	1.62	0.757	14.82
1218	A	23	X	7	40	45.0	214.90	33.540	15.51	39.64	1.52	0.788	13.01
1218	A	24	X	1	12	16.5	215.22	33.697	13.29	39.49	1.22	0.769	10.77
1218	A	24	X	1	50	54.5	215.60	33.734	14.84	39.20	1.24	0.779	12.49
1218	A	24	X	1	100	105.0	216.10	33.789	13.48	33.29	1.36	0.736	10.49
1218	A	24	X	2	7	11.5	216.25	33.807	13.33	35.72	1.59	0.715	10.66
1218	A	24	X	2	51	55.5	216.69	33.862	15.70	40.53	1.32	0.772	10.54
1218	A	24	X	3	100	104.5	217.18	34.197	11.89	29.50	1.13	0.798	10.10
1218	A	24	X	4	0	4.5	219.20	34.284	11.51	29.33	1.21	0.811	10.51
1218	A	24	X	4	102	106.5	220.22	34.462	12.24	32.77	1.20	0.793	10.58
1218	A	24	X	5	3	7.5	220.73	34.557	14.02	27.24	1.55	0.734	8.06
1218	A	24	X	6	3	7.5	222.23	34.976	12.96	35.07	1.15	0.801	7.71
1218	A	24	X	6	104	108.5	223.24	35.193	11.74	29.93	1.30	0.773	8.35
1218	A	24	X	7	0	4.5	223.70	35.286	25.93	37.96	1.55	0.798	5.37
1218	A	24	X	7	50	54.5	224.20	35.362	12.45	30.76	1.34	0.783	11.90
1219	A	17	X	2	40	42.0	150.40	33.623	13.10	38.01	1.54	0.765	9.98

1219	A	17	X	2	42	44.0	150.42	33.626	13.25	42.73	1.26	0.765	10.04
1219	A	17	X	2	44	46.0	150.44	33.629	13.14	35.99	1.28	0.752	8.98
1219	A	17	X	2	46	48.0	150.46	33.632	12.85	34.42	1.18	0.781	9.64
1219	A	17	X	2	48	50.0	150.48	33.635	13.13	34.82	1.18	0.792	9.33
1219	A	17	X	2	50	52.0	150.50	33.638	7.63	40.95	1.29	0.766	8.12
1219	A	17	X	2	52	54.0	150.52	33.641	12.86	37.92	1.32	0.771	9.29
1219	A	17	X	2	54	56.0	150.54	33.644	12.70	33.22	1.43	0.736	7.97
1219	A	17	X	2	56	58.0	150.56	33.646	12.83	34.46	1.24	0.767	8.37
1219	A	17	X	2	58	60.0	150.58	33.649	12.69	35.67	1.19	0.766	8.38
1219	A	17	X	2	60	62.0	150.60	33.652	11.93	32.93	1.18	0.751	8.13
1219	A	17	X	2	62	64.0	150.62	33.655	13.16	37.11	1.16	0.785	7.90
1219	A	17	X	2	64	66.0	150.64	33.658	13.07	34.31	1.11	0.779	9.24
1219	A	17	X	2	66	68.0	150.66	33.661	12.43	34.24	1.19	0.792	8.39
1219	A	17	X	2	68	70.0	150.68	33.664	11.91	32.44	1.20	0.768	6.93
1219	A	17	X	2	70	72.0	150.70	33.668	13.16	34.59	1.13	0.768	6.73
1219	A	17	X	2	72	74.0	150.72	33.671	13.39	38.18	1.14	0.803	8.16
1219	A	17	X	2	74	76.0	150.74	33.674	13.42	36.98	1.13	0.805	7.72
1219	A	17	X	2	76	78.0	150.76	33.678	12.71	36.09	0.98	0.790	6.66
1219	A	17	X	2	78	80.0	150.78	33.681	12.61	36.73	1.11	0.773	5.84
1219	A	17	X	2	80	82.0	150.80	33.684	13.43	42.49	1.27	0.792	7.93
1219	A	17	X	2	82	84.0	150.82	33.689	12.16	34.63	1.05	0.787	6.74

1219	A	17	X	2	84	86.0	150.84	33.695	12.24	41.92	1.22	0.813	6.67
1219	A	17	X	2	86	88.0	150.86	33.702	12.42	40.08	2.50	0.788	6.48
1219	A	17	X	2	88	90.0	150.88	33.708	12.17	35.79	0.86	0.806	5.61
1220	B	4	H	6	26	28.0	70.86	33.463629	13.53	38.40	1.27	0.772	9.55
1220	B	4	H	6	28	30.0	70.88	33.469708	13.89	34.85	1.41	0.732	9.85
1220	B	4	H	6	30	32.0	70.90	33.477001	12.68	33.90	1.32	0.733	8.64
1220	B	4	H	6	32	34.0	70.92	33.484295	9.99	52.40	1.57	0.732	8.75
1220	B	4	H	6	34	36.0	70.94	33.491589	13.17	44.66	1.39	0.717	10.80
1220	B	4	H	6	36	38.0	70.96	33.498883	12.42	35.54	1.37	0.709	8.59
1220	B	4	H	6	38	40.0	70.98	33.506177	14.08	33.40	1.76	0.701	11.93
1220	B	4	H	6	40	42.0	71.00	33.513471	13.67	35.13	1.44	0.730	7.66
1220	B	4	H	6	42	44.0	71.02	33.520765	12.93	34.32	1.37	0.705	8.24
1220	B	4	H	6	44	46.0	71.04	33.528059	12.82	37.50	1.43	0.736	10.15
1220	B	4	H	6	46	48.0	71.06	33.535353	12.76	34.45	1.40	0.712	8.00
1220	B	4	H	6	48	50.0	71.08	33.542647	13.45	36.07	1.42	0.724	8.58
1220	B	4	H	6	50	52.0	71.10	33.549941	13.49	36.43	1.56	0.731	9.71
1220	B	4	H	6	52	54.0	71.12	33.557235	13.84	36.33	1.47	0.722	8.55
1220	B	4	H	6	54	56.0	71.14	33.563313	14.55	40.03	1.62	0.746	10.42
1220	B	4	H	6	56	58.0	71.16	33.570607	12.93	35.41	1.32	0.744	8.98
1220	B	4	H	6	58	60.0	71.18	33.577901	13.24	39.70	1.32	0.752	9.02
1220	B	4	H	6	60	62.0	71.20	33.585195	13.33	36.48	1.39	0.744	8.51

1220	B	4	H	6	62	64.0	71.22	33.592489	12.59	33.95	1.39	0.735	9.25
1220	B	4	H	6	64	66.0	71.24	33.599783	12.36	32.72	1.48	0.691	9.02
1220	B	4	H	6	66	68.0	71.26	33.607077	12.31	32.57	1.40	0.711	8.12
1220	B	4	H	6	68	70.0	71.28	33.614371	12.53	34.68	1.29	0.730	7.74
1220	B	4	H	6	70	72.0	71.30	33.62288	12.43	33.55	1.28	0.725	8.07
1220	B	4	H	6	72	74.0	71.32	33.63139	13.10	39.01	1.23	0.738	9.68
1220	B	4	H	6	74	76.0	71.34	33.6399	10.76	34.39	1.30	0.738	8.39
1220	B	4	H	6	76	78.0	71.36	33.648409	13.12	36.90	1.22	0.745	8.25
1220	B	4	H	6	78	80.0	71.38	33.656919	12.11	38.29	1.10	0.757	7.90
1220	B	4	H	6	80	82.0	71.40	33.665428	10.71	57.88	1.18	0.792	7.07
1220	B	4	H	6	82	84.0	71.42	33.673938	14.13	33.89	1.25	0.769	6.77
1220	B	4	H	6	84	86.0	71.44	33.681232	12.17	35.45	1.05	0.771	6.42
1220	B	4	H	6	86	88.0	71.46	33.688526	11.10	44.53	1.05	0.777	6.82
1220	B	4	H	6	88	90.0	71.48	33.69582	10.76	55.93	1.14	0.803	5.89
1220	B	4	H	6	90	92.0	71.50	33.703114	10.15	37.50	0.95	0.785	4.93

8.4 Chapter 4

8.4.1 Data collected from ODP Leg 154 Sites.

Cibicidoides mundulus

Site	Hole	Section	Type	Interval	Top (cm)	Bottom (cm)	Depth (mbsf)	Age (Ma)	Li7/Ca43 μmol/mol	B11/Ca43 μmol/mol	Mg25/Ca43 mmol/mol	Sr88/Ca43 mmol/mol	U238/Ca43 nmol/mol
926	B	50	X	1	17	19	461.57	22.792	15.45	167.16	1.90	1.116	29.91
926	B	50	X	1	37	39	461.77	22.8	14.62		1.94	1.112	40.12
926	B	50	X	1	47	49	461.87	22.804	16.13		1.98	1.083	41.04
926	B	50	X	1	57	59	461.97	22.808	16.82	190.19	2.03	1.126	85.09
926	B	50	X	1	67	69	462.07	22.811	17.43		2.22	1.128	77.83
926	B	50	X	1	77	79	462.17	22.815			1.59	1.112	68.95
926	B	50	X	1	127	129	462.67	22.832	14.18	160.5	1.35	1.131	51.77
926	B	50	X	1	137	139	462.77	22.836	14.17		1.29	1.112	37.92
926	B	50	X	2	8	10	462.98	22.845	15.80	179.15	1.95	1.120	133.7*
926	B	50	X	2	18	20	463.08	22.849	15.80	175.26	1.78	1.121	27.28
926	B	50	X	2	66	68	463.56	22.869	15.31		1.63	1.104	31.64
926	B	50	X	2	88	90	463.78	22.878	12.89		2.03	0.97*	57.35
926	B	50	X	2	108	110	463.98	22.886	14.69	175.24	1.71	1.104	39.75
926	B	50	x	3	30	32	464.70	22.916	16.16		1.77	1.135	44.66

926	B	50	X	3	50	52	464.90	22.924	15.40	166.62	2.01	1.122	48.52	
926	B	50	X	3	70	72	465.10	22.931	18.39	200.78	2.50	1.132	49.30	
926	B	50	X	3	120	122	465.60	22.951			1.91	1.154		
926	B	50	X	3	140	142	465.80	22.959	16.68	168.27	1.92	1.124	47.77	
926	B	50	X	4	0	2	465.90	22.963	19.11		1.85	1.143	46.77	
926	B	50	X	4	10	12	466.00	22.967	18.62		1.96	1.107	38.64	
926	B	50	X	4	20	22	466.10	22.97	16.37		1.50	1.142	26.25	
926	B	50	X	4	27	29	466.17	22.973	21.70		2.15	1.118	41.71	
926	B	50	X	4	40	42	466.30	22.978	19.08		1.71	1.137	56.46	
926	B	50	X	4	50	52	466.40	22.982	21.34		2.01	1.146	54.54	
926	B	50	X	4	60	62	466.50	22.985	24.86		2.52	1.093	102.86	
926	B	50	X	4	80	82	466.70	22.993	19.06		1.59	1.130	61.72	
926	B	50	X	4	100	102	466.90	22.999	20.93		1.85	1.148	41.91	
926	B	50	X	4	110	112	467.00	23.003	17.18	174.81	1.86	1.155	30.86	
926	B	50	X	4	120	122	467.10	23.006	16.53		1.89	1.135	59.73	
926	B	50	X	4	140	142	467.30	23.013	16.88		2.11	1.115	62.01	
926	B	50	X	5	0	2	467.40	23.017	16.33		1.68	1.157	45.91	
926	B	50	X	5	20	22	467.60	23.024	16.37	156.74	1.61	1.134	43.43	
926	B	50	X	5	30	32	467.70	23.027	15.00	140.17	1.74	1.097	84.27	
926	B	50	X	5	61	63	468.01	23.038	18.50		1.93	1.147	46.56	
926	B	50	X	5	70	72	468.10	23.042	17.14		1.98	1.138	45.16	

926	B	50	X	5	80	82	468.20	23.045	18.82	175.91	2.01	1.114	85.33	
926	B	50	X	5	100	102	468.40	23.052	15.81		1.78	1.116	102.52	
926	B	50	X	5	110	112	468.50	23.056	16.46		1.49	1.108	80.15	
926	B	50	X	6	50	52	469.40	23.092	17.60		1.63	1.134	52.69	
926	B	50	X	6	60	62	469.50	23.096	16.13	176.98	2.12	1.155	57.41	
926	B	50	X	6	80	82	469.70	23.104	19.41		2.04	1.172	79.01	
926	B	50	X	6	120	122	470.10	23.121	13.66		1.77	1.047*	95.49	
926	B	50	X	6	130	132	470.20	23.125	16.57		1.60	1.126	57.50	
926	B	51	X	1	8	10	471.08	23.155	14.56	159.58	1.71	1.121	81.72	
926	B	51	X	1	16	18	471.16	23.158	13.76	148.44	1.62	1.120	53.45	
926	B	51	X	1	26	28	471.26	23.161	11.93		1.60	1.030*	82.62	
926	B	51	X	1	46	48	471.46	23.168	17.58		1.98	1.119	45.31	
926	B	51	X	1	47	49	471.47	23.168	14.44	132.33	1.80	1.140	50.57	
926	B	51	X	1	58	60	471.58	23.172	13.95	132.24	1.54	1.155	37.23	
926	B	51	X	1	66	68	471.66	23.174			1.45	1.116	42.33	
926	B	51	X	1	76	78	471.76	23.178	18.86		1.72	1.124	155.02*	
926	B	51	X	1	78	80	471.78	23.179	14.06	133.51	1.73	1.134	77.06	
926	B	51	X	1	86	88	471.86	23.181	16.52		1.51	1.157	174.05	
926	B	51	X	1	90	92	471.90	23.183	14.68	144.27	1.76	1.173	59.44	
926	B	51	X	1	106	108	472.06	23.189	15.23		1.72	1.136	102.68	
926	B	51	X	1	106	108	472.06	23.189	14.12	132.13	1.52	1.175	46.24	

926	B	51	X	1	126	128	472.26	23.197	15.76	164.6	1.54	1.132	54.68	
926	B	51	X	1	136	138	472.36	23.201	17.19		1.81	1.105	73.04	
926	B	51	X	1	147	149	472.47	23.205	13.73	127.26	1.56	1.156	32.71	
926	B	51	X	2	7	9	472.57	23.209	16.35	160.29	1.66	1.149	39.75	
926	B	51	X	2	8	10	472.58	23.209	13.20	124.59	1.53	1.153	30.89	
926	B	51	X	2	17	19	472.67	23.213	15.08	157.45	1.29	1.180	30.80	
926	B	51	X	2	27	29	472.77	23.217	16.35		1.75	1.133	42.40	
926	B	51	X	2	47	49	472.97	23.226			1.56	1.147	37.96	
926	B	51	X	2	53	55	473.03	23.228	14.17	128.21	1.71	1.169	62.16	
926	B	51	X	2	57	59	473.07	23.23	15.44		1.45	1.114	34.79	
926	B	51	X	2	67	69	473.17	23.234	14.76	155.86	1.44	1.159	36.78	
926	B	51	X	2	77	79	473.27	23.237			1.70	1.113	63.15	
926	B	51	X	2	87	89	473.37	23.241	16.06	160.42	1.73	1.136	36.41	
926	B	51	X	2	107	109	473.57	23.248	16.99		1.98	1.117	37.13	
926	B	51	X	2	118	120	473.68	23.252			2.27	1.101	12.18	
926	B	51	X	3	0	2	474.00	23.264	14.55	137.14	1.78	1.161	37.39	
926	B	51	X	3	8	10	474.08	23.268	15.41	147.11	2.00	1.091	76.57	
926	B	51	X	3	47	49	474.47	23.282	15.78		1.89	1.151	57.40	
926	B	51	X	3	56	58	474.56	23.285	17.95		1.91	1.124	123.29*	
926	B	51	X	3	66	68	474.66	23.288	18.34		2.04	1.165	63.93	
926	B	51	X	3	107	109	475.07	23.301	18.17	194.39	1.99	1.122	41.08	

926	B	51	X	3	112	114	475.12	23.302	15.44	123.69	2.21	1.123	38.76
926	B	51	X	3	117	119	475.17	23.304	17.15	176.22	1.70	1.132	39.33
926	B	51	X	3	127	129	475.27	23.308	22.22		2.06	1.140	62.87
926	B	51	X	3	133	135	475.33	23.31	14.98	138.15	1.89	1.162	72.34
926	B	51	X	4	107	109	475.57	23.317	16.79		1.83	1.245*	23.47
926	B	51	X	4	107	109	475.57	23.317	20.60		2.02	1.133	46.21
926	B	51	X	4	17	19	475.67	23.321	18.12		1.85	1.145	38.91
926	B	51	X	4	17	19	475.67	23.321	16.38		2.45	1.081	34.27
926	B	51	X	2	28	30	472.78	23.329	14.23	132.16	1.70	1.152	39.23
926	B	51	X	4	50	52	476.00	23.333	18.35	168.94	2.00	1.120	24.22
926	B	51	X	4	67	69	476.17	23.339	17.59	165.08	2.13	1.151	31.71
926	B	51	X	4	87	89	476.37	23.346	16.33		1.65	1.130	24.15
926	B	51	X	4	100	102	476.50	23.351	15.84		1.93	1.126	65.15
926	B	51	X	5	13	15	477.13	23.382	13.05	123.14	1.60	1.158	23.56
926	B	51	X	5	90	92	477.90	23.413	14.13	134.93	1.77	1.128	35.07

Site	Hole	Section	Type	Interval	Top (cm)	Bottom (cm)	Depth (mbsf)	Age (Ma)	Li7/Ca43 μmol/mol	B11/Ca43 μmol/mol	Mg25/Ca43 mmol/mol	Sr88/Ca43 mmol/mol	U238/Ca43 nmol/mol
929	A	34	X	4	0	2	315.2	22.577	13.41		1.57	1.010	39.09
929	A	34	X	4	10	12	315.3	22.579	12.50	125.47	1.56	1.014	42.38

929	A	34	X	4	33	35	315.53	22.585	12.05	122.33	1.27	1.030	54.58	
929	A	34	X	4	42	44	315.62	22.588	12.48	126.39	1.34	1.049	22.24	
929	A	34	X	4	50	52	315.7	22.590	13.29		1.43	1.032	28.46	
929	A	34	X	4	130	132	316.5	22.639	13.08	146.84	1.15	1.057	45.01	
929	A	34	X	5	10	12	316.8	22.660	12.50	121.84	1.44	1.025	40.19	
929	A	34	X	5	20	22	316.9	22.670	12.63	134.13	1.31	0.994	13.71	
929	A	34	X	5	30	32	317	22.678			1.24	1.044	20.21	
929	A	34	X	5	40	42	317.1	22.686	13.98		1.24	1.063	33.41	
929	A	34	X	5	60	62	317.3	22.702	13.77	156.69	1.38	1.050	17.59	
929	A	34	X	5	70	72	317.4	22.710	12.95	132.87	1.35	1.035	14.30	
929	A	34	X	5	80	82	317.5	22.716	12.71	142.91	1.28	1.037	10.38	
929	A	34	X	5	90	92	317.6	22.722			1.35	1.028	29.76	
929	A	34	X	5	100	102	317.7	22.728	13.15		1.35	1.040	25.12	
929	A	34	X	5	110	112	317.8	22.734	15.48		1.28	1.058	44.03	
929	A	34	X	5	120	122	317.9	22.740			1.36	1.048	33.88	
929	A	34	X	5	130	132	318	22.746		120.03	1.39	0.996	54.41	
929	A	34	X	5	143	145	318.13	22.755	13.83	145.11	1.34	1.017	24.22	
929	A	34	X	6	0	2	318.2	22.760	12.44	138.90	1.31	1.037	20.24	
929	A	34	X	6	10	12	318.3	22.767	12.90	151.17	1.22	1.086	12.06	
929	A	34	X	6	20	22	318.4	22.774	14.38		1.39	1.048	56.60	
929	A	34	X	6	40	42	318.6	22.788	12.86	127.85	1.33	1.021	22.77	

929	A	34	X	6	48	50	318.68	22.793	13.48	148.58	1.12	1.081	12.92	
929	A	34	X	6	60	62	318.8	22.800	13.28		1.26	1.045	20.08	
929	A	34	X	6	71	73	318.91	22.806	12.24	137.51	1.31	1.026	29.89	
929	A	34	X	6	78	80	318.98	22.810	14.62		1.34	1.023	56.43	
929	A	34	X	6	90	92	319.1	22.817	12.88	144.57	1.39	1.068	41.20	
929	A	34	X	6	100	102	319.2	22.822	13.11	137.42	1.42	1.021	37.89	
929	A	34	X	6	110	112	319.3	22.828	12.09	135.08	1.28	1.004	34.01	
929	A	34	X	6	121	123	319.41	22.834	13.24		1.40	1.043	37.40	
929	A	34	X	6	130	132	319.5	22.840			1.35	1.010	44.31	
929	A	34	X	6	140	142	319.6	22.845	14.40	156.87	1.68	1.036	34.59	
929	A	34	X	7	0	2	319.7	22.851	13.11		1.37	1.049	26.54	
929	A	34	X	7	10	12	319.8	22.857	13.27		1.24	1.058	23.46	
929	A	34	X	7	20	22	319.9	22.863	12.59	134.61	1.13	1.036	18.71	
929	A	35	X	1	30	32	320.7	22.933	14.42	160.27	1.68	1.014	36.87	
929	A	35	X	1	40	42	320.8	22.939	14.09	145.70	1.33	1.063	26.08	
929	A	35	X	1	50	52	320.9	22.944	13.68	143.24	1.49	1.056	25.68	
929	A	35	X	2	30	32	322.2	23.015	12.57	139.86	1.30	1.064	64.79	
929	A	35	X	2	40	42	322.3	23.020	12.85		1.35	1.060	30.20	
929	A	35	X	2	80	82	322.7	23.042	13.36	147.60	1.44	1.042	31.06	
929	A	35	X	2	90	92	322.8	23.047	13.06	150.47	1.32	1.056	49.93	
929	A	35	X	3	10	12	323.5	23.089	12.99		1.46	1.039	34.18	

929	A	35	X	3	20	22	323.6	23.096	12.86		1.60	1.006	55.15	
929	A	35	X	3	80	82	324.2	23.132	12.88		1.53	1.066	42.03	
929	A	35	X	3	105	107	324.45	23.146	11.88		1.17	1.079	66.52	
929	A	35	X	3	112	114	324.52	23.149	12.21	136.83	1.20	1.087	39.58	
929	A	35	X	4	30	32	325.2	23.182	11.08	124.91	1.24	1.071	17.82	
929	A	35	X	4	40	42	325.3	23.188	10.12	124.75	1.39	1.099	14.91	
929	A	35	X	4	88	90	325.78	23.226	12.31	138.97	1.34	1.099	24.48	
929	A	35	X	4	110	112	326	23.240	13.19	131.51	1.11	1.108	34.49	
929	A	35	X	4	140	142	326.3	23.257	12.62		1.43	1.081	81.77	
929	A	35	X	5	0	2	326.4	23.262	12.85		1.49	1.019	54.69	
929	A	35	X	5	40	42	326.8	23.284	12.29	134.84	1.40	1.075	88.87	
929	A	35	X	5	60	62	327	23.294	11.13		1.28	1.067	79.33	
929	A	35	X	5	68	70	327.08	23.299	14.44		1.22	1.073	34.46	
929	A	35	X	5	80	82	327.2	23.305	9.71		1.48	1.069	35.66	
929	A	35	X	5	90	92	327.3	23.310	11.64		1.29	1.063	24.89	
929	A	35	X	5	100	102	327.4	23.316	13.73		1.20	1.078	20.15	
929	A	35	X	6	10	12	328	23.352	15.29		1.19	1.055	26.80	
929	A	35	X	6	70	72	328.6	23.395	11.57	129.83	1.38	1.003	21.78	
929	A	35	X	6	80	82	328.7	23.402	12.13	140.53	1.42	1.035	16.79	
929	A	35	X	6	130	132	329.2	23.435	11.70	134.74	1.34	0.988	23.47	
929	A	35	X	6	140	142	329.3	23.442	14.02	139.92	1.30	1.040	22.86	

929	A	35	X	7	0	2	329.4	23.449	12.96		1.35	1.003	27.68
929	A	35	X	7	20	22	329.6	23.466	14.11		1.43	1.036	
929	A	35	X	cc	17	19	329.8	23.487	13.02	143.59	1.52	0.967	44.55
929	A	35	X	cc	28	30	329.91	23.499	12.72		1.50	0.998	54.69
929	A	36	X	1	1	3	330.01	23.507	13.25		1.55	1.066	32.36
929	A	35	X	cc	42	44	330.05	23.511			1.39	1.025	44.62
929	A	36	X	1	30	32	330.3	23.525			1.55	1.025	31.72
929	A	36	X	1	69	71	330.69	23.546	12.63		1.22	1.087	24.59
929	A	36	X	1	80	82	330.8	23.551	12.19	154.60	1.30	1.080	28.91

Oridorsalis umbonatus

Site	Hole	Section	Type	Interval	Top (cm)	Bottom (cm)	Depth (mbsf)	Age (Ma)	Li7/Ca43 μmol/mol	B11/Ca43 μmol/mol	Mg25/Ca43 mmol/mol	Sr88/Ca43 mmol/mol	U238/Ca43 nmol/mol
926	B	50	X	1	17	19	461.57	22.792		37.86	1.69	0.940	
926	B	50	X	1	37	39	461.77	22.800		28.71		0.890	
926	B	50	X	1	47	49	461.87	22.804	12.58	31.08	1.69	0.907	52.26
926	B	50	X	1	57	59	461.97	22.808	11.67	33.05	1.77	0.938	81.90
926	B	50	X	1	77	79	462.17	22.815		40.19*	1.81	0.967	
926	B	50	X	1	88	90	462.28	22.818	12.61	33.62	1.72	0.947	56.37

926	B	50	X	1	117	119	462.57	22.829		35.04	1.70	0.887	
926	B	50	X	1	127	129	462.67	22.832		38.40	1.54*	0.959	
926	B	50	X	1	137	139	462.77	22.836	12.91	29.01	1.67	0.901	48.53
926	B	50	X	1	147	149	462.87	22.840		43.42	1.70	0.928	
926	B	50	X	2	8	10	462.98	22.845		34.20		0.868*	
926	B	50	X	2	18	20	463.08	22.849		41.85	1.62	0.933	
926	B	50	X	2	28	30	463.18	22.853		35.83	1.82	0.916	
926	B	50	X	2	48	50	463.38	22.861	11.56	29.79	1.75	0.937	45.38
926	B	50	X	2	58	60	463.48	22.866	11.87	29.90	1.60	0.942	35.47
926	B	50	X	2	66	68	463.56	22.869	12.13	30.90	1.68	0.915	33.18
926	B	50	X	2	88	90	463.78	22.878		26.60		0.852	
926	B	50	X	2	108	110	463.98	22.886	11.42	25.98	1.64	0.918	39.24
926	B	50	X	2	118	120	464.08	22.890	11.27	31.91	1.86	0.862	
926	B	50	X	2	128	130	464.18	22.894		31.49	1.91	0.880	
926	B	50	X	2	138	140	464.28	22.899		25.82	1.92	0.863	54.20
926	B	50	X	2	148	150	464.38	22.903	11.41	28.10	1.87	0.878	35.13
926	B	50	X	3	10	12	464.5	22.908	12.66	33.58	1.89	0.924	51.87
926	B	50	X	3	20	22	464.6	22.912		25.61		0.857*	
926	B	50	X	3	40	42	464.8	22.920		33.27	1.75	0.948	
926	B	50	X	3	50	52	464.9	22.924		36.12	1.63	0.965	
926	B	50	X	3	60	62	465	22.928		45.43*	2.23*	0.929	

926	B	50	X	3	70	72	465.1	22.931		33.04	1.89	0.898		
926	B	50	X	3	80	82	465.2	22.935	13.28	30.62	2.07	0.935	43.44	
926	B	50	X	3	90	92	465.3	22.939		35.36	1.90	0.939		
926	B	50	X	3	110	112	465.5	22.947	12.66	38.99	1.78	0.914	37.25	
926	B	50	X	3	120	122	465.6	22.951	12.69	22.55	1.84	0.875		
926	B	50	X	3	130	132	465.7	22.955		28.66		0.891		
926	B	50	X	3	140	142	465.8	22.959	12.68	31.72	1.60*	0.938	29.98	
926	B	50	X	4	0	2	465.9	22.963		36.27	1.93	0.924		
926	B	50	X	4	10	12	466	22.967	13.48*	34.49	1.77	0.920	44.56	
926	B	50	X	4	20	22	466.1	22.970	13.01	34.15	1.81	0.918	47.84	
926	B	50	X	4	27	29	466.17	22.973		46.63	1.84	0.951		
926	B	50	X	4	40	42	466.3	22.978	12.66	55.13	1.63*	1.004	50.85	
926	B	50	X	4	50	52	466.4	22.982		33.98	1.79	0.927		
926	B	50	X	4	60	62	466.5	22.985		30.79		0.879		
926	B	50	X	4	70	72	466.6	22.989		35.57	1.73	0.887		
926	B	50	X	4	80	82	466.7	22.993	12.45	31.12	1.77	0.928	56.96	
926	B	50	X	4	100	102	466.9	22.999		38.78	1.80	0.919		
926	B	50	X	4	110	112	467	23.003		36.72	1.87*	0.930	75.87	
926	B	50	X	4	120	122	467.1	23.006	13.98*	39.18	1.77	0.946		
926	B	50	X	4	130	132	467.2	23.010		41.79	1.78	0.938		
926	B	50	X	4	140	142	467.3	23.013	12.74	33.83	1.70	0.947	56.77	

926	B	50	X	5	0	2	467.4	23.017	12.18	30.40	1.78	0.935	75.34	
926	B	50	X	5	10	12	467.5	23.020	12.68	31.09	1.88	0.926	80.31	
926	B	50	X	5	20	22	467.6	23.024	12.46	28.63	1.71	0.926	66.47	
926	B	50	X	5	30	32	467.7	23.027	13.68*	34.35	1.62	0.935	89.68	
926	B	50	X	5	40	42	467.8	23.031		45.22	1.67	0.950		
926	B	50	X	5	50	52	467.9	23.034		37.24	1.58	0.942		
926	B	50	X	5	61	63	468.01	23.038		37.74	1.71	0.952		
926	B	50	X	5	70	72	468.1	23.042		37.68	2.10*	0.922		
926	B	50	X	5	80	82	468.2	23.045		28.32		0.909		
926	B	50	X	5	100	102	468.4	23.052		34.61	1.81	0.926		
926	B	50	X	5	110	112	468.5	23.056	12.49	30.61	1.85	0.937	81.17	
926	B	50	X	5	120	122	468.6	23.060	12.71	31.29	1.68	0.955	65.78	
926	B	50	X	5	130	132	468.7	23.063	12.64	29.09	1.82	0.952	118.61	
926	B	50	X	5	140	142	468.8	23.067		34.07	1.50	0.935		
926	B	50	X	6	0	2	468.9	23.071	11.81	30.80	1.68	0.933	79.23	
926	B	50	X	6	10	12	469	23.075		35.40	1.47	0.963		
926	B	50	X	6	20	22	469.1	23.079	11.90	28.93	1.48	0.935	80.33	
926	B	50	X	6	30	32	469.2	23.083	12.66	29.74	1.50	0.934	120.69	
926	B	50	X	6	40	42	469.3	23.087	13.08	33.99	1.61	0.937	105.89	
926	B	50	X	6	50	52	469.4	23.092		29.24	1.65	0.955		
926	B	50	X	6	70	72	469.6	23.100		34.68	1.72	0.897		

926	B	50	X	6	70	72	469.6	23.100		38.61		0.956	
926	B	50	X	6	80	82	469.7	23.104	14.08	36.05	1.69	0.960	57.83
926	B	50	X	6	100	102	469.9	23.113	12.50	30.16	1.83	0.927	81.26
926	B	50	X	6	110	112	470	23.117	11.64	27.37	1.47	0.933	55.50
926	B	50	X	6	120	122	470.1	23.121	13.19	31.31	1.69	0.950	59.97
926	B	50	X	6	130	132	470.2	23.125		33.52		0.898	
926	B	51	X	1	0	3	471	23.152	12.48	29.74	1.76	0.949	57.21
926	B	51	X	1	18	16	471.16	23.158	12.57	30.97	1.82	0.934	65.17
926	B	51	X	1	30	32	471.3	23.162	11.95*	28.08	1.75	0.902	76.55
926	B	51	X	1	47	50	471.47	23.168	12.60	32.98	1.88	0.944	54.35
926	B	51	X	1	58	60	471.58	23.172	12.44	31.13	1.89	0.947	51.89
926	B	51	X	1	78	80	471.78	23.179	13.00	32.66	1.77	0.960	97.80
926	B	51	X	1	90	93	471.9	23.183	13.27	39.87*	1.67	0.975	60.97
926	B	51	X	1	108	106	472.06	23.189	13.52		1.66	0.969	66.04
926	B	51	X	1	117	120	472.17	23.193	12.82	31.17	1.74	0.968	62.40
926	B	51	X	1	132	135	472.32	23.199	11.98	29.39	1.82	0.934	26.15
926	B	51	X	1	147	149	472.47	23.205	12.20	31.51	1.73	0.964	38.43
926	B	51	X	2	8	10	472.58	23.209	12.49	32.73	1.71	0.949	37.54
926	B	51	X	3	62	65	474.62	23.217	13.11	32.12	1.91*	0.928	49.52
926	B	51	X	2	40	42	472.9	23.223	12.28	30.62		0.939	51.31
926	B	51	X	2	53	56	473.03	23.228	12.82	31.42	1.63	0.980	50.46

926	B	51	X	2	71	74	473.21	23.235	12.33	28.29	1.68	0.910	42.32	
926	B	51	X	2	85	89	473.35	23.240	13.64		1.77	0.994	28.35	
926	B	51	X	2	85	89	473.35	23.240	13.32		1.67	0.949	30.29	
926	B	51	X	2	100	102	473.5	23.246	12.14		2.02	0.922	42.13	
926	B	51	X	2	120	123	473.7	23.253	12.23	29.17	1.91	0.905	33.69	
926	B	51	X	2	130	132	473.8	23.256	12.69	31.03	2.05	0.933	54.73	
926	B	51	X	3	0	3	474	23.264	12.54	30.79	2.05	0.946	68.19	
926	B	51	X	3	24	27	474.24	23.274	12.28	27.78	1.93	0.967	51.98	
926	B	51	X	3	40	42	474.4	23.280	12.14	29.30	1.55	0.964	28.14	
926	B	51	X	3	57	60	474.57	23.285	12.19		1.74	0.961	41.13	
926	B	51	X	4	147	150	476.97	23.287	12.24	31.87	1.99	0.949	43.38	
926	B	51	X	3	68	70	474.68	23.289	12.80*	30.51	2.01	0.957	52.11	
926	B	51	X	3	101	103	475.01	23.299	12.07	30.13	1.93	0.949	45.07	
926	B	51	X	3	112	115	475.12	23.303	12.22	29.70	1.97	0.929	50.00	
926	B	51	X	3	133	135	475.33	23.310	12.65	31.91	2.11*	0.973	44.91	
926	B	51	X	4	10	13	475.6	23.318	11.88		1.90	0.933	43.74	
926	B	51	X	4	24	27	475.74	23.324	12.80	32.04	1.81	0.963	42.44	
926	B	51	X	2	28	31	472.78	23.329	11.86	30.76	1.86	0.937	29.38	
926	B	51	X	4	51	53	476.01	23.333	12.67	32.42	1.97	0.941	30.63	
926	B	51	X	4	72	74	476.22	23.341	12.26	29.86	1.93	0.941	34.10	
926	B	51	X	4	81	83	476.31	23.344	11.96	29.58	1.63	0.961	23.59	

926	B	51	X	4	100	103	476.5	23.351	12.08	29.66	2.00	0.912	48.07*	
926	B	51	X	4	117	119	476.67	23.358	11.87	30.56	1.73	0.966	31.15	
926	B	51	X	4	130	132	476.8	23.365	12.51	32.35	1.87	0.920	25.03	
926	B	51	X	4	38	40	475.88	23.373	12.36	32.05	1.89	0.950	51.40	
926	B	51	X	5	13	15	477.13	23.382	13.20*	30.26	2.01	0.957	38.12	
926	B	51	X	5	29	32	477.29	23.390	12.55		1.75	0.915	48.25	
926	B	51	X	5	44	46	477.44	23.396	12.22		1.74	0.925	56.39*	
926	B	51	X	5	60	62	477.6	23.402	14.51*		1.98	0.939	41.07	
926	B	51	X	5	73	76	477.73	23.406	12.42	31.22	1.89	0.922	39.38	
926	B	51	X	5	90	92	477.9	23.414	12.02	30.84	1.75*	0.965	33.14	
926	B	51	X	5	103	105	478.03	23.420	12.69		1.88	0.931	53.28	
926	B	51	X	5	122	125	478.22	23.431	12.83	31.37	1.88	0.939	53.60	
926	B	51	X	5	131	133	478.31	23.436	11.86*	27.98*	1.77*	0.891	63.67*	
926	B	51	X	5	148	150	478.48	23.443	12.90	33.05	1.83	0.939	48.95	
926	B	51	X	6	0	3	478.5	23.444	13.06	32.34	1.85	0.926	47.57	
926	B	51	X	6	15	17	478.65	23.450	13.68		1.91	0.946	34.03	
926	B	51	X	6	30	32	478.8	23.469	13.32		1.83	0.963	45.90	
926	B	51	X	6	46	49	478.96	23.494	12.07		1.76	0.986	30.70	
926	B	51	X	6	72	74	479.22	23.533	12.86		1.67	0.979	38.79	
926	B	51	X	6	72	74	479.22	23.533	12.83		1.84	0.968	57.77	
926	B	51	X	6	89	92	479.39	23.555	12.51		1.72	0.900	48.00	

926	B	51	X	6	108	110	479.58	23.569	12.68	39.33	1.89	0.923	52.59

Site	Hole	Section	Type	Interval	Top (cm)	Bottom (cm)	Depth (mbsf)	Age (Ma)	Li7/Ca43 μmol/mol	B11/Ca43 μmol/mol	Mg25/Ca43 mmol/mol	Sr88/Ca43 mmol/mol	U238/Ca43 nmol/mol
929	A	34	X	4	0	2	315.2	22.577			1.44	0.870	42.40
929	A	34	X	4	10	12	315.3	22.579	12.63		1.42	0.837	48.61
929	A	34	X	4	20	22	315.4	22.582	12.17	35.30	1.40	0.886	28.28*
929	A	34	X	4	33	35	315.53	22.585	13.22	34.90	1.46	0.874	45.80
929	A	34	X	4	50	52	315.7	22.590	11.71		1.31*	0.831*	47.37
929	A	34	X	4	71	73	315.91	22.603	12.60	33.66	1.44	0.855	71.34
929	A	34	X	4	80	82	316	22.611	12.26	34.85	1.45	0.881	
929	A	34	X	4	90	92	316.1	22.619	12.97	33.65	1.46	0.876	58.26
929	A	34	X	4	100	102	316.2	22.624	13.57	36.10	1.52	0.848*	60.55
929	A	34	X	4	110	112	316.3	22.629	12.73	35.18	1.35	0.856	19.46*
929	A	34	X	4	130	132	316.5	22.639	13.57	38.52	1.53	0.867	58.75
929	A	34	X	4	140	142	316.6	22.644		49.47*	1.64	0.850	39.26
929	A	34	X	5	10	12	316.8	22.660		32.81	1.51	0.855	37.40
929	A	34	X	5	20	22	316.9	22.670		38.62	1.44	0.796	17.95
929	A	34	X	5	30	32	317	22.678	14.96*	45.31	1.30	0.876	13.98
929	A	34	X	5	70	72	317.4	22.710		38.92	1.31	0.828	15.98

929	A	34	X	5	80	82	317.5	22.716		38.92	1.34	0.851	13.96	
929	A	34	X	5	90	92	317.6	22.722	12.85	33.89	1.45	0.843	19.85	
929	A	34	X	5	100	102	317.7	22.728		42.87	1.74	0.844	26.71	
929	A	34	X	5	120	122	317.9	22.740		39.75	1.48	0.867	42.36	
929	A	34	X	5	130	132	318	22.746	12.23	31.96	1.42	0.832	23.35	
929	A	34	X	5	143	145	318.13	22.755		35.00	1.77*	0.813	33.02	
929	A	34	X	6	0	2	318.2	22.760		31.02	1.57	0.824	27.64	
929	A	34	X	6	10	12	318.3	22.767	12.21	33.22	1.59	0.832	29.67	
929	A	34	X	6	20	22	318.4	22.774		36.21	1.58	0.877*		
929	A	34	X	6	31	33	318.51	22.782		30.16	1.46	0.803	28.08	
929	A	34	X	6	40	42	318.6	22.788		38.92	1.29	0.826	21.46	
929	A	34	X	6	48	50	318.68	22.793		38.45	1.54	0.874	19.52	
929	A	34	X	6	60	62	318.8	22.800		40.98	1.29	0.862	16.23	
929	A	34	X	6	71	73	318.91	22.806		39.77	1.43	0.841	43.07	
929	A	34	X	6	90	92	319.1	22.817		41.13	1.40	0.882	45.51	
929	A	34	X	6	100	102	319.2	22.822		49.52*	1.22	0.850	29.97	
929	A	34	X	6	110	112	319.3	22.828	12.38	33.93	1.05*	0.871	22.40	
929	A	34	X	6	121	123	319.41	22.834	13.04	36.12	1.41	0.841	34.85	
929	A	34	X	6	130	132	319.5	22.840	13.82*	40.32	1.38	0.869	45.97	
929	A	34	X	6	140	142	319.6	22.845		39.12	1.54*	0.805*		
929	A	34	X	7	0	2	319.7	22.851	12.64	33.08	1.35	0.860	64.396*	

929	A	34	X	7	10	12	319.8	22.857	12.91	35.58	1.28	0.852	25.06	
929	A	34	X	7	20	22	319.9	22.863		43.98	1.55	0.903*	17.97	
929	A	34	X	cc	0	2	320.06	22.872		39.54	1.29	0.855	12.81	
929	A	34	X	cc	20	22	320.26	22.893		34.10	1.66	0.832	32.07	
929	A	35	X	1	13	15	320.53	22.922	12.48	36.77	1.55	0.830	40.05	
929	A	35	X	1	20	22	320.6	22.928		67.12*	1.99*	0.849	41.87	
929	A	35	X	1	40	42	320.8	22.939		41.33	1.46	0.875	28.24	
929	A	35	X	1	50	52	320.9	22.944	13.07	36.95	1.42	0.856	28.36	
929	A	35	X	1	60	62	321	22.949	13.29	35.93	1.38	0.850	34.491*	
929	A	35	X	1	67	69	321.07	22.953		38.64	1.31	0.853	27.33	
929	A	35	X	1	80	82	321.2	22.960			1.47	0.854	23.59	
929	A	35	X	1	90	92	321.3	22.966			1.62*	0.848	25.25	
929	A	35	X	1	100	102	321.4	22.971	12.79		1.36	0.814	26.17	
929	A	35	X	1	110	112	321.5	22.977		38.13	1.42	0.839	30.93	
929	A	35	X	1	120	122	321.6	22.982		39.71	1.41	0.883	23.01	
929	A	35	X	1	130	132	321.7	22.988			2.42*	0.796	29.16	
929	A	35	X	1	140	142	321.8	22.993		43.95	1.38	0.866	56.14	
929	A	35	X	2	0	2	321.9	22.998			1.50	0.902	26.10	
929	A	35	X	2	10	12	322	23.004		41.73	1.61	0.795*	72.71	
929	A	35	X	2	30	32	322.2	23.015	12.89	34.24	1.42	0.870	71.90	
929	A	35	X	2	40	42	322.3	23.020	13.27*	33.44	1.50	0.854	45.45	

929	A	35	X	2	50	52	322.4	23.026		34.44	1.18	0.868	50.51	
929	A	35	X	2	60	62	322.5	23.031	12.96	36.53	1.25	0.869	24.92	
929	A	35	X	2	70	72	322.6	23.036		38.76	1.35	0.868	21.37	
929	A	35	X	2	80	82	322.7	23.042	12.66	35.98	1.28	0.865	24.45	
929	A	35	X	2	90	92	322.8	23.047	13.22	33.35	1.68*	0.828	82.27	
929	A	35	X	2	100	102	322.9	23.053	12.55	34.72	1.39	0.855	28.54	
929	A	35	X	2	110	112	323	23.058	12.68	48.12*	1.41	0.827	78.42	
929	A	35	X	2	120	122	323.1	23.064	12.50	34.87	1.32	0.873	21.01	
929	A	35	X	2	130	132	323.2	23.070	12.30		1.36	0.852	36.56	
929	A	35	X	2	140	142	323.3	23.076			1.22	0.872	14.37	
929	A	35	X	3	0	2	323.4	23.083	11.88		1.30	0.858	71.35	
929	A	35	X	3	10	12	323.5	23.089		35.29	1.52	0.856	52.49	
929	A	35	X	3	20	22	323.6	23.096	13.03	37.14	1.39	0.858	36.48	
929	A	35	X	3	30	32	323.7	23.102		40.90*	1.39	0.866	25.27	
929	A	35	X	3	40	42	323.8	23.108		37.99	1.30	0.852	28.74	
929	A	35	X	3	50	52	323.9	23.114	14.16*	37.30	1.33	0.865	25.09	
929	A	35	X	3	60	62	324	23.120	12.80		1.36	0.866	23.97	
929	A	35	X	3	71	73	324.11	23.126		35.13	1.56	0.839	53.94	
929	A	35	X	3	80	82	324.2	23.132	12.74	33.62	1.41	0.854	43.72	
929	A	35	X	3	105	107	324.45	23.146	14.62*		1.48	0.887	87.45	
929	A	35	X	3	112	114	324.52	23.149		44.92*	1.44	0.869	71.62	

929	A	35	X	3	118	120	324.58	23.152			1.55	0.895	54.86	
929	A	35	X	3	130	132	324.7	23.157	13.04	34.07	1.45	0.851	31.92	
929	A	35	X	3	141	143	324.81	23.162	12.26	33.54	1.34*	0.840	23.90	
929	A	35	X	4	0	2	324.9	23.166	14.06	39.00	1.51	0.861	53.97*	
929	A	35	X	4	10	12	325	23.171		36.77	1.51	0.856	33.46	
929	A	35	X	4	20	22	325.1	23.176		32.01	1.49	0.831	27.50	
929	A	35	X	4	30	32	325.2	23.182		32.11	1.54	0.805	24.10	
929	A	35	X	4	40	42	325.3	23.188	12.80	35.09	1.46	0.843	17.79	
929	A	35	X	4	60	62	325.5	23.205		40.54	1.41	0.877	15.71	
929	A	35	X	4	67	69	325.57	23.211		39.19	1.38	0.900	24.30	
929	A	35	X	4	76	78	325.66	23.218		40.02	1.54	0.879	18.64	
929	A	35	X	4	88	90	325.78	23.226	13.66	36.83	1.39	0.901	27.10	
929	A	35	X	4	100	102	325.9	23.234		35.20	1.25	0.876	16.19	
929	A	35	X	4	110	112	326	23.240	12.43	30.56	1.19	0.885	24.40	
929	A	35	X	4	130	132	326.2	23.252		40.79*	1.52	0.866	33.42	
929	A	35	X	4	140	142	326.3	23.257	11.93	34.38	1.45	0.859	50.77	
929	A	35	X	5	0	2	326.4	23.262			1.66	0.838*		
929	A	35	X	5	10	12	326.5	23.268			1.61	0.866	75.49	
929	A	35	X	5	20	22	326.6	23.273	10.82*		1.18*	0.856	39.00	
929	A	35	X	5	30	32	326.7	23.278	12.13	33.56	1.48	0.885*	41.83	
929	A	35	X	5	40	42	326.8	23.284		36.92	1.63	0.851	116.62	

929	A	35	X	5	50	52	326.9	23.289		34.60	1.60	0.858	121.21	
929	A	35	X	5	60	62	327	23.294		40.50	1.71	0.839	92.04	
929	A	35	X	5	68	70	327.08	23.299	12.74	31.28	1.51	0.895	42.18	
929	A	35	X	5	90	92	327.3	23.310	12.68	33.90	1.66	0.877	30.50	
929	A	35	X	5	100	102	327.4	23.316	13.00	37.40	2.10*	0.834*	31.33	
929	A	35	X	5	110	112	327.5	23.321		35.44	1.41	0.901	20.05	
929	A	35	X	5	130	132	327.7	23.332			1.67	0.882	61.92*	
929	A	35	X	5	140	142	327.8	23.338		31.22	1.79	0.819*	36.44	
929	A	35	X	6	0	2	327.9	23.345		42.24	1.39	0.879	15.60	
929	A	35	X	6	10	12	328	23.352	11.63*	32.93	1.13	0.869	23.77	
929	A	35	X	6	50	52	328.4	23.381		41.09	1.63	0.856	26.29	
929	A	35	X	6	60	62	328.5	23.388		32.41	1.67	0.743*	29.35	
929	A	35	X	6	70	72	328.6	23.395		39.09	1.42	0.876	15.21	
929	A	35	X	6	80	82	328.7	23.402		30.70	1.53	0.818	21.99	
929	A	35	X	6	90	92	328.8	23.409	12.89	37.72	1.40	0.879	18.87	
929	A	35	X	6	100	102	328.9	23.415		48.65*	1.51	0.866	31.15	
929	A	35	X	6	120	122	329.1	23.429		34.24	1.52	0.835	43.26	
929	A	35	X	6	130	132	329.2	23.435		30.46	1.47	0.797*	24.76	
929	A	35	X	6	140	142	329.3	23.442		34.56	1.52	0.869	59.23	
929	A	35	X	7	10	12	329.5	23.456			1.59	0.840	28.35	
929	A	35	X	7	20	22	329.6	23.466		41.58	1.43	0.846	43.78	

929	A	35	X	cc	0	2	329.63	23.469		37.23	1.44	0.868	30.10
929	A	35	X	cc	10	12	329.73	23.480		32.43*	1.71*	0.793*	48.55
929	A	35	X	cc	17	19	329.8	23.487		39.78	1.48	0.826	52.89
929	A	36	X	1	1	3	330.01	23.507	13.25	37.38	1.58	0.863	60.59
929	A	35	X	cc	42	44	330.05	23.511		36.44	1.47	0.889	39.17
929	A	36	X	1	10	12	330.1	23.513		36.98	1.39	0.880	33.57
929	A	36	X	1	18	20	330.18	23.518	13.05	33.41	1.32	0.876	27.95
929	A	36	X	1	30	32	330.3	23.525		33.18	1.52	0.837	34.82
929	A	36	X	1	40	42	330.4	23.530		40.11	1.56	0.872	49.26*
929	A	36	X	1	50	52	330.5	23.536		58.68*	1.44	0.846	37.66
929	A	36	X	1	80	82	330.8	23.551		48.50	1.35	0.887	35.22
929	A	36	X	1	90	92	330.9	23.556		38.32	1.37	0.862	26.86
929	A	36	X	1	110	112	331.1	23.567		59.13*	1.40	0.887	44.40

8.5 Chapter 5

8.5.1 Data collected from ODP Leg 130 Sites.

Trace metal data

Site	Hole	Section	Type	Interval	Top (cm)	Bottom (cm)	Depth (mbsf)	Age (Ma)	Li7/Ca43 μmol/mol	B11/Ca43 μmol/mol	Mg25/Ca43 mmol/mol	Sr88/Ca43 mmol/mol	U238/Ca43 nmol/mol
803	D	22	H	3	80	85	192.40	11.269	13.77	33.06	1.62	0.877	12.01
803	D	22	H	5	70	75	195.30	11.552	12.43	31.74	1.70	0.848	7.82
803	D	23	H	1	70	75	198.80	11.900	12.44	31.98	1.75	0.822	7.99
803	D	23	H	3	70	75	201.80	12.204	15.14	36.70	1.56	0.814	8.99
803	D	24	H	1	70	75	208.30	12.880	14.29	32.44	1.70	0.813	6.59
803	D	24	H	3	80	85	211.40	13.210	14.87	34.60	1.56	0.839	6.45
803	D	25	H	1	70	75	217.80	13.904	14.36	35.62	1.44	0.855	5.95
803	D	25	H	3	80	85	220.90	14.246	14.35	34.28	1.70	0.888	7.48
803	D	26	H	3	70	75	230.50	15.324	13.41	28.14	1.60	0.837	8.41
803	D	29	H	5	80	85	262.30	18.985	12.97	34.29	1.55	0.838	12.17
806	B	44	x	2	82	87	409.52	12.116	12.13	31.77	1.96	0.888	14.09
806	B	45	x	5	81	86	423.71	12.477	12.21	30.89	2.02	0.902	13.36
806	B	46	x	2	82	87	428.82	12.606	12.39	31.80	1.94	0.938	11.60
806	B	46	x	5	82	87	433.32	12.721	13.41	31.90	2.03	0.908	11.32

806	B	47	x	2	70	75	438.30	12.847	12.07	31.47	2.04	0.932	10.68	
806	B	47	x	5	38	43	442.48	12.953	11.89	29.79	1.89	0.920	12.90	
806	B	48	x	2	64	69	447.94	13.092	12.38	31.00	1.99	0.944	28.22	
806	B	48	x	5	60	65	452.40	13.205	12.88	33.05	1.76	0.960	7.12	
806	B	49	x	2	68	73	457.68	13.339	11.92	28.99	1.92	0.942	20.36	
806	B	49	x	5	63	68	462.13	13.452	12.09	31.98	2.01	0.939	8.41	
806	B	50	x	2	70	75	465.80	13.546	12.87	31.31	2.17	0.948	17.99	
806	B	51	x	2	68	73	475.48	13.792	12.14	178.71	2.00	0.955	2.14	
806	B	51	x	5	80	85	480.10	13.909	14.60	68.07	2.67	0.958	21.02	
806	B	52	x	2	88	93	484.98	14.033	11.17	28.49	1.79	0.966	17.70	
806	B	52	x	5	77	82	489.37	14.144	11.95	31.30	2.05	0.983	14.77	
806	B	53	x	2	71	76	494.51	14.275	11.84	29.40	1.89	0.960	7.93	
806	B	53	x	4	80	85	497.60	14.354	13.05	30.41	2.00	0.933	8.34	
806	B	54	x	2	71	76	504.11	14.519	11.79	27.99	1.83	0.983	10.71	
806	B	54	x	5	66	68	508.56	14.632	12.69	29.05	1.91	0.972	9.20	
806	B	55	x	2	80	85	513.90	14.768	13.25	31.33	2.09	0.979	5.71	
806	B	55	x	5	80	85	518.40	14.882	12.16	31.28	2.13	0.978	5.50	
806	B	56	x	2	87	92	523.67	15.016	11.55	28.67	2.19	0.954	5.32	
806	B	56	x	4	69	74	526.49	15.087	11.66	30.01	2.45	0.865	6.80	
806	B	57	x	2	70	75	533.10	15.255	13.57	29.55	2.34	0.962	9.85	
806	B	57	x	5	80	85	537.70	15.372	21.83	391.86	2.53	0.948	11.37	

806	B	58	x	2	70	75	542.70	15.499	10.93	26.53	2.09	0.978	7.58
806	B	58	x	5	75	80	547.25	15.615	11.19	27.98	2.06	0.963	5.62
806	B	59	x	2	70	75	552.40	15.746	11.38	27.98	2.01	0.950	6.60
806	B	59	x	5	80	85	557.00	15.862	12.36	34.72	2.16	0.967	6.47
806	B	60	x	2	80	85	562.20	15.995	12.21	33.49	1.71	0.969	8.04
806	B	60	x	5	36	41	566.26	16.098	11.35	31.71	1.81	0.977	6.62
806	B	61	x	2	70	75	571.80	16.238	12.62	32.28	1.91	0.984	6.25
806	B	62	x	2	110	115	581.90	16.495	11.67	32.71	2.42	0.854	11.94
806	B	62	x	5	80	85	586.10	16.602	12.81	30.18	2.20	0.944	8.95
806	B	63	x	2	70	75	591.20	16.731	10.83	29.18	2.24	0.910	14.98
806	B	63	x	5	78	83	595.78	16.848	12.89	31.71	1.95	0.961	8.73

Stable isotope data

Site	Hole	Section	Type	Interval	Top (cm)	Bottom (cm)	Depth (mbsf)	Age (Ma)	Species	$\delta^{13}C$ (PDB)	$\delta^{18}O$ (PDB)
803	D	22	H	3	80	85	192.40	11.269	*C. mundulus*	0.93	2.39
803	D	22	H	5	70	75	195.30	11.552	*C. mundulus*	0.69	2.29
803	D	23	H	1	70	75	198.80	11.900	*C. mundulus*	0.87	2.49
803	D	23	H	3	70	75	201.80	12.204	*C. mundulus*	0.88	2.60
803	D	24	H	1	70	75	208.30	12.880	*C. mundulus*	1.14	2.56

803	D	25	H	1	70	75	217.80	13.904	*C. mundulus*	1.12	1.95
803	D	26	H	3	70	75	230.50	15.324	*C. mundulus*	1.52	1.58
806	B	44	X	2	82	86	409.52	12.116	*Cibicidoides* spp.	0.83	2.34
806	B	45	X	5	81	86	423.71	12.477	*Cibicidoides* spp.	0.86	2.35
806	B	46	X	2	82	87	428.82	12.606	*Cibicidoides* spp.	0.91	2.33
806	B	46	X	5	82	87	433.32	12.721	*Cibicidoides* spp.	1.13	2.37
806	B	46	X	5	82	87	433.32	12.721	*C. mundulus*	0.99	2.34
806	B	47	X	2	70	75	438.30	12.847	*C. mundulus*	0.82	2.36
806	B	47	X	2	70	75	438.30	12.847	*C. wuellerstorfi*	0.91	2.37
806	B	47	X	5	38	43	442.48	12.953	*C. mundulus*	0.84	2.43
806	B	47	X	5	38	43	442.48	12.953	*Cibicidoides* spp.	0.99	1.37
806	B	48	X	2	64	69	447.94	13.092	*Cibicidoides* spp.	0.80	2.30
806	B	48	X	2	64	69	447.94	13.092	*C. wuellerstorfi*	0.94	2.26
806	B	48	X	5	60	65	452.40	13.205	*Cibicidoides* spp.	0.94	2.16
806	B	49	X	2	68	73	457.68	13.339	*C. wuellerstorfi*	1.17	2.18
806	B	49	X	2	68	73	457.68	13.339	*C. mundulus*	1.08	2.24
806	B	49	X	5	63	68	462.13	13.452	*C. wuellerstorfi*	1.24	1.94
806	B	50	X	2	70	75	465.80	13.546	*C. wuellerstorfi*	1.10	1.71
806	B	51	X	2	68	73	475.48	13.792	*C. mundulus*	1.70	2.23
806	B	51	X	2	68	73	475.48	13.792	*C. wuellerstorfi*	1.77	1.92
806	B	51	X	5	80	85	480.10	13.909	*C. mundulus*	1.78	2.13

806	B	51	X	5	80	85	480.10	13.909	*Cibicidoides spp.*	1.83	2.05
806	B	52	X	2	88	93	484.98	14.033	*C. wuellerstorfi*	0.88	2.30
806	B	52	X	5	77	82	489.37	14.144	*C. wuellerstorfi*	1.56	1.38
806	B	53	X	2	71	76	494.51	14.275	*C. wuellerstorfi*	1.67	1.27
806	B	53	X	4	80	86	497.60	14.354	*C. wuellerstorfi*	1.66	1.31
806	B	54	X	2	71	76	504.11	14.519	*C. wuellerstorfi*	1.52	1.38
806	B	54	X	5	66	68	508.56	14.632	*C. wuellerstorfi*	1.39	1.55
806	B	55	X	2	80	85	513.90	14.768	*C. wuellerstorfi*	1.40	1.26
806	B	55	X	2	80	85	513.90	14.768	*C. mundulus*	1.39	1.39
806	B	55	X	5	80	85	518.40	14.882	*C. wuellerstorfi*	1.04	0.82
806	B	55	X	5	80	85mc	518.40	14.882	*C. mundulus*	1.20	1.17
806	B	56	X	2	87	92	523.67	15.016	*C. mundulus*	1.61	1.23
806	B	56	X	4	69	74	523.67	15.016	*C. mundulus*	1.07	0.90
806	B	57	X	2	70	75	533.10	15.255	*C. mundulus*	1.65	1.53
806	B	57	X	5	80	85	537.70	15.372	*C. mundulus*	1.81	1.56
806	B	58	X	2	70	75	542.70	15.499	*C. mundulus*	1.73	1.55
806	B	58	X	5	75	80	547.25	15.615	*C. mundulus*	1.40	1.18
806	B	61	X	2	70	75	571.80	16.238	*C. mundulus*	0.69	1.33
806	B	62	X	2	110	115	581.90	16.495	*C. mundulus*	0.41	1.31
806	B	62	X	5	80	85	586.10	16.602	*C. mundulus*	0.77	1.54
806	B	62	X	5	80	85	586.10	16.602	*C. wuellerstorfi*	0.79	1.32

806	B	63	X	2	70	75	591.20	16.731	*C. mundulus*	0.29	1.26
806	B	63	X	5	78	83	595.78	16.848	*C. mundulus*	0.74	1.72

*Denotes samples removed from plots using the screening method of Lear et al, (2004).